# Opportunities from Renewable Resources: From biobased chemicals to biomaterials

**Yang Gao**

**Doctor of Philosophy**

University of York
*Chemistry*

June 2020

# Dedication

*I dedicate this work to my dear father, mother and Sister: Ling Gao, Yuzhi Yang and Huiping Gao*

# Abstract

Renewable resources and materials are considered as sustainable alternatives to their petroleum-derived counterparts which are often associated with negative social and environmental impact. In particular, where renewable resources occur as a by-product or waste as a consequence of primary and secondary processing, they can be viewed as a potential source of carbon neutral biobased chemicals, materials and (bio)energy through a process termed valorization.

This thesis presents the valorization of unavoidable food supply chain wastes (UFSCW), namely, pea-, ginger- and agricultural straw-waste to afford biobased chemicals, materials and (bio)energy. Pea and ginger wastes were successfully defibrillated in to microfibrillated celluloses (MFC) via acid-free microwave hydrothermal treatment as evidenced by changes in IR, TGA, $^{13}C$ CPMAS NMR, SEM, TEM, XRD, CrI and their ability to form hydrogels. The hydrolysate was rich in sugars, organic acids and, interestingly, starch (only for ginger waste). The effect of extrusion on pea waste gave higher CrI (*approx.* 1%-15%) and thermal stability (around 1-11$^{o}$C), reduced lignin and hemicellulose content, narrower fibril width (about 0.4-3.3 nm), better water holding capacity (5 to 40 % higher) and higher surface area compared (*approx.* 7-20 $m^2/g$) with their non-extruded counterparts. Ginger essential oils were successfully isolated in good yield (heptane; ~4%) with a composition similar to industrial grade ginger oil. Microwave pyrolysis of ginger afforded hydrochars (20 - 24.5 MJ $kg^{-1}$) and bio-oils of variable quality dependent on the processing conditions.

Bioboards (maximum IBS:0.25 $N/mm^2$) were successfully manufactured from agri-straws and biosilicate binders, and initial attempts to produce foam materials, as an inner layer of a structural insulation panel (SIP) are reported. Preliminary attempts to increase hydrophobicity via silanization are reported.

In conclusion, this thesis shows that biorefineries that deliver chemicals, materials and (bio)energy can be envisaged from valorization of pea, ginger and agri-straw UFSCWs.

# List of contents

# List of Figures

# List of Tables

# Acknowledgements

First and foremost, I would like to thank my supervisor, Dr. Avtar Matharu for his kind, patient, scrupulous supervision and support that he gave me throughout my PhD training in York. I also appreciate Dr. Duncan Macquarrie as my Independent Panel Member (IPM).

My many thanks to all dear green chemistry fellows and technicians providing nice working atmosphere which I really enjoyed. I would like to thank Paul Elliott. Dr. Fangru Xing, Dr. Hannah Briers, Dr. Richard Gammons, Dr. Thomas Dugmore, Dr. Suranjana Bose, Dr Mustafa Ozel, Dr. Tabitha Petchey and Dr. Maria Garcia Gallarreta for their kind help during my project especially the first year. I'd like to acknowledge the helpful support I received during my research that brought many contributions to my work: Meg Stark, Heather Fish, Karl Heaton and Prof Menaka Jha.

I would like to thank my friends, Long, Xiangju, Xia, Zhicheng, Tianzong, Xudong, Allyn and Andy for the help with my research in the past four years.

Finally, I'd like to thank my family, which has always supported me. Thank you very much for everything you had done for me.

Thank you all.

# Author’s declaration

I hereby declare that all the work in this thesis is my own except where stated. This work has not previously been presented for an award at this, or any other, University. All sources are acknowledged as References.

# Publications and Conferences

The work in this thesis has been published and presented as follows:

1. Gao, Y.; Mustafa. Z.O.; Dugmore, T. I. J.; Sulaeman, A.; Matharu, A. S. Spent industrial ginger biomass for production of high value products – a value added strategy for resource recovery. *Journal of Hazardous Materials*, 2021, **401**,123400.
2. Gao, Y.; Xia, H.; Sulaeman, A.; de Melo, E. M.; Dugmore, T. I. J.; Matharu, A. S. Defibrillated celluloses via dual twin-screw extrusion and microwave hydrothermal treatment (MHT) of spent pea biomass. *ACS Sustainable Chemistry & Engineering*, 2019, **13**, 11861-11871.
3. Gao, Y.; Xing, F.; Jha, M.; Yadav, K. K.; Yadav R.; Matharu, A. S. Towards Novel Biocomposites from Unavoidable Food Supply Chain Wastes and Zirconia (Submitted: ACS Sustainable Chemistry & Engineering, 07/06/2020).
4. Jiang, Z.; Fan, J.; Budarin, V. L.; Macquarrie, D. J.; Gao, Y.; Li, T.; Hu, C.; Clark, J. H. Mechanistic understanding of salt-assisted autocatalytic hydrolysis of cellulose. *Sustainable Energy & Fuels*, 2018, **2**, 936-940.
5. Influence of physical fractionation on unavoidable pea waste followed by microwave hydrothermal treatment (MHT) for micro fibrillated cellulose. Poster. Systems Change Thinking - Creating Value and Closing the Loop from Unavoidable Food Supply Chain Wastes. UK, York (3/12/2018).

6. New insights into physical fractionation on unavoidable pea waste and microwave processing for production of microfibrillated cellulose. Poster. 15th International Conference on Renewable Resources & Biorefineries, France, Toulouse (4/06/2019).

# How to use this thesis

This thesis is intended for those either new to green and sustainable chemistry and/or experienced researchers. The thesis is divided in to 4 chapters and in accordance with University of York rules and regulations. The references are consolidated towards the end of the thesis rather at the end of each chapter. The abbreviations are listed at the end of the thesis.

Chapter 1: Introduction and Aims. This chapter contextualizes the need for this research with reference to 'big picture' concepts, *i.e.*, impending sustainability issues associated with global megatrends, UN Sustainable Development Goals, green chemistry and the biorefinery concept and the importance valorization of UFSCW. These are then consolidated in to an overall, global aim, which is subdivided in to specific objectives: *Part A: Production, characterization and applications of defibrillated celluloses via dual twin-screw and microwave hydrothermal treatment (MHT) of spent pea biomass; Part B: Spent ginger biomass: A biorefinery strategy for resource recovery, and: Part C: Towards Novel composite bioboards and structural insulation panels from waste agri-fibres.*

Chapter 2: Experimental. This chapter is written in sufficient detail to enable final year undergraduates, postgraduates and those skilled-in-the-art to complete procedures, isolate materials and proceed to their characterization. This chapter consolidates all experimental details that are commensurate with the intended aims and objectives (as reported in Chapter 1) and supports the results and discussion thereof, in Chapter 3.

Chapter 3: Results and Discussion. This chapter is divided into 3 parts, namely: *Part A: Production, characterization and applications of defibrillated celluloses via dual twin-screw and microwave hydrothermal treatment (MHT) of spent pea biomass; Part B: Spent ginger biomass: A biorefinery strategy for resource recovery, and; Part C: Towards Novel composite bioboards and structural insulation panels from waste agri-fibres*, enabling connectivity with the intended aims listed in Chapter 1 and experimental in Chapter 2.

A significant volume of results is presented and critically discussed based on their characterization. Attempts are made to correlate key information across several techniques.

Chapter 4: Conclusions and Future Work. This chapter consolidates the entire research undertaken providing key conclusions and, importantly, provides an insight in to future work.

References

All references are listed in numerical order and cited as follows:

1. For journals: Surname, Initials, Manuscript title. *Journal title*, **publication year**, *volume number*, page numbers. For example, Amidon, T. E.; Wood, C. D.; Shupe, A. M.; Wang, Y.; Graves, M.; Liu, S. Biorefinery: conversion of woody biomass to chemicals, energy and materials. *Journal of Biobased Materials and Bioenergy,* **2008,** *2*, 100-120
2. For PhD thesis: Surname, Initials, Thesis title, University, **publication year**. For example, Tian, G. Renewable materials from renewable resource. PhD

Thesis, University of York: **2015**.

3. For book and book chapters: Surname, Initials, *Book title*, Publisher: **publication year.** For example, Brunner, G., *Hydrothermal and supercritical water processes*. Elsevier: 2014.

Certain references and documents are cited from the internet. For those, the URL is given followed by the date it was last accessed.

United Nations. World Population Prospects 2019: Key findings and advance tables. https://population.un.org/wpp/Download/Standard/Population/ (accessed 28 October 2019).

Chapter 1

# 1 INTRODUCTION and AIMS

## 1.1. Global problem and opportunity

It is quite startling that global population is expected to reach 10.9 billion by 2100 (**Figure 1.1**), from its current value of 7.8 billion (2020).[1] Our planet faces unprecended resource and consumption challenges as a direct consequence of population rise and allied megatrends of increasing urbanisation, industrialisation, quality of health, increased life span, and the need to protect our environment. In 2017, approximately 89 Gt of virgin resource was extracted which is expected to increase to 167 Gt by 2060 (**Figure 1.2**).[2] Our material, chemical, and energy needs continue to be sourced mainly from petroleum and fossil fuels.[3] However, their continued utilization is fraught with various environmental and social problems, let alone dwindling availability since crude oil is finite resource.[4] The known reserves of accessible oil, nature gas and coal are finite and not infinite. Our production and consumption are based on a linear economy that takes from Planet Earth (cradle), makes (manufactures), uses and disposes (grave). Our current production and consumption rates are unsustainable as we use and dispose too much resource, for example, plastics in the environmment.[5] Now is the time for a paradigm shift in our thinking that considers alternative feedstocks to crude oil, makes better of by-products and wastes, and develops circular (cradle to cradle)[6] rather than linear thinking (cradle to grave), keeping resource functional for longer.

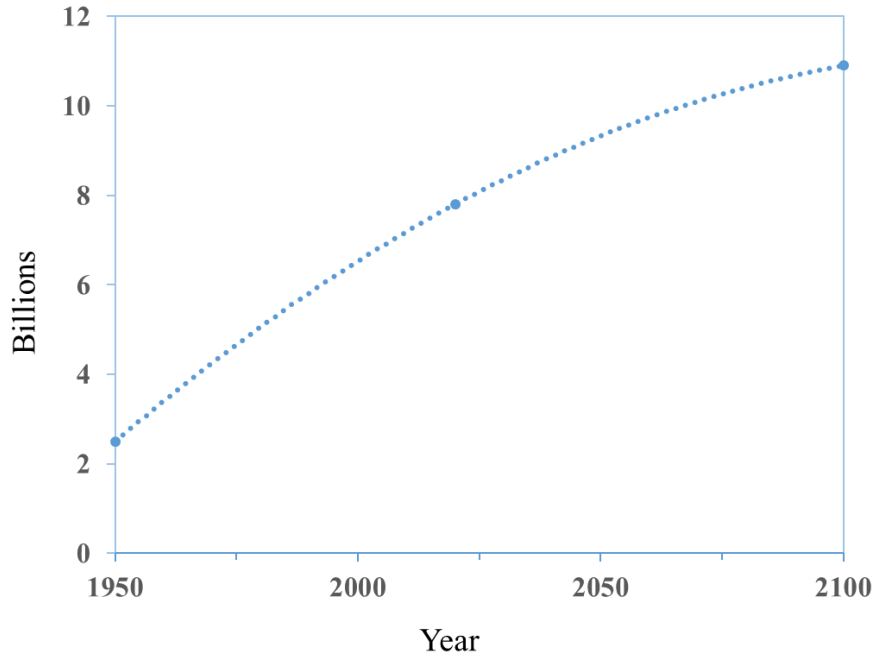


Figure 1. 1 Human population projection. Adapted from Cilluffo *et al.*[7]

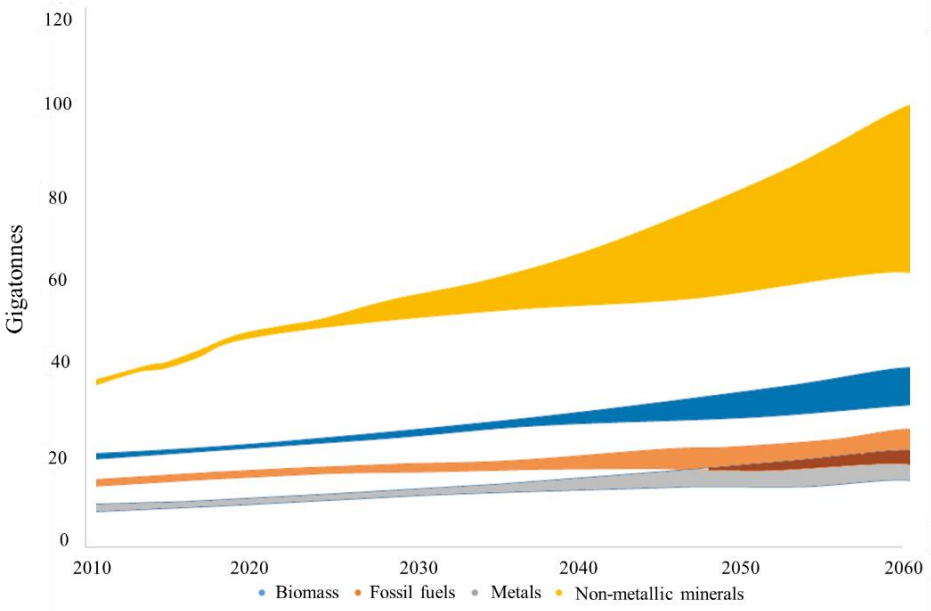


Figure 1. 2 Material use trends (2010-2100). Adapted from Agrawala *et al.*[2]

In this context using biomass as a feedstock and, in particular, where it occurs as a by-product of primary and secondary processing offers a potentially sustainable alternative to the continued use of crude oil for our chemicals, materials and energy

need. This transition away from crude oil is becoming a global grand challenge as Nations are advocating sustainability as part of a connected effort to protect our planet through committed policy actions, such as the United Nations Sustainable Development Goals (SDGs).[8]

### 1.1.1. UN Sustainable Development Goals, COP21 and to date

As a global project of action for our planet, people, peace, partnership and prosperity, 17 Sustainable Development Goals (SDGs, see **Figure 1.3**) were established at the United Nations (UN) Sustainable Development Summit in 2015.[9] The international development framework set a focus on integration and balance among social, economic, environmental aspirations in both developing and developed countries.[10]

Alongside the development of UN SDGs, in 2015, the Paris Conference of the Parties (COP21) and the Parties to the United Nations Framework to Combat Climate Change (UNFCCC) reached a landmark agreement to combat climate change and to accelerate and intensify actions and investments needed for a sustainable low carbon future, known as the Paris Agreement.[11] The Paris Agreement's central aim was to strengthen the global response to the threat of climate change by keeping a global temperature rise this century below 2 $^{o}$C above pre-industrial levels and to pursue efforts to limit the temperature increase even further to 1.5 $^{o}$C. Additionally, the agreement aimed to increase the ability of countries to deal with the impacts of climate change, and make finance flows consistent with low GHG emissions and climate-resilient pathways.

To date, COP25 (December 2019: Chile-Madrid Time for Action), held in Madrid but under the auspices of the Chilean Government, continues to develop the UN SDGs and the Paris Agreement within an holistic approach of climate action work in areas including finance, the transparency of climate action, forests and agriculture, technology, capacity building, loss and damage, indigenous peoples, cities, oceans and gender. The need for scientific innovation and intervention was deemed extremely important.[12] The highlighted green ovals in **Figure 1.3** show how the work in this thesis is linked to the SDGs and are further expanded in the Aims and Objectives section later.

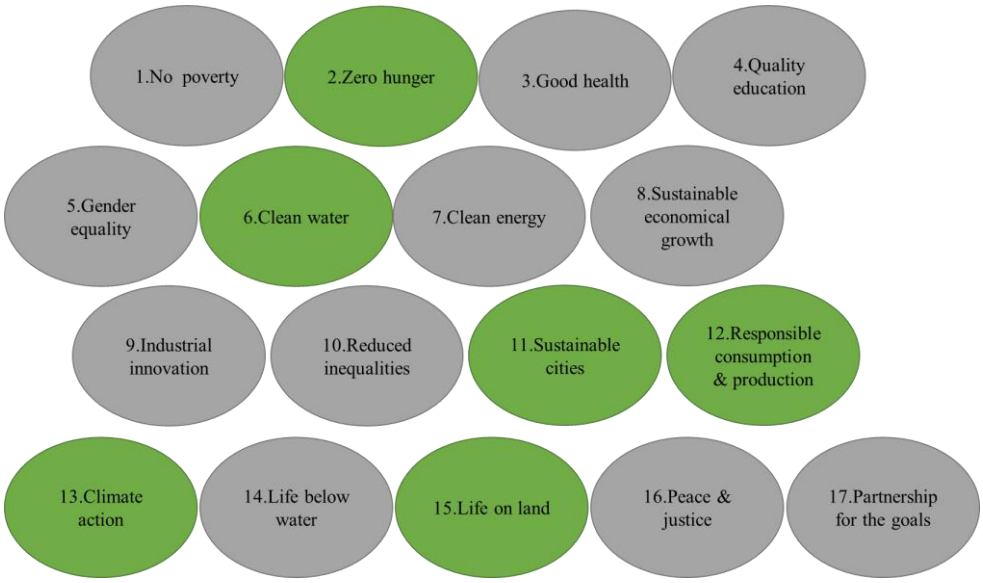


Figure 1. 3 The 17 UN Sustainable Development Goals.

Interestingly, much of the terminology and guiding principles described in the SDGs and the Paris Agreement resonate with the practice of green chemisty and the 12 Principles of Green Chemistry first established by Anastas and Warner in 1998.[13]

## 1.2 Green chemistry and the Biorefinery Concept

### 1.2.1 Green chemistry

"*Green chemistry consists of environmentally friendly, sustainable chemicals and processes whose use results in reduced waste, safer outputs, and reduced or eliminated pollution and environmental damage. Green chemistry encourages innovation and promotes the creation of products that are both environmentally and economically sustainable*." [14]

The *12 principles of green chemistry* (see **Figure 1.4**) provide a set of guidelines for performing better chemistry. The economic value of green chemistry of green and sustainable chemistry should not be underestimated for a sustainable 21st Century. Globally, the chemicals industry is worth approximately $5.7 trillion (USD) and supported 120 million jobs in 2017.[15] . In UK, the Chemistry Council (formerly known as Chemistry Growth Partnerships) recognises the importance of green and sustainable chemistry to deliver advanced materials, green supply chains and green energy in its Sector Deal.[16]

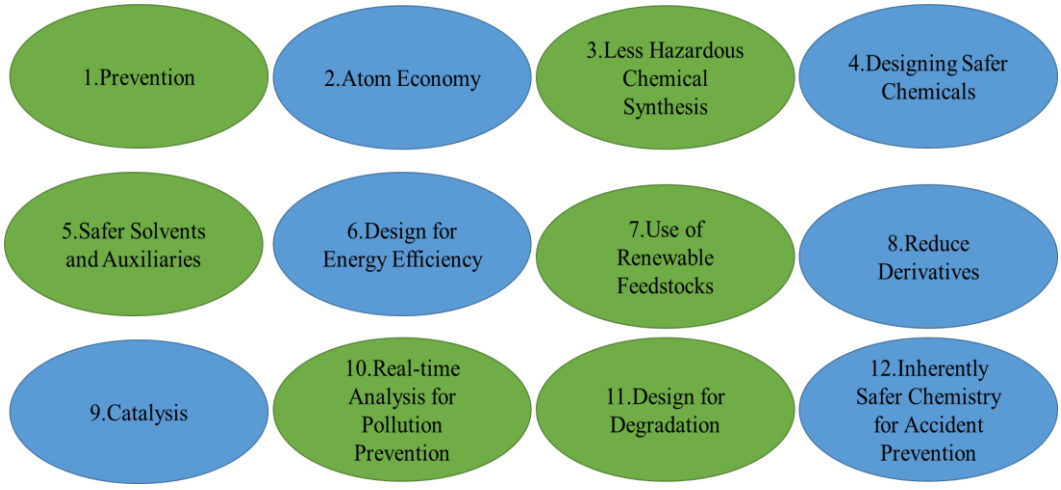


Figure 1. 4 The 12 Principles of Green Chemistry (the green ovals link to the work in this thesis)

### 1.2.2 The Biorefinery Concept

*"A biorefinery is a facility that integrates biomass conversion processes and equipment to produce fuels, power, and value-added chemicals from biomass."*[17]

The biorefinery concept is similar to a petroleum refinery where crude oil is fractionated and refined to produce energy[18] and chemicals but biomass (*e.g. straws, corns, grass, wood, biological waste*) is used instead (**Figure 1.5**). A biorefinery utilises already embedded carbon dioxide within renewable resources and are often said to be carbon neutral. However, this is debatable as resource inputs (land, chemicals, energy fertilizer, machinery, etc) to grow feedstock are sometimes discarded in calculations. Nevertheless, where by-products or waste is used then this is more akin to carbon saving or neutrality.[19]

According to the type of feedstock, technology, and products a biorefinery can be classified into three types:[20] i. one feedstock to one main product with only one process, for example, the production of biodiesel from vegetable oil or bioethanol from corn grain without valorisation of other products; ii. one feedstock to various main products with multiple processes (physical, chemical, biochemical etc), and; iii. different raw materials to diverse products with multiple processes (specially, sometimes multiply feedstocks to one main product via one approach also belong this type, *e.g.* lignocellulosic-based feedstock to biogas via anaerobic digestion, namely, LCF biorefinery).[21]

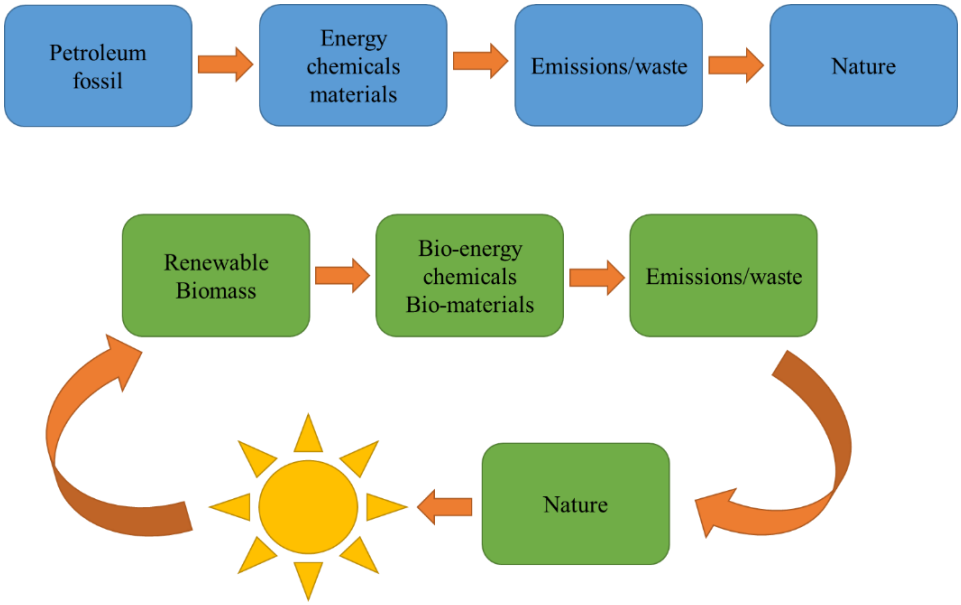


Figure 1. 5 Moving from a petroleum to a biorefinery economy

However, despite the conceptual advantages of a biorefinery concept, commercial acceptance is still reserved because: i. it is still an immature technology despite fermentation being a centuries old process;[19, 22] ii. feedstock has a high oxygen content which is problematic for fuel-like applications;[23] seasonal feedstock and variability, and; struggles to compete economically especially the price of crude oil is very low.[f] Nevertheless, at an academic level the biorefinery concept to deliver biobased products continues to gain much attention. Many feedstocks and processes have been explored. For example, Vernès *et al*. report a biorefinery approach for microalgae including cultivation, harvesting, and extraction of high value added molecules to different final potential products.[24] Yang *et al*. report a biorefinery based on crustacean shell waste with a simple, low-cost and environmentally friendly fractionation method

[f] This thesis was written during the time of Covid-19 (2020), a global pandemic, which saw the price of crude oil fall to as low as $11.50 (USD) per barrel (commensurate with 1990 price) and is now hovering at $25 (USD) per barrel.

to obtain a high purity chitins.[25] Khan *et al*. report several pretreatments for lignin anaerobic digestion to produce biogas.[26]

## 1.3 Composition of biomass: a renewable resource

Typically, terrestrial agricultural biomass comprises 40–50% cellulose, 20–40% hemicellulose and 20 to 30% for lignin, in addition to lipids, waxes, proteins, flavonoids, etc.[27] Traditionally, plant cell walls can be described as shown in **Figure 1.6**: hemicellulose embraces cellulose fibrils forming a cross-link structure, and lignin gradually fills the space between them via ester and ether linkages.[28, 29] The hierarchical structure of cellulose is aggregated into parallel elementary microfibrils which are stabilized through a network of hydrogen bonds.[30] The elementary microfibrils form into larger macroscopic fibers which consist of two major domains: highly organized crystalline, and unorganized amorphous.

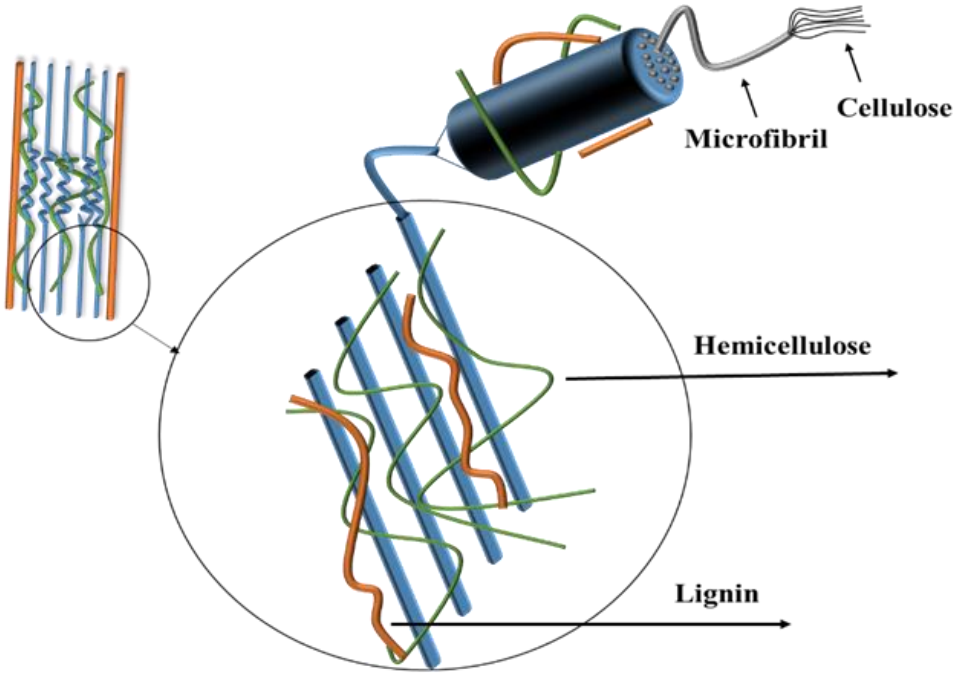


Figure 1. 6 Structure of lignocellulosic biomass

Due to the inherent, strong cross-linked composition of the original lignocellulosic matrix, crude biomass can only be utilized inefficiently and with difficulty.[31,32] Thus, pretreatment becomes a crucial technique to make lignocellulosic biomass easier to convert to high-value chemicals or materials.[33,34] Normally, the pretreatment process can be classified into chemical (*e.g.* acid, alkali, ionic liquid treatment),[35-39] physical (mechanical splintered, microwave, ultrasonic treatment),[40-42] biological (*e.g.* white rot fungi, brown rot fungi, enzymatic)[43] or physicochemical combined methods (*e.g.* steam explosion, $CO_2$ explosion).[44,45]

### 1.3.1 Cellulose

As the most abundant organic polymer on earth, cellulose is widely existing in plant cell walls. The linear homopolysaccharide is composed of glucose units linked together by β-(1-4) glyosidic bonds. A single chain may contain around 5000–14,000 glucose molecules.[46] The chains stack side by side and packed into microfibrils by hydrogen bonds (see **Figure 1.7**).[47] The strong intermolecular hydrogen bond between the chains make cellulose insoluble in water and most solvents.[48]

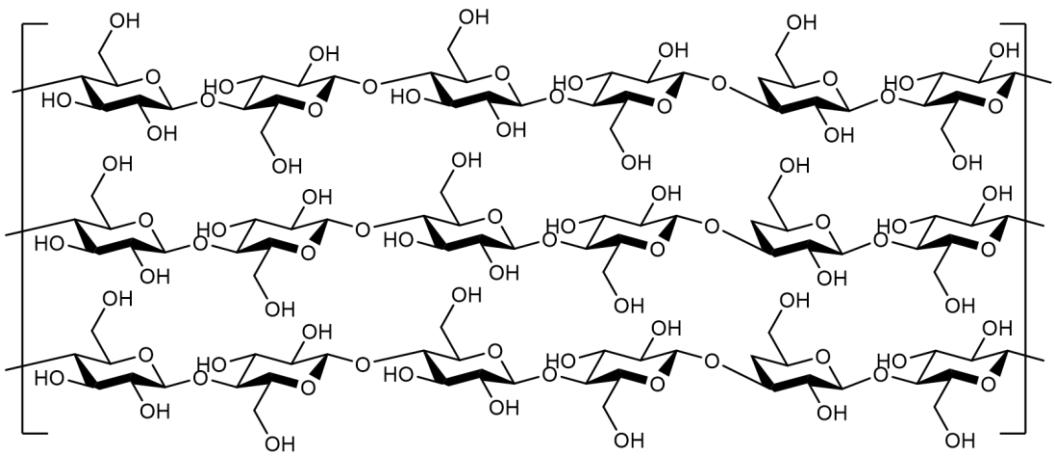

Figure 1.7 The chemical structure of cellulose

There are 4 four different crystalline polymorphs according to their state of aggregation: cellulose I, II, III, and IV (see **Figure 1.8**). Cellulose I is native cellulose and can be divided into two forms dependent on its the layer packing along the c direction: the cellulose $I_\alpha$ and cellulose $I_\beta$.[49] Cellulose $I_\alpha$ and $I_\beta$ can coexist even in the same microfibril;[50] Cellulose II is normally found in marine algae, and can also be obtained from cellulose I by alkali treatment. The difference is that in parallel fibrils the crystals of cellulose II are in opposite direction.[50] Cellulose III is derived from ammonia (or mono-, di-, and tri-amines)[51] treatment of cellulose I, producing a structure with high degree of inter- and intra-molecular hydrogen bonding. [52] Cellulose IV is formed from high temperature treatment with glycerol.

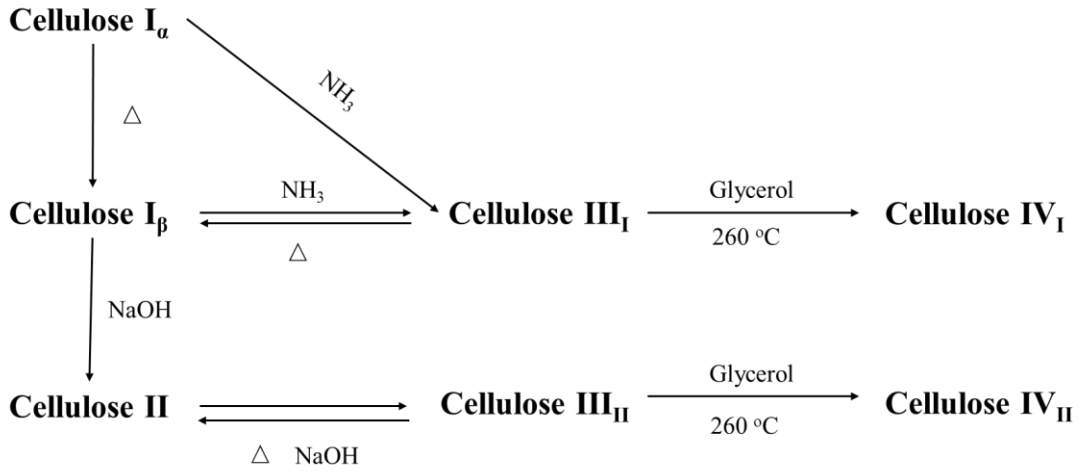


Figure 1. 8 Diagram of the conversion of various crystalline forms of cellulose Adapted from Santon.[53]

### 1.3.2 Hemicellulose

As the second most abundant constituent in biomass, hemicellulose is a heterogeneous polymer comprising many different sugar monomers (see **Figure 1.9**): five carbon xylose, rhamnose, arabinose; six carbon glucose, mannose, galactose, and; sugar acids based on the nature of the biomass.[54] This is different compared with cellulose which

is only made from glucose. The sugars in hemicellulose are normally linked by β-1,4- or β-1,3-glycosidic bonds.[55]

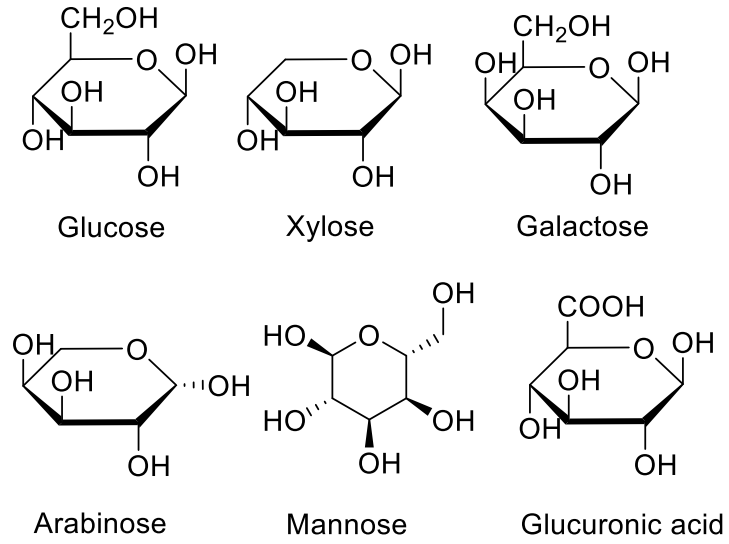


Figure 1. 9 The structures of different monomers in hemicellulose

Hemicelluloses are generally branched with low degree of polymerization (500–3,000 sugar units),[56] making it easier to degrade to with respect to cellulose. In terms of a biorefinery concept, hemicellulose is an ideal sustainable feedstock to produce bio-based energy (*e.g.* sugars to bioethanol via fermentation), materials and high value-added chemical including furfural and xylan.[57]

### 1.3.3 Lignin

Lignin is a complex cross-linked aromatic polymer which is formed by repeat phenolic monomers including (see **Figure 1.10**) *p*-coumaryl alcohol (H-units), coniferyl alcohol (G-units), and sinapyl alcohol (S-units) via ether linkages and C-C connection.[33] According to the plant species, growth duration and growing location, lignin presents different structures and repeat units.[58] As a structural material, lignin fills the spaces between cellulose, hemicellulose and other components (*e.g.* pectin)

and plays a critical role in ensuring the mechanical strength of plant cell walls.[59] The lignin content is based on the type of biomass, for example, there is approximately 28% in softwoods and 20% in hardwoods.[60] Physical pretreatment, (milling or ultrasound), pyrolysis, organic solvent , liquid hot water, steam explosion and ozonation are some common approaches to deligninfication.[61]

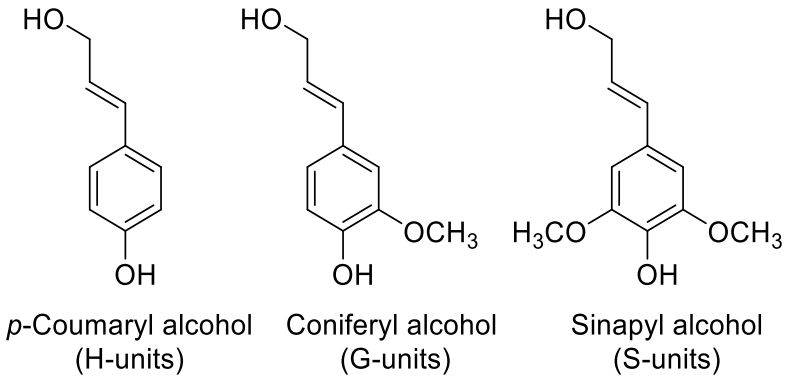


Figure 1. 10 The three main types of monolignols: *p*-coumaryl, coniferyl, and sinapyl alcohols

Lignin itself had received considerable attentions due to its physicochemical properties, abundance resource, low cost and biocompatibility,[58] it can be used as adsorbents, hydrogels,[62] reinforced bioplastic composites,[63] adhesives, resins and even nanostructured materials.[64]

## 1.4 Food waste as a biomass resource

By 2100, solid waste is set to exceed 11 million tonnes (Mt) per day – triple than today's rate,[65] with cities such as Mexico City, and Shanghai, producing more than 10,000 tonnes per day. Agricultural arisings and food waste are a significant contributor to the global waste problem. According to the Food and Agriculture Organization (FAO), it is striking that 1.3 billion tonnes of food[66] which equals to 1/3

of all food produced in the world (more than $1 trillion in economic costs)[67] is wasted every year.

**Figure 1.11** shows typical losses and wastes throughout the food supply chain (FSC), from initial harvesting to final household consumption.[68] Normally, the first 3 phases: food production and harvest, storage, processing and packaging belong to upstream waste, and the last 3 phases contribute to downstream waste.

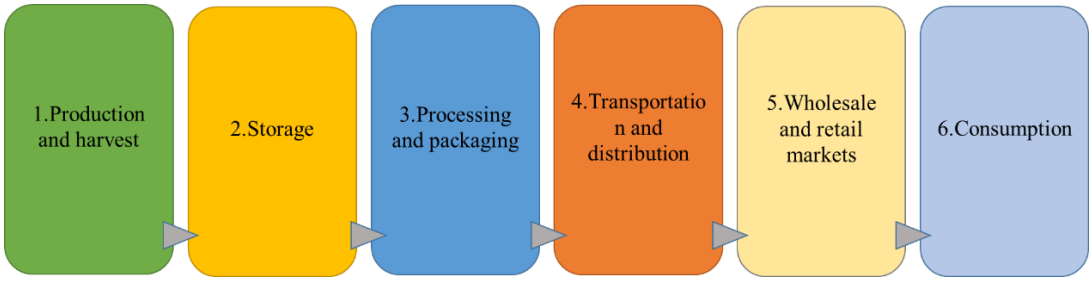


Figure 1. 11 Loss and waste along food supply chain

**Figure 1.12** displays the distribution of food waste by region and by phase of the supply chain. It is obvious that the type of food waste in the FSC is determined by geographical region: in high-income developed regions, the proportion of lost and wasted food is much higher in downstream waste especially in the consumption stage. This may due to food quality regulations and misconceptions between supplier and consumers,[69] *e.g.*, "best before date" and "use by date".[70] Conversely, in developing countries, food waste is mainly upstream especially in harvesting and storage stages. This may be due to low-tech and/or lack of infrastructure to keep harvest free from spoilage.[70]

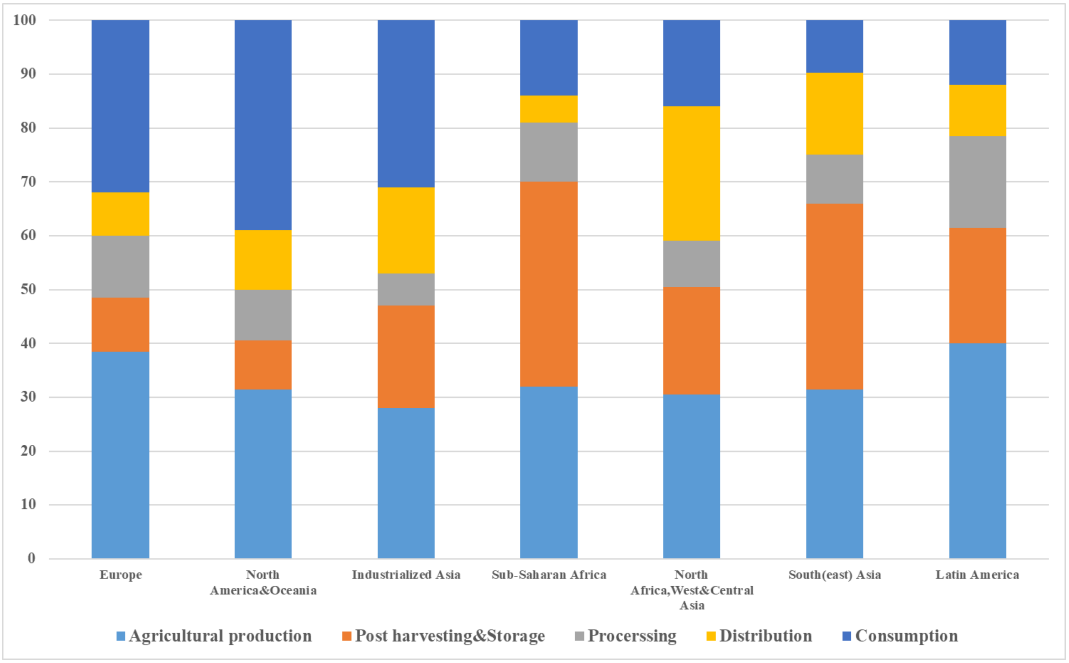


Figure 1. 12 Distribution of food waste by region and phase of supply chain

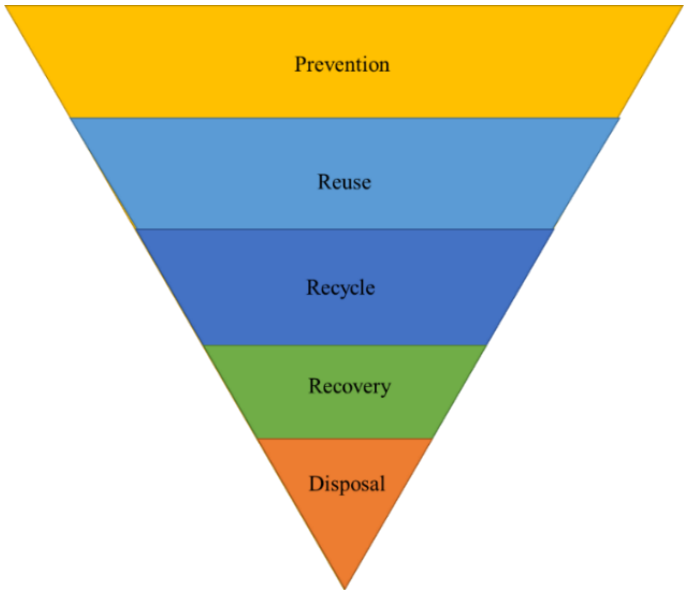


Figure 1. 13 Food waste hierarchy（Adapted from Effie *et al*. 2014[71]）

There are measures to reduce avoidable food waste through prevention and reuse (see **Figure 1.13**), but unavoidable food supply chain waste (UFSCW), which consists of unsellable or inedible food that cannot be consumed by human, is deemed as waste.

Obtained from post-harvesting and processing phases (*e.g.*, peeling, chopping, shredding, preserving, boiling, etc) [72] of the FSC, UFSCW (*e.g.* straws, husks, leaves, peels, seeds or pods) can be regarded as the "periodic table of fit for purpose biobased chemicals"[72] which contain extractable functional biomolecules, *e.g.*, fibres, proteins, polysaccharides, fats or oils, enzymes, flavors and aromas, pigments, and antioxidants).[69, 73, 74] Furthermore, compared to fossil fuel-derived products, biomass naturally comprises heteroatom C, H, O, N and S functionality.[69] The decomposition timescale of agricultural/food waste is 3–12 months. This is at most 80 times better than wood (25–80 years) and 280 million times better than fossil-based product (more than 280 million years).[69, 75] Thus, UFSCW is an important, renewable feedstock for future chemicals, materials and energy requirements. Three examples of feedstock are given in the following sections, namely: peas; ginger root, and; agricultural straws, which are relevant to the work described in this thesis.

### 1.4.1. Peas

As the second most important legume after the common green bean,[76] peas (*Pisum sativum*) are not exotic but grown globally.[77] Peas have been cultivated since approx. 6,500 B.C.[78] In 2018, China (12.9 Mt), India (5.4 Mt) and France (0.25 Mt) were the top three global pea producers.[79] Pea seeds are rich in protein, starch, fibre and micronutrients including minerals (*e.g. zinc, magnesium, calcium, phosphorous and iron*) and vitamins (*e.g. A, B6, C, K* ).[80] The especially high protein content (22% to 24%), including albumins (20%) and globulins (50% to 60%), of pea seeds makes pea an important source of vegetal protein.[81]

In 2018, 38000 hectares of pea were grown in the UK, (see **Table 1.1**) yielding an average of 3.8 tons per hectare.[82] In general, more than 30% (w/w) waste comprising leaves, vines, pods and stalks, (also known as haulm) is produced during pea harvesting and processing. Traditionally, the fresh or ensiled pea vines can be used as animal feed as they have a higher protein content than cereal straws. The pods after peeling are also rich in crude protein (around 19.8 %), soluble sugars, phenolics and other nutrition and, thus, eaten by ruminants.[83]

Table 1. 1 Protein crops (Peas and Beans) production (thousand tonnes, Adapted from Agriculture in the United Kingdom 2018[82])

| | 2014 | 2015 | 2016 | 2017 | 2018 |
|---|---|---|---|---|---|
| **Peas for harvesting dry** | | | | | |
| Area (thousand hectares) | 32 | 44 | 51 | 40 | 38 |
| Yield (tonnes per hectare) | 4.0 | 4.1 | 3.7 | 4.0 | 2.8 |
| **For animal feed** | | | | | |
| Volume of harvested production | 70 | 100 | 65 | 85 | 90 |
| Value of production (£million) | 13 | 12 | 9 | 12 | 18 |
| **For human consumption** | | | | | |
| Volume of harvested production | 68 | 95 | 121 | 75 | 17 |
| Value of production (£million) | 13 | 14 | 18 | 11 | 3 |

The composition of dried pea biomass is listed in **Table 1.2**. The differences in data may due to crop type, growth environment or testing method. Despite reuse opportunities like animal feed, haulm is often left on farmland;[84] anecdotally, more than enough pea waste is left on land than is required to maintain good soil health and

nutrition. Thus, there is an excess which serves no additional benefit and probably decays. Reutilization or valorization of unavoidable pea waste, represents a significant lignocellulosic resource for chemical and economic exploitation,[85] but also an opportunity to improve the environment by diverting decaying waste.[86-88]

Table 1. 2 Composition of dried pea biomass from Åman and Graham (1987) and Treviño, Centeno and Caballero, (1986) (Adapted from Phillips)[80]

| | Åman and Graham | | | | Treviño, Centeno and Caballero | | | |
|---|---|---|---|---|---|---|---|---|
| Nutrient type | Whole plant | Stem | Leaf | Pod/flower | Whole plant | Stem | Leaf | Pod seed |
| Cellulose | 23-31 | 14-35 | 9-25 | 14-35 | 14-14 | 23-31 | 12-22 | 7-10 |
| Hemicellulose | 10 | 15 | 9 | 19 | 5-12 | 8-13 | 5-12 | 10 |
| Lignin | 5-8 | 10.5-16.5 | 4.4-14.5 | 2-9 | 4-6 | 6-13 | 3-7 | 2 |
| Pectin | 5-9 | 7-10 | 9-14 | 4-10 | - | - | - | - |
| Protein | 22-40 | 3-9 | 15-22 | 5-35 | 16-20 | 11-22 | 8-11 | 20-26 |
| Starch | 4-24 | 1-6.5 | 1-7 | 5-9 | 8-22 | 4-7 | 6-8 | 14-34 |
| Lipids | 1-4 | 1-2 | 1-4 | 1 | - | - | - | - |
| Ash | 6-8 | 4-6 | 6-8 | 2-6 | 8-9 | 9-11 | 9-14 | 4-5 |

### 1.4.2 Ginger root

Ginger (*Zingiber officinale*), originally derived from Southeast Asia and now cultivated in a number of countries including India, China, Nepal, and Nigeria, is a flowering plant whose rhizome, ginger root or ginger, is used in food, flavors, fragrances and medicinal products.[89, 90] In 2016, 3.3 million tonnes of ginger was produced[91] and with rising concerns towards health and a demand of herb-based products, global production of ginger is set to increase.[92]

Ginger is often processed for its high-value oleoresins and volatile oils.[93-96] Ginger oleoresin (the compounds present in ginger oils like gingerols, shogaol, and paradols are shown in **Figure 1.14**) contains on average 20–30% of volatile oil, 10% of fixed oil, 50–70% of pungent resinous matter and only accounts for 4–10% of the total dry weight of the rhizome. Thus, there is a significant amount (by weight) of spent industrial ginger wastes, which are currently used as low value animal feed (ginger waste meal) [97] or discarded. Actually, 40-55% starch and cellulose can be obtained from the dried ginger after extraction of the oils.[98] Nevertheless, current scenarios for re-utilisation of spent ginger wastes are limited, especially those that seek to explore resource recovery (valorization) in the form of chemicals, materials and energy within the context of a biorefinery.

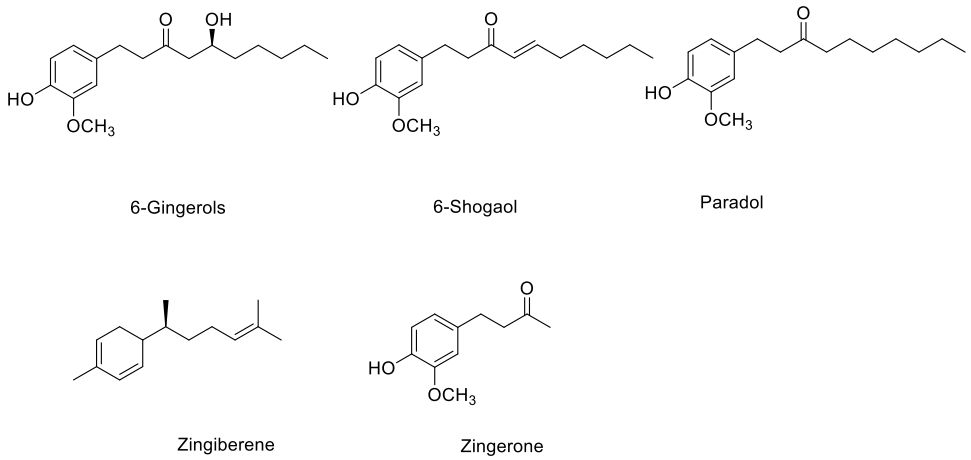

Figure 1. 14 Examples of valuable compounds found in ginger.

### 1.4.3 Agricultural straws

In 2018, maize, wheat, and rice were the top three global cereal crops (see **Table 1.3**) supporting enough food for our increasing population. Every year, millions of tons of cereals are cultivated and havested, producing a considerable amount of agricultural

byproduct, namely, straw.

Table 1. 3 Annual production of cereals in 2018 [79] (Mt)

| | Maize | | Rice | | Wheat |
|---|---|---|---|---|---|
| World | 1147.6 | World | 782 | World | 734 |
| US | 392.5 | China | 212.1 | China | 131.4 |
| China | 257.2 | India | 172.6 | India | 99.7 |
| Brazil | 82.8 | Indonesia | 83 | Russian | 72.1 |
| Argentina | 43.5 | Bangladesh | 56.4 | US | 51.2 |
| India | 28.7 | Vietnam | 42.8 | France | 36.9 |

Traditionally, because of the low economic value of straws, they are used for animal bedding, animal feed (poor quality), over-wintering of carrots, general tilling and more seriously, landfill and burning (now banned in many countries but still practised illegally).[99] Based on economic and environmental concerns, the re-utilisation of the agricultural straws has attracted widespread attention during last few decades, [100, 101] including manufacture of biocomposites and as a source of renewable energy.[102] However, currently the conversion of agricultural straws to bioethanol is an expensive procedure and the seasonality of raw materials restricts its development.[102, 103]

Straws can also be processed in to composite panels (*e.g. particleboard*) as alternatives to using wood.[104] Wood-based panels are sheet materials comprising chips of wood glued together with organic binders (urea-formaldehyde (UF) or phenol-formaldehyde (PF)) to afford particle boards (PB), plywood and oriented strand boards (OSB). Due to their good mechanical and physical properties,[105] these products have various applications in furniture, table tops, cabinets, home construction, kitchen worktops and other industrial products (see **Figure 1.15**). According to the Wood Based Panel Market Size, Share & Trends Analysis Report, in 2019, the value of wood based board

market in the US was about $144.67 bn (USD) and anticipated to increase (see **Figure 1.16**).[106]

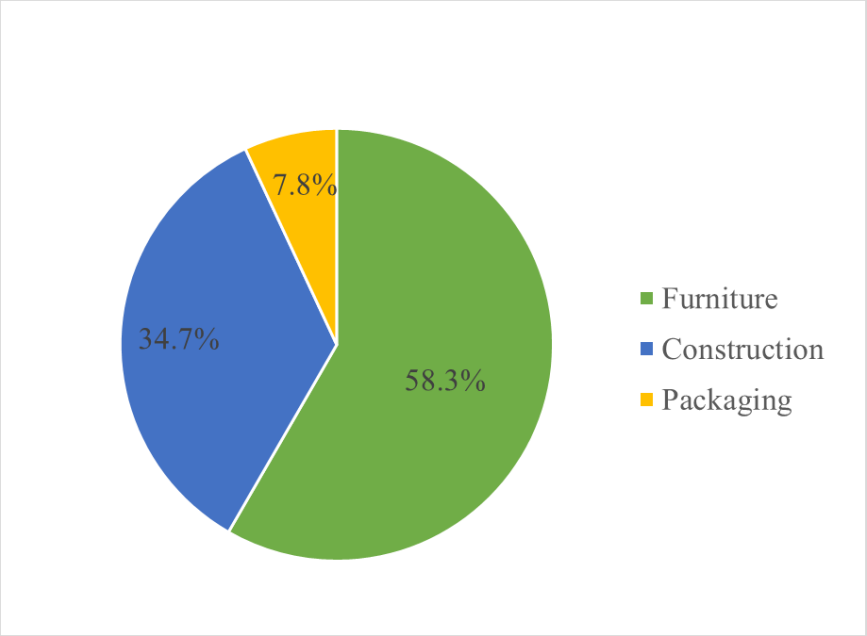


Figure 1. 15 US wood-based panel market size, by product,2016 to 2027. Adapted from Grand View Research.[106]

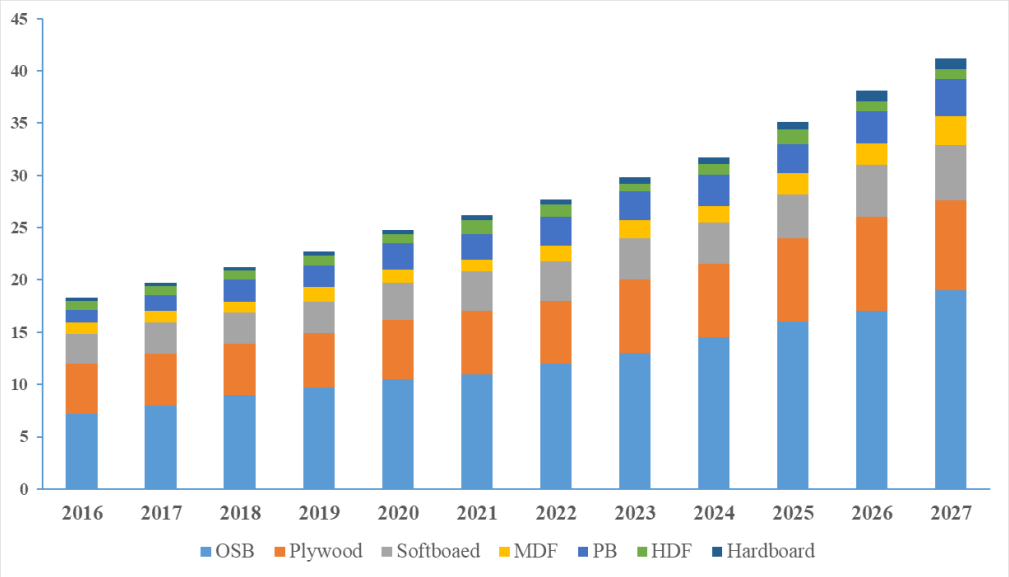


Figure 1. 16 Global wood-based panel market share, by application. Adapted from Grand View Research.[106]

However, due to accelerating deforestation and the use of toxic binders (UF, PF and isocyanates),[107] it is becoming environmentally unfriendly to use wood based products,

especially reconstituted. The use of medium-density fibre board (MDF) is already banned in California State, USA.

The continued use of wood, even though it may be sustainably managed, is environmentally unsound and as a resource is limited. Hence, to avoid unnecessary deforestation, alternative materials, especially those arising as 'waste or residues' from processing industries represent an interesting alternative to wood.

Following the production of first commercial straw board in 1995 by Prime Board, North Dakota, USA,,[108] the utilisation of this raw material for board manufacture has received considerable attention. Petra *et al*. investigated the influence of enzymatic treatment on the properties of wheat boards.[109] Juan *et al.* developed fiberboards from wheat straw fibers without any bonding agent via enzymatic treatment.[110] Štěpán studied different types of wheat straw pretreatment (alkaline, plasma and hydrothermal) on properties of the particle boards.[111] Not linited to wheat straw, rice husks/straws,[112-114] and sunflower stalks,[115, 116] which are also available in significant volumes, have been used to substitute wood as a resource. Nicolao *et al.* studied the enforcement of jute fabric for rice husk particleboards with soybean adhesive.[117] Mahieu *et al.* compared the properties of bioboards made of two agricultural by-products: flax shives and the sunflower bark.[118] Mesquita *et al.* investigated the enhancement of cellulose nanocrystals for sugarcane bagasse particleboards.[119] Hýsková produced particleboards with enzymatic modified wheat and rapeseed straw and found the enzymatic treatment may be not effective.[109] In addition, bamboo,[120] maize stock,[121] and even *Prunus avium* fruit[122] can be processed to bioboards.

## 1.5 Aim and objectives

Thus, the overall aim of this thesis is to explore the potential utilization of unavoidable food supply chain wastes: pea; ginger root, and; agricultural straw (mainly wheat) as a renewable resource of biobased chemicals, materials and (bio)energy.

The abovementioned overall aim is sub-divided in to three parts outlined as follows:

- *Part A: Production, characterization and applications of defibrillated celluloses via dual twin-screw extrusion and microwave hydrothermal treatment (MHT) of spent pea biomass*

The defibrillation of lignocellulosic matter from pea waste using a dual approach of twin-screw extrusion and microwave hydrothermal treatment (MHT) in the presence of water alone from 120 to 200°C will be investigated to afford microfibrillated[f2] celluloses (PEA and EPEA), ultimately (see **Figure 1.17**). Prior to MHT both PEA and EPEA will be boiled in hot solvent (ethanol and heptane) to ascertain quantity and type of extractives.

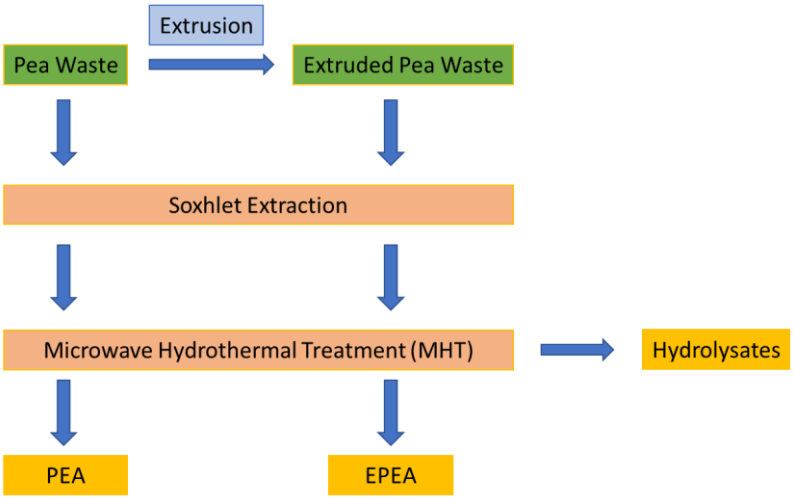


Figure 1. 17 Process diagram to produce MFC using MHT.

[f2] the term microfibrillated cellulose is used in a generic context and once evidenced by TEM/SEM can be subdivided into micro- and nano-fibrillated cellulose

Nanocelluloses are interesting materials because of their application in food,[123] electronics,[124] catalysis,[125] hydrocolloids,[126] biomedical materials.[127,128] Nanocellulose possesses excellent properties including high mechanical strength, high surface area and enhanced optical properties.[129,130] In 2017, the market size was $240.7 million (USD) and is expected to increase to $661.3 million (USD) by 2023.[131]

Generally, nanocellulose is classified into three types which are further sub-divided: i. nano-objects, namely, cellulose nanocrystals (CNC or NCC, width = 3-10 nm, aspect ratio = 5-50) and cellulose nanofibrils (CNF or NFC, width = 5-30 nm, aspect ratio>50); ii. nanostructured celluloses, namely, microcrystalline cellulose (CMC or MCC, width = 10-15 μm, aspect ratio<2), and; iii. microfibrillated cellulose (MFC or CMF, width = 10-100 nm, length=0.5-10 μm) according to TAPPI WI3021(see **Figure 1.18**).[132,133]

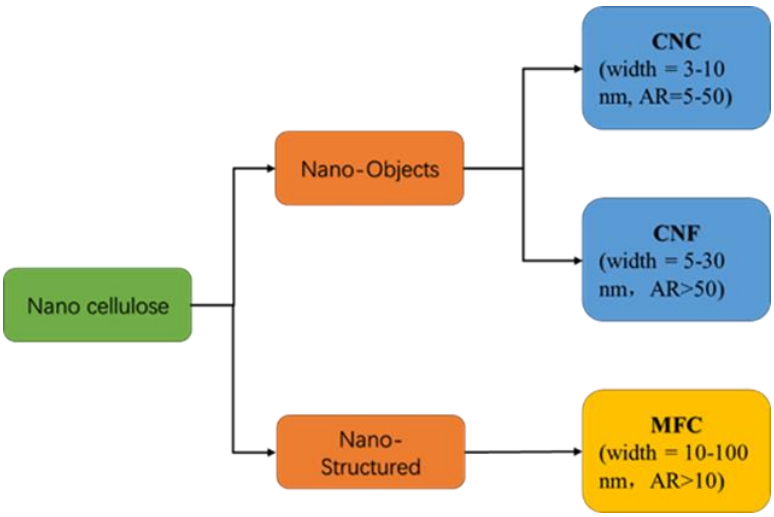


Figure 1. 18 Standard nomenclature for cellulose nanomaterials (TAPPI W13021). W = width, AR = length/width aspect ratio.

Traditionally, nanocellulose is produced from wood pulp. An extensive number of studies have been carried out on production of nanocellulose through conventional mineral acid-catalysed hydrolysis and/or enzymatic digestion followed by physical

processing (*e.g.* ultrasound, mechanical shear).[134,135] However, such treatments are deemed energy- and time-consuming, costly and environmentally-hazardous but are necessary due to the inherent, stable, inter-twined structure of the lignocellulosic matrix.[31,32] New approaches for the production of cellulose, such as, ionic liquids, TEMPO (2,2,6,6-tetramethylpiperidine-1-oxyl radical) oxidation, microorganisms (fungi or bacteria), metal salt catalysts have been reported as alternative to the conventional approach.[136]

Our approach explores a dual approach of twin-screw extrusion and microwave hydrothermal treatment (MHT) in the presence of water alone from 120 to 200 ºC, *i.e*, acid-, alkali-, oxidant, TEMPO, ionic liquid-free.

As a low-energy, non-ionizing form of electromagnetic radiation ranging from 300 MHz to 300 GHz (wavelength in air or vacuum between 1m and 1 mm), microwaves are increased being used to process biomass and waste.[137, 138] Through the ionic conduction and dipole rotation mechanism of ions and polar molecules, the microwave radiation transforms the electromagnetic energy in calorific energy, achieving in fast and selective heating of matter.[69, 139] The efficiency of microwave depends on the dielectric properties of solvent and the matrix, and water is superior solvent due to its excellent dielectric constant (80.4 at r.t. and 2.45 GHz).[69] As biomass is inherently wet (even *dry* biomass contains up to 10% by weight bound water), the combination of microwaves and biomass enables rapid internal heating. Microwave heating is known to directly interact with cellulose in biomass.[140] In the amorphous region, the electrical conductivity rises when the glass transition temperature (above 180ºC) is reached

whereby the ionic current increases.[141] Hot spots can be created within cellulose because of differences in conductivity between amorphous and crystalline cellulose (see **Figure 1.19,** the hot spot is in red).

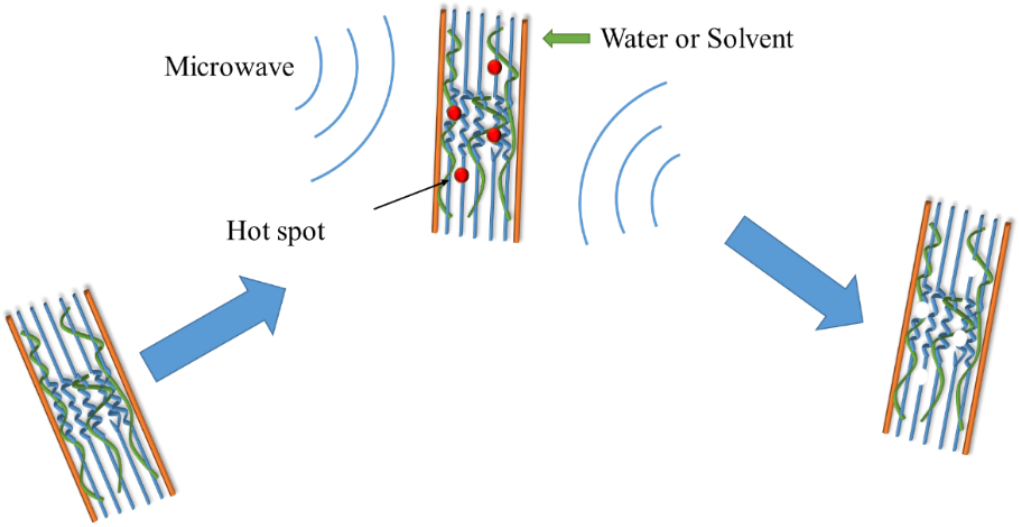


Figure 1.19 Schematic of the interaction of microwaves with lignocellulosic matter (Adapted from Alejandra *et al*. 2017[141]).

Thus, pea waste will be subjected to the following microwave processing conditions (see **Table1.4**) in order to investigate influence of processing time on material and hydrolysate quality but also the influence of extrusion as a pretreatment technology.

Table 1. 4 MHT experiments

| **Raw material** | **Temperature (ºC)** | **Ramp time (min)** | **Hold time (min)** | **Sample code** |
|---|---|---|---|---|
| Pea waste | 120 | 15 | 15 | P120 |
| | 140 | 15 | 15 | P140 |
| | 160 | 15 | 15 | P160 |
| | 180 | 15 | 15 | P180 |
| | 200 | 15 | 15 | P200 |
| Extruded pea waste | 120 | 15 | 15 | EP120 |
| | 140 | 15 | 15 | EP140 |
| | 160 | 15 | 15 | EP160 |
| | 180 | 15 | 15 | EP180 |
| | 200 | 15 | 15 | EP200 |

- Part B: *Spent ginger biomass: A biorefinery strategy for resource recovery*

The valorisation of spent ginger biomass will be investigated via a cascade approach as outlined in **Figure 1.20** and **Table 1.5** in order to explore its potential as a feedstock for a zero waste biorefinery. The spent ginger will be explored for its extractives (Soxhlet extraction; ethanol and heptane) to afford ginger oil. The oil-free residues will be subjected to microwave pyrolysis to yield bio-oil and biochar. The latter may serve as a potential source of bioenergy and its calorific value will be determined. The oil-free residues will also be subjected to acid-free microwave hydrothermal treatment (MHT) to investigate the formation of defibrillated celluloses and their propensity to form hydrogels and films. As stated earlier, ginger root is a rich source of starch and the hydrolysate is expected to yield starch, oligosaccharides, sugars and small molecule organic acids.

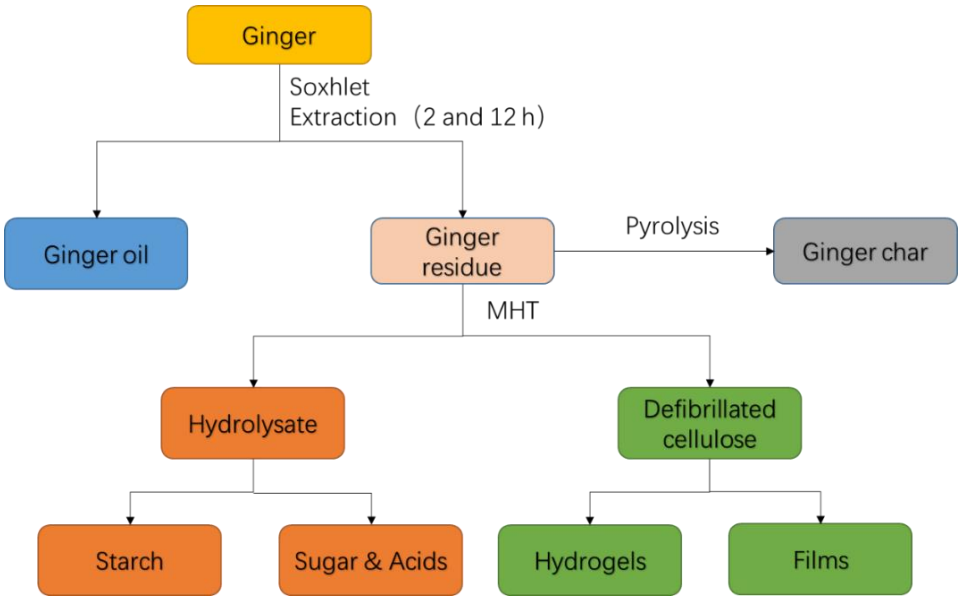


Figure 1. 20 Process diagram for a potential zero-waste biorefinery for spent ginger waste.

Table 1. 5 MHT and Pyrolysis experiments

| Raw material | Temperature (°C) | Ramp time (min) | Hold time (min) | Sample code |
|---|---|---|---|---|
| MHT | 120 | 15 | 15 | GMFC120 |
| | 140 | 15 | 15 | GMFC140 |
| | 160 | 15 | 15 | GMFC160 |
| | 180 | 15 | 15 | GMFC180 |
| | 200 | 15 | 15 | GMFC200 |
| Prolysis | 220 | 0 | 0 | GC2200 |
| | 220 | 3 | 0 | GC2203 |
| | 220 | 6 | 0 | GC2206 |
| | 220 | 9 | 0 | GC2209 |
| | 240 | 0 | 0 | GC2400 |
| | 240 | 3 | 0 | GC2403 |
| | 240 | 6 | 0 | GC2406 |
| | 240 | 9 | 0 | GC2409 |
| | 260 | 0 | 0 | GC2600 |
| | 260 | 3 | 0 | GC2603 |
| | 260 | 6 | 0 | GC2606 |
| | 260 | 9 | 0 | GC2609 |
| | 280 | 0 | 0 | GC2800 |
| | 280 | 3 | 0 | GC2803 |
| | 280 | 6 | 0 | GC2806 |
| | 280 | 9 | 0 | GC2809 |

- *Part C: Towards Novel composite bioboards and structural insulation panels from waste agri-fibres*

This part aims to explore valorization of agricultural straws into UF, PF and isocyanate-free bioboards, which then could be developed in to structural insulation panels (SIPS) comprising a foamed renewable resource inner core, *e.g.*, from waste paper, agri-straws, microfibrillated celluloses and or/blend, as outlined in **Figure 1.21**. The formation of SIPS is new research within the GCCE and builds on well-established production of bioboards using silicate and protein binders. Silicate binders

once cured are fireproof and relatively waterproof. Ideally, the whole SIP should be constructed from a single renewable source.

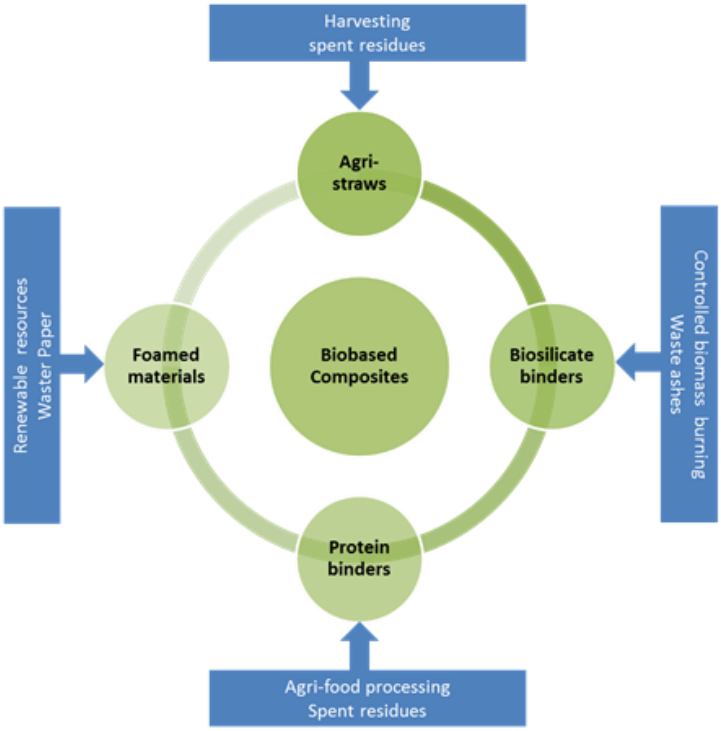


Figure 1. 21 Material portfolio for making biobased composites

Structural insulation panels (SIPs) comprise different layers akin to sandwich-like structures (See **Figure 1.22**) to create a product that is firm, air-tight, lightweight, thus providing good insulation and lightweight. SIPs can be used for walls, floors and roofs as part of a modular off-site building.[142, 143]

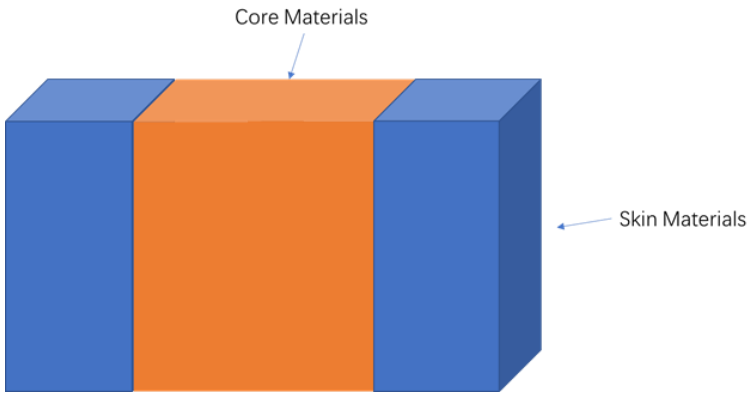


Figure 1. 22 Structural Insulated Panel.

The outer two layers can be sheet metal, plywood, cement, and the core materials are often foam polymers such as expanded polystyrene foam (EPS), extruded polystyrene foam (XPS), polyisocyanurate foam (PIR), polyurethane foam (PU) or composite honeycomb (HSC).[144] Huge numbers of skin materials are produced by researchers based on different SIP applications[145] such as, metal, fibre cement, cement, calcium silicate, fibre reinforced polymer, and oriented strand board.

As a relatively cheap material, oriented strand board (OSB) is widely used but it is flammable and affected easily by insects; metal is fire-resistant but is unable to keep the core warm. Wood has better thermal insulation properties compared to metal.[146] Cement is fire resistant but brittle; calcium silicate board can insulate the core and is fire resistant but has practical and logistical problems, *i.e.*, it is unable to be made in to a large size panel. Polymer composites are lightweight, insect and waterproof, but are potentially flammable and possess low compressive strength.[147]

The core material of a SIP is commonly made of plastic foam, carbon foam, clay, fibre glass, sheep wool, and even waste from agriculture.[148, 149] Most of the core materials can insulate effectively, are lightweight and easy to handle but as recently evidenced by the tragic events of the Grenfell fire, blown or expanded polymer films polythene (PE) and expanded polystyrene are flammable.[150, 151] Pentane is used in the manufacture of expanded PE thus creating a structure that represents a *fuel within a fuel* and hence, highly flammable. Clay as a filler is cheap but may be too heavy, fibre glass has insulation properties but it is expensive and associated with health risks. Foamed biobased materials make for interesting filler materials as they are lightweight

and based on readily available fibres.[151-153] However, there are still challenges to achieve, such as, mechanical fragility, flame retardancy and moisture ingress. The latter is problematic especially with renewable resources such as paper and de-waxed agricultural straws which are susceptible to water penetration.

To improve hydrophobicity, a hydrophobic surface can be produced in two ways: one is to increase the rough structure of the surface to prevent water from spreading, and; second is chemical modification to lower surface free energy.[154, 155] A variety of methods have been used for surface roughening, for example, plasma-etching[156] and deposition of nanoparticles[157-161] to provide a roughened, nanometer-scale surface which is so small that the hydrophile cannot permeate. Chemical modification with organosilanes, such as, aminopropyltriethoxy silane (APTES),[162-164] 3-aminopropyltriethoxy silane (APTMS)[165, 166] and methyltrimethoxy silane (MTMOS),[167, 168] is used commonly to induce hydrophobicity.

Thus, initially bioboards comprising agricultural residues (wheat straw, barley straw and lemongrass) and aqueous biosilicate solutions will be explored. The use of lemongrass, widely grown and used in the Far East, as an aggregate with biosilicate binder is novel. Existing formulations of aggregate:biosilicate:protein will be explored and the mechanical strength (internal bond strength) of the boards will be measured. The biosilicate solution will be leached (KOH-assisted hydrothermal leaching) from the wheat straw ash and its concentration will be determined by ATR-IR spectroscopy and compared with commercial silicate solution (K120 as supplied by PQ Corp).

The incorporation of zirconia powders (as supplied by collaborators in India) will be explored in order to increase the internal bond strength and flame retardancy of bioboards. The presence of zircoinia will be evidenced by powder X-ray diffractions. Thereafter, the production of a range of novel biobased foam materials as potential core layers within structural insulation panels (SIPs) will be explored. Initial trials will be conducted using waste paper and foaming agents. Subsequently, the preparation of novel foam materials mixed with defibrillated celluloses derived from orange peel residues (OPR) will be explored. OPR was chosen because of its availability in the GCCE but also because it is a high volume feedstock from citrus juicing industries. To improve water resilience of the inner layer, waste paper and cellulose will be chemically modified with aminopropyltriethoxy silane (APTES).

### 1.5.1 Links to Green Chemistry and SDGs

The aims and objectives are connected with the UN SDGs (see **Figure 1.3** earlier) as follows:

*Goal 2.3 By 2030, double the agricultural productivity and incomes of small-scale food producers, in particular women, indigenous peoples, family farmers, pastoralists and fishers, including through secure and equal access to land, other productive resources and inputs, knowledge, financial services, markets and opportunities for value addition and non-farm employment*

The valorization of unavodiable food supply chain wastes (UFSCW) which have limited economic value would raise famers'income and expand employment, benefiting local economy.

*Goal 11.1 By 2030, ensure access for all to adequate, safe and affordable housing and basic services and upgrade slums*

The manufacture of bioboards and SIPs will avoid the use of toxic binders such as formaldehyde, isocyanates, phenols and urea by using aqueous silicate solutions leached from biomass ashes and proteins from spent residues from food processing, providing safer living environment.

*Goal 12.3-5. By 2030, halve per capita global food waste at the retail and consumer levels and reduce food losses along production and supply chains, including post-harvest losses.*

*By 2020, achieve the environmentally sound management of chemicals and all wastes throughout their life cycle, in accordance with agreed international frameworks, and significantly reduce their release to air, water and soil in order to minimize their adverse impacts on human health and the environment.*

*By 2030, substantially reduce waste generation through prevention, reduction, recycling and reuse.*

UFSCW is transformed to useful materials/chemicals,reduce the waste along with food supply chain, prevents the burning of the UFSCW to release harmful emissions to atmosphere, minimizes environment pollution.

*Goal 13.3. Improve education, awareness-raising and human and institutional capacity on climate change mitigation, adaptation, impact reduction and early warning*

The utilization of the UFSCW and paper waste as resource instead of fossil reduces

the emission of greenhouse gas by recycling of carbon, mitigate the influence on the climate change.

*Goal 15.2 By 2020, promote the implementation of sustainable management of all types of forests, halt deforestation, restore degraded forests and substantially increase afforestation and reforestation globally*

The work avoids the use of virgin materials such as natural wood which is currently used in structural boards by using renewable agri-food residues.

With respect to Green Chemistry Principles 1, 7 and 10, namely: raw materials are from a renewable source (waste), and fits within a biorefinery concept, *i.e.*, "an integrated factory to process crops (biomass) in to refined fractions," which provide our future need for chemicals, materials and energy. A successful biorefinery will deliver maximum chemical, material and energy value from its incoming feedstock. Principles 3 and 5, toxic solvents or chemicals to defibrillate cellulose; aqueous silicate solutions leached from biomass ashes and proteins from food processing were applied to replace toxic binders including formaldehyde, isocyanates, phenols and urea in bio bioboards manufacture; Principle 11, the materials divert under- or poorly-utilised agro-food, *e.g.*, straws, via a process of valorisation (adding value), some of which may be left to decompose in fields thus acting as an environmental burden.

Chapter 2

# 2 EXPERIMENTAL

## 2.1 Materials & Methods

All reagents and solvents used were analytical or high-performance liquid chromatography (HPLC) grade purchased from either Sigma-Aldrich and/or Fisher Scientific. Whey protein (brand: Myprotein) was bought on-line (Amazon) whilst soy protein was obtained from the Yuwang Group in China. Nano-zirconia was provided by Dr Menaka Jha's Group, India. Commercial K120 silicate solution was supplied by PQ Corp.

Pea (*Pisum sativum)* waste comprising leaves, vines and stems (collectively known as haulm) was collected immediately after harvesting from farmland nearby York (Green Pea Company, Driffield, England, United Kingdom). The fresh biomass was then passed through a twin-screw press juicer (Angelia, 7500 Series, 180W) with a continuous shearing force between the screws and barrel to obtain the extruded pea fibres and pea juice. The latter was sent to University of Nottingham as part of a seaparate research project. Subsequently, both non-extruded pea waste and extruded pea waste fibres were dried at room temperature for 2 weeks (see **Figure 2.1**), milled (Retsch™ Knife Mill Grindomix GM300) and sieved (200 μm). The samples were then subjected to Soxhlet extraction (40 g with 400 ml ethanol, 24 h, around 80 $^{o}$C) to remove pigments and other organic compounds, *i.e.,* extractives, prior to the microwave hydrothermal treatment.


Figure 2. 1 Dried virgin pea vine (a) and extruded pea vine waste (b).

Ginger (*Zingiber officinale Roscoe*) waste was supplied by a commercial company (name to remain confidential). The biomass was milled in a knife miller (Retsch™ Knife Mill Grindomix GM300) and sieved (200 μm). Then, the samples were subjected to either Soxhlet extraction (heptane, 24 h) to remove extractives.

The wheat straw and wheat straw ash were sourced from within the Green Chemistry Centre of Excellence.

### 2.1.1 Microwave hydrothermal treatment (MHT) of pea and ginger waste for production of microfibrillated cellulose

For pea waste, the appropriate raw materials (either pea or extruded pea) were processed in a CEM Mars 6® closed vessel Microwave, operating in 1200 W, 2.45 GHz with EasyPrep Plus® closed vessels (Teflon, 100 mL). Dried pea waste or extruded pea fibres (2 g) after Soxhlet extraction was mixed with distilled water (70 mL) with a ratio of 1: 35 (w/v) and subjected to MHT at different temperatures (120 $^{o}$C to 200 $^{o}$C), the ramping time and holding time were both 15 min. Subsequently, the mixtures were separated via a centrifuge with 3000 rpm for 20 min (the G-force was approximately 4000). Supernatant was isolated and stored for sugar analysis via HPLC.

The pellet was washed with ethanol (2 x 300 ml) and freeze-dried for 24 h to obtain the desired MFC. The latter were stored in glass vials until further required and coded as follows: sample type microwave processing temperature. For example, P120 refers to the non-extruded pea waste that was subjected to 120 ℃ MHT and EP160 refers to the extruded pea waste subjected to MHT at 160 ℃. The images of both MFC and hydrolysates are shown in **Figures 3.2**, section 3.1, Chapter 3.

The yield of the microfibrillated cellulose (MFC) was calculated according to **Equation 2.1**:

$$\text{Yield (\%)} = (\text{mass of MFC} / \text{mass of dried raw material}) \times 100 \qquad \text{(Equation 2.1)}$$

For ginger waste, the residues after extraction (Soxhlet) were processed with a SynthWave Microwave Processor, operating at 1500 W, 2.45 GHz, 60% stirring power and using PTFE vessels (900 ml). Dried ginger waste (10 g) was mixed with distilled water (350 mL) with a ratio of 1:35 (w/v) and processed to MHT in different temperatures (120 to 200 $^{o}$C).

The ramping time and holding time were both 15 min. The resulting slurry was filtered whilst hot. The residue (crude ginger cellulose) and filtrate were separated and an equal volume of ethanol was added to the latter (filtrate), stored in a fridge overnight to effect precipitation (of starch), centrifuged (20 min, 3000 rpm) to separate starch (pellet) and hydrolysate (supernatant). The crude ginger cellulose (residue) was washed with hot water (300 ml for 15 min), hot ethanol (2 x 300 mL, 15 min. each), cold ethanol (300 mL, 15 min), cold acetone (300 mL, 15 min.) and dried to afford ginger MFC. The cellulose product was coded as GMFC (Ginger microfibrillated

cellulose), starch was coded as GS and the hydrolysate was coded as GH based on the temperature, for example, GMFC120 refers the cellulose sample with 120 $^{o}$C microwave hydrothermal treatment, and GS160 refers to the starch were extracted from the hydrolysate which was subjected to 160 $^{o}$C MHT. The images of hydrolysate are shown in **Figure 3.14**, section 3.2, Chapter 3: Results and Discussion.

The procedure was shown in **Figure 1.20**. The yield of the Ginger microfibrillated cellulose (GMFC) was calculated accordingly to **Equation 2.1** (see earlier), whilst the yield of starch was calculated according to **Equation 2.2**.

Yield (%) = (mass of starch /mass of dried raw material) × 100 (Equation 2.2)

**2.1.2 Microwave pyrolysis**

Pyrolysis experiments were performed using a CEM Discover SP microwave reactor with 30 mL borosilicate glass vessels. Ginger powder (1 g after Soxhlet extraction) was subjected to microwave pyrolysis, at fixed power (95 W) and variable temperature (220, 240, 260 and 280 $^{o}$C) and variable hold time (0, 3, 6 and 9 mins). Post hold time, the vessels were cooled with compressed air and the pyrolysis residues (mixture of bio oil and biochar) were washed with ethyl acetate (10 ml) and the latter was evaporated *in vacuo* to afford GbioOil. The ethyl acetate washed residues were dried (60 $^{o}$C, 48 h) to yield biochar. The chars were coded GC (Ginger char) and based on the temperature and reaction time. For example, GC2206 refers to the sample with 220 $^{o}$C and 6 min residence time.

The yield of biochars and bio oils were calculated according to **Equations 2.3** and **2.4**. The yield of non-condensable gases was based on a mass balance (**Equation 2.5**)

Biochar Yield (%) = (mass of char/mass of dried raw material) x 100 (Equation 2.3)

Bio oil yield (%) = (mass of oil/mass of raw sample) x 100 (Equation 2.4)

Biogas yield (%) = 100 - biochar yield (%) – bio oil yield (%) (Equation 2.5)

### 2.1.3 MFC-based hydrogels

The appropriate MFC (250-400 mg) was mixed with deionised water (10 ml) to produce concentrations in the range (2.5 – 4% w/v). The mixture was subjected to high-shear homogenisation (Ystral X10/20 E3 homogeniser, 3 min, 20000 rpm) to obtain potentially hydrogels. The tube inversion test was implemented to test quality of the gel; the sample was placed in to a small vial, closed and turned the upside down (inverted). The ability for the gel to remain held without falling to the bottom was indicative of gel quality

### 2.1.4 Water Holding Capacity (WHC) [169]

The method was according to Traynham *et al*:[170] The appropriate MFC (2 g) was placed in a pre-weighed centrifuge tube and dispersed in water (38 ml). The mixture was shaking for 10 min, centrifuged (30 min, 3000 rpm) supernatant discarded whist the wet pellet was weighed. The WHC was calculated according to **Equation 2.6** and the measurement was repeated twice.

WHC (g water/g) = (mass of wet sample - mass of dried sample)/mass of dried sample (Equation 2.6)

### 2.1.5 Water Retention Value (WRV) [171]

The water retention value (WRV) was measured according to SCAN-C 62:00 test method. A 2.5% wt/v concentration of dispersion with sample and water were

centrifuged at 3000 rpm for 15 min and then dried (105 $^{o}$C, 24 h). The WRV was calculated according to **Equation 2.7** and measured were performed in duplicate.

$$WRV\ (\%) = (m_{wet} - m_{dried})/m_{dried} \times 100 \qquad \text{(Equation 2.7)}$$

Where $m_{wet}$ is the mass of wet sample, $m_{dried}$ is the mass of the dried sample.

### 2.1.6 Crystalline index (CrI)

The crystalline index (CrI) of MFC samples was determined from ratio of amorphous and crystalline areas at C4 carbon region (79–93 ppm), the CI is calculated by x/(x+y) which X is related to crystalline region and Y is amorphous region in **Figure 2.2**.

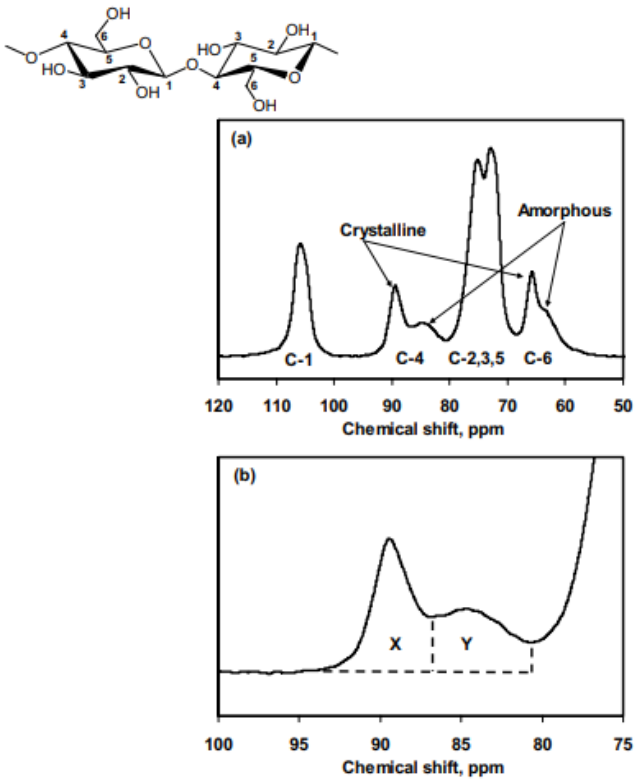


Figure 2. 2 a) Whole spectrum displaying the carbon peak in cellulose and b) expand spectrum assigned to the C4. Adapted from S. Park.[172]

### 2.1.7 Wax extraction (general method)

The appropriate, milled, agricultural straw (40 g) and solvent (600 ml, ethanol) was

heated under reflux for 2 h. Thereafter, the straw was separated from solvent and allowed to air dry for 48 h. The solvent was evaporated to dryness in *vacuo*.

### 2.1.8 Hydrothermal extraction of silicate solution from wheat ash

Wheat straw bottom ash (18 g), KOH (8.4 g) and deionised water (30 ml) contained within a PTFE round bottle were heated at either 140 $^{o}$C or 180 $^{o}$C for 6 h, 12 h, 18 h and 24 h. Thereafter, the extraction mixture was subjected to centrifugation (15 mins, 3000 rpm). The desired supernatant biosilicate was decanted and stored in sealed plastic bottles prior to silicate concentration determination. The samples are shown in **Figure 2.3**.

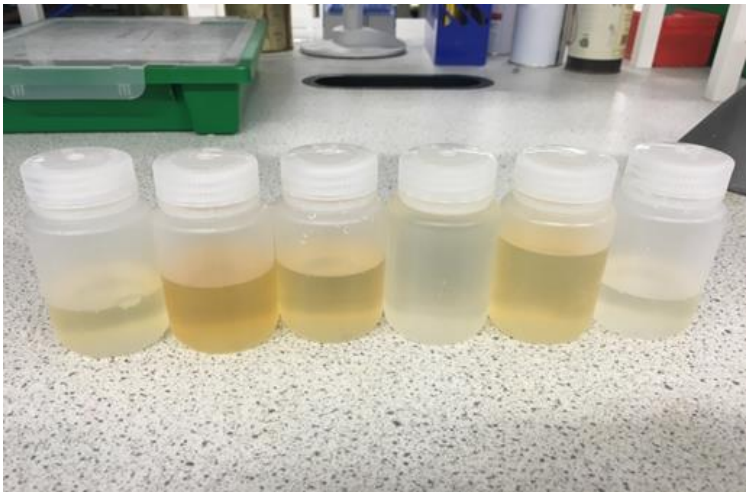

Figure 2. 3 Silicate solutions prepared in different conditions

After extraction, the mixtures were centrifuged and the upper clear potassium silicate solutions obtained.

### 2.1.9 Silicate concentration determination - Titration method

Freshly prepared methyl red indicator (1-2 drops; methyl red (100 mg) in 60%-aqueous ethanol (100 ml)) was added to biosilicate solution (0.5 ml) in de-ionised water (20 ml). The resultant solution was titrated against aqueous HCl (0.5 mol dm$^{-}$

$^{3}$) until endpoint was achieved (first permanent red tinge).

Thereafter, an excess of solid sodium fluoride (approximately 2.5 g) and methyl red indicator (1-2 drops) were added and the mixture was titrated with aqueous HCl (0.5 mol $dm^{-3}$) until endpoint was achieved (first permanent red tinge).

The first titration determines $K_2O$ concentration whilst the second titration determines $SiO_2$ concentration. As titration is a complex and time-consuming procedure, thus, an IR absorbance method was employed.

### 2.1.10 Silicate concentration determination – ATR method

ATR spectra were recorded for commercial K120 at different concentrations in order to establish a calibration plot as shown in the 'Results and Discussion' section (3.3.2.2 Determination of concentration of $K_2O$ and $SiO_2$).

### 2.1.11 Preparation of foam materials

A schematic for preparation of foamed composites is outlined in **Figure2.4**. A solution of PVA (10 g) in distilled water (200 ml) was added to a rapidly, stirred (2500 rpm) slurry of milled waste paper fibres (40 g) in distilled water (1000 ml) contained in a Retsch GM 300 knife-mill, followed by the appropriate silicate solution (28 g), wheat starch (10 g), SDS (1.5 g), sodium hydrogen carbonate (2 g) and aluminium sulfate (11 g) at 2 minutes' intervals. The resulting foamed mixture was stirred for a further 5 minutes to mix evenly, then the slurry was poured into a mould and dried under constant temperature (80 $^{o}$C) for 7 h. The function and dosage are shown in **Table 2.1** and the properties of the dried foamed materials are described in the 'Results and Discussion' section.

Table 2. 1 Formulation of Fibre Foam Materials

| Agents | Function | Dosage (g) |
|---|---|---|
| Polyvinyl alcohol (PVA) | Adhesive | 10 |
| Starch | Adhesive | 10 |
| sodium silicate | Adhesive | 28 |
| aluminium sulfate | flame retardant | 11 |
| SDS | blowing agent | 1.5 |
| Sodium hydrogen carbonate | blowing agent | 2 |

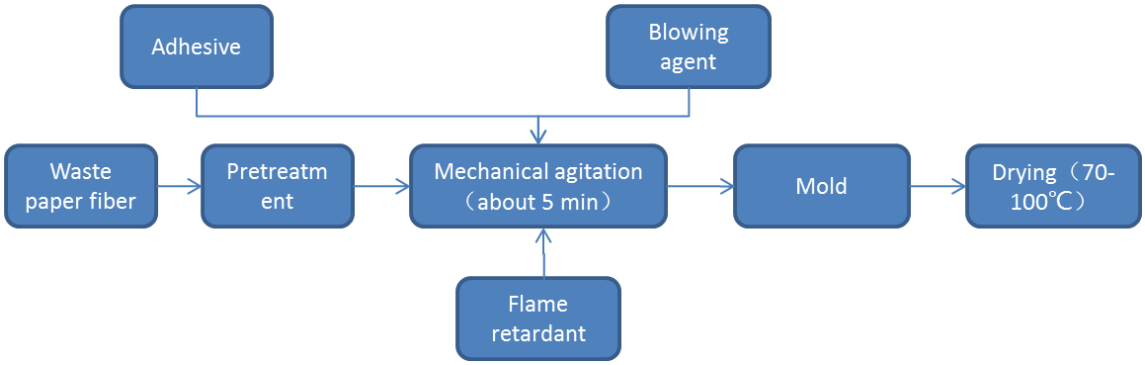


Figure 2. 4 Process flowchart for making foam materials

When processing the paper foam materials combined with MFC, the MFC (the weight is depending on total weight and ratio, for example, 10%MFC represent 4 g MFC) extracted from orange peel were added into water and mixing for 5 minutes with a homogenizer, then the papers were added into mixtures and the slurries were under ultrasonic condition for 40 min, subsequently the mixtures were added with a solution of PVA (1.2 g) in distilled water (50 ml) and stirred rapidly in a Retsch GM 300 knife-mill, at last , the biosilicate solution (2.4 g), wheat starch (1.2 g), SDS (0.12 g), sodium hydrogen carbonate (0.24 g) and aluminium sulfate (1.2 g) at 2 minute intervals were added. The resulting foamed mixture was stirred for a further 5 minutes, poured into a mold (5 cm x 15 cm x 3 cm) and dried (80 $^{o}$C) overnight until constant weight was achieved.

### 2.1.12 Preparation of composite bioboards (General method)

The process of making composite bioboards is summarised in **Figure 2.5** and images of crude and trimmed boards are shown in **Figure 2.6**. Full details of formulations are: silicate binders or commercial K120 (12 g), protein (3.6 g; either soy or whey) with different concentrations and straw (40 g; wheat, barley or the mixtures). Either waxed or dewaxed milled wheat straw (40 g) was mixed with the binders and poured into a metal mold (10 x 10 cm) and pre-pressed (manually) for 1-5 min. The metal mold was removed, the crude pre-pressed bioboard was covered with an aluminium platen and transferred to a hot press machine. The boards were pressed for 8 min at temperature of 210 ℃ (10 tons pressure). At the same time, the space between the two hot plates was approximately 11.7 mm to make sure the thickness of bioboard was 10 mm after hot pressing. The bioboards were machine cut to 5 x 5 cm squares for further analysis.

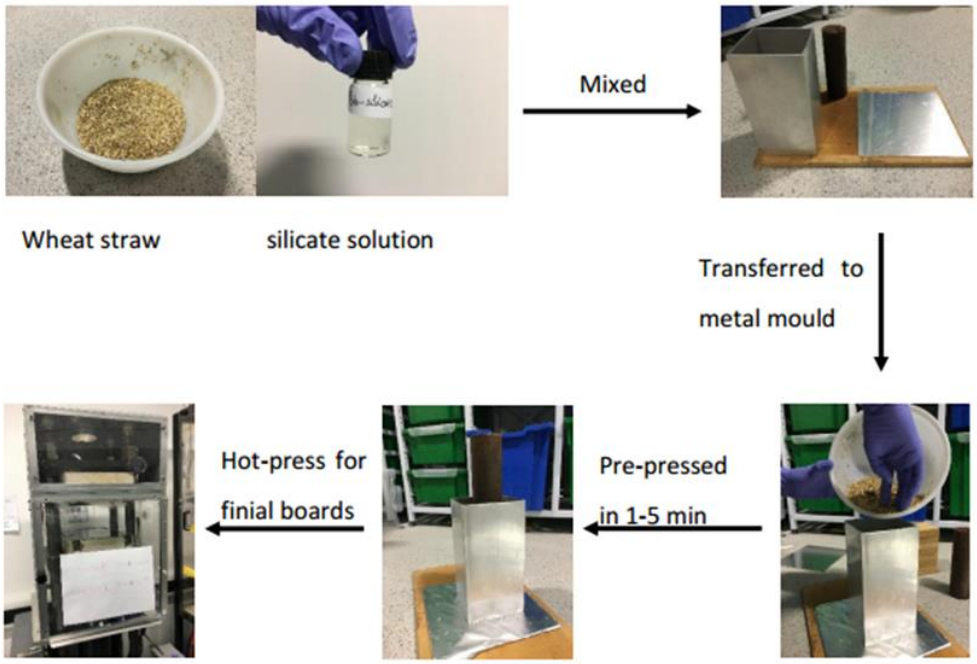


Figure 2. 5 Process of Bioboards. Adapted from Tian.[173]


Figure 2. 6 Crude 10 cm x 10 cm bio-boards

### 2.1.13 Internal bond Strength (IBS)

The internal bond strength was determined using an Instron 3367 tensiometer with BlueHill software. The appropriate size composite blocks were glued (commercial 'super' glue) in the jaws of the tensiometer and pulled apart with a force operating at 10mm/min until failure. The process is seen in **Figure 2.7**, maximum load (point at which board split in to two) was recorded and the IBS was calculated according to **Equation 2.8**:

IBS=Maximum load (N) / surface Area ($mm^2$) (Equation 2.8)

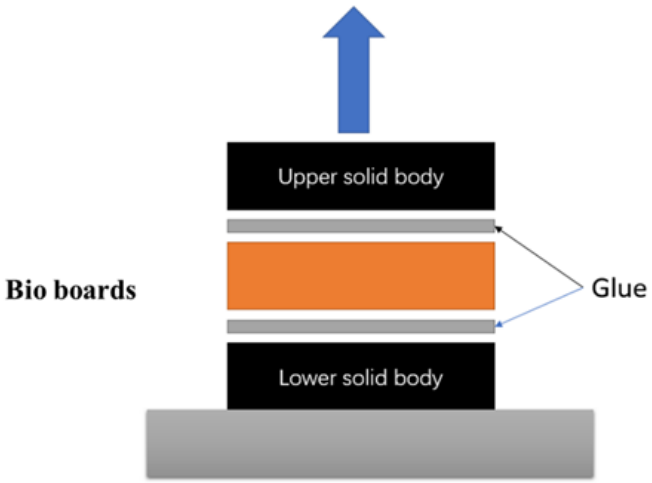


Figure 2. 7 Internal Bond Strength Test.

### 2.1.14 APTES Treatment

Waste paper (2 g A4 sheet) was cut into small pieces with a scissors and put into to blender to form slurry with 100 ml water, then dried for a few days (water content less than 2 %). APTES (5 wt%) was added to 80%-aqueous ethanol or aqueous acetone (80 ml) and allowed to stir for 2 h at room temperature. The appropriate cellulosic material (commercial cellulose, waste paper) was added and stirred for a further 3 h at room temperature. Thereafter, the pH of the slurry was adjusted with acetic acid to 4 and dried under vacuum oven for 2 h at 120 ℃.

## 2.2 Instrumentation

### 2.2.1 Attenuated Total Internal Reflectance Infrared Spectroscopy (ATR-IR)

Attenuated Total Internal Reflectance Infrared Spectroscopy (ATR-IR) was recorded on a Perkin Elmer FT-IR Spectrometer using Spectrum software. 16 background scans and 8 sample scans were recorded each sample and the scan range is from 650 $cm^{-1}$ to

4000 $cm^{-1}$. A small amount of sample was placed on a ATR crystal and then turn pressure tower down to push the samples firmly on the crystal, at last, the samples were scanned and recorded with the software.

### 2.2.2 Thermogravimetric Analysis (TGA)

The thermal decomposition properties of the samples were recorded using a PL Thermal Science STA 625 instrument. The samples (approx. 10 mg) were weighed accurately in an aluminum crucible and analyzed in a nitrogen atmosphere from 20 ℃ to 625 ℃ at a heating rate of 10 ℃ /min with respect to an empty aluminium pan as reference. The first derivatives of thermograms were calculated and smoothed with Origin 9.0.

### 2.2.3 X Ray Diffraction (XRD)

XRD was performed using a Bruker AXS D8 Advance Diffractometer controlled by XRD Commander software, the 1.54184 Å wavelength monochromatic K-α radiation was generated by Cu source and detected by PSD Lynx eye. The samples were grounded to fine powders before testing. The scan type was set at locked coupled, operating voltage of 40 kV (current, 40 mA), scan speed of 0.2 sec/step and the scan scope from 5Θ to 38 Θ (for MFC) and 5 Θ to 90 Θ (for other samples including ash, zirconia). Background subtraction and trace smoothing were implemented after data obtained.

### 2.2.4 Solid state $^{13}C$ CP-MAS Nuclear Magnetic Resonance ($^{13}C$-MAS NMR)

The Solid State $^{13}C$ Cross Polarization Magic Angle Spinning (CP-MAS) NMR was obtained on Bruker JEOL 400S, the spectra were collected by using a Bruker 4mm

H(F)/X/Y triple-resonance probe, the $^{13}C$ frequency was 10 KHz, Magic-angle spinning was performed at10000 ± 2Hz, recycle delays was 3 seconds, and the scan number was 1024. Chemical shifts were corresponding to TMS and adamantane (29.5 ppm) was used as an external secondary reference.

### 2.2.5 Inductively Coupled Plasma (ICP)

The elemental analyses were carried on an Agilent ICP Axial OES by an external provider (YARA Analytical Services, Pocklington, York)

### 2.2.6 Scanning Electron Microscope (SEM)

The morphology of the samples was imaged using a JEOL JSM-6490LV instrument. The samples were placed on a copper shim, to avoid the disturbance the samples were coated with gold, then the shim was mounted under liquid nitrogen conditions and analysis was performed by Meg Stark from Dept. of Biology, University of York.

### 2.2.7 Transmission Electron Microscopy (TEM)

A TEM Tecnai 12 BioTWIN with a SIS Megaview 3 camera at a 76-acceleration voltage of 120 kV was used to obtain TEM images of the microfibrillated cellulose. The analysis was performed by Meg Stark and Karen Hodgkinson from Dept. of Biology, University of York. Before capturing the image, 2% mass ratio of the samples were dispersed in water with a 1500 W ultrasound bath for 20 min in order to get good clarity images. The widths of MFC were calculated by ImageJ software.

### 2.2.8 CHN Analysis (CHN)

The CHN analysis was performed by Dr Graeme McAllister, Dept. of Chemistry, University of York, on an Exeter Analytical CE-440 Analyser, in conjunction with a Sartorius SE2 analytical balance. The samples were burned at 975 ℃ in an oxygen

atmosphere and then the gas was detected by several thermal conductivity detectors. Measurements were in conducted in duplicate.

### 2.2.9 $N_2$ porosimetry

A Micromeritics TriStar Surface Area and Porosity Analyser was used to characterize the textural properties of microfibrillated cellulose, the dried fine samples were put in a porosimetry tube and weighted, and degassed at 120 $^{o}$C for 7 h under flowing nitrogen. The weight of tube and samples were recorded again for further analysis. TriStar software was used to process the data, specific surface areas were calculated according to the Brunauer-Emmett-Teller (BET) method whilst, desorption pore volume and average pore diameter were calculated using Barrett-Joyner-Halenda (BJH) equations. All analyses were conducted in duplicate.

### 2.2.10 High-performance Liquid Chromatography (HPLC)

The samples of each hydrolysate were collected after MHT, were filtered through a disk filter (0.22 μm pore) and analysed by HPLC by Dr. Richard Gammons, Dept. of Chemistry, University of York.

For levoglucosan, glucose, xylose, and organic acids (lactic): the samples were analysed by using an Agilent 1260 equipped with a Agilent Hi-Plex H (300 x 7.7mm, 8um particle size) column, 0.005M $H_2SO_4$ as mobile phase, isocratic mode (no gradient), flow-rate is 0.4 mL/min, the column temperature is 60 ℃, refractive index detector is 55 °C, injection volume is 5 μL and the total run time are 35 minutes.

For furfural, levoglucosenone, 5-HMF, the samples were analysed by using an ACE C18 (250 × 4.6 mm, 5 μm particle size) column with acetonitrile: water (25/75) mobile

phase, isocratic mode, 0.8 ml/min flow-rate, column temperature is 30 ℃, injection volume is 5 µL and total run time are 22 minutes.

### 2.2.11 Gas Chromatography-mass Spectrometry (GCMS)

Gas Chromatography-Mass Spectrometry was carried out on PerkinElmer Clarus 560S mass Spectrometer and Clarus 500 Gas Chromatography instrument equipped with a Restek Rxi-5HT column (30 m x 0.25 mm ID x 0.25 µm) and operating at EITHER General 2 Method: the initial temperature is 50 ℃ and hold for 4 min, then heat to 290 ℃ at a 10℃ ramp rate and hold for 10 min, the split ratio is 5:1 and injector temp at 290ºC, OR, Sensitive 2 Method: the initial temperature is 60 ℃ and hold for 1 min, then heat to 340 ℃ at a 8 ℃ ramp rate and hold for 30 min, the split ratio is 5:1 and injector temp at 340 ºC.

### 2.2.12 Differential Scanning Calorimetry (DSC)

Differential Scanning Calorimetry was carried out on a Mettler DSC Q2000 machine with Q Series software. Around 10 mg sample was weighted in an aluminium crucible. The whole system was filled with nitrogen and, at a heating/cooling of 10 ºC/min, the sample was heated from 25℃ to 110 ℃, cooled to -50℃ and held for 3 min, the sample was heated again to 110℃ and at last was cooled to -50℃.

### 2.2.13 Liquid 1H Nuclear Magnetic Resonance ($^1$H NMR)

Bruker AV500 spectrometer was used to record $^1$H spectra. The samples were dissolved in chloroform-d (normally 4 wt.%) and chemical shifts (δ) of the spectra were based on tetramethylsilane (TMS) reference value (0.0 ppm). For $^1$H, the experiments were run with 64 scans.

### 2.2.14 Zeta potential

The Zeta potential of defibrillated cellulose from ginger waste were analysed by a Malvern Zeta sizer instrument., The appropriate cellulose sample was dispersed in deionized water with 0.005% (w/v) and homogenised for 5 min. Then, the suspension was injected to a capillary with a proper syringe, at last the capillary was carefully transferred to the Malvern Zeta sizer and the data was recorded by the software. The experiment was performed three times.

### 2.2.15 Bomb calorimetry

The Higher heating value (HHV) of the ginger and its char product after pyrolysis treatment was measured by a Parr 6200 Calorimetry equipped with a standard 1108 oxygen bomb. The dry ginger powder or char (both approximately 0.3 g) was placed into a metal pan and then transferred the pan to a bomb cylinder with a firing wire on the bomb head, for determination of the calorific value, the temperature of 2809 g bucket water and jacket would be stabilized during the burning procedure.

### 2.2.16 Estimation of higher heating value

The simple estimation of HHV for ginger powder and its char product after microwave pyrolysis was calculated via modified form of Channiwala's formula[174] as shown in **Equation 2.9**:

$$HHV\ (MJ/kg) = 0.3491C\ (wt.\%) + 1.1783H\ (wt.\%) - 0.1034O\ (wt.\%) - 0.015\ N\ (wt.\%) \quad \text{(Equation 2.9)}$$

Where the C, H, N were obtained from the elemental analysis, and oxygen content was calculated by subtraction of C, H, N content from total, namely,

oxygen (%) =100%-carbon (%)-nitrogen (%)-hydrogen (%)  (Equation 2.10)

Chapter 3

# 3 RESULTS and DISCUSSION

For ease of clarity, this chapter is divided in to three parts based on the aims and objectives outlined in chapter 1:

1. *Part A: Production, characterization and applications of defibrillated celluloses via dual twin-screw and microwave hydrothermal treatment (MHT) of spent pea biomass. The work from within this part has been published.*

   Gao, Y.; Xia, H.; Sulaeman, A.; de Melo, E. M.; Dugmore, T. I. J.; Matharu, A. S. Defibrillated celluloses via dual twin-screw extrusion and microwave hydrothermal treatment (MHT) of spent pea biomass. *ACS Sustainable Chemistry & Engineering*, 2019, **13**, 11861-11871.

2. *Part B: Spent ginger biomass: A biorefinery strategy for resource recovery. The work from this section is under review.*

   Gao, Y.; Mustafa. Z.O.; Dugmore, T. I. J.; Sulaeman, A.; Matharu, A. S. Spent industrial ginger biomass for production of high value products – a value added strategy for resource recovery. *Journal of Hazardous Materials*, 2021, **401**,123400.

3. *Part C: Towards Novel composite bioboards and structural insulation panels from waste agri-fibres. (Submitted: ACS Sustainable Chemistry & Engineering, 07/06/2020)*

## 3.1 Part A: Production and characterization of defibrillated Celluloses from Spent Pea Biomass

This section reports the defibrillation of lignocellulosic matter from pea waste using a dual approach of twin-screw extrusion and microwave hydrothermal treatment (MHT) in the presence of water alone from 120 to 200 ºC. Gradual "scissoring" of biomass macrofibres to microfibrils was observed alluding to the Hy-MASS (Hydrothermal Microwave-assisted Selective Scissoring) concept.[175,176, 177] The latter was introduced to describe the microwave-assisted hydrolysis process of lignocellulose: in the first step (120-180 ℃), the amorphous part including starch, hemicellulose and part of non-crystalline cellulose is selectively removed (scissoring) from the biomass; and the second step (above 180℃), the amorphous cellulose softens and the lignin which embedded in cellulose microfibrils are released through a proton transfer mechanism generated through the dipolar polarization of water molecules.[175, 177]

Defibrillated celluloses from PEA (non-extruded) and EPEA (extruded) wastes were successfully produced and characterized. The EPEA samples gave higher crystallinity index and thermal stability, reduced lignin and hemicellulose content, narrower fibril width, better water holding capacity and higher surface area compared with their non-extruded counterparts (PEA). Twin screw extrusion as a pretreatment method followed by MHT represents a potential way to produce microfibrillated cellulose with improved physico-chemical performance compared to the raw biomass. The process

of defibrillation and the samples post MHT are summarized in **Figure 3.1**.

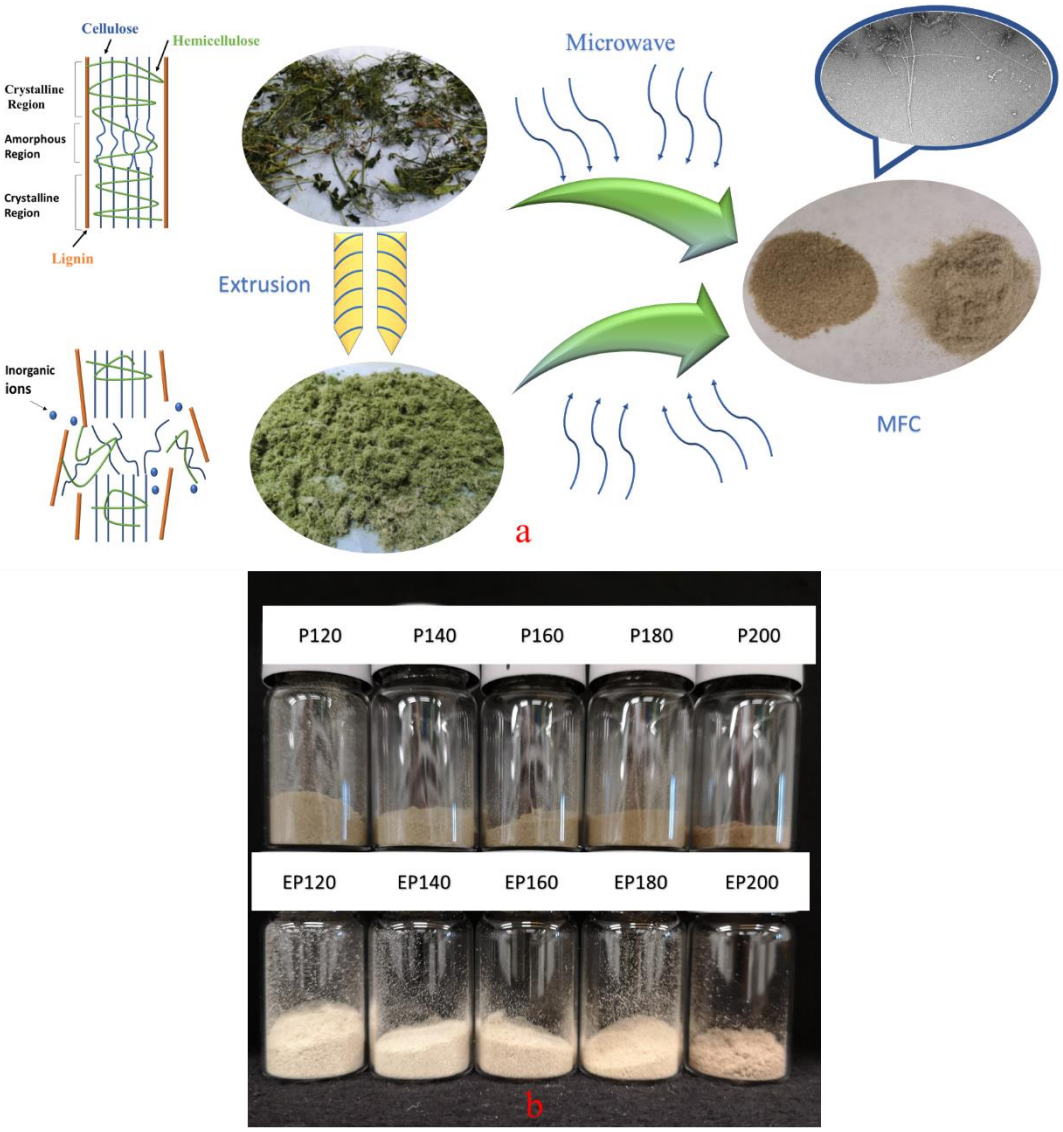


Figure 3. 1 a. Scheme of the experimental procedure; b. PEA and EPEA residues post MHT (120 –200 ℃).

### 3.1.1 Yield of MFC

The yields of PEA and EPEA produced at several MHT temperatures (120 -200 ºC) are shown in **Figure 3.2**. During MHT, the yield of PEA and EPEA falls from 52.7 % to 32.4 % and from 66.0 % to 42.0 %, respectively as the processing temperature increases. In general, the EPEA samples display a higher yield than PEA at the same processing temperatures. The yield of PEA samples starts to decrease sharply

(approximately 6.1 %) after 140 ºC. For EPEA celluloses, the yield appears to remain relatively stable from 120 to 160 ºC and then decreases sharply.

The difference in yield between PEA and EPEA may be due to the effect of extrusion which breaks the ordered structure of biomass and removes some non-lignocellulosic matter, such as hemicelluloses and sugars, by the shearing force between screws, biomass and the barrel. Thus, the material is more cellulosic in character with less hydrolysable content.

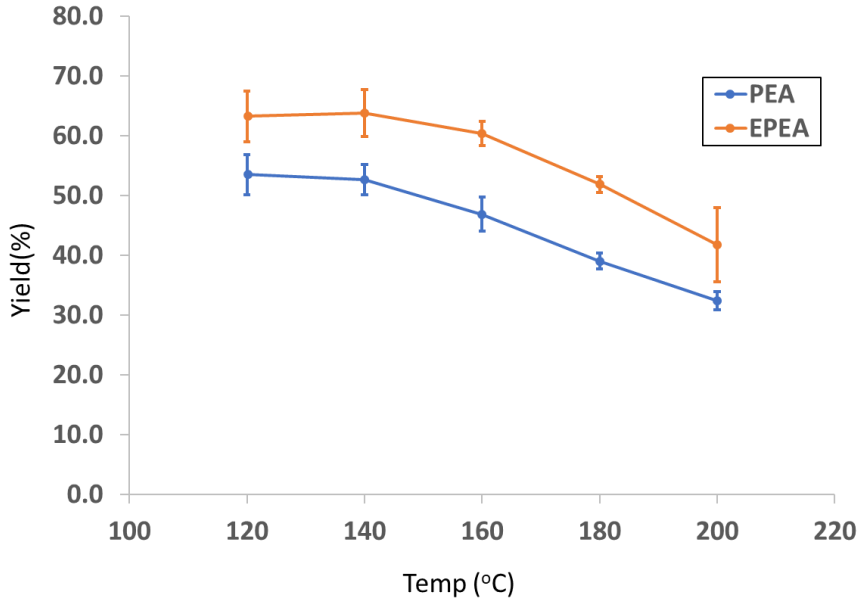


Figure 3. 2 The yield (%) of MFCs from of PEA and EPEA. Error bars represent standard deviation (n = 3)

### 3.1.2 Thermogravimetric analysis (TGA)

The TGA, and respective first derivatives (DTG), profiles of PEA and EPEA cellulose are shown in **Figure 3.3**. PEA gives a higher residue content than EPEA (approximately 25.6% for PEA and 19.2% for EPEA), probably due to the fact that during extrusion water-soluble inorganic salts, for example, potassium, phosphorus, aluminium and iron, present in the biomass were removed, which correlated well with

the ICP analysis (see **Figure 3.5**). Furthermore, during MHT dissolvable inorganic minerals, except calcium, were removed and thus, no significant difference in the final residue mass was noted. Three main stages were observed from the DTG: i. loss of moisture and volatiles, (around 4% to 10%, Td=50-125 °C); ii. Due to the strong interactions between hemicellulose and cellulose, the peak for hemicellulose decomposition was not fully resolved [178] and presented itself as a front shoulder of the main peaks ranging from 250-280 °C, and the peaks indicative of hemicellulose for both PEA and EPEA samples started to disappear with increasing MHT temperature and in samples treated at 200 °C these peaks were no longer detectable (see blue arrows of DTG of PEA and EPEA in **Figure 3.3**) and; iii. a large mass loss (approximately 60%) between 280-390 °C due to (ligno)cellulose decomposition. Meanwhile, with increasing MHT temperature, for both PEA and EPEA samples, the decomposition signature of cellulose became sharper and with increased intensity, indicating removal of hemicellulose and amorphous cellulose.[178]

Furthermore, the decomposition temperatures of cellulose are shifted to higher temperatures (see black arrows of DTG of PEA and EPEA in **Figure 3.3**), *i.e.*, for non-extruded pea waste: native PEA (Td, 313.2 ºC); P120 (Td, 344.1 °C); P140 (Td, 346.8 °C); P160 (Td, 351.3 °C); P180 (Td, 365.8 °C); P200 (Td, 373.9 °C), and for extruded pea waste: native EPEA (Td, 335.3 °C); EP120 (Td, 345 °C); EP140 (Td, 345.7 °C); EP160 (Td, 354 °C); EP180 (Td, 364 °C); EP200 (Td, 373.2 °C) (Td is temperature of decompositionas measured by the maximum on the DTG curve). This can be explained by the action of MHT which depletes the amorphous regions within the

cellulose fibrils [179] leaving behind highly compact crystalline cellulose with increased decomposition temperature. EPEA samples gave a higher decomposition temperature than their PEA counterparts showing the effectiveness of pretreatment.

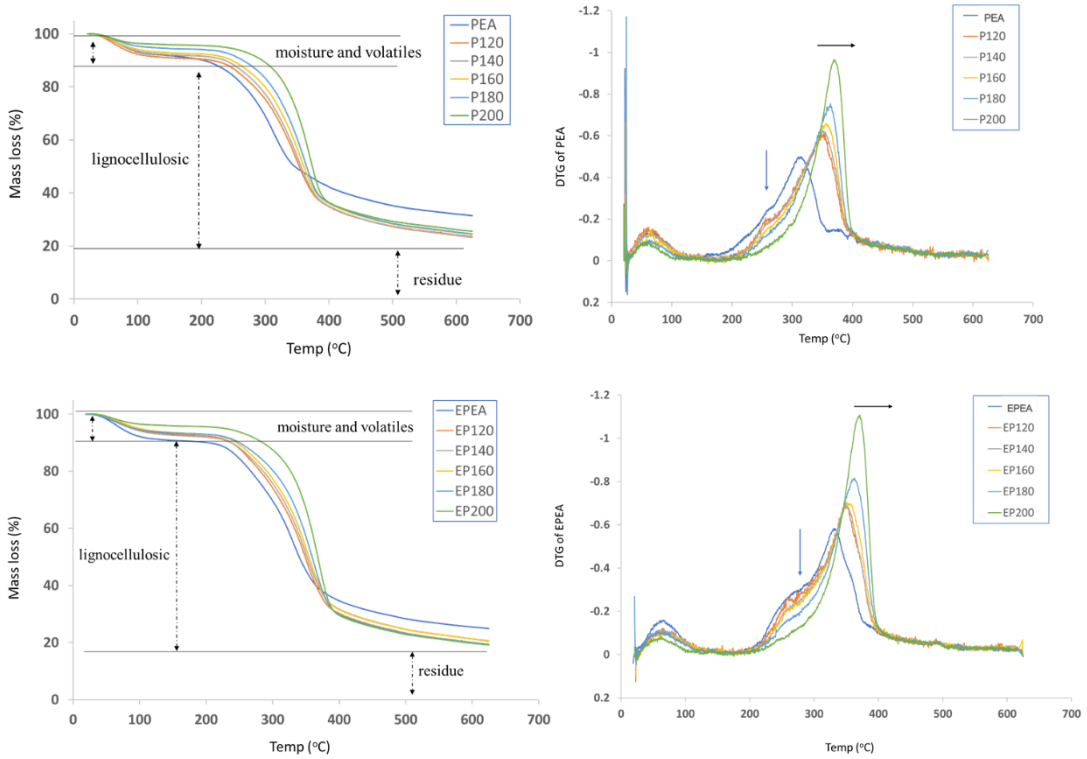


Figure 3. 3 TGA thermograms of PEA and EPEA: a) TG of PEA, b) DTG of PEA, c) TG of EPEA and d) DTG of EPEA.

### 3.1.3 X-Ray powder diffraction analysis (XRD)

The XRD patterns of PEA and EPEA are shown in **Figure 3.4**. Characteristic peaks for crystalline cellulose type-I peaks were observed (2θ: 16.5°, 22.5° and 34.5°) and with higher MHT temperature the crystalline diffraction peaks at 16.5° seemed to be more intense which revealed higher crystallinity (as already evidenced by $^{13}C$ CPMAS in **Figure 3.6**). These results indicated that after high temperature MHT both PEA and EPEA samples had higher decomposition temperatures indicative of an increase in the degree of crystallinity, loss of amorphous cellulose and removal of hemicellulosic impurities as discussed previously. With the increasing MHT the XRD patterns for

insoluble calcium salts (*e.g.* $CaC_2O_4$) which exist in plant cell wall and vacuoles[180] in both PEA and EPEA samples became more intense due to the hydrolysis of amorphous polysaccharides and organic molecules from the lignocellulosic matrix. Also, the EPEA samples show a higher crystallinity than the non-extruded PEA, probably due to the extrusion disrupting cell wall structure of pea waste and aiding leaching of amorphous contents.

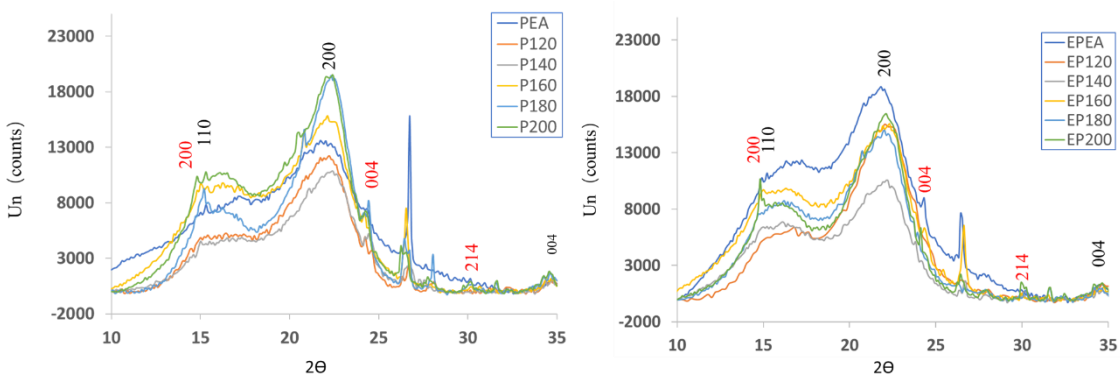


Figure 3. 4 XRD diffractograms of a) PEA and b) EPEA varying from 120 to 200 ºC. The cellulose peaks are shown in black and $CaC_2O_4$ peaks in red.

For the samples without MHT, the virgin pea sample displays more intense calcium salts peaks than EPEA samples. This may due to extrusion pretreatment which destroys the structure of cell walls and thus the salts were removed with the juice. Interestingly, after MHT, the calcium content in EPEA samples are higher, (see **Figure 3.5**) and the peaks of the calcium salts are detected obviously at 200 ºC.

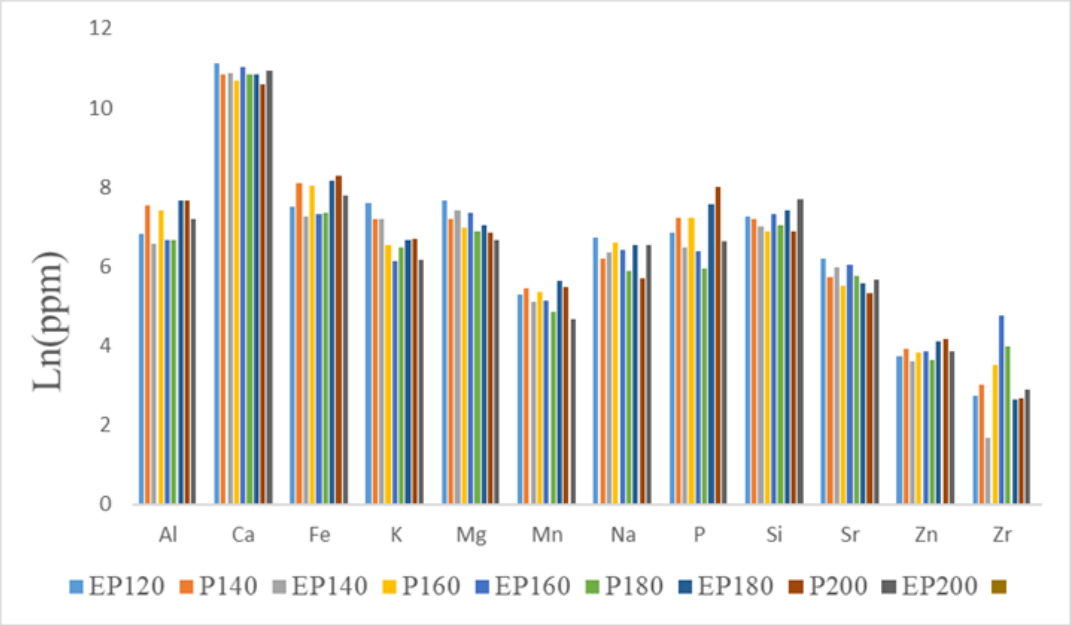


Figure 3. 5 ICP analysis for PEA and EPEA samples.

### 3.1.4 ATR-IR

The ATR-IR spectra of the defibrillated celluloses are shown in **Figure 3.6**, and their assignments listed in **Table 3.1**. It can be surmised that the O-H stretching vibration at about 3300 $cm^{-1}$ might be correlated to the hydroxyl moieties in cellulose I.[181] Bands at 2920 $cm^{-1}$ refer to C-H stretch from cellulose/hemicellulose. The absorption bands at 1735 $cm^{-1}$ were attributed to the carbonyl group from residual hemicellulose and lignin present in PEA and EPEA. The intensity of these bands decreased with increasing MHT temperature indicating that hemicellulose/lignin were gradually removed from cellulose during the microwave treatment (also possible that the hemicellulose could remain in its deacetylated form, as loss of the acetates could occur at a low temperature such that the polymer backbone is unchanged).[182] Minor O-H bending vibration at about 1620 $cm^{-1}$ was attributed to bonded water existing in the material. The bands at 1030 $cm^{-1}$ corresponded to C–O and C-C stretching[183]

confirming the presence of cellulose in PEA and EPEA, which became more evident at higher MHT temperatures since the non-cellulosic matter was gradually removed and therefore showed a purer cellulose spectrum.

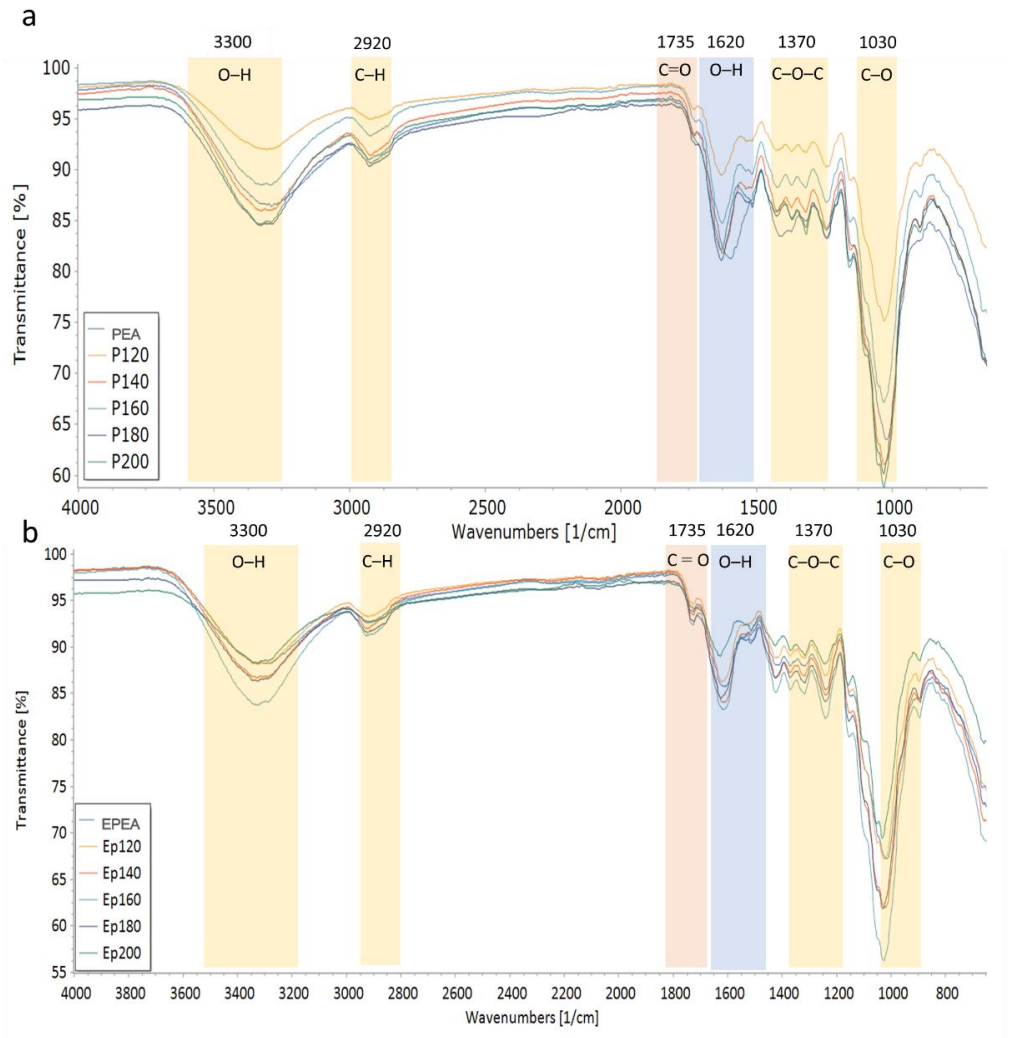


Figure 3. 6 ATR-IR of a) PEA and b) EPEA varying from 120 to 200 ºC.

Table 3. 1 FTIR spectra of lignocellulosic major band assignments [184-186]

| Absorption band ($cm^{-1}$) | Assignment | Component |
|---|---|---|
| 3300 | O-H stretching | Cellulose/hemicellulose/lignin |
| 2920 | C-H asymmetric and symmetric vibration in saturated $CH_2$ | Cellulose/hemicellulose |
| 2907 | C-H stretching in $CH_3$ and $CH_2$ groups | Cellulose/hemicellulose/lignin |
| 2934,2845 | C-H stretching vibration in | Lignin |

| | | |
|---|---|---|
| | the methyl and methylene groups | |
| 1735 | C = O stretching of carboxyl and acetyl groups | Hemicellulose |
| 1708 | C=O stretching vibration in aromatic skeleton | Lignin |
| 1660 | C=O stretching | Lignin |
| 1640 | O-H bending | Bonded water |
| 1600 | Aromatic ring vibrations and C=O stretching or $COO^-$ stretching | Hemicellulose/lignin |
| 1508 | Aromatic skeletal vibrations | Lignin |
| 1462 | C-H bending in $CH_2$ and $CH_3$ | Lignin |
| 1554 | O-H in plane bending | Cellulose/hemicellulose |
| 1422 | O-H in plane bending or C-H bending in $CH_3$ | Cellulose/hemicellulose/lignin |
| 1380 | $COO^-$ stretching | Hemicellulose |
| 1370 | C-H bending | Cellulose/hemicellulose |
| 1355 | O-H in plane bending | Cellulose/hemicellulose |
| 1335 | O-H in plane bending or C-H bending in G unit | Cellulose/hemicellulose/lignin |
| 1325 | C-O stretching vibration | Lignin |
| 1315 | O-H in plane bending | Cellulose/hemicellulose |
| 1267,1264 | C-O stretching vibration of G | Lignin |
| 1253 ,1096 | C-O stretching of aromatic ether | Lignin |
| 1248 | C-O single bond associated with an ester or a carboxylic acid | Hemicellulose |
| 1240 | C-O stretching vibration | Hemicellulose |
| 1226 | C-C,C-O,C=O stretching | Lignin |
| 1205 | O-H deformation | Cellulose/hemicellulose |
| 1156 | C-O-C asymmetric stretching | Cellulose/hemicellulose |
| 1150, 1125 | Aromatic C-H in-plane deformation (typical for G units) | Lignin |
| 1156 | C1-O-C4 asymmetric stretching | Cellulose/hemicellulose |
| 1110 | C2-O2H stretching | Cellulose/hemicellulose |

| | | |
|---|---|---|
| 1052 | C3-O3H stretching | Cellulose/hemicellulose |
| 1030 | C4-O6H stretching dominant or | Cellulose/ lignin |
| 988 | C6-O6H stretching minor or C-stretching or CH=CH out of plane bending | Cellulose/lignin |
| 897 | C-O-C vibration at β-(1-4)-glycosidic | Cellulose/hemicellulose |
| 875 | $CH_2$ bending | Hemicellulose |
| 860,817 | CH-CH out of plane bending | Lignin |
| 808 | In-phase ring stretching of mannosyl residues | Hemicellulose |

### 3.1.5 Solid state $^{13}$C CPMAS NMR and Crystallinity Index (CrI)

The stacked $^{13}$C CPMAS NMR spectra of PEA and EPEA samples with respect to increasing MHT temperature are shown in **Figure 3.7**. The signals at 175 ppm correspond to the carbonyl carbon of carbonyl/carboxylic groups which presenting in strongly bound cell wall polysaccharides (*e.g.* hemicelluloses) in pea waste.[187] The signals for cellulose carbons (C1 to C6)[188-191] are shown ranging from 110 ppm to 60 ppm. The peaks at 20 ppm may be attributed to $CH_3$ in polysaccharides (*e.g.* hemicelluloses) existing in the pea waste.[192-197] With increasing MHT temperature the signals of hemicellulose and/or lignin started to disappear especially after 180 °C, indicated the hydrolysis and depolymerization of the non-cellulosic matter[198] and resulted in the matter which was more similar to pure cellulose. At the same time, a significant change in cellulose structure was observed; the ratio of cellulosic surface/amorphous in C4 and C6 (84 ppm and 62 ppm, respectively) and interior/crystalline in C4 and C6 (89 ppm and 65 ppm, respectively)[199] was observed (arrows in yellow area **Figure 3.7**). The peaks representing crystalline regions start to

increase whilst the amorphous peaks start to reduce. This suggests that amorphous parts from the cellulose surface were also gradually hydrolyzed by MHT and the crystalline character of cellulose increased, this also provided the evidence for the formation of cellulose nanocrystals at higher temperatures as proved by TEM. These results correlated well with thermogravimetric data reported earlier and HPLC results to be discussed later.

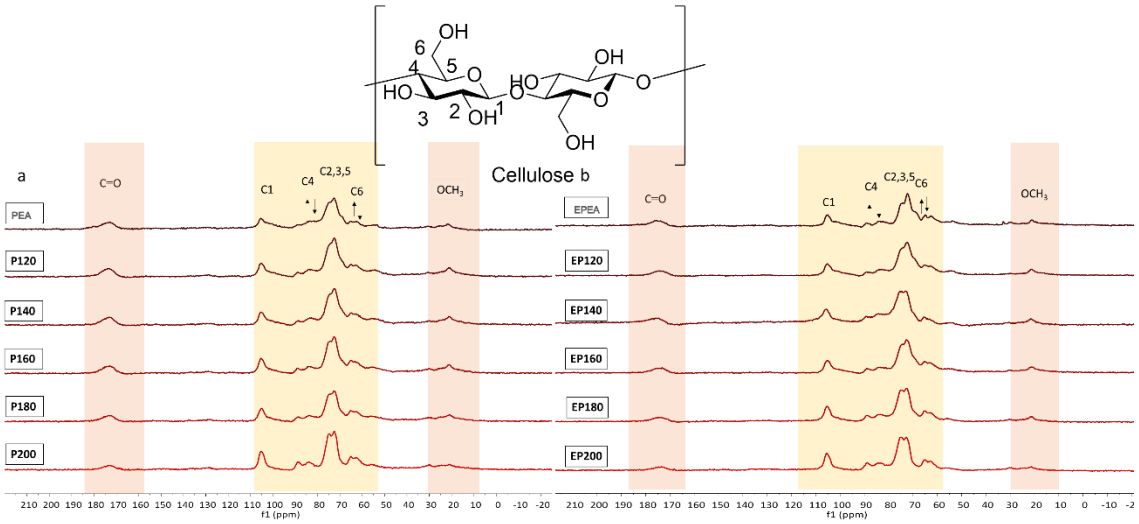


Figure 3. 7 $^{13}$C CPMAS NMR spectra of a) PEA and b) EPEA samples with a labelled illustration of a cellulose moiety. Arrows show the ratio of crystalline/interior: amorphous/surface cellulose.

The change in CrI (crystallinity index) of PEA and EPEA, determined from $^{13}$C CPMAS spectroscopy, with respect to MHT processing temperature is presented in **Figure 3.8**. As an important factor of cellulosic materials, the crystallinity affects several properties of the cellulose including thermal stability, mechanical strength, biodegradability, and saccharification.[200] Crystallinity index (CrI) can be determined via several methods: i. XRD： In XRD the height ratio between the crystalline peak ($I_{002}$ - $I_{AM}$) and total intensity ($I_{002}$) with no cellulose background signal subtraction is determined.[172] ii. solid-state $^{13}$C NMR. In solid state NMR the area of the signal

corresponding to C4 crystalline carbons (87 to 93 ppm) with respect to the amorphous carbons (80-87 ppm) is calculated.[172] In this thesis, the NMR method was adopted because it was relatively convenient and more accurate than the XRD height method. The EPEA samples display a higher CrI than their corresponding PEA counterparts. With increasing MHT temperature, an obvious increase in the CrI is noted after 180 ºC for PEA while the CrI of EPEA significantly increases after 160 ºC (approx. Δ =1.65 %-6.3 % for PEA and 2.6 %–5 % for EPEA). These differences could be related to the two stages of the Hy-MASS concept[175], *i.e.*, in the first step, the amorphous part in biomass (starch, hemicellulose) was selectively and progressively removed (scissoring) from the lignocellulosic matrix (120-180 ºC)[201] which correlated well with compositional data: NMR, XRD, TGA (see later) and, in the second step, softened amorphous cellulose and lignin embedded in cellulose microfibrils were released through a proton transfer mechanism at higher temperatures (>180 ºC). Extrusion as a pretreatment "softens" the material such that it can be hydrolyzed easier at a lower temperature (160 ºC compared with 180 ºC).

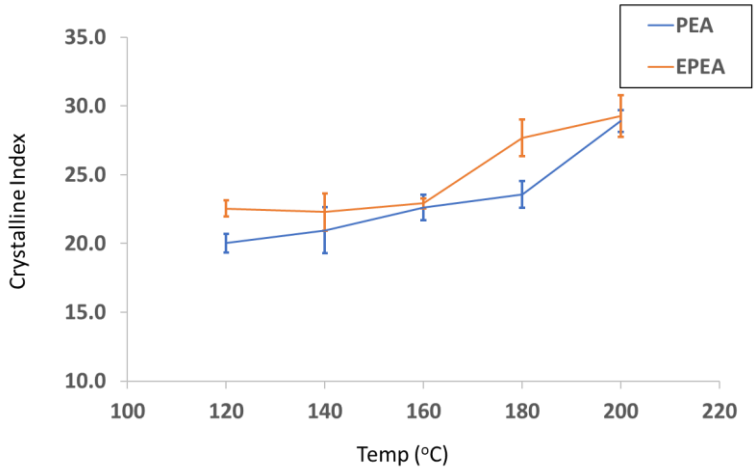


Figure 3. 8 Crystallinity index of PEA and EPEA calculated from $^{13}$C CPMAS NMR data. Error bars represent standard deviation (n = 3).

### 3.1.6 TEM and SEM

Defibrillated celluloses were successfully evidenced as microfibrillated cellulose (MFC) and cellulose nanocrystals (CNC) by high resolution TEM based on their fibrillar dimensions (**Figure 3.9**). The TEM images provide a clear understanding of the defibrillation during MHT: in MFC the microfibrils and elementary fibrils (3–5 nm in width and a few μm in length) in both amorphous and crystalline regions[199, 202, 203] were present. The cellulose nanocrystals (width 5–70 nm and length <500 nm) which originated from crystalline regions of elementary fibrils were found in EP180, P200 and EP200 after the hydrolysis of amorphous regions at high temperature (above 180 °C) (see **Figure 3.9**). This further confirmed the effect of the Hy-MASS concept, *i.e*. during MHT non-cellulosic biopolymers and amorphous regions of cellulose are hydrolyzed and cellulose nanocrystals are released above 180 ºC.[204] Comparison of the two samples revealed that the EPEA series displayed a narrower width than their non-extruded counterparts (difference of *ca.* 2-4 nm). Also, nanocrystals were detected only in EPEA samples at 180 ºC possibly implying that amorphous regions of cellulose were breached during extrusion and thus became easier to hydrolyse during MHT process.

The grey regions which surround the nanofibrils are possibly residual amorphous matter (mainly include hemicellulose, lignin and some probably amorphous superficial cellulose).[175] With increasing MHT temperature, the gradual removal of grey regions occurred but some still persisted entangled with the nanofibrils and crystals even at a temperature of 200 ºC (see **Figure 3.9**). It could be that

hemicellulose were “scissored” gradually during MHT but the residual lignin fragments could not be totally removed or the pseudo-lignin which is defined as “an aromatic material that yields a positive Klason lignin value that is not derived from native lignin” were formed during the (MHT) process.[205] Interestingly, the extruded samples presented a less dark grey area than compared with their non-extruded counterparts. These results also proved that there were two steps in MHT: i. the outside amorphous regions in microfibrillated cellulose were “cut” progressively by microwave treatment up to 180 ºC, and; ii. the nanocrystals which existed in elementary fibrils were released after 180–200 °C.

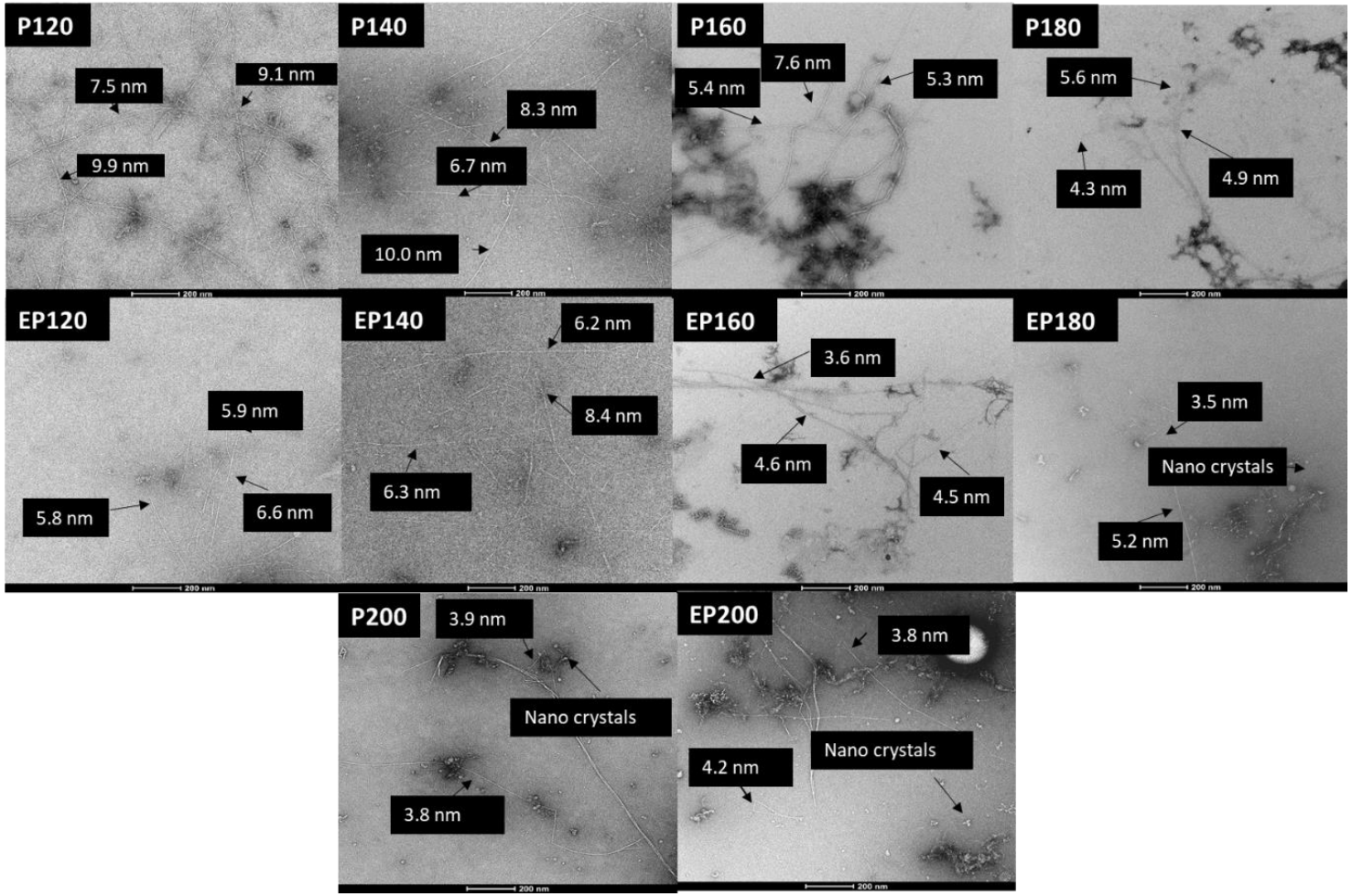


Figure 3. 9 TEM images of PEA and EPEA samples varying from 120 to 200 ºC (scale bar = 200 nm). The width of the MFC were labeled.

The SEM images from the surfaces of PEA and EPEA varying from 120 to 200 ºC are shown in **Figure 3.10**. This provided the morphologies and structures of the PEA and EPEA samples during the microwave hydrolysis procedure. It can be observed that the P120 sample presents a more complete and compacted morphology while EP120 displays smoother, thinner and heavily distorted fibres due to high shear created by extrusion. During the MHT Process, with the temperature increasing, the fibrillar moieties of both PEA and EPEA samples were separated via the hydrolysis of amorphous regions, and the EPEA samples seem to tend towards exhibiting a more porous and corrugated surface while the fibre matrix of PEA samples presented a rough and more intact structure, implying that the pretreatment made it easier for MHT to disrupt the tissue network of MFC.[206]

Due to the rich hydroxyl groups of MFC, the individual fibrils of the samples might aggregate and become hornified during the drying process.[207] In order to obtain better evidence of the defibrillation, several operations could be carried out including freeze-drying technology[208] and more diluted and well-dispersed of the suspension via homogenized or ultrasound treatment.[69]

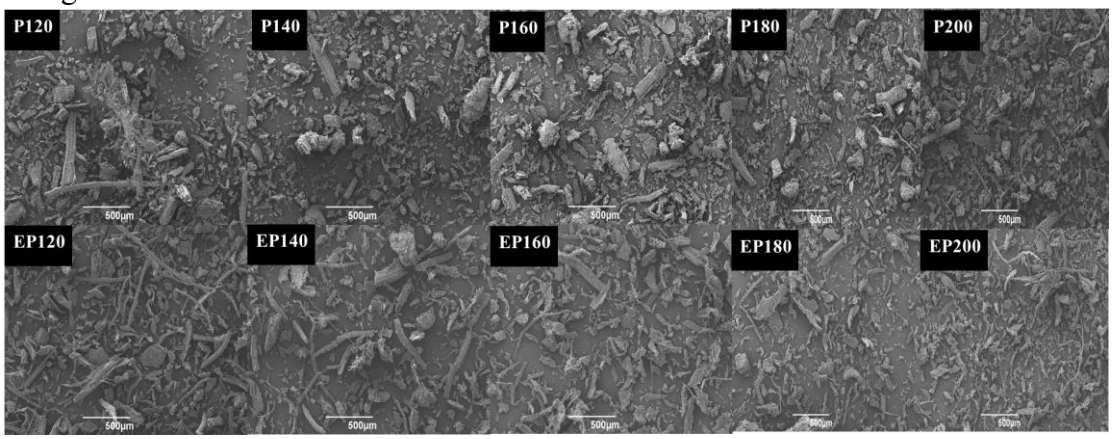


Figure 3. 10 Morphological features of PEA and EPEA varying from 120 ℃ to 200 ℃ (scale bar = 500 μm).

### 3.1.7 HPLC

The HPLC analyses of the hydrolysate obtained from MHT of the two samples (PEA and EPEA) are presented in **Figure 3.11(a)**. The main chemicals in the hydrolysate are soluble sugars (mainly monosaccharides), organic acids and furans. The monosaccharides were all derived from the hydrolysis of polysaccharides presented in the biomass, and the acids and furans were from decomposition of these sugars. The conversion pathways are presented in **Figure 3.11(b)**, it should be emphasized that the fructose and xylose cannot be resolved via the HPLC method used. Considering the biomass type,[209] here we assumed that fructose was not a major carbohydrate in pea waste. The results showed that glucose and xylose were the main monosaccharides in the hydrolysate. In general, the sugar yield from PEA hydrolysate remained higher than the EPEA series. The yield of glucose decreased (0.32 to 0.04 mg/ml and 0.14 to 0.15mg/ml, separately) with increasing MHT processing temperature (120 to 200 ºC), 5-hydroxymethylfurfural (HMF) and furfural appeared after 180 °C. This could be related to the hydrolysis of polysaccharides in water below 220°C.[179] Glucose could be derived from amorphous cellulose and hemicellulose, and 5-hydroxymethylfurfural (HMF) is considered the major secondary byproduct from glucose degradation. Levoglucosan, which is derived from amorphous cellulose hydrolysis [179] could be detected in all hydrolysates and distinctly increased after 180 °C (the maximum concentration was 0.26 mg/mL in P200 hydrolysate), implying its conversion from glucose was more common at high temperature. Xylose was mainly derived from residual hemicellulose since, the hydrolysis product was mainly from the amorphous part of the biomass and

the crystalline region would not take part in the MHT reaction, thus the high amount of amorphous cellulose and hemicellulose would induce a higher sugar yield. After 180 °C， the part of glucose converted to HMF led to a yield reduction, and a significant increase of HMF is observed. Conversely, the xylose conversion to furfural did not affect its yield, hence, it may be reasonable to suppose that with higher temperature, hemicellulose has a higher conversion to monosaccharides.[210]

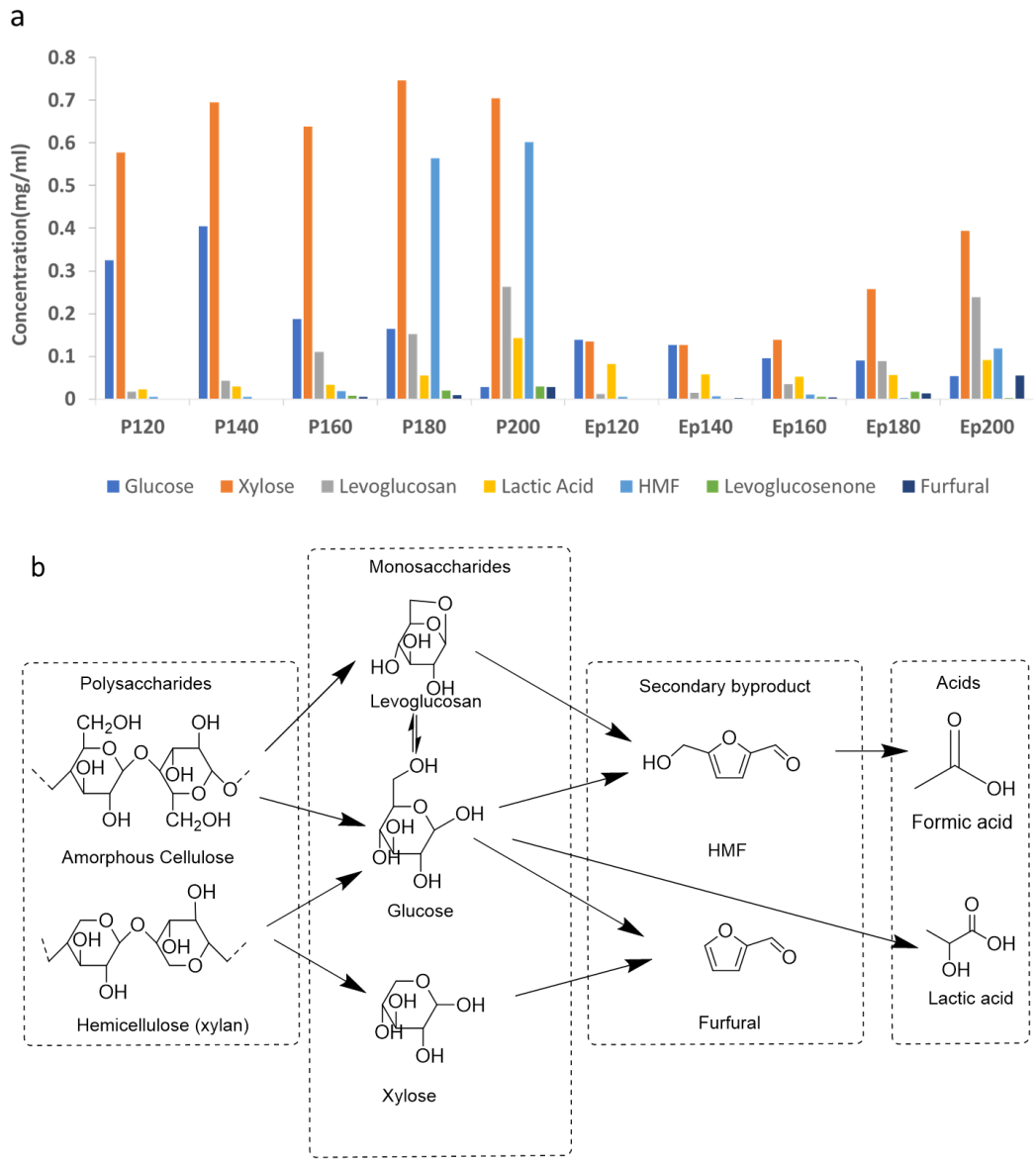


Figure 3. 11 HPLC data for hydrolysates from PEA and EPEA after MHT (a) Products and sub-products from lignocellulosic, (b) polysaccharides conversion pathways to acids

### 3.1.8 Water Holding Capacity (WHC)

The water holding capacity (WHC) of cellulose samples is shown in **Figure 3.12**. The EPEA samples displayed a higher WHC than their non-extruded PEA counterparts (approximately 5 to 15% higher), implying that the extrusion broke the structure of the cell walls, making the feedstock easier to hydrolysis during MHT, consequently enlarging the surface area of samples. Both types of starting material (native biomass) had lower hydration capacity compared to their MFC products, indicated that the MHT had a significant influence on the WHC of the samples. As mentioned before, the treatment changes the structural of the cellulosic fibres and simultaneously increase the surface area, thus the insoluble cellulose can hold more water by absorbing water in their fibril network through swelling properties.[175, 211]

During the gradual selective removal of amorphous matters by microwave treatment, particle size diminished and consequently the surface area of cellulose increased (this can be proved in SEM image), improving hydration capacity. However, from our data, the water holding capacity of PEA and EPEA samples remained constant irrespective of MHT temperature (7 g and 8 g, respectively) which may due to the higher crystalline index of cellulose making it more hydrophobic. Meanwhile, the recalcitrant pseudo-lignin which formed from degradation of carbohydrates at high temperature could also increase the hydrophobicity of MFCs and thus reduced the values of WHC. However, even the WHC was a common approach to evaluate the water holding abilities of the cellulose, due to the defects in experimental operation (*e.g.* the remaining water in samples cannot be drained completely), the result may be not

precise, thus the water retention value (WRV) using the centrifuge was an appropriate alternative method to replace WHC.

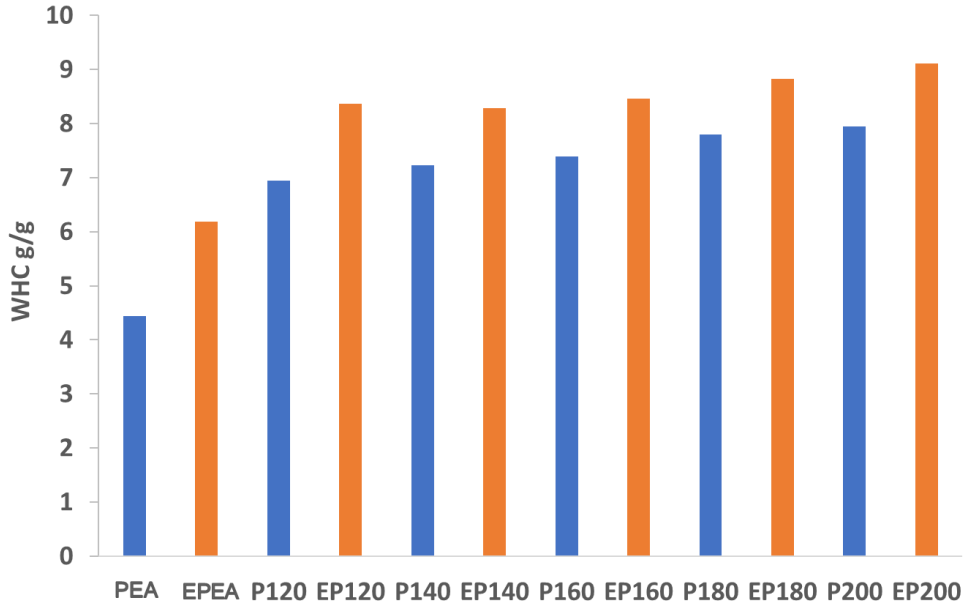


Figure 3. 12 WHC of PEA and EPEA (g of water per g of dry sample). Values are average of duplicate experiments.

### 3.1.9 $N_2$ Adsorption porosimetry

The BET surface area, BJH average pore size and BJH pore volume for PEA and EPEA samples are shown in **Figure 3.13**. Both types of MFC display considerable surface area and porosity. For PEA samples, the BET specific surface area decreases initially up to 160 ºC, and then increases from 160 to 200 ºC; the BET surface area of EPEA samples decreased significantly from 120 to 160 ºC (30 to 15 $m^2/g$) and then rose from 160 to 200 ºC (15 to 37 $m^2/g$) which agrees with the scissoring of amorphous polysaccharides and other components and lignin from cellulosic matrix by means of the MHT. In general, EPEA samples displayed a higher BET surface area than their PEA counterparts (about 2-30 $m^2/g$ higher), which could be explained by the destructive nature of the extrusion process destroying the original lignocellulosic

construct. [199,212] The BJH average pore diameter was approximately 10 nm and, according to the IUPAC mesoporous classification (average pore size ranged between 2 and 50 nm), these materials can be classified as mesoporous.[175] Mesoporous materials have promising applications including drug delivery agents, filters, membranes, adsorbents, catalysis, and carbonaceous materials.[213]

The pore volume of both samples presents the same pattern as for BET surface area: the pore volume of PEA and EPEA samples slightly decrease at first but then increase. The decrease in pore volume at may be associated with pores collapsing or becoming blocked which then become unblocked (melting and leaching of material from within pores) at higher MHT temperatures.

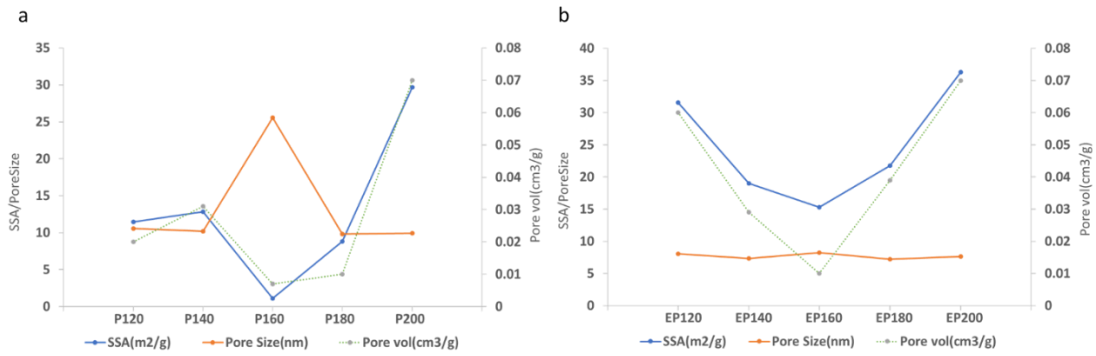


Figure 3. 13 Porosimetry data (BET Specific surface area – SSA, BJH pore volume and BJH average pore size) for PEA (a) and EPEA (b) samples.

Nevertheless, even though some useful information was obtained from $N_2$ adsorption porosimetry, this method is not the optimum technique for the analysis of "soft materials" such as cellulose (even though the samples were degassed at 120 °C for several hours). The fibrils may irreversibly aggregate via the interfibrillar hydrogen bonding,[208, 214, 215] namely, hornification. Meanwhile, the pores in sample may also disrupt, leading a reduction of the surface area and pore volume.[216] Researchers have

found that the drying method (*tert*-butanol freeze-drying, supercritical $CO_2$ and liquid $CO_2$ evaporation) was an important procedure which influences the results.[217] Thus, alternatives to nitrogen porosimetry should be considered. For example, Spence *et al.* used the Congo red dye adsorption method to test the SSA values of (un)bleached pulp MFC without drying process.[218] Cryo-DSC and Cryo-NMR are also reported to better methods for determining porosity of 'soft materials'.[219, 220] Despite all this, the increasing SSA values could still provide the evidence that the cellulose fibrillated to microfibrils along with other components are removed from the cellulosic matrix and constitutive open pores form during MHT procedure (160 to 200 ºC).

Thus, the MFCs were successfully obtained from pea waste via MHT treatment, to investigate whether the treatment is feasible on other cellulose rich food waste, the spent industrial ginger waste was also attempted to produce the valuable products via microwave technology.

## 3.2 Part B Spent ginger biomass: A biorefinery strategy for resource recovery

An integrated biorefinery approach using spent industrial ginger (post-industrial liquid-$CO_2$ extracted) waste for resource recovery is reported. Products including essential oils, starch, MFC (microfibrillated cellulose), bio-oil and hydrochar were obtained either via Soxhlet extraction (heptane) or microwave hydrolysis or pyrolysis. Approx. 4% residual essential oil with a profile similar to commercial ginger oil can be recovered via Soxhlet extraction (heptane). The oil-free ginger residues were processed with two microwave techniques: starch, microfibrillated celluloses (MFC) and sugar-rich hydrolysates were gained through hydrothermal acid-free microwave processing (120 to 200 $^{o}$C in water alone), whilst chemical-rich bio-oils (both aliphatic and aromatic compounds) and energy-dense hydrochar (20 - 24.5 MJ $kg^{-1}$) were obtained via conventional microwave pyrolysis procedure (220 to 280 $^{o}$C). The morphology and properties of these products were characterized through a variety of analytical techniques. The ginger MFC (GMFC) exhibited increasing crystallinity with increasing processing temperature, increased propensity to form microfibrillated cellulose (as evidenced by TEM) with increasing temperature and nanocrystalline cellulose at the highest temperature (200 $^{o}$C). These changes are commensurate with the leaching and decomposition of the amorphous regions within cellulose. Starch was obtained (approx. 50 wt%, T = 140 $^{o}$C) from within the hydrolysate which was also rich in sugars (glucose, xylose, levoglucosan) and small molecules (lactic acid, acetic acid, furfural) resonant with cellulose hydrolysis. The molecules and materials isolated

have further downstream applications, thus, industrial spent ginger waste (resource) is significant resource for consideration within a biorefinery concept. This study presents an eco-friendly value-added strategy for spent industrial ginger for production of chemicals (essential oil, bio-oil, starch), materials (MFC, hydrochar) and (bio)energy (hydrochar) within the context of a zero waste biorefinery.

Interestingly, it should be noted that the precipitate of hydrolysate from pea and ginger are quite different: a significant amount (approx. 50% by weight) of starch from ginger hydrolysate post microwave hydrolysis was obtained (**Figure 3.14**). To our best knowledge, this may be the first time starch has been extracted from ginger waste via microwave hydrothermal treatment (MHT).

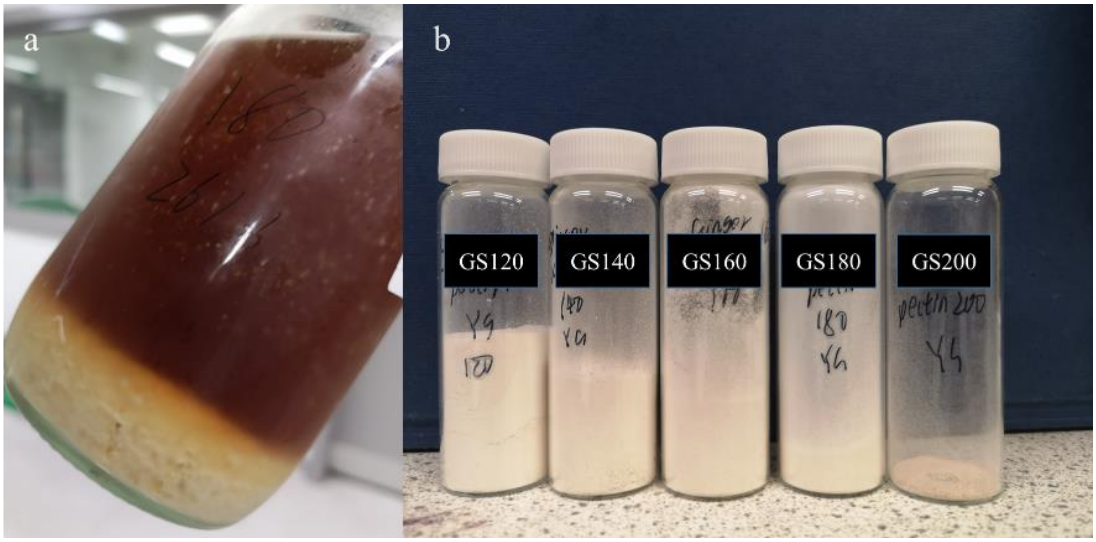


Figure 3. 14 a. Hydrolysate treated with ethanol to afford a precipitate; b isolated ginger starch post MHT (120 – 200 ℃).

### 3.2.1 Essential oil recovery

The composition of the essential oil as recovered via Soxhlet extraction (hot heptane; (1.58 g, 3.95 %)) and determined by GC-MS is shown in **Table 3.2** (the raw spectrum is shown in Appendix, **Figure A1**). Interestingly, α-curcumene, zingiberene, α-

farnesene, β-sesquiphellandrene, zingerone, isoshogaol and shogaol and gingerol were identified. These are known key molecules present in commercial ginger oil, thus, immediately representing a potential valorization opportunity. Depending on the quality/grade of ginger oil and its intended application, its value can range from £100 to £500/kg.

Table 3. 2 Major identified compounds from Soxhlet extraction

| Compound | Retention Time (min)[b] | % Area[c] |
|---|---|---|
| α-Curcumene | 22.17 | 9.03 |
| Zingiberene | 22.65 | 22.65 |
| α-Farnesene | 22.89 | 2.62 |
| β-Bisabolene | 22.99 | 4.1 |
| β-Sesquiphellandrene | 23.48 | 9.28 |
| Zingerone | 26.8 | 2.28 |
| 6-Shogaol | 42.59 | 7.32 |
| 6-Gingerol | 44.66 | 11.17 |
| Unknown | 46.84 | 1.27 |
| 10-Isoshagaol | 48.27 | 2.17 |
| 10-Shogaol | 49.13 | 4.14 |
| γ-sitosterol | 54.24 | 2.1 |

### 3.2.2 Microwave pyrolysis

#### 3.2.2.1 Bio-Oils

Gas chromatography-mass spectrometry (GC-MS) characterization was performed to identify the organic compounds obtained in pyrolysis of spent ginger to afford bio-oils. **Tables 3.3** shows the possible main identified compounds at different temperature (220, 240, 260 and 280 $^{o}$C) with same holding time (9 min). The conditions were coded according to temperature and time, for example, 2209 refers to the sample with 220 $^{o}$C and 9 min residence time. The qualified constituents can be classified by functional group: cellulose/hemicellulose derived furanic structures (furfural and 2-furanmethanol) and 3-Methyl-1,2-cyclopentanedione, lignin-derived

phenolic-like compounds including methoxyphenol, cyclopentanol, catechol and 2-hydroxy-5-methylacetophenone. Meanwhile, due to the samples being washed with ethyl acetate, the water soluble carbohydrate sugars (*e.g.* levoglucosan) were not detected and they may still stay in the char. Interestingly, some essential oils (zingerone, shagaol) were still detected possibly due to their thermal stability.

Table 3. 3 Chemical composition of ginger oils obtained with pyrolysis

| **Compounds**[a] | **RT (min)**[b] | **% Area**[c] | | | |
|---|---|---|---|---|---|
| | | 2209 | 2409 | 2609 | 2809 |
| Furfural | 3.32 | 6.66 | 5.82 | 5.33 | 5.07 |
| 2-Furan-methanol | 3.68 | 28.46 | 28.40 | 32.26 | 27.74 |
| Butyrolactone | 4.73 | 5.94 | 5.52 | 7.04 | 7.03 |
| 3-Methyl-1,2-cyclopentanedione | 7.49 | 4.61 | 5.15 | 4.27 | 3.59 |
| Methoxy phenol | 9.23 | 2.16 | 1.79 | 2.14 | 2.07 |
| Cyclopentanol | 9.64 | 5.89 | 7.63 | 5.50 | 3.06 |
| Catechol | 13.04 | 0.74 | 1.40 | 0.39 | 2.59 |
| 2-Hydroxy-5-methylacetophenone | 16.58 | 1.90 | 2.09 | 1.03 | 0.49 |
| Zingerone | 26.68 | 0.49 | 0.34 | 0.40 | 0.41 |
| Shagaol | 42.43 | 1.36 | 0.88 | 0.91 | 0.04 |

Thus, spent industrial ginger waste can be pyrolysed in to biobased chemicals both aliphatic and aromatic. Furanics are interesting as a source of biobased platform molecules for conversion in to further molecules of industrial interest such as 5-hydroxymethyl furfural, itaconic acid, furan-2-, 5-dicarboxylic acid.

#### 3.2.2.2 Yield of char

The yields of microwave pyrolysis gas, bio-oil and char with respect to temperature at fixed holding time (9 min) are displayed in **Figure 3.15**. It can be seen that with increasing temperature (220 to 280 $^{o}$C), the gas yield increases from 9.28% to 15.28%. Yields of oil also increase from 14.06% to 33.38%, with both the gas and oil yields

reaching the maximum at 280 ºC. Conversely, yields for the chars reduce from 76.66% to 52.19%, with the char yield reduction being attributed to biomass depolymerization during pyrolysis and subsequent, increased volatilization (including CO, $CO_2$ and $H_2O$) and aromatization.[221] Generally, increasing temperature would lead to a decreased char yield but with high carbon concentration.[222] Compared to the traditional heating method, in this thesis, the microwave pyrolysis treatment presents relatively low oil and gas yield (even at 280 ºC and 9 min, the yield of gas and oil are 15.43% and 33.38%,respectively) compared to other literatures.[223, 224] But the yield can be controlled via maximising the heating rate at the same temperature.[225] In this experiment, in order to avoid the explosion of glass tube during the heating process (rapid gas pressures), the power was set to 95 W, and the microwave heating was a much faster reaction than conventional heating. Considering the high energy cost in traditional heating (normally the temperature reaches 600 ºC while the temperature of microwave pyrolysis ranging between 200 ºC and 300 ºC), the microwave pyrolysis is a promising way to obtain gas, oil and char.

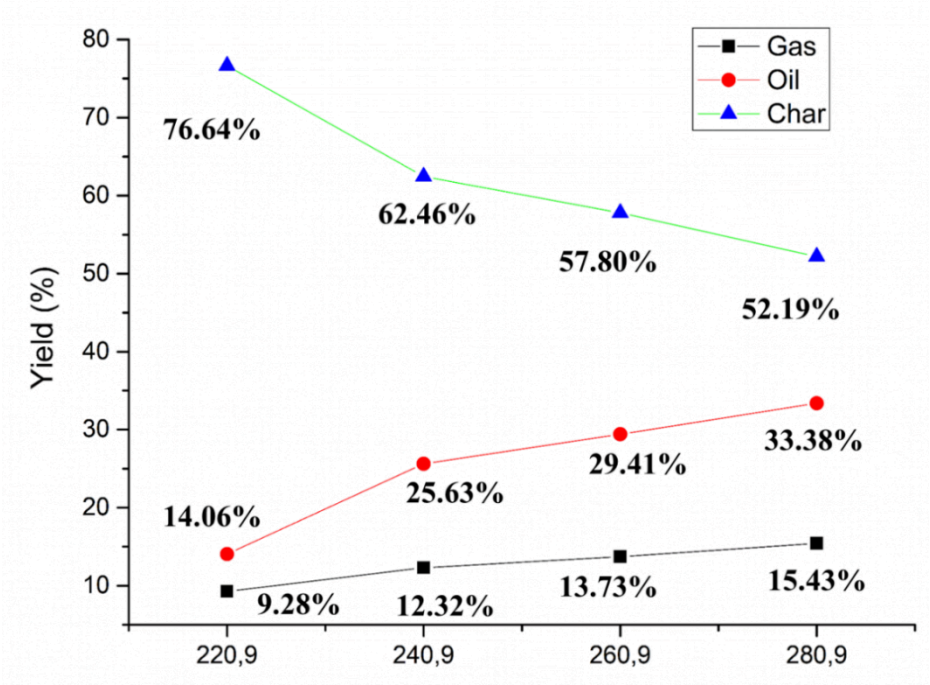

Figure 3. 15 Yield of pyrolysis products with respect to temperature.

### 3.2.2.3 Higher heating value (HHV) of char

The calorific value or higher heating value (HHV) of the resultant chars was determined both experimentally and theoretically via bomb calorimetry and elemental analysis, respectively, and is shown in **Figure 3.16** (where GP refers to virgin, non-pyrolysed spent ginger and GCXXXY refers to ginger char (GC), processed at temperature XXX $^{o}$C for Y minutes). Compared with the original ginger waste (16.29 MJ kg$^{-1}$), the concept of energy densification is noted as the calorific value increases upon char formation (20 - 24.5 MJ kg$^{-1}$). Meanwhile the empirical values from bomb calorimetry are higher than values from CHN at around 1-2 MJ kg$^{-1}$. This may attribute to the sulfur and phosphorus content not being accounted in **Equation 2.9**. Overall, the values increase with higher temperature and holding time, with the average maximum HHV (23.26 MJ kg$^{-1}$) is obtained at 280 $^{o}$C for 9 min. Theoretically, higher calorific values may be achieved at higher temperatures or more residence time (*e.g.*

300 °C). Restricted by the capability of the instrument, a higher calorific value may be achieved at higher temperature or more residence time (*e.g.* 300 °C or greater). This indicated that the ginger waste had undergone energy densification through microwave pyrolysis, and thus could be utilized as an available energy source (*e.g.* heating, electric generation, or gas turbine).

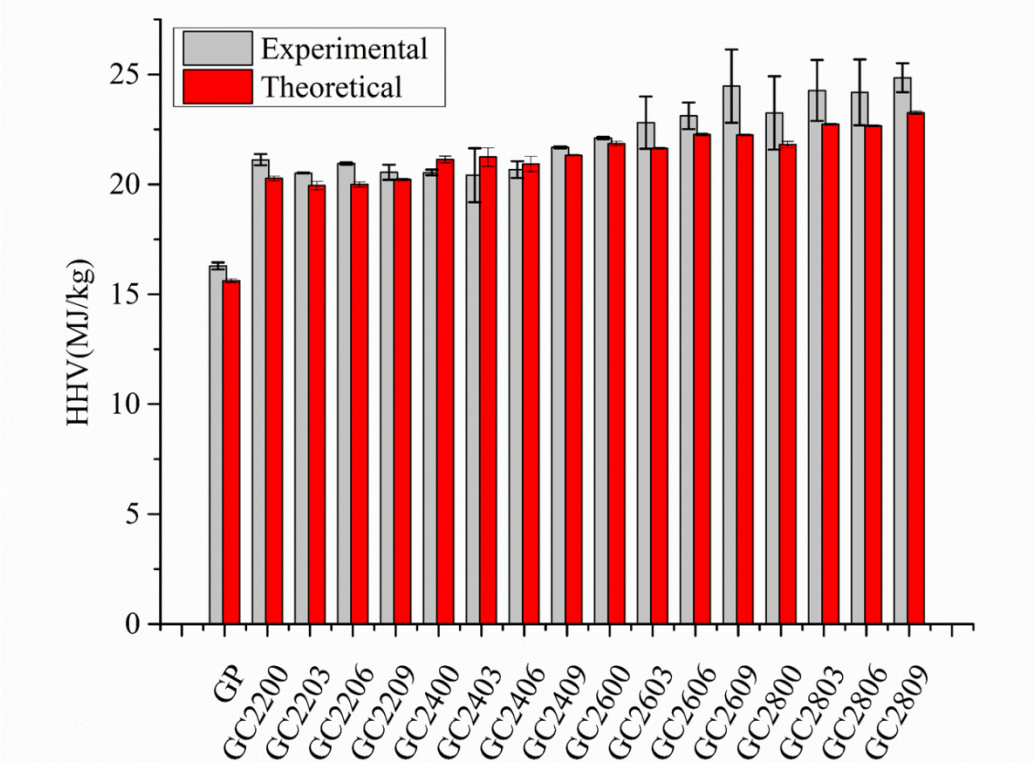


Figure 3. 16 Higher heating value of ginger and its chars from bomb calorimeter (Experimental) and theoretical HHV from CHN calculation (Theoretical). Values are average of duplicate experiments.

Also, in comparison with other selected biomass char types based on internal and external data (**Figure 3.17),**[85] it can be observed that most of the HHV of raw biomass types are similar (about 16 - 17 MJ $kg^{-1}$) except for soft wood (20 MJ $kg^{-1}$). This may be due to the high lignin content in soft wood.[85] Ginger char is also comparable to other char types. However, these values are for qualitative analysis only as the chars

have been produced by different methods.

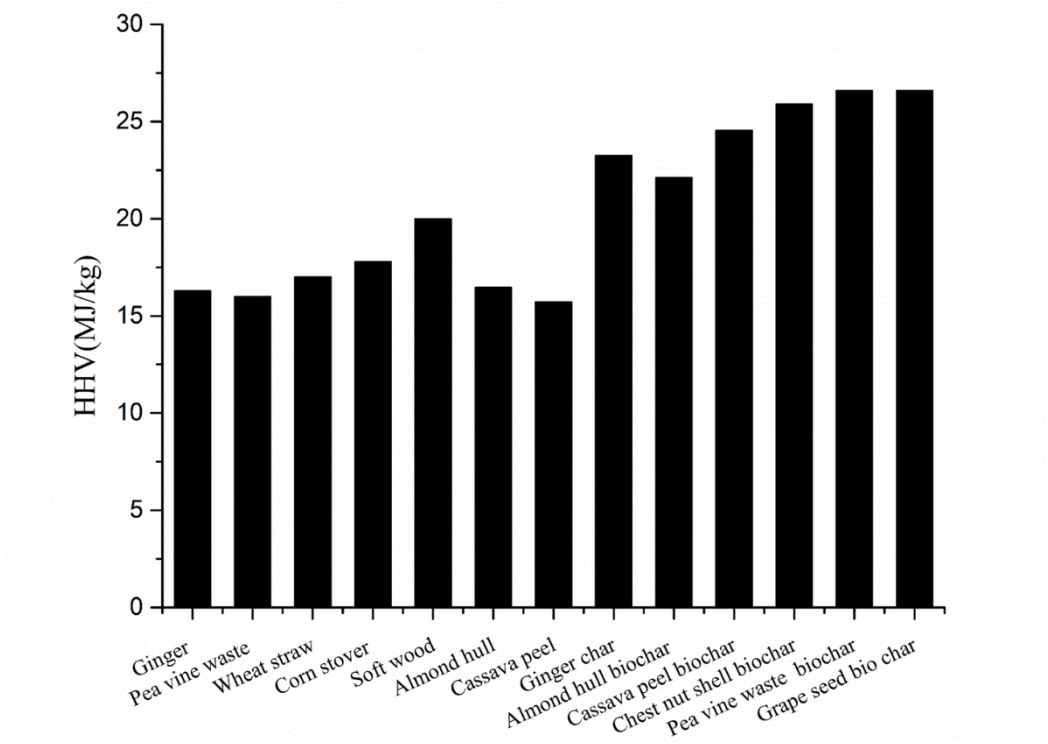


Figure 3. 17 HHV of different biomass and their chars.

The van Krevelen diagram for ginger and its chars obtained from different pyrolysis conditions is displayed in **Figure 3.18**. The O/C and H/C ratios (the ratios were calculated by elements percent from CHN analysis over atomic weights of the elements with the O content being assumed to be 100%- (%C + %H)) can be used to present the degree of carbonization, the O/C ratio describes the polarity and higher ratio indicate more polar functional groups, and the H/C ratio indicates potential aromaticity in the biochar.[226] It can be observed that O/C and H/C ratios of ginger residue are around 0.98 and 1.9, respectively, and with increasing temperature (220 to 280 $^{o}$C) and residence time (0 to 9 min), the O/C and H/C ratios both decreased through the pyrolysis (from 0.58 to 0.42 and 1.23 to 1.01, respectively), suggesting the

displacement of polar surface functional groups to aromatic structures of char with removal of H- and O-containing volatiles.[227] Thus the carbon content is "concentrated" with harsher conditions resulting in a higher degree of carbonisation.[228] Ideally, the optimum H/C and O/C ratios of biochar should be less than about 0.6 and 0.4 respectively( see the yellow area in **Figure 3.18**).[229] In this instance the char product produced from spent ginger may be classified as a hydrochar with high oxygen functional groups, more alkyl moieties instead of aromatic structure and higher nutrient retention capacity than biochar.[230] The formation of a hydrochar or *pseudobiochar* rather that a biochar is further evidenced by thermogravimetric analysis (see **Figure 3.19**) which still shows a significant decomposition fingerprint for (ligno)cellulose. In an ideal char, this decomposition should be absent.

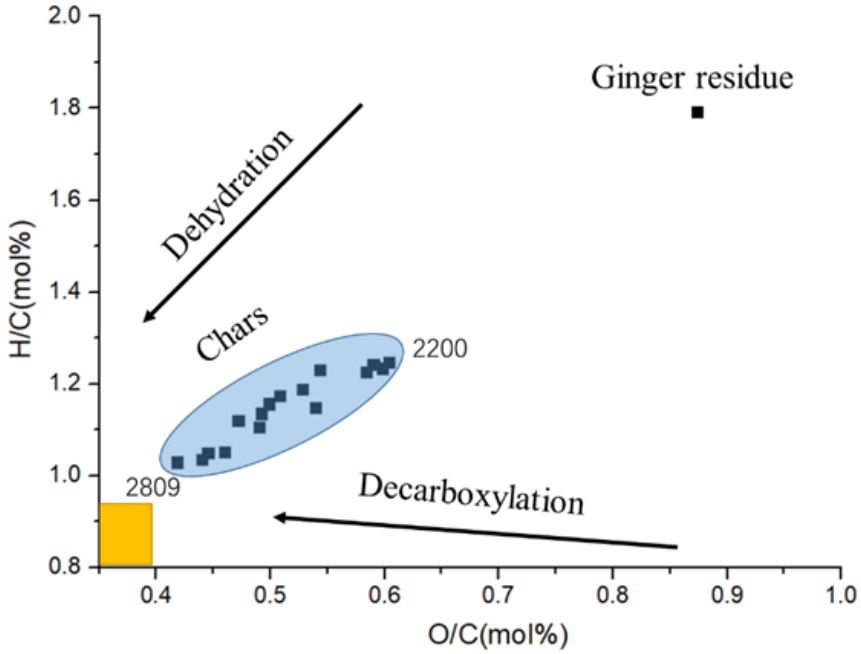


Figure 3. 18 Van Krevelen diagram for ginger and its chars obtained at different conditions, optimum H/C and O/C ratios of char is in yellow area.

### 3.2.2.4 Thermogravimetric analysis (TGA) of char

The TGA, and respective first derivative (DTG), of the chars produced are shown in **Figure 3.19**. From the TGA curves, it can be observed that all chars exhibit a similar trend, and at higher pyrolysis temperatures and longer holding times, result in better thermal stability. Namely, the mass loss decreases with increasing temperature and residence time: 2200 (61.49%), 2203 (59.28%), 2206 (55.7%), 2209 (53.88%); 2400 (56.61%), 2403 (51.23%), 2406 (51.19%), 2409 (49.93%); 2600 (53.40%), 2603 (53.36%), 2606 (53.61%), 2609 (51.83%), 2800 (49.49%), 2803 (45.42%), 2806 (42.56%) and 2809 (40.57%). This is due to the fact that the mass loss during pyrolysis is firstly from the decomposition of the relatively unstable hemicelluloses; harsher conditions during pyrolysis will remove more such materials, thus the more stable the resulting residues will be at higher temperatures and longer residence times.

The DTG results provide further information of the biochar properties. For all samples, there are two distinct decomposition bands observed in DTG curves. The first is between 30 and 100 $^{o}$C which corresponds to the loss of moisture and other volatiles and accounts for approximately 3% of the sample. The second is between 220 and 360 $^{o}$C which corresponds to remnant cellulose and accounts for between 40-60% of the sample. There is also a small band (see arrow in Figure 3.20 a) at about 380 $^{o}$C which may be attributed to lignin existing in GC2200 and GC2203. However, with increasing temperature and residence time, the bands disappear, indicating the decomposition of organic compounds. Interestingly, with higher temperatures, the height of the peaks become shorter, this may be due to harsher conditions causing the amount of

remaining cellulosic materials to decrease, thus the total decomposition time shortened and reduced the decomposition rate.

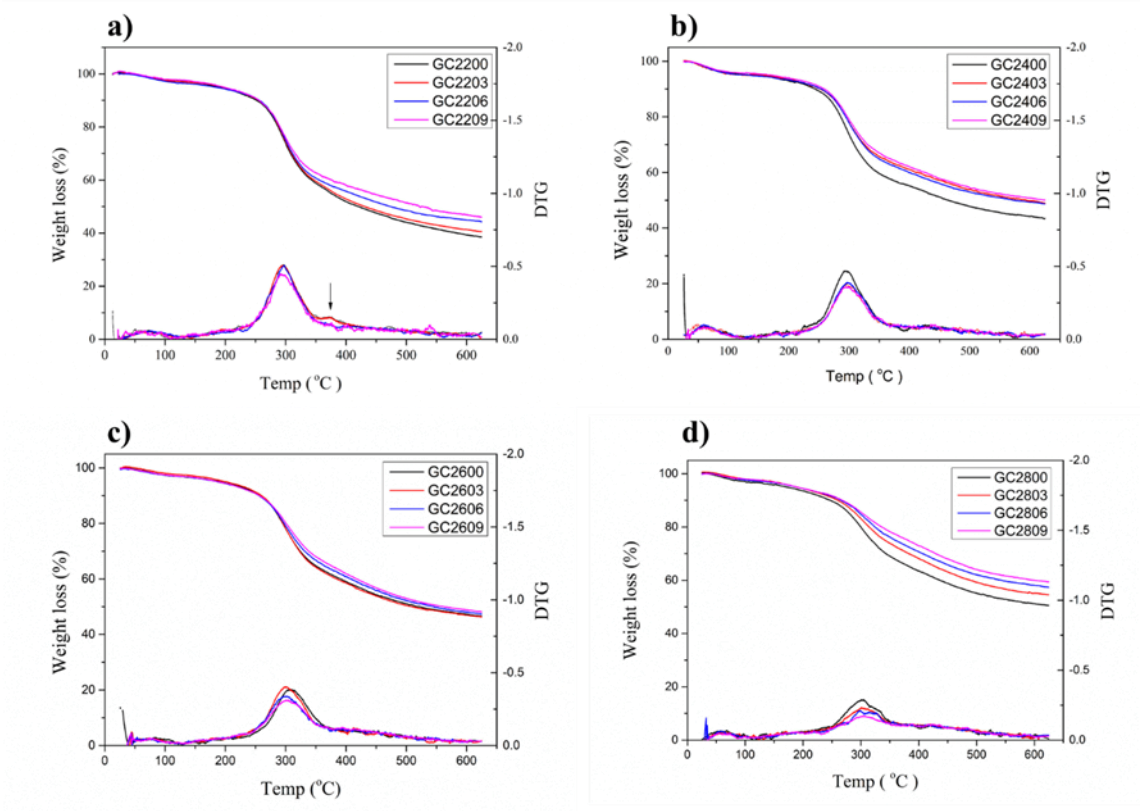


Figure 3. 19 TGA thermograms of ginger char samples.

### 3.2.2.5 ATR-IR of char

ATR-IR analysis of the chars also supports this notion of a hydro- rather than bio-char. The stacked FTIR spectra of the initial ginger powder and its char samples produced at different temperatures (220 to 280 °C) and same resident time (9 min) are shown in **Figure 3.20**. The broad bands at around 3300 $cm^{-1}$ are O-H groups stretching corresponding to hydroxyl moieties in hemicellulose or cellulose. The bands centred at about 2920 $cm^{-1}$ are due to the symmetric and asymmetric $–CH_2$ and $–CH_3$ stretching which belongs to hemicellulose. Two small peaks at around 1700 $cm^{-1}$ and 1600 $cm^{-1}$ are assigned to C=O stretching and C=C stretching in phenolic esters,

lactones, conjugated ketones or quinones which are derived from lignin pyrolysis.[228] The peaks at approximately 1620 $cm^{-1}$ confirm the existing of bonded water in biomass, the bands at about 1340 $cm^{-1}$ refer to aromatic C=C in lignin.[228] The sharp peak centered at 1010 $cm^{-1}$ may attributed to C–O and C-C stretching in cellulose/ hemicellulose, the small peaks at about 760 $cm^{-1}$ is likely due to the aromatic C-H in lignin/hemicellulose.[228]

The spectrum of ginger shows characteristic lignocellulosic bands (3300 $cm^{-1}$, 2920 $cm^{-1}$, 1340 $cm^{-1}$, 1010 $cm^{-1}$ and 760 $cm^{-1}$) due to its main components (cellulose, hemicellulose and lignin). But during the pyrolysis process, these major bands gradually disappear in the char samples and are substituted by new, smaller bands (1700 $cm^{-1}$ and 1600 $cm^{-1}$) which correspond to aromatic structure compounds, indicating that the raw biomass converts to a char which is broadly (there are still significant amounts of H and O present) polycyclic aromatic in character through carbonisation and aromatisation processes [231, 232] Although, the ratio of O/C and H/C in biochars could further be reduced at higher temperature through more complete pyrolysis indicating that ginger waste can be a potential feedstock for biochar production and bioenergy, needless to say other application such as soil improver, catalytic support, and remediation agent.

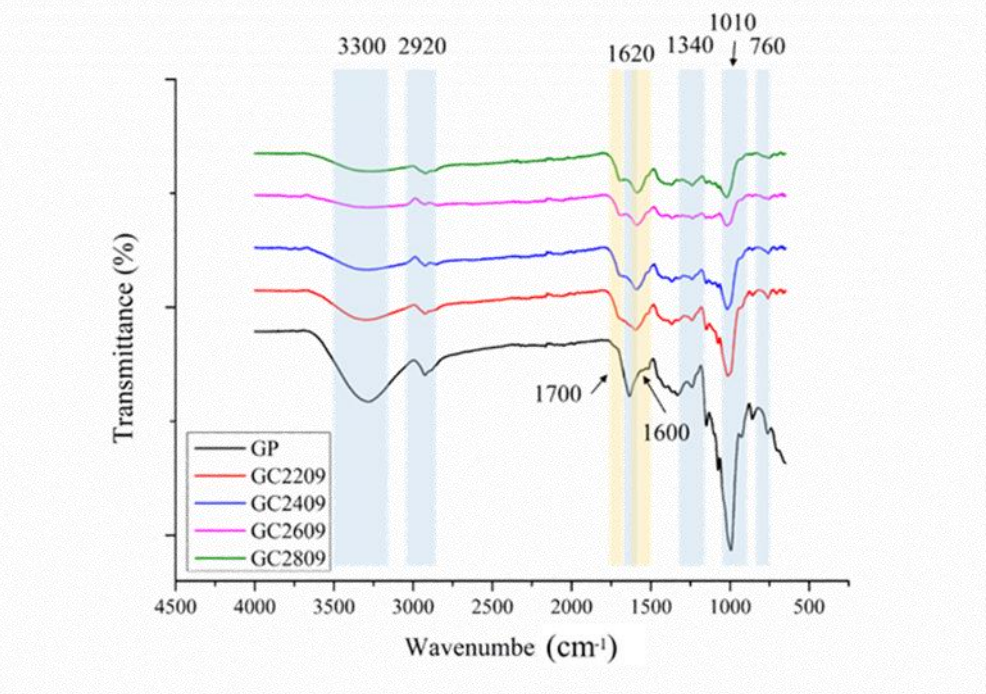


Figure 3. 20 ATR-IR of char varying from 220 to 280 $^{o}$C with 9 min.

### 3.2.3 Microwave Hydrothermal Treatment for ginger MFC

#### 3.2.3.1 Yield of MFC

The yield and Crystallinity Index of the MFC obtained from hydrothermal microwave processing at different temperatures (120 to 200 $^{o}$C) are shown in **Figure 3.21**. The yield decreases from 21.6% to 7.8% with increasing processing temperature; the greatest drop is between 120 to 140 $^{o}$C ($\Delta$=6.4%). This may be due to the loss of starch (see section **3.2.4.1**: yield of starch). The yield decreases with a stable trend per temperature interval ($\Delta$=2-3%).

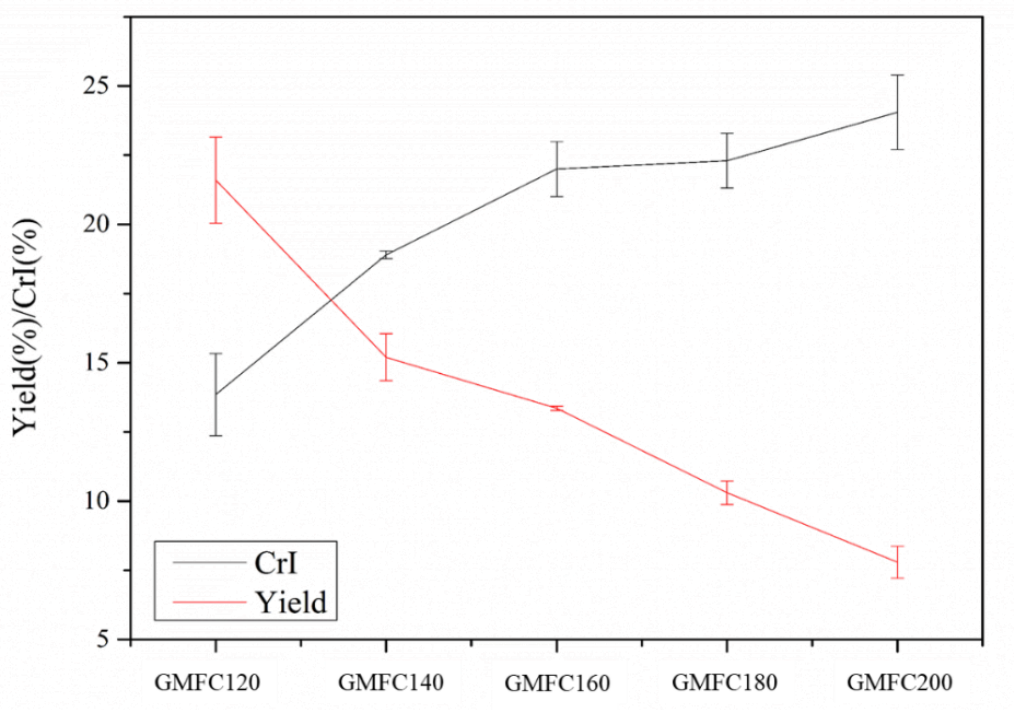


Figure 3. 21 Crystallinity Index (CrI) from solid state $^{13}C$ CPMAS NMR and Yield for GMFC. Values are average of duplicate experiments.

### 3.2.3.2 Thermogravimetric analysis

The thermograms and DTG of thermograms of GMFC are presented in **Figure 3.22**, from which, the composition can be calculated. The mass of moisture/volatiles account for 4-10% of the industrial ginger waste, and the mass of lignocellulose accounts for approximately 70%. The mass of residue appears to remain approximately the same (21-24%) despite different processing temperatures. Three major bands are observed in DTG. The first was due to the moisture and volatiles (4-8.5%) between 30-110 ℃. The second main band at 240-330 $^{o}$C is attributed to hemicellulose decomposition. Finally, the third peak between 330-390 ℃ is associated with the decomposition of cellulose.[233] Interestingly, the height of the band between 240 to 330 ℃ starts to reduce with the increasing microwave treatment and then can no longer be detected when the MHT temperature reaches 200 ℃ (blue arrow of DTG

in **Figure 3.22**). This can be explained by considering that the amorphous hemicellulose was hydrolysed gradually during the MHT and was almost removed at 200 ºC. Meanwhile, the main peaks referring to cellulose start to shift to the right (higher decomposition temperatures) with increasing MHT temperature, *i.e.*, DC120 (Td=349.5ºC); DC140 (Td=352.9ºC); DC160 (Td=353.1ºC); DC180 (Td=359.1ºC); DC200 (Td=364ºC). Implying that the decomposition temperature of cellulose increased after the MHT, this was due to CrI resulting in higher decomposition temperature.

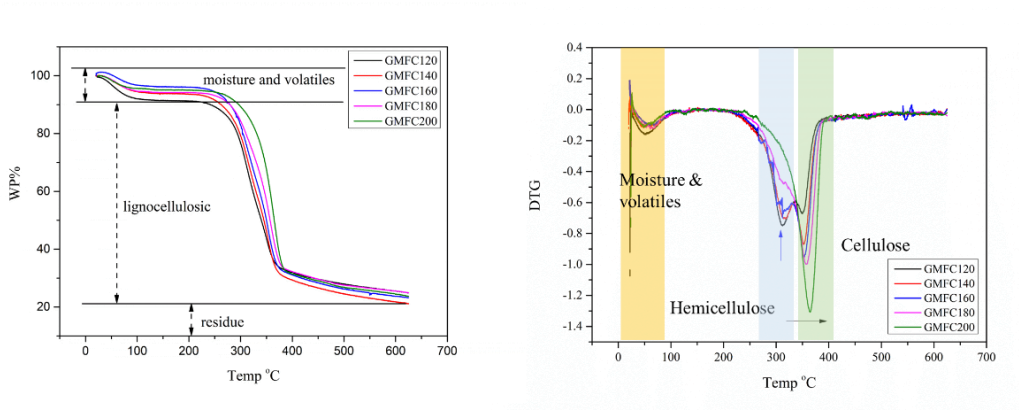


Figure 3. 22 TGA thermograms of GMFC with different temperatures.

### 3.2.3.3 X-Ray powder diffraction analysis (XRD)

The XRD patterns of ginger powder and MFC are presented in **Figure 3.23**, the peaks for crystalline cellulose were observed at 2θ: 16.5°, 22.5° and 34.5° corresponding to Miller Indices of 110, 200 and 004, respectively. With the MHT temperature increasing, the peaks at 22.5 ° and 34.5 ° became more intense implying higher crystallinity. This is due to the gradual removal of hemicellulose and amorphous cellulose during the microwave treatment.

The additional peaks at 15 °, 24.3 ° and 30 ° may be attributed to the insoluble calcium

salts (mostly $CaC_2O_4$) which exists in the plant cell wall and vacuoles,[69, 234] and the increasing temperature makes the peaks of salts more intense (loss of amorphous matters in high temperature increased crystal regularity of cellulose).

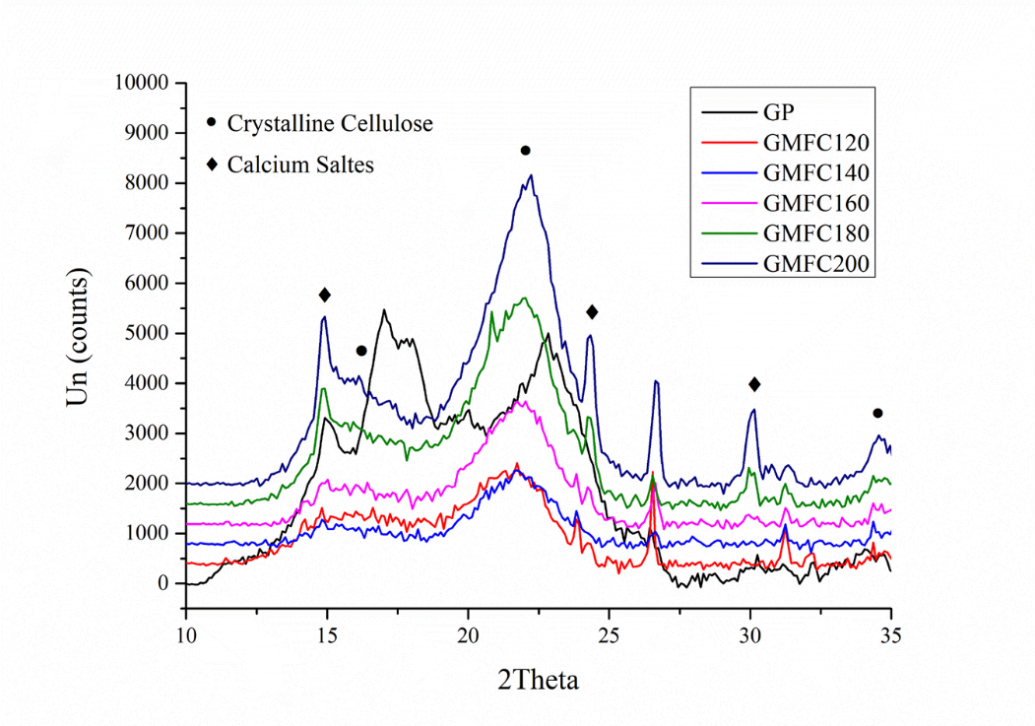


Figure 3. 23 XRD diffraction patterns of GMFC varying from 120 to 200 ºC.

### 3.2.3.4 ATR-IR

The ATR-IR confirms that the cellulose is the main component of the product, with residual hemicellulose or lignin as the impurities, the spectra is shown in **Figure 3.24**. The broad peaks between 3600 $cm^{-1}$ and 3100 $cm^{-1}$ correspond to the hydroxyl moieties in the carbohydrate backbone, with the 2920 $cm^{-1}$ C-H stretch attributed to cellulose/hemicellulose. The absorption bands at about 1745 $cm^{-1}$ are attributed to the carbonyl group which confirms the existence of lignin/hemicellulose in the biomass. Simultaneously, with the increasing microwave temperature, the intensity of the C=O bands decrease, this is attributed to the removal of hemicellulose/lignin;[235] and the O-

H bending vibration at 1635 $cm^{-1}$ is assigned to the bonded water which existing in the material. Finally, the sharp bands at about 1025 $cm^{-1}$ correspond to C–O and C-C stretching and confirm the presence of cellulose in resulting product from ginger residue.

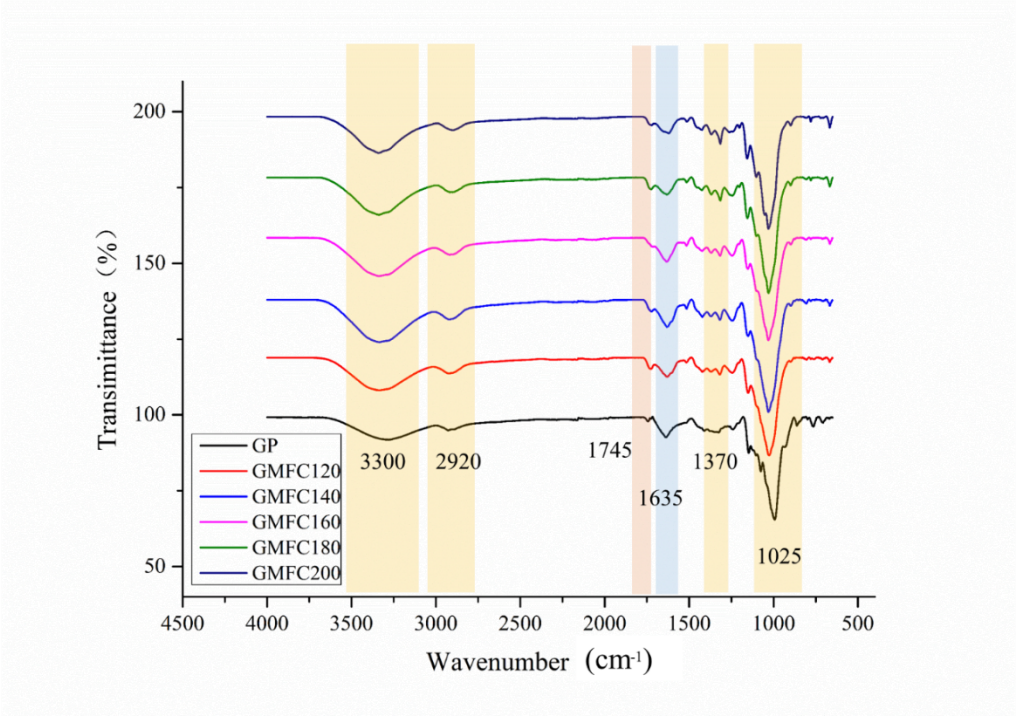


Figure 3. 24 ATR-IR of GMFC varying from 120 to 200 ºC.

### 3.2.3.5 TEM

TEM images successfully proved the defibrillated cellulose to be MFC via measurement of the fibril dimensions as shown in **Figure 3.25**. Both microfibrils (width = 10-100 nm, length=0.5-10 µm ) and elementary fibrils (3–5 nm in width and a few µm in length) in amorphous and crystalline regions were displayed [199, 203] and cellulose nanocrystals (width 5–70 nm and length <500 nm) were observed at 180 ºC and above. This can be explained by the two step Hy-MASS (Hydrothermal Microwave-assisted Selective Scissoring) concept previously discussed.[69] Firstly, the

non-cellulosic matters and amorphous parts of cellulose are selectively and progressively hydrolyzed from the lignocellulosic matrix. Secondly, the softened amorphous cellulose and lignin which are embedded in MFC were released through the proton transfer mechanism.

Meanwhile, the residual amorphous matters can also be observed in TEM images (grey regions which surround the nanofibrils),[69] and the grey regions seem to reduce with increasing temperature which corresponds to the gradual removal of amorphous cellulose. The dark grey regions may be *pseudo*-lignin which is defined "an aromatic material that yields a positive Klason lignin value that is not derived from native lignin".[205] As can be seen at **Figure 3.24**, the carbonyl band (~1745 $cm^{-1}$) re-emerges at temperature above 180 $^{o}$C indicative of pseudo-lignin from decomposition amorphous cellulose.

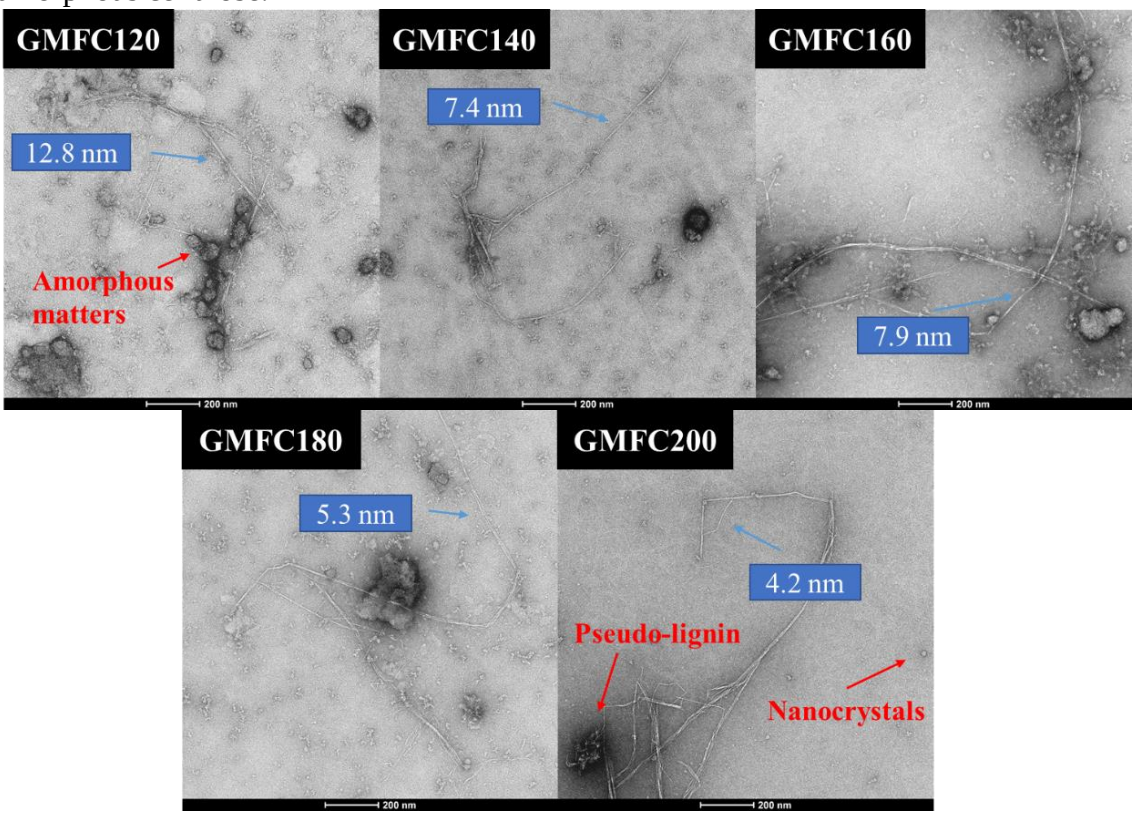


Figure 3. 25 TEM images of GMFC (120 to 200 $^{o}$C) (scale bar = 200 nm). The width of the MFC were labeled.

### 3.2.3.6 Solid state $^{13}$C CPMAS NMR and Crystallinity Index (CrI)

The stacked $^{13}$C CPMAS spectra of ginger powders and GMFC processed at different MHT temperatures are presented in **Figure 3.26**. The carbonyl carbon signals at approximately 174.5 ppm are assigned with polysaccharides which exist strongly bound in cell walls (*e.g.* hemicellulose).[187] The signals ranging from 110 ppm to 60 ppm are attributed to cellulose carbons (C1 to C6).[191, 236, 237] The signals at about 20 ppm may be associated to acetyl group in hemicelluloses.[195, 238] The signals of hemicellulose (174.5 ppm and 20 ppm) start to reduce with increasing MHT processing (120 to 200 $^{o}$C), especially after 180 $^{o}$C, indicating depolymerization and hydrolysis of the amorphous, non-cellulosic materials. Meanwhile, the signals of cellulose show interesting changes: the signals for the crystalline regions in C4 and C6 (89 ppm and 66 ppm, respectively) begin to appear and increase with higher temperature. The ratio of cellulosic surface/amorphous and interior/crystalline for C4 and C6 decreases,[69] implying that the amorphous matter from the cellulose surface were also gradually removed by MHT. Thus the crystalline character of cellulose increases (see arrows in **Figure 3.26**). This result corresponds well to the TGA and XRD data discussed earlier.

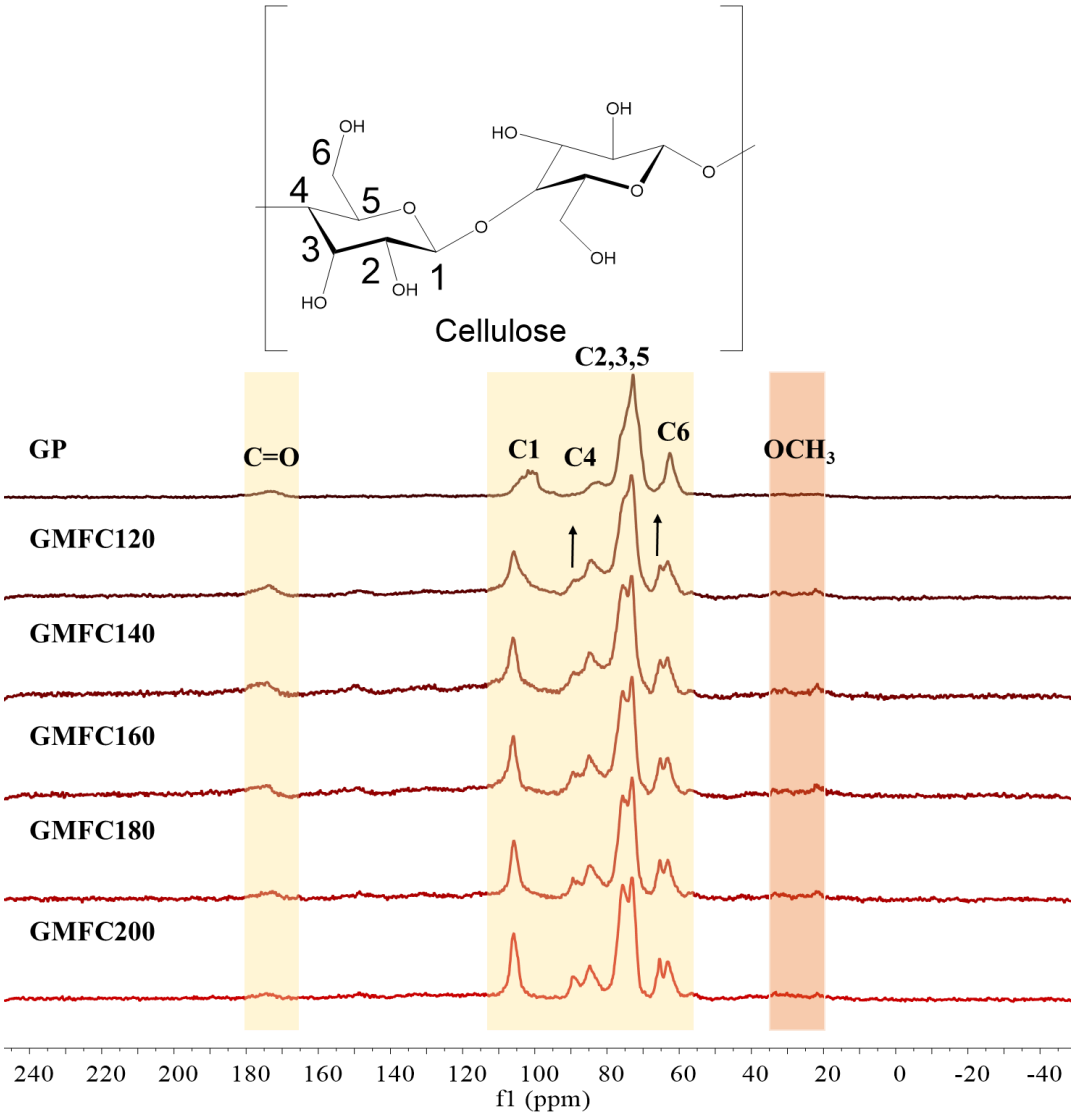


Figure 3. 26 $^{13}$C CPMAS NMR spectra of GMFC with a labelled illustration of a cellulose moiety. Arrows show the ratio of crystalline/interior: amorphous/surface cellulose.

The change in CrI (crystallinity index) of GMFC calculated from $^{13}$C CPMAS spectroscopy are presented in **Figure 3.21** and goes up from13.9º to 24.1º with the increasing temperature (120 to 200 ºC). A rapid rise between 120 to 160 ºC (approximately 8.1º) is observed. This can be explained that the non-crystalline region in biomass were gradually and selectively removed (scissoring) from the lignocellulosic matrix by MHT, and after 180 ºC, due to the softened amorphous cellulose and lignin embedded which in cellulose microfibrils was released via a

proton transfer mechanism,[69] the CrI increased slightly (Δ=2°).

### 3.2.3.7 WRV

The water retention value (WRV) of GMFC's produced is presented in **Figure 3.27**. The raw ginger powder has a lower hydration capacity (2-3 g water per g) than the GMFC products. It is well known that the insoluble cellulose can hold water by absorbing water in their fibril network through fibre swelling properties.[69] Smaller particle size and larger surface area would increase the WRV of cellulose.[211, 239] The hydrothermal microwave process reduces particle size, increases surface area of the material due to the removal of amorphous matter, thus improving hydration capacity. However, with increasing temperature, amorphous regions were removed and the crystalline cellulose holds less water due to the compact and strongly bonded (via hydrogen bonding) structure, resulting in the more hydrophobic cellulose.

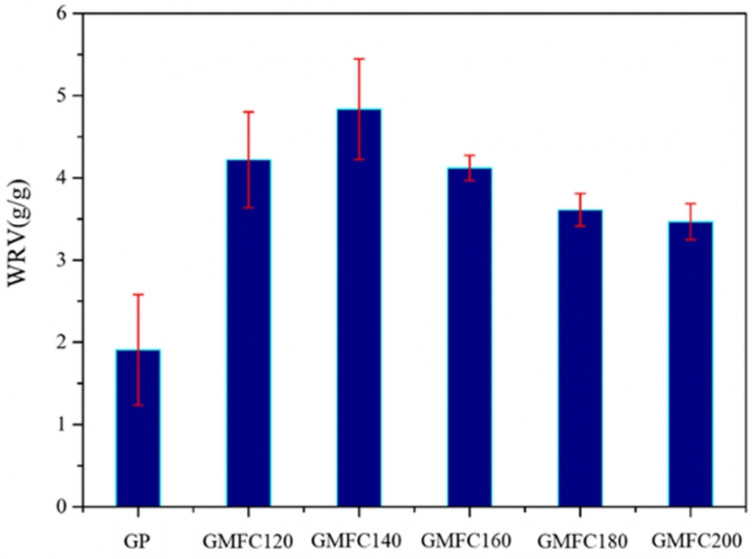


Figure 3. 27 WRV of GMFC (g of water per g of dry sample). Values are average of duplicate experiments.

Thus, within the context of a spent ginger waste biorefinery microwave processing produces microfibrillated celluloses with improved water retention capacity compared

to the virgin material. The ability to retain water makes for interesting applications such as hydrogels and/or biobased rheology modifiers for use in food and non-food applications (pharmaceuticals and cosmetics).

#### 3.2.3.8 $N_2$ Adsorption porosimetry

The textural properties (surface area, pore volume and pore diameter) of the GMFC from ginger residue were analysed using a Micromeritics TriStarII Surface Area and Porosity Analyser and the results are presented in **Figure 3.28**. The specific surface area (SSA) and pore volume (PV) follow a similar trend: the values decrease to a minimum in GMFC160 (3.6 $m^2$ $g^{-1}$ and 0.000762 $cm^3$ $g^{-1}$, respectively), then increase to a maximum in GMFC200 (13.0 $m^2$ $g^{-1}$ and 0.003 $cm^3$ $g^{-1}$, respectively), which corresponds to the gradual removal of amorphous hemicellulose/lignin from the cellulosic matrix. The BJH average pore diameter is between 16 to 20 nm and thus these materials can be classified as mesoporous.[69] However, the analysis of "soft materials", like cellulose, via $N_2$ porosimetry is not always reliable. The extended high temperature degassing period (>100 $^oC$, several hours), causes cellulose to aggregate via irreversible interfibrillar hydrogen bonding[214, 215] through a process known as hornification. The pores collapse and the structure becomes extremely rigid. This process is very difficult to control. So, alternative methods like cryoporosimetry (DSC and NMR), Congo red dye adsorption or radiation scattering may be better to determine porosity.[218, 220]

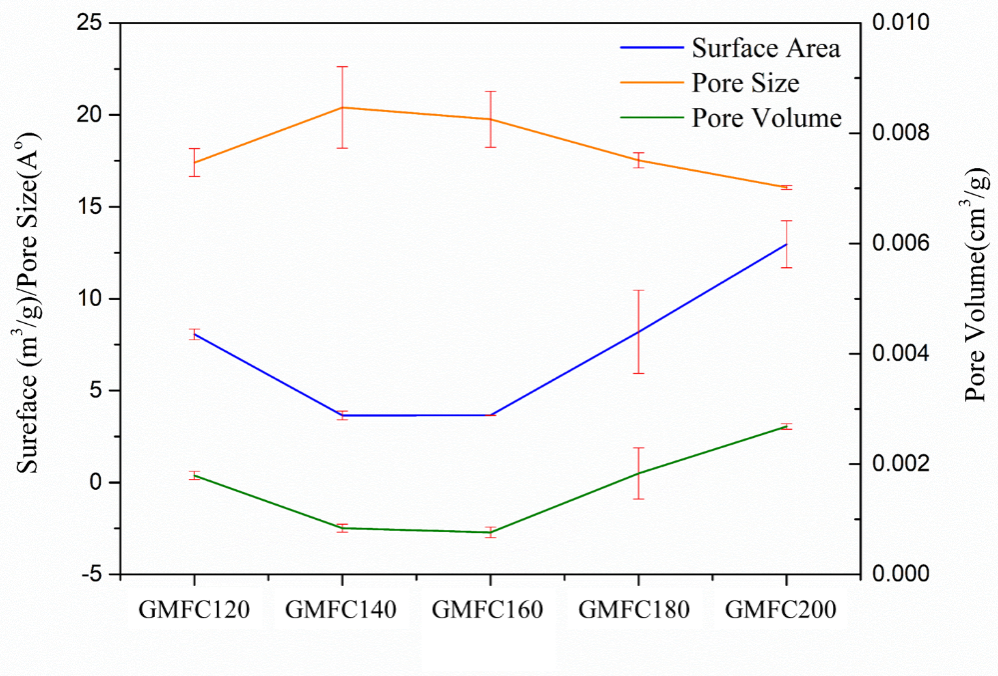


Figure 3. 28 Porosimetry data (BET Specific surface area – SSA, BJH pore volume and BJH average pore size) for GMFC.

### 3.2.3.9 Elemental analysis

The percentage composition of carbon, hydrogen and nitrogen for ginger powder and its GMFC processed with different temperatures (120 to 200 $^{o}$C) are displayed in **Figure 3.29**. The carbon content increase slightly after MHT (39.7 % to 41.5%) and continues to rise with increasing temperature (41.5% at 120 $^{o}$C to 43.4% at 200 $^{o}$C). The presence of nitrogen can contribute to ammonium groups which belong to proteins in the biomass. The nitrogen content of raw ginger powder is about 1.42% (the protein content can be determined with a conversion factor of 4.64).[240] After MHT, due to the hydrolysis of the proteins, the content decreases to about 0.5%.

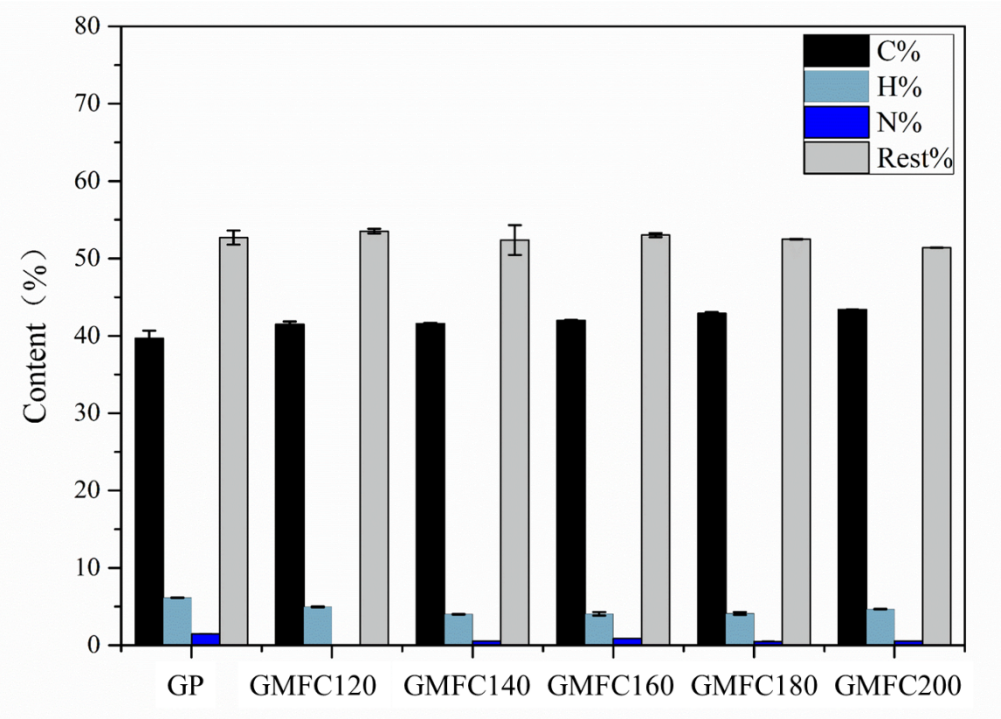


Figure 3. 29 CHN analysis of ginger and its defibrillated cellulose obtained from MHT (120 to 200 $^{o}$C)

### 3.2.3.10 Zeta potential

When a material is immersed in a liquid, the functional groups on surface will contact and react with the surrounding medium resulting in a surface charge. The charge can attract the opposite ions, and the counter ions accumulate and form the so-called electrochemical double layer, the sum of the initial surface charge and the accumulated layer is defined as zeta potential. This parameter provides some information on stability of the dispersed particles, surface functionality and interaction between dissolved compounds in liquid and surface of the material. Thus, for nanoparticles, zeta potential plays a very important role in physical stability of a colloidal dispersion which reflecting the ability of the nanoparticles to electrostatically push each other. The magnitude of the zeta potential electrically indicates repulsion between the particles: when the value is around ±40-60 mV, a good stability colloid can be formed.

With the decreasing of zeta potential, the colloid will show moderate stability (±30 - 40 mV) and incipient instability (±10-30 mV). Very low zeta potential values (±0-5 mV) which have the high electrostatic attraction but low repulsion between particles tend to rapidly coagulate or flocculate.[241]

The zeta potential of GMFCs obtained from MHT with different temperatures (120 to 200 °C) determined in neutral water are shown in **Figure 3.30**. It can be seen that microwave treatment has a big influence on the zeta potential of the GMFC. The zeta potential of initial untreated ginger is approximately -33 mV, which increases significantly after MHT. At 120 °C, the value of corresponding GMFC is about -17 to -20 mV. With increasing temperature, the zeta potential decreases slowly from around -23mV (140 °C) to -24 mV (160 °C), -26 mV (180 °C). However, after 180 °C, the zeta potential sharply drops to -32.5 mV (200 °C). The higher negative zeta potential (in water) of GMFC contributes to high repulsion between particles, implying better hydrophobic performance.[242]

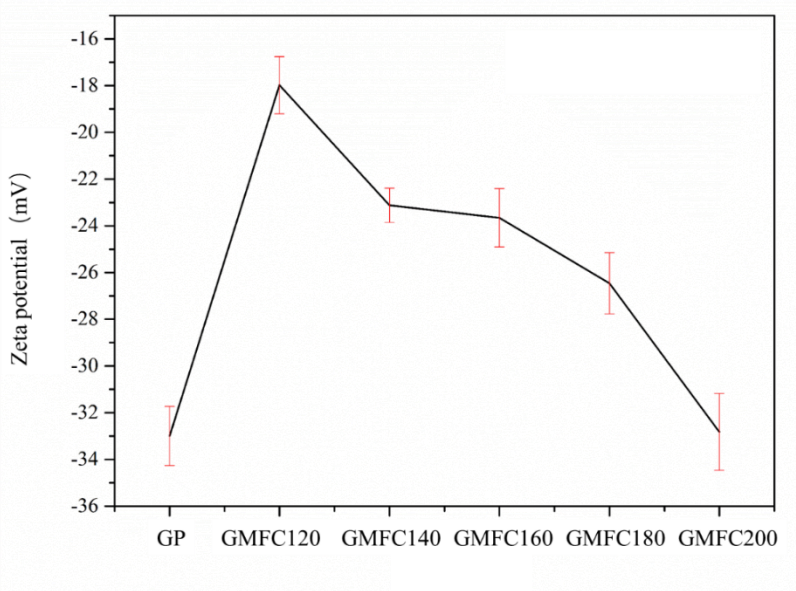


Figure 3. 30 Zeta potential of GMFC after MHT.

### 3.2.3.11 Hydrogel formation

The polysaccharide-based hydrogels extracted from biomass (*e.g.* food waste) have attracted extensive attention due to their excellent performance including biodegradability, high-water retention value, high surface to volume ratio and high tensile strength.[243, 244] The chemical and physical interactions determine the hydrogel 3D network structure. Chemically, covalent bonding provides strength and stability of the network and followed by physical interaction. When water fills voids within the material, the fibres entangle via hydrogen bonding or van der Waals forces.

Even though cellulose alone is not water-soluble in water, the entanglement of micro- and nanofibers results in a cross-linking 3D network structure. The GMFC was successfully characterised as a nanostructured material (MFC). The gel formation was qualitatively assessed through the tube inversion test (see **Figure 3.31**). With higher MHT temperature, the GMFC become easier to form hydrogels (5% to 2.5%). This may due to high surface area and aspect ratio. However, the ginger powder after Soxhlet extraction hardly formed a hydrogel even with the increasing concentrations (around 5%). This is due to the cellulose still being in its passive, hydrophobic state with very strong internal hydrogen bonding. Conversely, the GMFC has high-affinity for fibres and water, hence, they can form the hydrogel at relatively low concentrations.

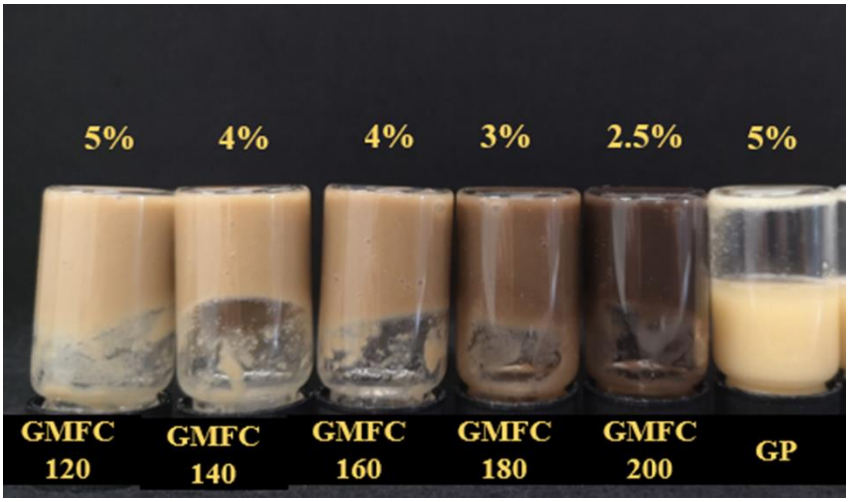


Figure 3. 31 Inversion test for hydrogel at minimum concentration

In comparison with other biomass types within the GCCE, for the MFCs produced at 120 $^{o}$C, the minimum gel formation concentration of almond husk, cassava peel, peas, and orange peel are 2% (w/v), 5% (w/v), 4% (w/v) and 1.5% (w/v), respectively. According to de Melo's study,[69] the minimum concentration of commercial pure CNC is about 3% (w/v). Unlike pure CNC which is 100% cellulose, our materials still retain some hemicellulosic and/or lignaceous matter. These additional materials provide enhanced anionic surface charges enabling strong gel formation even at low concentration.[126] For example, pectin if retained within the MFC, can form strong networks.[245]

### 3.2.4 Microwave Hydrothermal Treatment for starch

3.2.4.1 Yield of starch

The starch yield with respect to microwave processing temperature is displayed in **Figure 3.32**, which shows an initial increase, peaking at 140 $^{o}$C (48.6%) before slowly decreasing to 40.2% at 180 $^{o}$C, followed by a sharp decrease at 200 $^{o}$C (1.95%). It is well known that microwave-induced heating can lower the decomposition temperature

of biopolymers such as cellulose, hemicellulose and starch by approximately 100 $^{o}$C. Thus, as the temperature increases starch is initially leached without any significant decomposition but at 200 $^{o}$C, significant decomposition occurs which is also noted by the number and type of compounds detected by HPLC in the hydrolysate.

Thus, spent industrial ginger waste is also a source of starch. Close to 50% by weight of starch can recovered at 140 $^{o}$C with respect to dry input feedstock. Starch is a commodity chemical with multifarious applications.

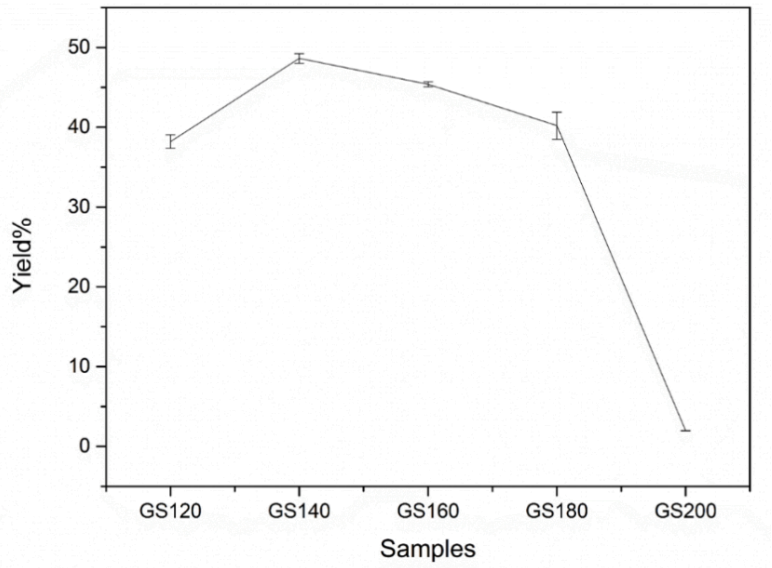


Figure 3. 32 Yield for ginger starch with different temperatures.

### 3.2.4.2 NMR

The NMR spectra provides evidence for the possible presence of starch as the component of the hydrolysates, and the stacked $^{13}$C CPMAS spectra of starch which extracted from hydrolysates at different temperatures are presented in **Figure 3.33**. The signals for starch carbons (C1 to C6) range from 110 to 55 ppm, the peaks at approximately 20 ppm may refer to acetyl group in polysaccharides [187, 194]

Interestingly, even with the increasing MHT temperature, the signals of starch still keep the same intensity meaning that the starch structure is not changing, and the temperature had no obvious influence on the properties of starch. At the same time, a sharp peak was observed after 160 $^{o}$C, this may due to the complex compounds which appeared in high temperature by the hydrolysis of lignocellulose.

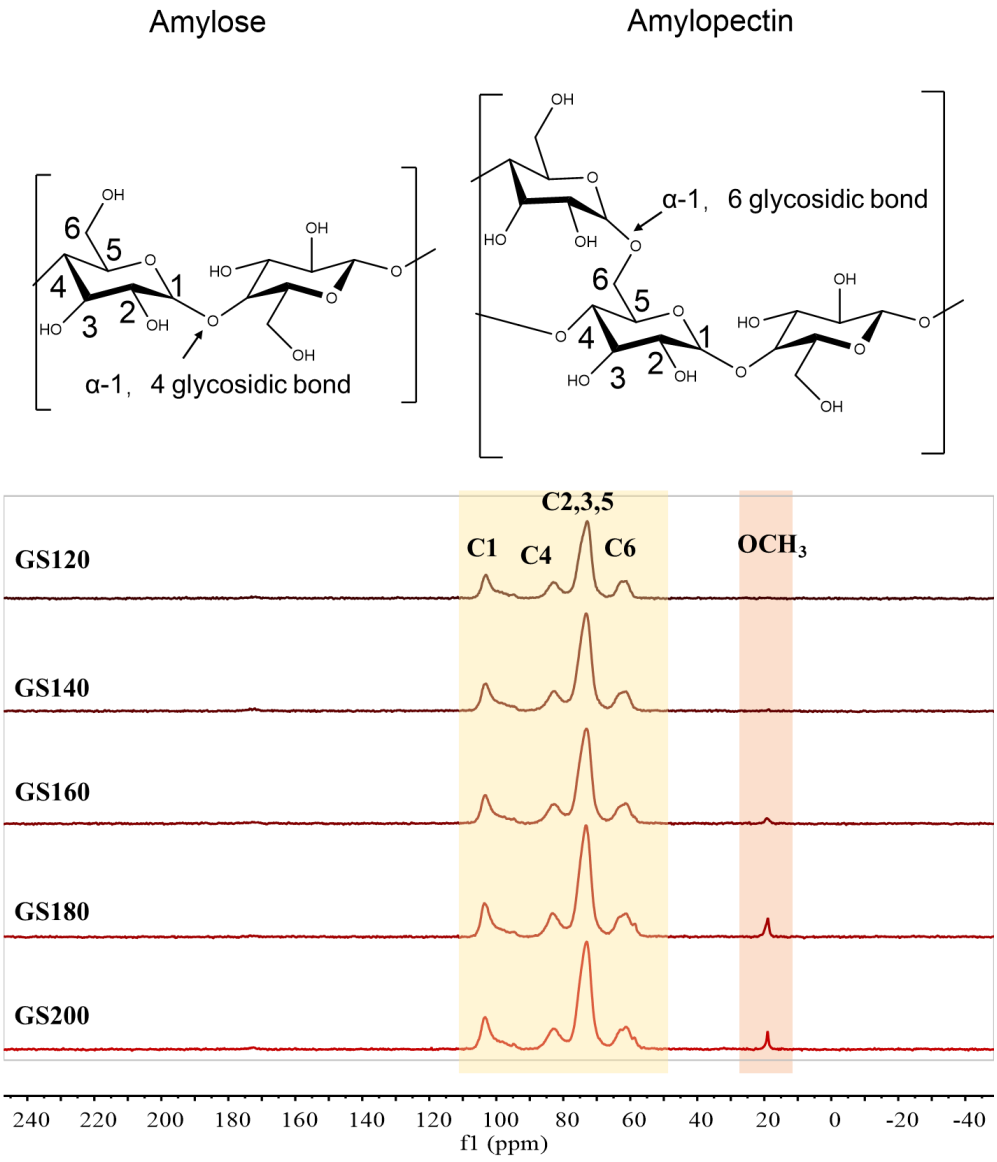


Figure 3. 33 $^{13}$C CPMAS NMR spectra of starch with a labelled illustration of a starch moiety.

### 3.2.4.3 ATR-IR

ATR-IR provides the evidence to confirm the white matter which extract from hydrolysates was starch, and the spectra was shown in **Figure 3.34**. The common signals of starch were displayed: the broad bands at about 3300 $cm^{-1}$ are attributed to O-H stretching vibration which referring to hydroxyl moieties in starch; the bands at 2930 $cm^{-1}$ and 1370 $cm^{-1}$ are related to C-H stretch, and the peaks located at 1640 $cm^{-1}$ may refer to bonded water which exists in biomass. Finally, the bands at 1150 $cm^{-1}$ and 1020 $cm^{-1}$ are associated with C-O or C-C stretching vibration in starch.

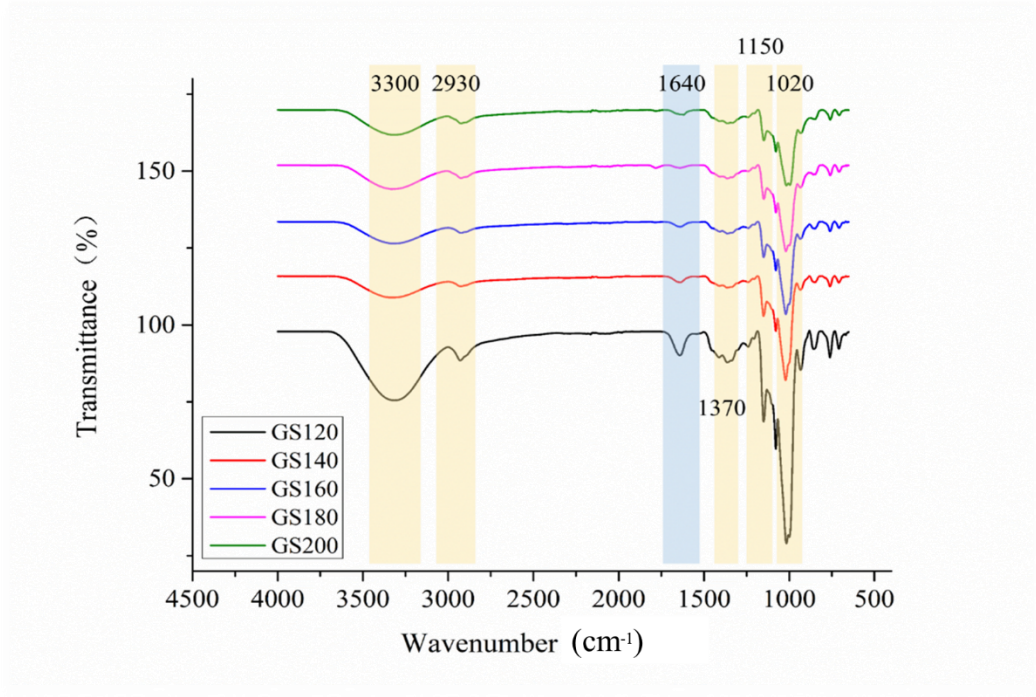


Figure 3. 34 ATR-IR of ginger starch ranging from 120 to 200 ºC.

### 3.2.4.4 Thermogravimetric analysis

The thermograms and DTG of thermograms of starch obtained from MHT (120-200 ºC) are presented in **Figure 3.35**. All samples contain same moisture and volatile content (around 10%), and residue content of GS120, GS140 and GS200 is quite similar (approximately 22%). Interestingly, for GS160 and GS180, the residues are

about 16%, this may due to that with higher temperatures, increased leaching of metal salts (*e.g.* K, Mg, Ca).

The DTG shows only two bands: i. the first peak (Td=30-110 ℃) is attributed to loss of moisture and volatile content, and; ii. the second stronger transition (Td=330-310 ℃) corresponds to starch decomposition. It can be observed that the decomposition temperatures of GS120, GS140 and GS200 are similar (about 310 $^{o}$C) while for GS160 and GS180 they present higher thermal stability (320 $^{o}$C). The difference may be due to highly crystalline structures [246] which are formed at high temperature via removal of amorphous regions. Meanwhile, the sharp peaks also indicate that the starch which from MHT treatment is relatively pure, this provide a feasibility approach for production of starch via microwave from high starch content agro waste.

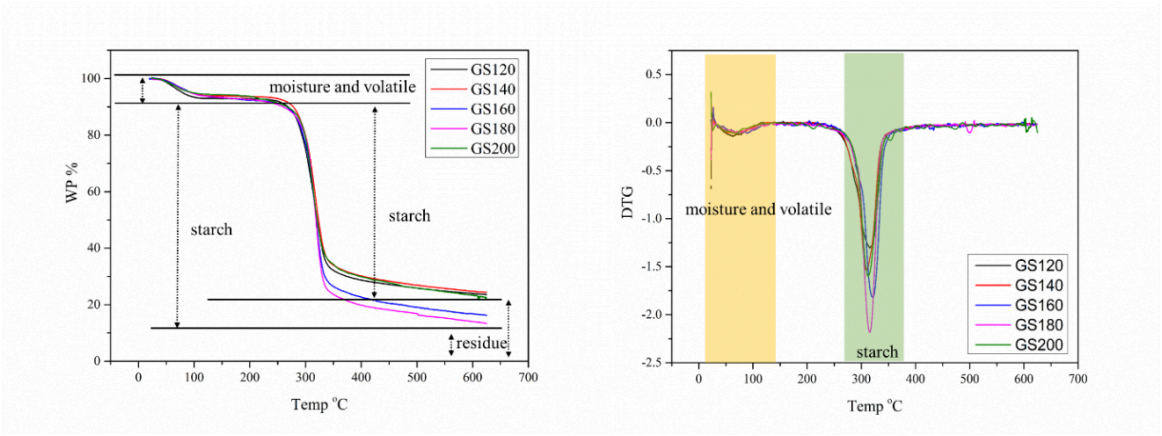


Figure 3. 35 TGA thermograms of starch with different temperatures

### 3.2.4.5 Elemental analysis

The percentage composition of carbon, hydrogen and nitrogen for starch obtained from ginger waste via MHT procedure is displayed in **Figure 3.36**. The carbon content increases slightly (39.7% to 43.4 % from 120 to 180 $^{o}$C) but then reduces to 41.4%. Nitrogen content is observed before 140 $^{o}$C albeit with a very low percentage (0.3%

to 0.4%) but then can no longer be detected at higher temperature.

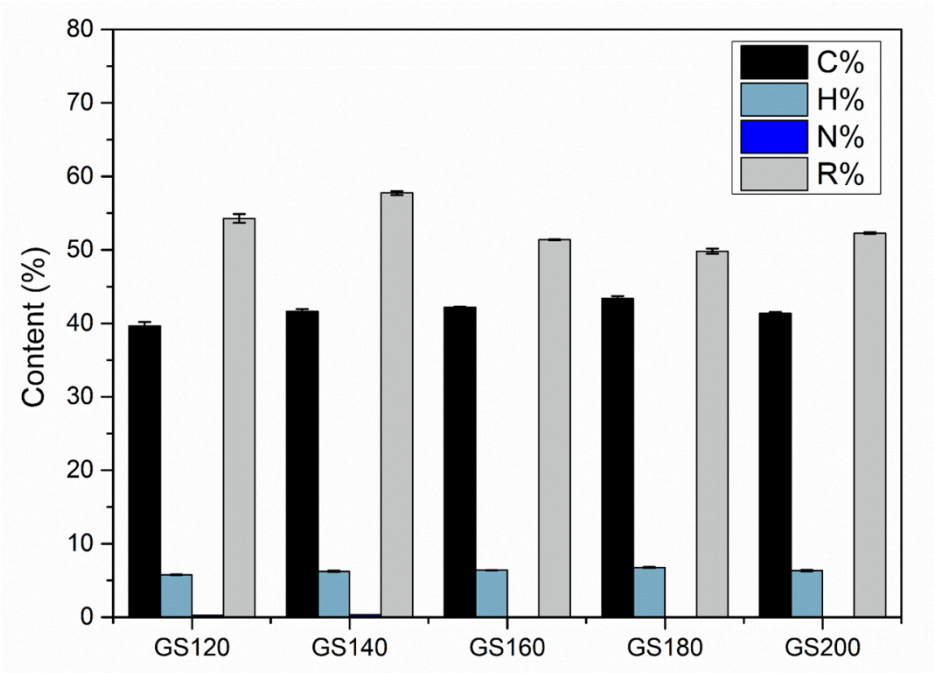


Figure 3. 36 Elemental analysis of starch obtained from MHT.

### 3.2.5 Microwave Hydrothermal Treatment for Hydrolysates

The HPLC analyses of the hydrolysate from hydrothermal microwave processing of ginger residues are summarised in **Figure 3.37**. In general, the yield of sugars (*e.g.* glucose, xylose) decrease with increasing microwave processing temperature, and the concentrations of levoglucosan, lactic acid, formic acid, acetic acid were opposite. A small number of 5-hydroxymethylfurfural (HMF) and furfural are observed after 180 ℃. The reason could be explained by the microwave-assisted hydrolysis of polysaccharides in water below 220 ℃: glucose and xylose were mainly derived from amorphous cellulose and hemicellulose of the ginger residue. In high temperature especially after 180 ℃, part of glucose converted to HMF which was regarded as the major secondary byproduct from glucose degradation, and xylose converted to the furfural, acids are the final product of biomass depolymerization. Herein the yield of

the sugars reduced and acids, HMF, furfural increased at higher MHT temperatures.

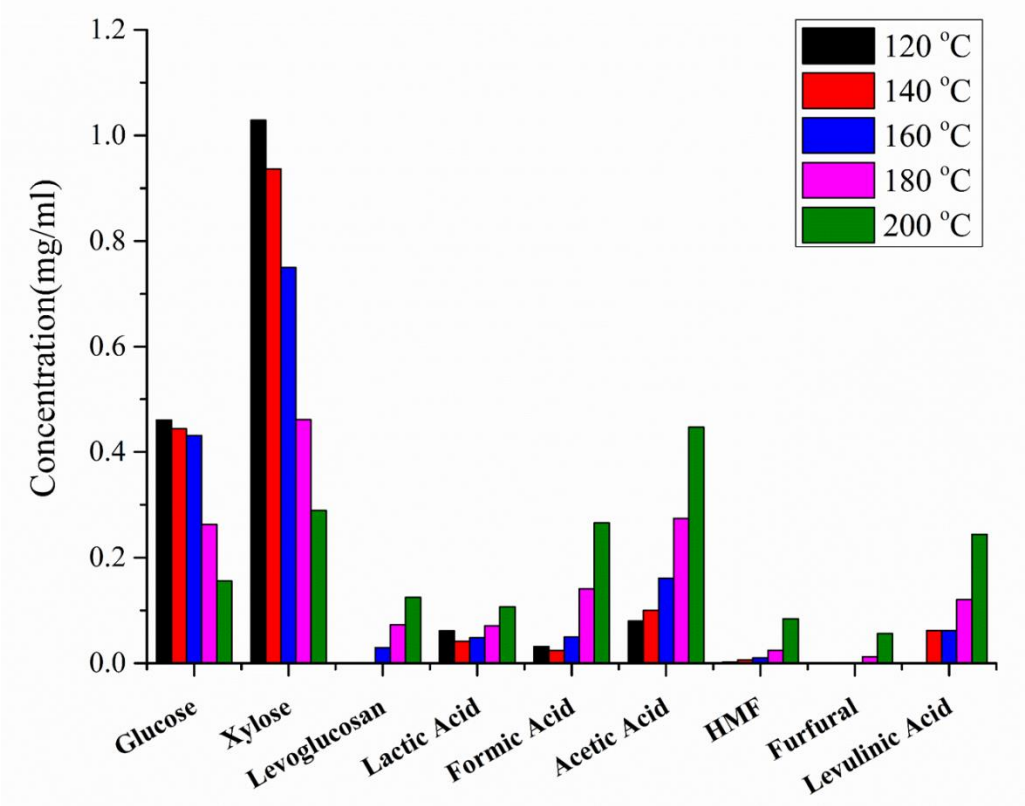


Figure 3. 37 Products and sub-products from hydrolysate after MHT.

## 3.3 Part C Towards Novel composite bioboards and structural insulation panels from waste agri-fibres

The synthesis and characterization of novel biocomposites, herein termed bioboards, derived from agricultural residues (wheat straw, barley straw and lemongrass) and aqueous biosilicate solutions, as binder, are reported. The addition of a small amount of protein significantly enhances board strength. The internal bond strength (IBS) increases from 0.0498 to 0.0688 $N/mm^2$. Prior to adhesion, the agricultural residues were de-waxed (ethanol), making them more amenable to aqueous wetting. The aqueous biosilicate binder was obtained via KOH-assisted hydrothermal leaching of spent ashes derived from the combustion of wheat straw. The concentration of biosilicate was determined by ATR-IR spectroscopy and compared with commercial silicate solution (K120). Zirconia powders were introduced to increase internal bond strength and flame retardancy of bioboards. The presence of zirconia was evidenced by powder X-ray diffraction studies. Thus, the bioboards reported represent 'greener' alternatives to conventional, commercial particle and medium density fiber boards because they are wood-free, use waste as a renewable resource (agricultural straws) and, importantly do not use any harmful phenol-formaldehyde and isocyanate binders. In an attempt to develop a range of novel biobased foam materials as potential core layers within structural insulation panels (SIPs), initial trials were conducted using waste paper and foaming agents. The preparation of novel foam materials mixed with nanostructured cellulose derived from depectinated orange peel residues (OPR) was attempted but with limited success. The composites were characterised via TGA IR,

SEM and NMR to see the chemical change of combination. To investigate water resilience of the inner layer via chemical modification, waste paper and cellulose, were silylated (aminopropyltriethoxy silane, APTES). Qualitative contact angle test showed increased hydrophobicity.

### 3.3.1 Ash yield of lemon grass and wheat straw

The ash remaining after combustion of wheat straw and lemongrass at various temperatures is shown in **Table 3.4**. It can be observed that the ash remaining for lemongrass and wheat straw decrease (7.7% to 5.0% and 4.7% to 4.2%, respectively) with rising temperature (400 to 800 $^{o}$C). The ash remaining of lemongrass were a bit higher than wheat straw. Interestingly, there is an obvious mass loss for lemongrass samples from 600 to 800 $^{o}$C, this may attribute to some components which is hard to decompose in samples.

Table 3. 4 Ash remaining after burning

| Sample | Type | Temperature (°C) | Ash Remaining (%) |
|---|---|---|---|
| LA-1 | Lemongrass | 400 | 7.7 |
| LA-2 | Lemongrass | 600 | 7.3 |
| LA-3 | Lemongrass | 800 | 5.0 |
| WA-1 | Wheat | 400 | 4.7 |
| WA-2 | Wheat | 600 | 4.5 |
| WA-3 | Wheat | 800 | 4.2 |

#### 3.3.1.1 ATR-IR Analysis

The IR spectra for ashes generated from the combustion of lemon grass (LA1-LA3) and wheat (WA1-WA3) are depicted in **Figure 3.38**. Absorption bands for carbonate are noted at 1410 cm$^{-1}$ to 1490 cm$^{-1}$ in both wheat (WA1) and lemongrass ash (LA1) burned at 400 $^{o}$C for 2 h. But as the temperature increases, these bands are less evident

due to carbonate decomposition. The intensity of broad silicate asymmetric stretching band from 900 $cm^{-1}$ to 1190 $cm^{-1}$ significantly decreases as the temperature increases. The symmetric bridge stretching vibration at 784 $cm^{-1}$ is assumed with Si-O-Si and disappear with rising temperature. However, the IR data should be treated with caution as there could some uncarbonised biomass which retains significant organic content (C, H, O) which also have absorption bands in the above-said regions.

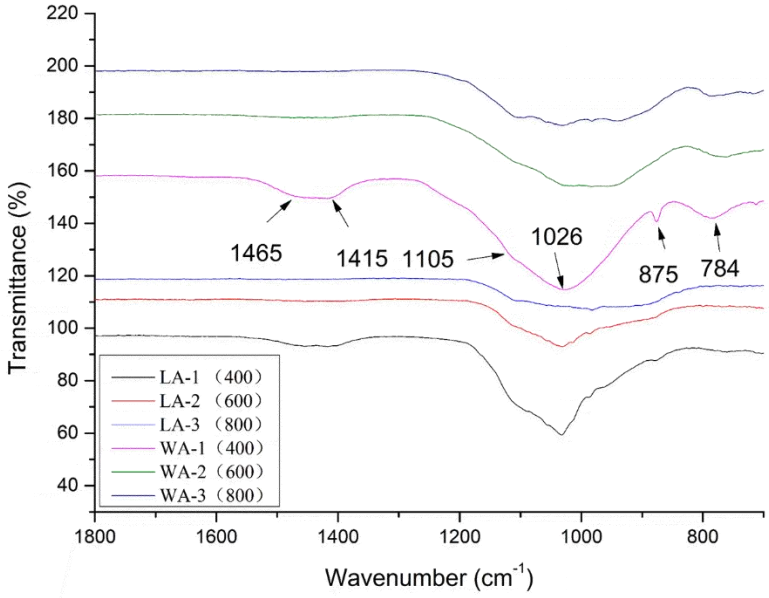


Figure 3. 38 ATR-IR of lemongrass and wheat ashes obtained at different processing temperatures.

### 3.3.1.2 XRD Analysis

The **Figure 3.39** shows XRD patterns of lemongrass and wheat ash burned at different temperatures. Signatures for different crystallographic forms of potassium chloride are numbered 1 whilst crystalline silicate dioxide in numbered 2. Further interpretation of this data is still needed. Quartz, tridymite and cristobalite are the common crystalline phases of silica, and they are always formed with $Q^4$ tetrahedral crystal structures.[247] In plants, soluble silica has a higher concentration than that in the soil because of the

flora' strong ability to accumulate silica. Silica content between plant type varies, with rice having one the highest concentrations of silica: rice >> wheat > triticale > sorghum > rye > maize > barley.[248] The roots will store silica firstly in the form of silicic acid. Then within the transpiration stream the silica acid moves via the xylem to shoots, stems and leaves. The latter usually contains high silica concentration due to evaporation and polymerization.

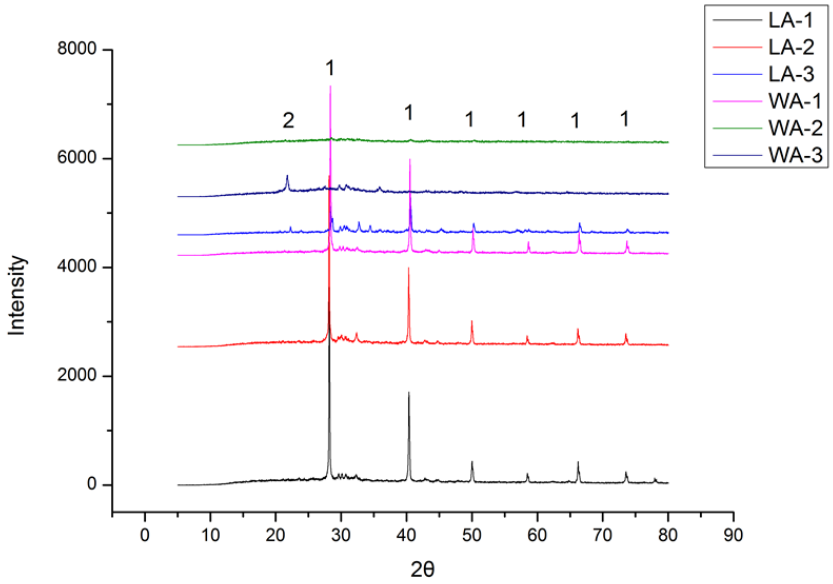


Figure 3. 39 XRD patterns of lemongrass and wheat straw ashes after 2 h combustion from 400 to 800 ℃.

### 3.3.2 Biosilicate leaching

#### 3.3.2.1 Silica binders

As a polymeric, inorganic and alkaline silica based materials, the silica binders is composed of alkali material ($Na_2O$ or $K_2O$), silica ($SiO_2$) and water, and the performance (viscosity, solubility and reactivity) of final silicate binders is determined by mass ratio of silica and alkali material.[173] The silicate solutions leached from biomass ashes were used as binder instead of traditionally used urea, formaldehyde,

phenol and isocyanate systems. Compared to the organic binders which include the Volatile Organic Compounds (VOCs), the silica solution is non-toxic and non-flammable. Simultaneously, the silicate binders have some other advantages such as high tensile strength, strong bacteria and water resistant abilities.[173] This makes it a promising adhesive in the future.

The mechanisms of the silica binder bond can be explained by dehydration (evaporation of water) and chemical mechanism, namely, i. the hydroxyl groups on the surface of the silicate form siloxane bonds (Si-O-Si) with dehydration and results in a three-dimensional network;[249] ii the silica binders can also simultaneously react with acidic/soluble metal compounds and polymerize.

In this section, the hydrothermal extraction of silicate solution from biomass ashes (resultant solution from herein is termed biosilicate) at different ash:water ratios and different times and the determination of sodium and potassium silicate concentration using titrimetric and infra-red spectroscopic methodologies is discussed. The biosilicate solution acts as our binder instead of traditionally used urea, formaldehyde, phenol and isocyanate systems.[250, 251] The biosilicate solution is compared with commercial silicate solution, namely, K120, as supplied by PQ Corp.

#### 3.3.2.2 Determination of concentration of $K_2O$ and $SiO_2$

The silica content can be determined directly through titration. However, it is a complex and time-consuming procedure, so an IR method was developed by testing the area of the IR absorbance bands (1250-650 $cm^{-1}$) for known K120 samples as standard. Normally, for solid silicate, three strongest absorbance bands relating to

silicate are centered at around 1070 $cm^{-1}$ (with a high frequency shoulder at around 1200 $cm^{-1}$), 810 $cm^{-1}$ and 457 $cm^{-1}$: the most intense peak contributes to the asymmetrical stretching of Si-O-Si bond, the band at about 810 $cm^{-1}$ is assumed with symmetrical stretching /bending of Si-O-Si bond. The band at 457 $cm^{-1}$ correlates to rocking /bending of bridging O-atom.[173] But in silicate solution, due to the negative influence of strong absorption of water, the main peaks related to Si-O-Si bond seem to be at approximately 1010-977 $cm^{-1}$ (see **Figure 3.40**). When the biosilicate solution was diluted to different concentrations (5, 10, 20, 30 and 50% of the original concentration) and recorded by ATR-IR spectra (**Figure 3.40**), the absorption bands for silica (shown enlarged in **Figure 3.41**) changed with the effect of water. In this thesis, the strongest main peaks were studied to determine concentration of silicate content in solutions due to the influence of water absorption on the determination of band location and area.

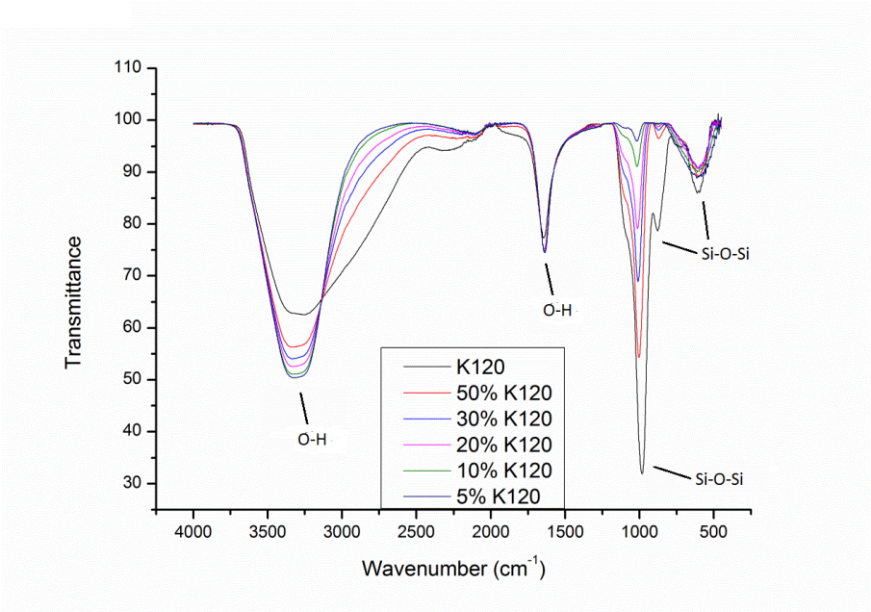


Figure 3. 40 ATR-IR of K120 solution at various concentrations relative to the original solution

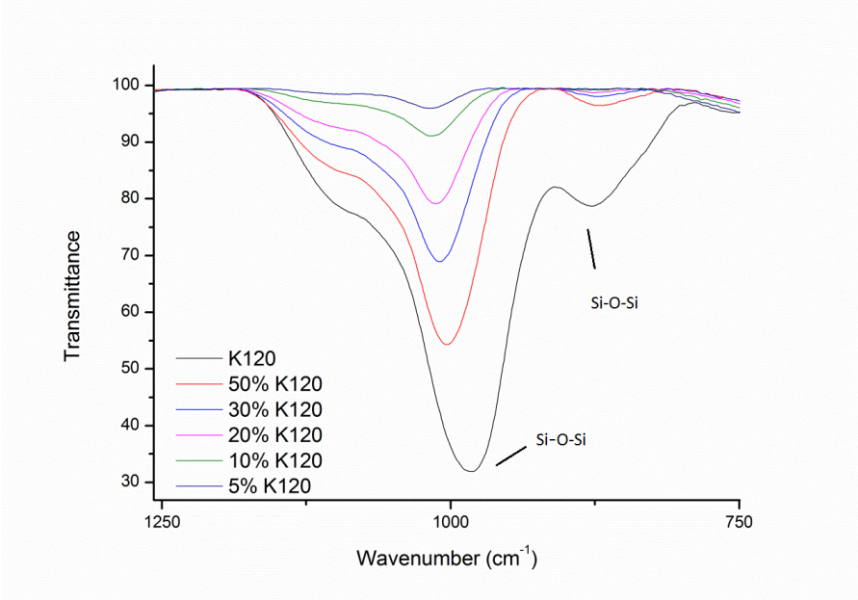


Figure 3. 41 Expanded ATR-IR showing silica absorption bands for K120 solutions

According to concentration of silicate from the titration method and area from infrared integral, it is no doubt that a strong linear correlation with the silicon concentration for K120 is noted (**Figure 3.42**). The data suggest that the IR integral is an effective and alternative approach for determination of the silica concentration in our potassium silicate solutions. After this pre-experiment, the application of this method to our biosilicate solutions is shown by IR spectral traces in **Figure 3.43** and **Figure 3.44.**

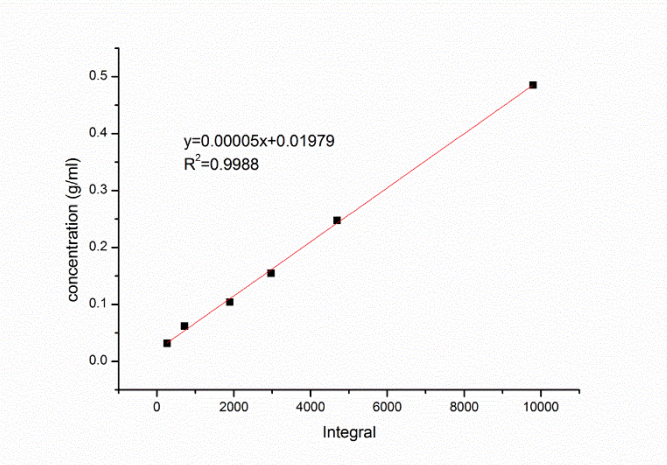


Figure 3. 42 Correlation between the concentrations of K120 silicon measured by ATR-IR

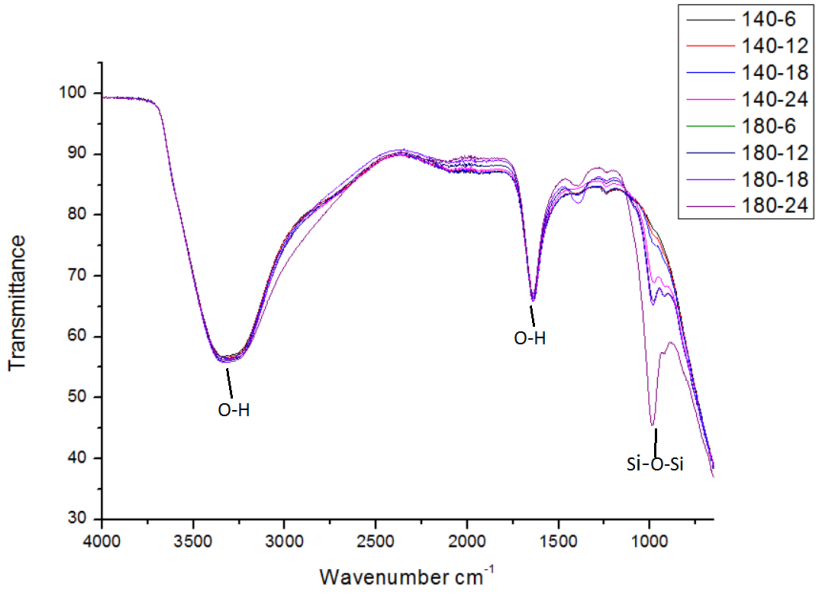


Figure 3. 43 ATR-IR showing silica/silicate absorption bands at different hydrothermal extraction conditions.

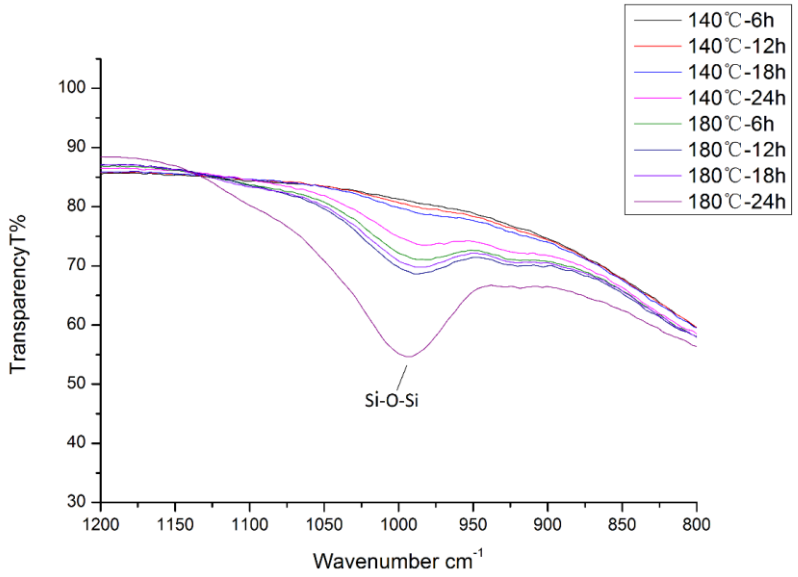


Figure 3. 44 Expanded ATR-IR showing silica/silicate absorption bands for different silicate solutions

The results calculated from the IR method are displayed in **Table 3.5**. It can be seen that harsher conditions (temperature or time) results in higher silicon concentration (from 0.0209 g/ml to 0.0752 g/ml). When extraction condition was 180 $^{o}$C and 24 h, highest concentration 0.0752 g/ml could be obtained. Meanwhile, the temperature

seems to have more influence on the silicon concentration, indicating that the concentration of silicate can be controlled by the change of conditions.

Titrimetry was also used to determine silica concentration which also gives the potassium: silicon ratio. The results of K120 with different concentrations and the biosilicate solutions with different conditions obtained from titration methods are shown in **Table 3.5**.

Table 3. 5 Ratio of $K_2O$:$SiO_2$ and concentration of Si (Titration)

| **Sample** | **Concentration (g/ml)** | | **$K_2O$:$SiO_2$** |
|---|---|---|---|
| | **$K_2O$** | **$SiO_2$** | |
| K120 (standard) | 0.3243 | 0.48525 | 1:1.50 |
| 50% K120 | 0.16685 | 0.2475 | 1:1.48 |
| 30% K120 | 0.10575 | 0.1545 | 1:1.46 |
| 20% K120 | 0.0658 | 0.10425 | 1:1.58 |
| 10% K120 | 0.0376 | 0.0615 | 1:1.64 |
| 5% K120 | 0.0188 | 0.0315 | 1:1.68 |
| 180 $^oC$-6h | 0.1974 | 0.0645 | 1:0.33 |
| 180 $^oC$-12 h | 0.2068 | 0.087 | 1:0.42 |
| 180 $^oC$-18 h | 0.1974 | 0.0705 | 1:0.36 |
| 180 $^oC$-24 h | 0.1786 | 0.0855 | 1:0.48 |
| 140 $^oC$-6 h | 0.19035 | 0.0105 | 1:0.06 |
| 140 $^oC$-12 h | 0.19505 | 0.0165 | 1:0.08 |
| 140 $^oC$-18 h | 0.1927 | 0.0195 | 1:0.10 |
| 140 $^oC$-24 h | 0.2021 | 0.05025 | 1:0.25 |

Although the ATR-IR method is more convenient, it is pleasing to note that the Si concentrations between titration and integral ATR from both methods (IR and titrimetry) were relatively in close agreement (see **Table 3.6**).

Table 3. 6 Comparison of Si concentration between titration and integral ATR in biosilicate solutions

| | **[Si] by Titration** (g/ml) | **[Si] by integral ATR** (g/ml) |
|---|---|---|
| 180 °C - 6 h | 0.0645 | 0.0635 |
| 180 °C -12 h | 0.087 | 0.0786 |
| 180 °C -18 h | 0.0705 | 0.0667 |
| 180 °C - 24 h | 0.0855 | 0.0752 |
| 140 °C - 6 h | 0.0105 | 0.0209 |
| 140 °C -12 h | 0.0165 | 0.022 |
| 140 °C - 18 h | 0.0195 | 0.0233 |
| 140 °C - 24 h | 0.0503 | 0.0491 |

### 3.3.2.3 K120 and silicate solution

A range of blends of commercial K120 and biosilicate solution were prepared (K120, 80% K120, 60% K120, 50% k120, 40% K120, 20% K120 to pure biosilicate solution (180 ℃ 24 h)) in order to have a range of potassium: sodium silicates (see **Figure 3.45**). The ideal blend would be one with a similar $K_2O$:$SiO_2$ ratio to commercial K120 as the latter is known to produce bioboards with high strength. Replacing as much K120 with biosilicate adds to the 'green' credentials of K120.

It can be seen that with decreasing K120 concentration and increasing biosilicate concentration the ratio of $K_2O$ and $SiO_2$ increases slowly at first and then begins to rise in an exponential-like manner. The lower ratio means a higher content of $SiO_2$, and a high $SiO_2$ content can provide a better performance for bioboards. Thus, according to **Figure 3.45** 40% K120 would perform best and gives the biggest utilization of biosilicate solution at the same time.

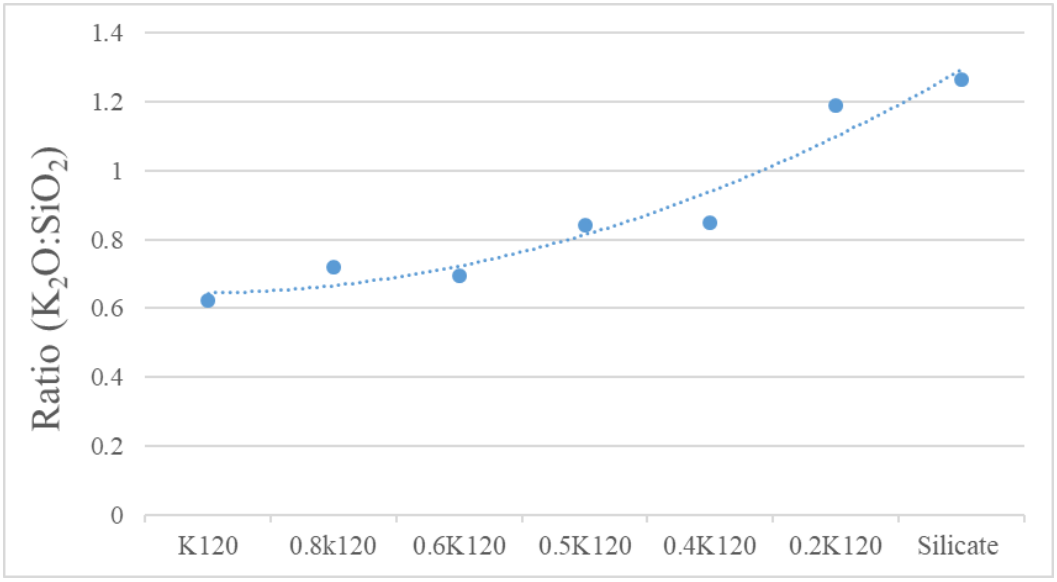

Figure 3. 45 Ratio of $K_2O$ and $SiO_2$ at different concentration of K120 with respect to biosilicate solution.

### 3.3.3 Production of bioboards

The production of bioboards involves the mixing of biosilicate solution (binder) with agri-straws (aggregate; wheat, barley and lemongrass) and a small amount of protein (co-binder or accelerant). A range of protein co-binders, namely: whey protein and soy protein which can be obtained from residues resulting from primary and secondary processing of agrifoods, were investigated. Proteins have been known to accelerate or enhance silica/silicate polymerization. Prior to board manufacture, the aggregates were dewaxed.

#### 3.3.3.1 Wax extraction

Wax removal is necessary in order for effective binding of straws as our binder is aqueous based (biosilicate). The extraction yields are approximately 1.5% and melting crude of extract, as determined by DSC, is shown in **Figure 3.46**. The IR and GC-MS data are reported in Appendices (**Figure A4** and **Figure A5**). DSC is frequently used as an analytical technique to characterize the thermal properties (melting point,

crystallization, decomposition, heat capacity and oxidative point) of oils, fats and waxes. It provides unique energy profile information which especially measures the temperature and heat flow associated with the material transitions as a function of time and temperature.

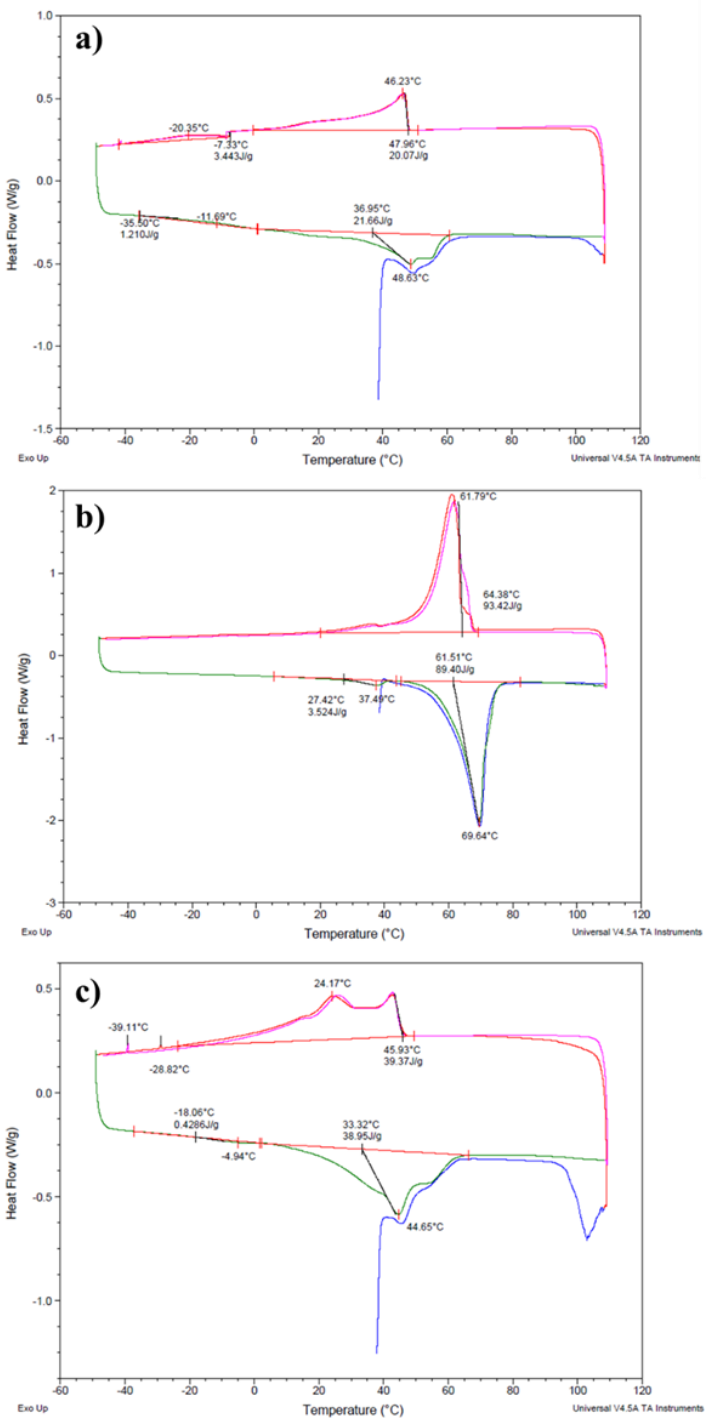


Figure 3. 46 DSC of wax from a) wheat, b) lemongrass and c) barley

The thermal profiles of wheat and barley wax are fairly similar, *i.e.*, show several transitions over a broad temperature range, with peak at maximum temperature (T*p*) approximately 45 $^{o}$C (**Table 3.7**). Interestingly, the transitions for extract from lemongrass are tightly grouped with T*p* at 69.64$^{o}$C (Table 3.4), approximately 25 $^{o}$C higher than that for barley and wheat straw wax. The valorization (to seek added value) of these waxes is not the prime focus of this research but the difference in melting behaviour is noteworthy.

Table 3. 7 Melting points of three waxes

| Wax | T*p* (℃) |
|---|---|
| Wheat | 48.63 |
| Barley | 44.65 |
| Lemon grass | 69.64 |

### 3.3.3.2 Effect of protein (with wheat straw only)

The internal bond strength (IBS) of bioboards with different composition (K120, soy protein and whey protein) are displayed in **Table 3.8**. It is obvious to notice that the boards without dewaxed straws present a very low IBS (0.0036 N/mm$^2$). Compared to their dewaxed counterparts (wheat straw is considerably higher (0.0498N/mm$^2$)). This is due to the hydrophobic wax present on the exterior surface of the straw which hinders the combination between an aqueous based binder (K120) and an organic surface.

The introduction of soy protein decreases the IBS of bioboards with K120, which may due to the pH of the solution. pH is an important factor for silicate binders. Soy protein has a pH of 7.0-8.5, its influence on the overall pH of the system might not be enough to bring the pH down far enough, or there may be kinetic reasons, to induce effective

silica polymerization. It is worth noticing that whey protein performed better in enhancing the IBS than soy protein and higher concentration led to higher IBS value (0.047 to 0.0539 N/mm$^2$). As already mentioned, pH plays an important role in binder property. Whey protein (pH≈6.5 via our test) is more acidic than soy protein thus sufficiently lowers the pH of the solution (for K120, the pH is about 7) to initiate effective silica polymerization.

Table 3. 8 Internal bond strength of bioboards with different additions

| **Entry** | **Straw** | **Biosilicate solution** | **Protein** | **Internal bond strength (N/mm$^2$)** |
|---|---|---|---|---|
| **1** | waxed straw | K120 | | 0.0036 |
| **2** | de-waxed straw | | soy protein solution (5%) | 0.0038 |
| **3** | de-waxed straw | | soy protein solution (10%) | 0.0041 |
| **4** | de-waxed straw | K120 | | 0.0498 |
| **5** | de-waxed straw | K120 | soy protein solution (5%) | 0.039 |
| **6** | de-waxed straw | K120 | soy protein solution (10%) | 0.0433 |
| **7** | de-waxed straw | K120 | whey protein solution (10%) | 0.047 |
| **8** | de-waxed straw | K120 | whey protein solution (25%) | 0.0539 |

Another reason for the poor performance of soy protein may be associated with its solubility in the biosilicate solution itself. As shown in **Figure 3.47**, soy protein did not dissolve completely in biosilicate solution.

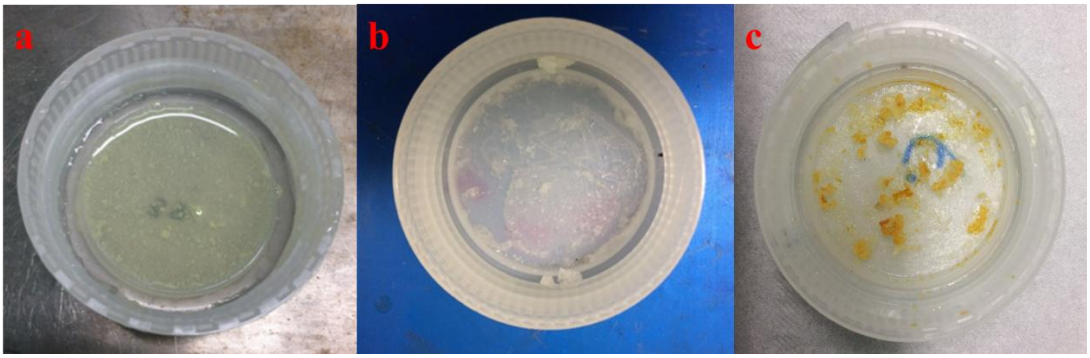


Figure 3. 47 Dried silicate solution and protein (a mixture of biosilicate solution and soy protein; b dried biosilicate solution; c mixed and dried sample of biosilicate solution).

### 3.3.3.3 Effect of aggregates (wheat, barley and lemongrass)

IBS of different raw materials such as wheat straw, barley straw and lemongrass was determined and the data is listed in **Table 3.9**, where: WKW is wheat straw with K120 and whey protein; WBW is wheat straw with biosilicate solution which is 180-24 and whey protein; BBW is barley straw with biosilicate solution and whey protein and; BKW is barley straw and K120 whey protein. As shown in **Table 3.9** WKW has the highest IBS (around 0.23 $N/mm^2$) compared with other boards (around 0.1 to 0.15 $N/mm^2$) which are relatively similar to each other. Normally, the commercial K120 is a better binder than biosilicate solution. But the result of barley straw as a raw material is opposite: the biosilicate solution performs better than K120. The reason for this is still unknown.

WLE and WLH are wheat (75%) and lemongrass (25%) de-waxed with ethanol and heptane mixed with K120 and whey protein. The WLE shows a lowest IBS, indicating that heptane dewaxing was better than ethanol dewaxing. This is not a surprise as ethanol is a polar solvent and less amenable to solvating waxes. Thus WLH display a relative higher IBS, but it is still weaker compared to the WKW, this may be because

the lemongrass fibre content is lower than wheat straw.

Table 3. 9 Sample details of boards with different raw materials

| ID | Length (mm) | Width (mm) | Thickness (mm) | Weight (g) | Density ($g/cm^3$) | IBS ($N/mm^2$) |
|---|---|---|---|---|---|---|
| **WKW** | 50.86±0.12 | 50.78±0.29 | 9.36±0.30 | 11.45±0.50 | 0.47±0.02 | 0.20±0.05 |
| **WBW** | 45.24±0.04 | 45.19±0.02 | 9.17±0.31 | 10.99±0.10 | 0.46±0.02 | 0.14±0.01 |
| **BBW** | 50.84±0.02 | 50.57±0.18 | 8.94±0.28 | 10.30±0.15 | 0.45±0.01 | 0.16±0.02 |
| **BKW** | 50.73±0.19 | 50.88±0.09 | 9.18±0.31 | 11.69±0.44 | 0.49±0.01 | 0.13±0.02 |
| **WLE** | 50.95±0.34 | 51.01±0.65 | 9.58±0.02 | 11.87±0.40 | 0.47±0.02 | 0.07±0.01 |
| **WLH** | 51.25±0.07 | 51.29±0.11 | 9.24±0.39 | 11.11±0.39 | 0.45±0.03 | 0.16±0.11 |

### 3.3.3.4 Effect of Zirconia

Zirconia was explored to improve bond strength and flame retardancy. Initially, biosilicate and zirconia mixtures in the absence of straw were made in to glasses and examined by XRD for structural changes and thereafter, straw boards were made and their flammability was tested by Prof Menaka Jha' s group (Institute of Nanoscience and Technology, Mohali, Punjab, India, for images see Appendix **Figure A2** and **Figure A3**). Zirconia was also provided by Prof Menaka Jha: i. monoclinic; ii. tetragonal, and; iii. monoclinic mixed with tetragonal. On receipt, the samples were milled and their crystallinity investigated by XRD as shown in **Figure 3.48**. From a knowledge of the initial crystalline states then any changes as a result of mixing with silicate solutions could be better evidenced. Zirconium dioxide ($ZrO_2$), sometimes known as zirconia, is a white crystalline oxide of zirconium. Baddeleyite, is its most naturally occurring form, with a monoclinic crystalline structure. Three phases are known: monoclinic <1,170 ℃; tetragonal 1,170–2,370 ℃, and; cubic >2,370 ℃. A minor percentage of the oxides of calcium or yttrium are often present which stabilize the cubic phase. Unlike $TiO_2$, which features six-coordinate Ti in all phases,

monoclinic zirconia consists of seven-coordinate zirconium centres. This difference is attributed to the larger size of Zr atom relative to the Ti atom.

From the **Figure 3.48** it can be seen that the $ZrO_2$ contains two crystalline phases. By comparing the intensities of these two crystalline phases, it can be concluded that there are some monoclinic zirconia peaks in tetragonal zirconia, this may be because tetragonal zirconia can only form in a very high temperature, some monoclinic zirconia did not change the structure during the process.

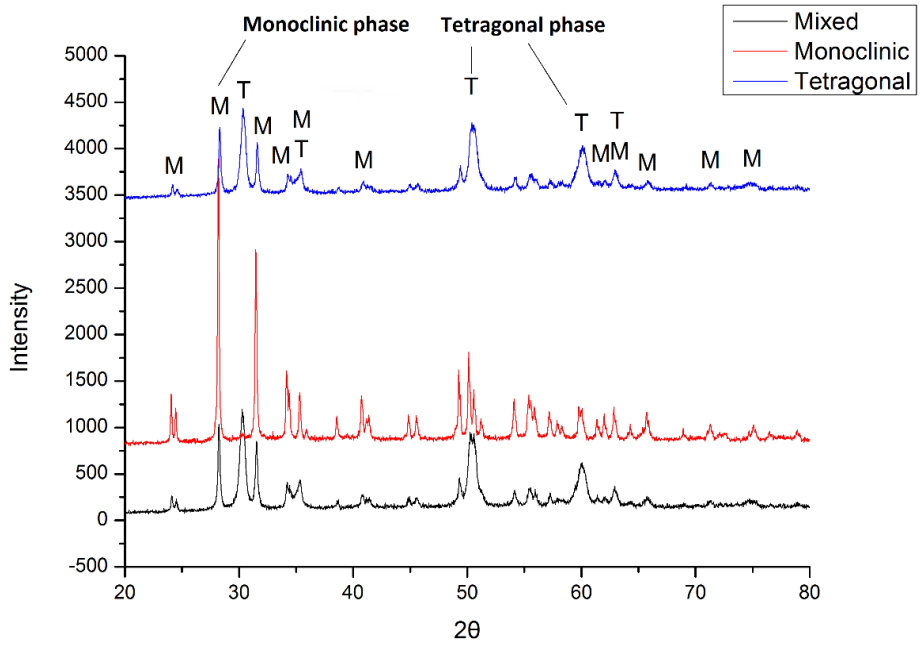


Figure 3. 48 XRD patterns of the phases present in as-received samples of mixed, monoclinic and tetragonal zirconia (M= monoclinic phase； T= tetragonal phase).

The IBS of zirconia-containing bioboards are listed in **Table 3.10** (where: M2, M4, M6 refer to biosilicate solution with 2% 4% 6% mass fraction of as received monoclinic zirconia, and T2, T4, T6 mean biosilicate solution with 2% 4% 6% mass fraction of as-received tetragonal zirconia) and the formulations were the same, *i.e.*, 40 g wheat straw, 3.6 g whey protein solution) except K120 silicate solution. The

addition of zirconia seems to make IBS worse overall even though different mass fraction of zirconia was added.

Table 3. 10 Internal bond strength (IBS) of bioboards with different phase and mass fraction of zirconia

| Sample | length (mm) | Width (mm) | Thickness (mm) | Weight (g) | Density ($g/cm^3$) | IBS ($N/mm^2$) |
|---|---|---|---|---|---|---|
| **M2** | 50.17 | 50.27 | 9.47 | 10.48 | 0.43 | 0.1 |
| **M4** | 50.23 | 50.97 | 9.63 | 10.82 | 0.43 | 0.07 |
| **M6** | 50.3 | 50.36 | 9.52 | 10.74 | 0.44 | 0.09 |
| **M2** | 50.26 | 50.21 | 8.9 | 10.67 | 0.47 | 0.09 |
| **M4** | 50.24 | 50.28 | 9.51 | 10.64 | 0.44 | 0.08 |
| **M6** | 49.71 | 49.76 | 9.58 | 10.8 | 0.45 | 0.08 |
| **A** | 50.14 | 50.19 | 9.51 | 11.23 | 0.46 | 0.09 |

The flammability of boards is a very important property due to their potential application in furniture. Flame retardancy and flammability tests (flame retardancy test determines the ability of a material to withstand a fire for a period of time while flammability testing determines how easily a material will ignite or burn when exposed to heat) were conducted by Prof Menaka Jha's group and are depicted in **Figure 3.49**. The introduction of zirconia improved the fire resistance ability of bioboards. The incorporation of 4% $ZrO_2$ showed an almost 2.5-fold enhancement in performance than for boards without $ZrO_2$. For fire retardancy, the two boards showed approximately show the same burning time, but the boards without $ZrO_2$ completely deformed on touch, *i.e*, cinder-like texture whilst, the boards with 4% $ZrO_2$ gave a more robust char (**Figure 3.49**).

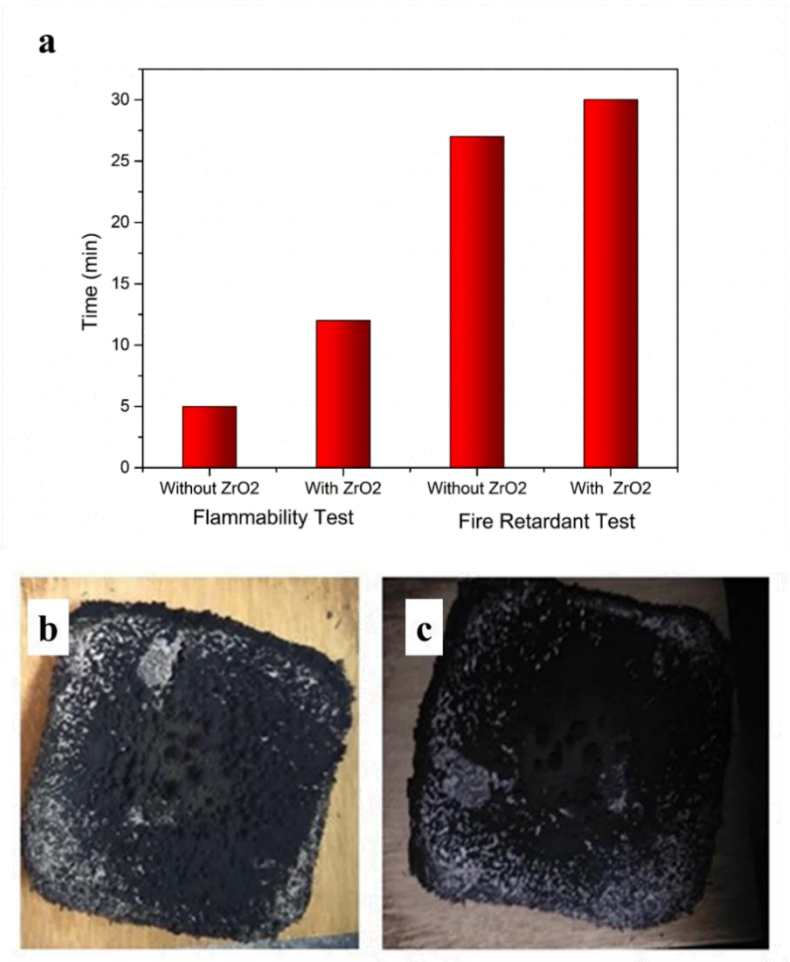


Figure 3. 49 a. Flammability and fire retardancy bioboards with and without zirconia; Fire retardant test (b) Without $ZrO_2$; (c) with $ZrO_2$.

Following work of making bioboards with different straws (wheat, barley and lemongrass) and the short study on the role of zirconia, the next aim was to explore the making of a novel SIP comprising a biobased foamed inner core.

### 3.3.4 Structural insulation panels: foam materials

#### 3.3.4.1 Foam materials with microfibres

Initial trials were conducted using waste paper and foaming agents (See **Figure 3.50**). Waste paper was chosen because it is an example of significant cellulosic resource. In 2017, globally 419.7 million tons of paper was used.[252] It is predicted that world demand for paper and board will reach 489 million tons by 2030,[253] making paper the

3rd largest industrial pollutant.[254] As the most widely recycled material in the world, the global market for waste paper recycling was valued at $41.7 billion (USD) in 2019.[255] However, contrary literature which often mis-quotes that paper can recycled upto seven times, in practice, recycling is limited to 3 times as the cellulose fibres become too short for binding.[256] Thus, waste paper is a significant renewable resource. Furthermore, since 1 January 2018, China imposed much stricter quality restrictions on imported cardboard as well as banning the importation of all plastic waste and mixed paper rubbish from all over the world.[257] The new quality standards mean that Chinese authorities will only accept cardboard if it is uncontaminated with other waste products; contamination rates must be <0.5%, rather than the <1.5% as previously applied. At the time of this research, the UK used to export around 3 million tonnes of cardboard waste to China each year but some or all of this could be rejected under the new restrictions.

Figure 3. 50 Waste paper foam materials (3-Dimensional porous is displayed).

At first the cellulose from orange peel wastes (OPR) was combined with waste paper. Several pre-experiments (shown in **Figure 3.51** a and b) showed that the materials failed to foam, this may due to the low surface area of the cellulose which lead to a

weak combination between the materials. Microfibrillated celluloses (MFC) from orange peel waste (MFC120, MFC160, MFC200) were tried to combine with the waste papers (shown in **Figure 3.51** c and d). It should be noted that MFCs processing with higher temperature (120 to 200 $^{o}$C) and less mass ratio (50% to 10%) have a better foam quality (depend on foaming extent) in foam materials. The textures of materials are displayed in **Table 3.11**.

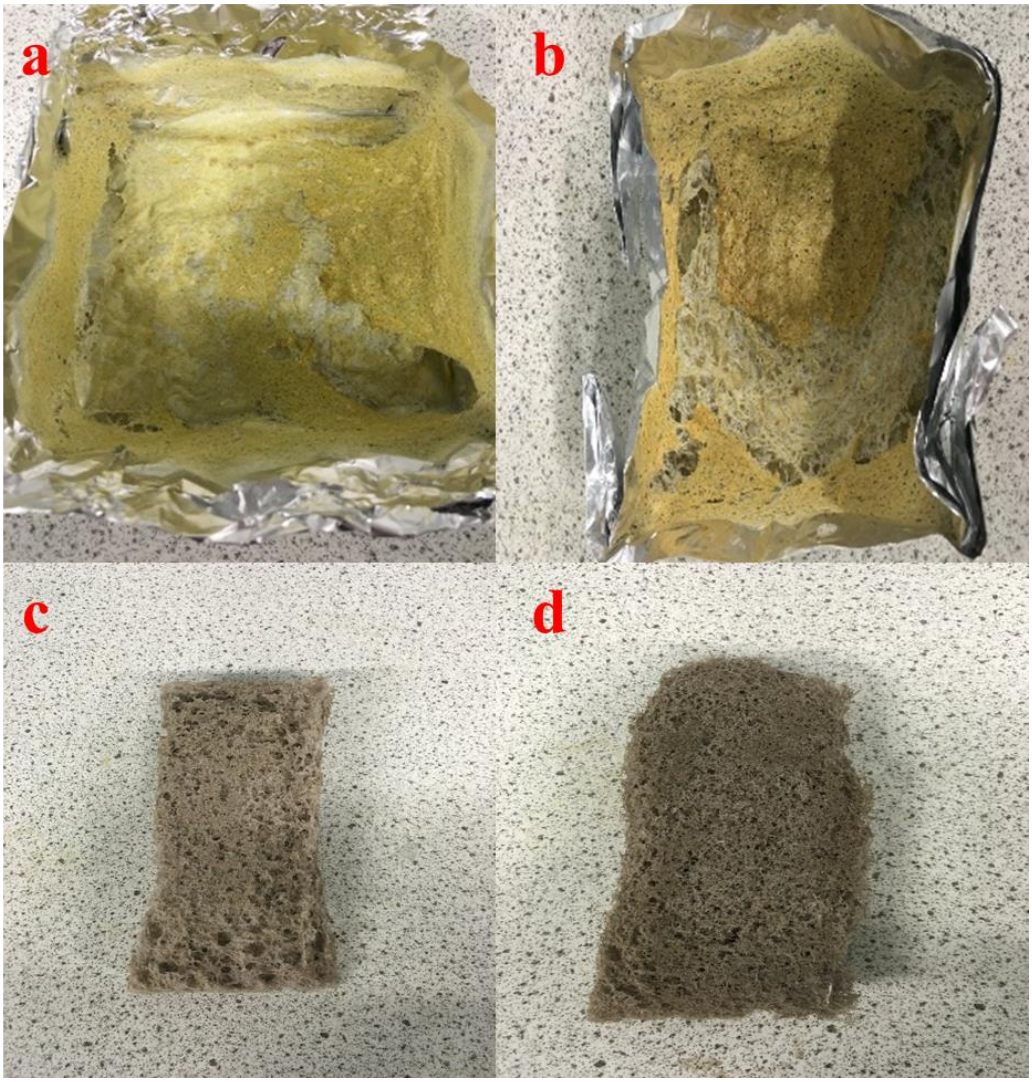


Figure 3. 51 Foam materials made of paper with OPR (a and b) and paper with MFC (c and d)

Table 3. 11 Texture of foam materials made of MFC and paper

| Sample | Waterproof | Texture | Foam Quality |
|---|---|---|---|
| 10% MFC120 | No | Soft | Poor |
| 25% MFC120 | No | Soft | Poor |
| 50% MFC120 | No | a little hard | Poor |
| 10% MFC160 | No | Soft | Good |
| 25% MFC160 | No | Soft | Poor |
| 50% MFC160 | No | a little hard | Poor |
| 10% MFC200 | No | Soft | Excellent |
| 25% MFC200 | No | Soft | Good |
| 50% MFC200 | No | a little hard | Poor |

Thermal degradation of the foam materials with different ratio of MFCs were studied by their mass loss and decomposition temperature through thermogravimetric (TG) analysis (**Figure 3.52**). The initial mass loss between 50 to 90 $^{o}$C is related to moisture loss in the materials. The decomposition bands at about 200 $^{o}$C were only observed in 25% MFC 140, 10% MFC 200 and the broad peaks at around in 10% MFC 120 and MFC 160 may due to the agents (*e.g.* sodium bicarbonate or other) in the foam materials. The major peaks are attributed to the cellulose which is the main component of foam materials. It also can be shown that MFCs present a relatively lower thermal stability compared to the mixed materials, indicating the bonding with agents during the foaming process results in a higher thermal stability. Interestingly, the decomposition temperatures of MFC increase from 298.1 to 330.1 ℃ with rising

process temperature, this is due to the removal of amorphous non-cellulosic matters leading to a higher crystalline index which we discussed before. Meanwhile, the mass losses in same MFCs decrease with the content reduced (approximately from 40% to 20%). This may be due to that when the foam materials were processed, the nanoparticles with larger surface area could absorb more silicon from the water glass via hydrogen bonds and thus the samples contained more silicon which could not decompose below 625 ℃.

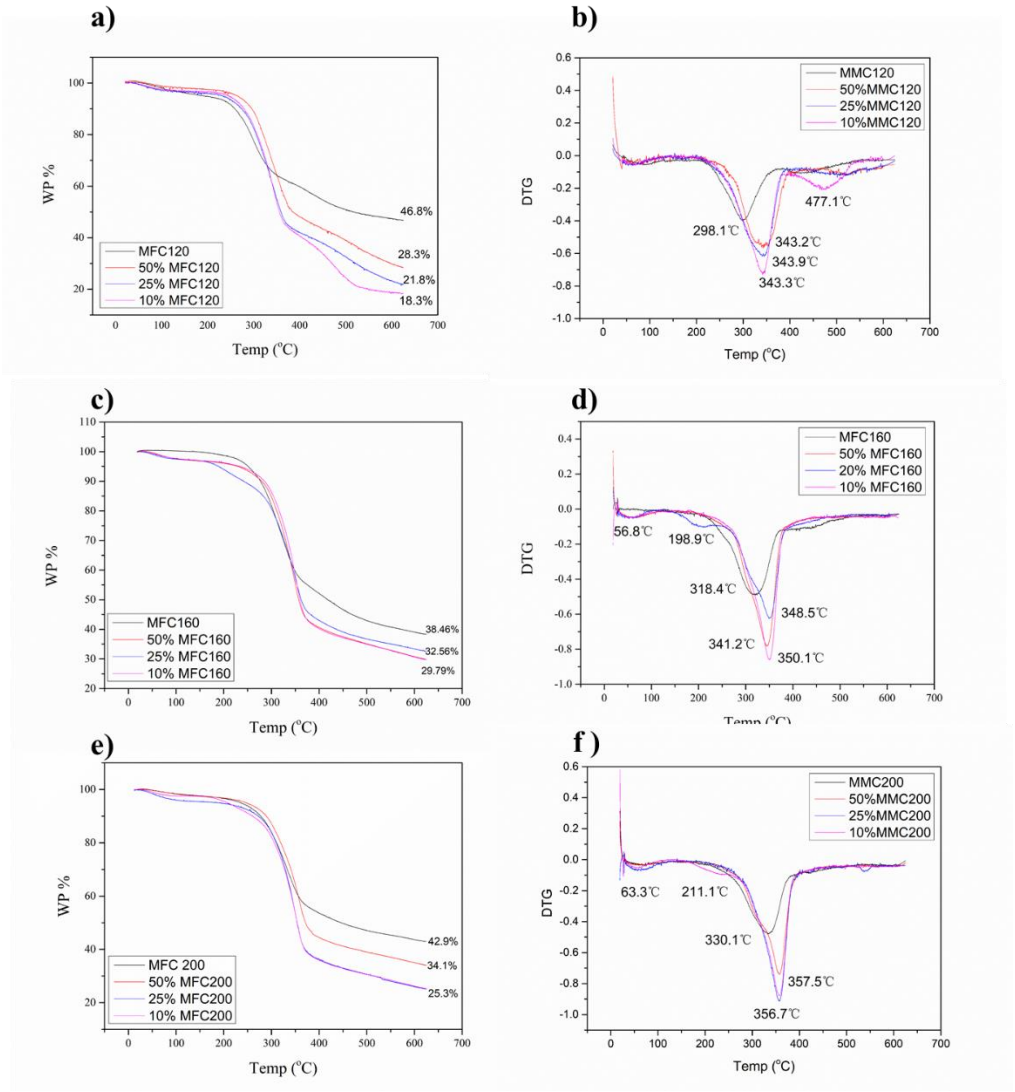


Figure 3. 52 The thermal stability and degradation profile of foam materials with MFC: a) TG of MFC120, b) DTG of MFC120, c) TG of MFC160, d) DTG of MFC160, e) TG of MFC200 and f) DTG of MFC200.

### 3.3.4.2 Solid state $^{13}$C CPMAS NMR

The stacked $^{13}$C CPMAS NMR spectra of the foamed materials are displayed in **Figure 3.53**. Typical resonances for cellulose are observed from 60 to 120 ppm:[258] the main assignments are anomeric C1 (δ ≈ 105 ppm); C4 (86−92 ppm crystalline and 79−86 ppm amorphous); C2, C3, and C5 (72−79 ppm); and in the end the C6 carbon (δ ≈ 64 ppm). The NMR data indicate that no obvious new resonances are detected when mixing different mass of MFC (120,160) with paper.

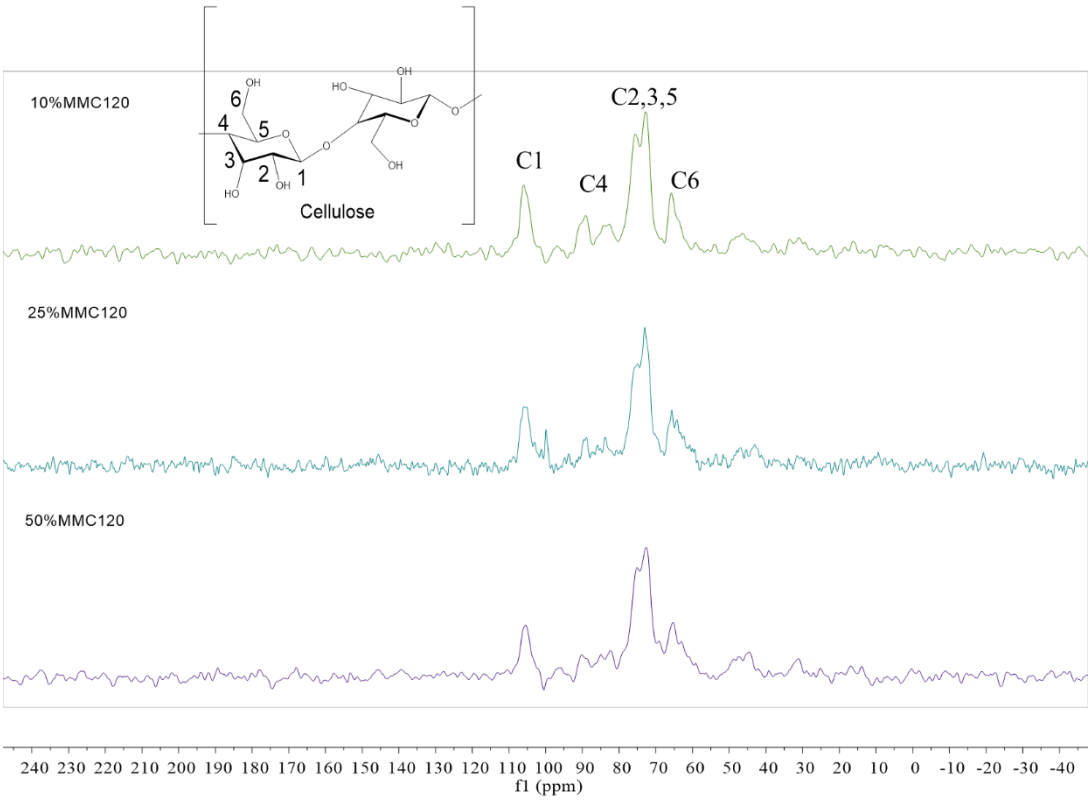

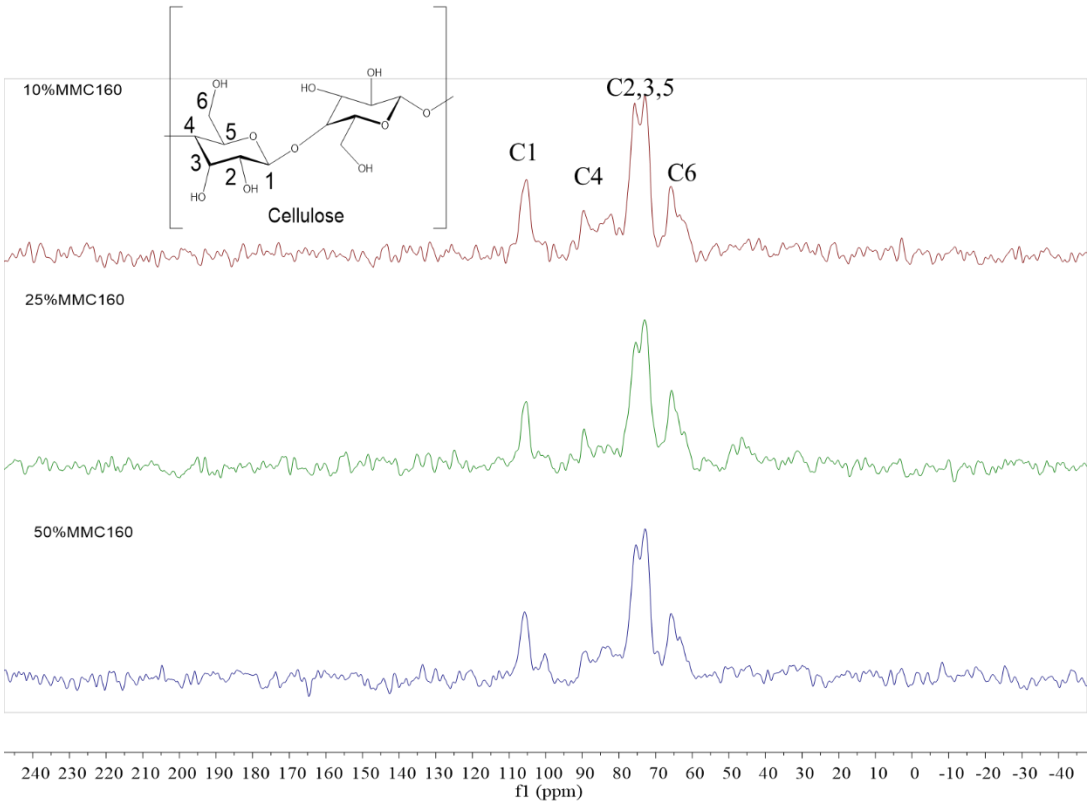


Figure 3. 53 solid-state $^{13}C$ NMR spectra for foam materials with MFC120 (top) and MFC160 (bottom)

### 3.3.4.3 ATR-IR

The ATR-IR for MFCs and the foam materials with 10%, 25%, 50% MFC are displayed in **Figure 3.54**. According to the summarized FTIR spectra of lignocellulose in **Table 3.1**, the signals at about 3400 $cm^{-1}$ is due to intramolecular OH stretching. the bonds at 2893 $cm^{-1}$ are CH and $CH_2$ stretching, the absorption bands at 1642 $cm^{-1}$ is corresponding to OH from absorbed water. Bands at 1427 $cm^{-1}$ correspond to $CH_2$ symmetric bending and the vibrations at around 1063 $cm^{-1}$ are due to C-O/C-C stretching.

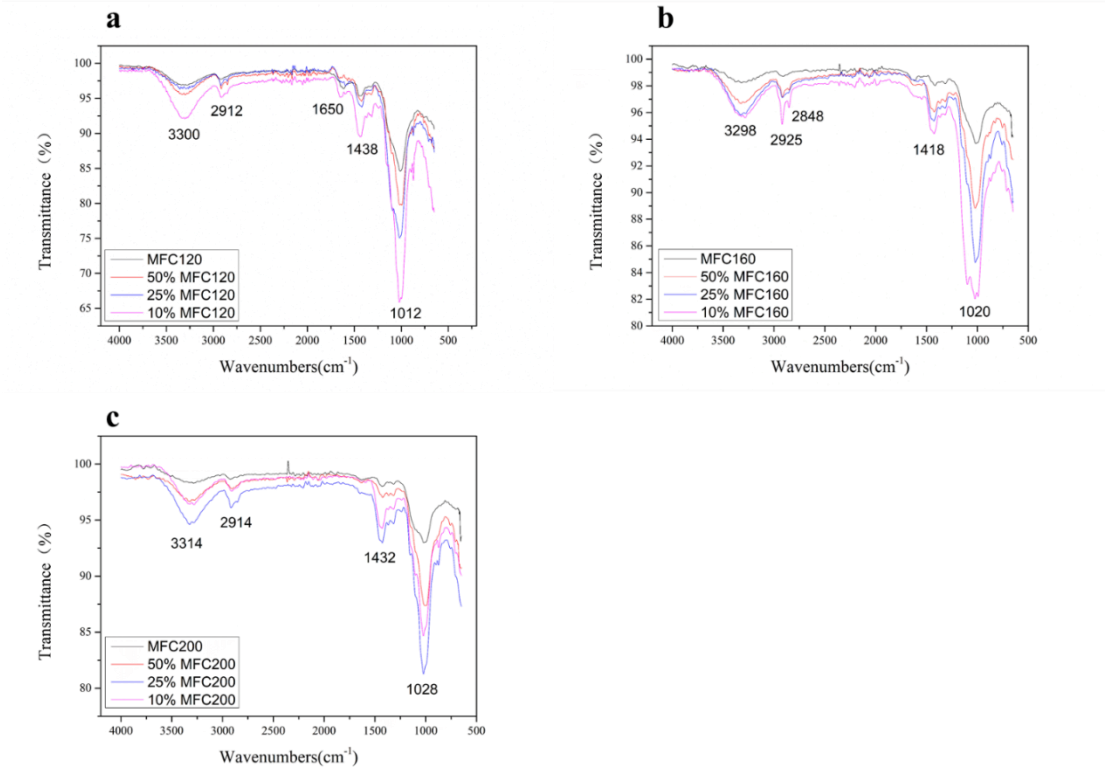


Figure 3. 54 ATR showing foam materials with different MFCs absorption bands: a. MFC120; b. MFCC160; c. MFC200.

### 3.3.4.4 SEM

The SEM images of the foamed materials are shown in in **Figure 3.55**. The paper fibres present long and flat morphological features. The introduction of MFC120 (10%, 25% and 50%) gives rise to small(er) particles and aggregates on, and possibly within, the surface of the paper fibres. This may be tentative evidence as to intimate mixing between paper and MFC.

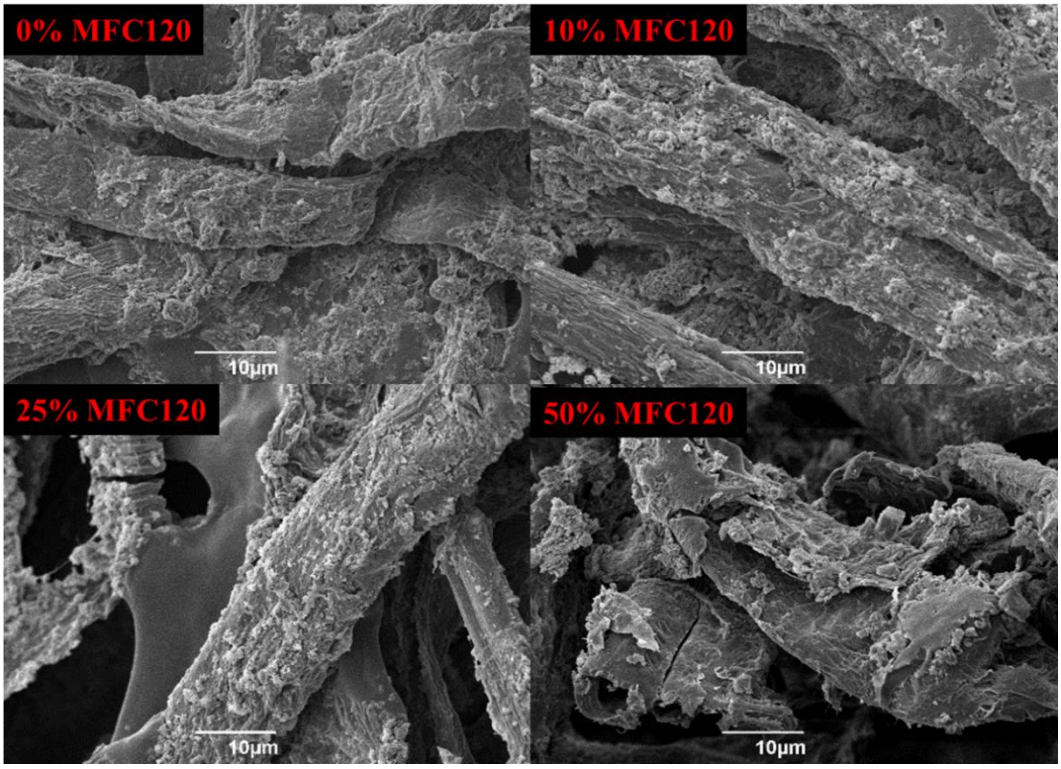

Figure 3. 55 Micromorphology of foam materials with different ratio of MFC120(0%,10%, 25%, and 50%).

### 3.3.5 APTES treatment

In order to improve the water resilience of the paper-MFC foams, silylation with aminopropyltriethoxy silane (APTES) was investigated. APTES treatment is well-known in the literature for chemical modification but not so much so for spent or waste cellulosic residues such as MFC. Silylation was evidenced by solid state NMR, in particular $^{29}$Si and ICP and, its effect observed qualitatively via a simple contact drop test with water. The mechanism of APTES functionalization is shown in **Figure 3.56** (in ethanol/water):

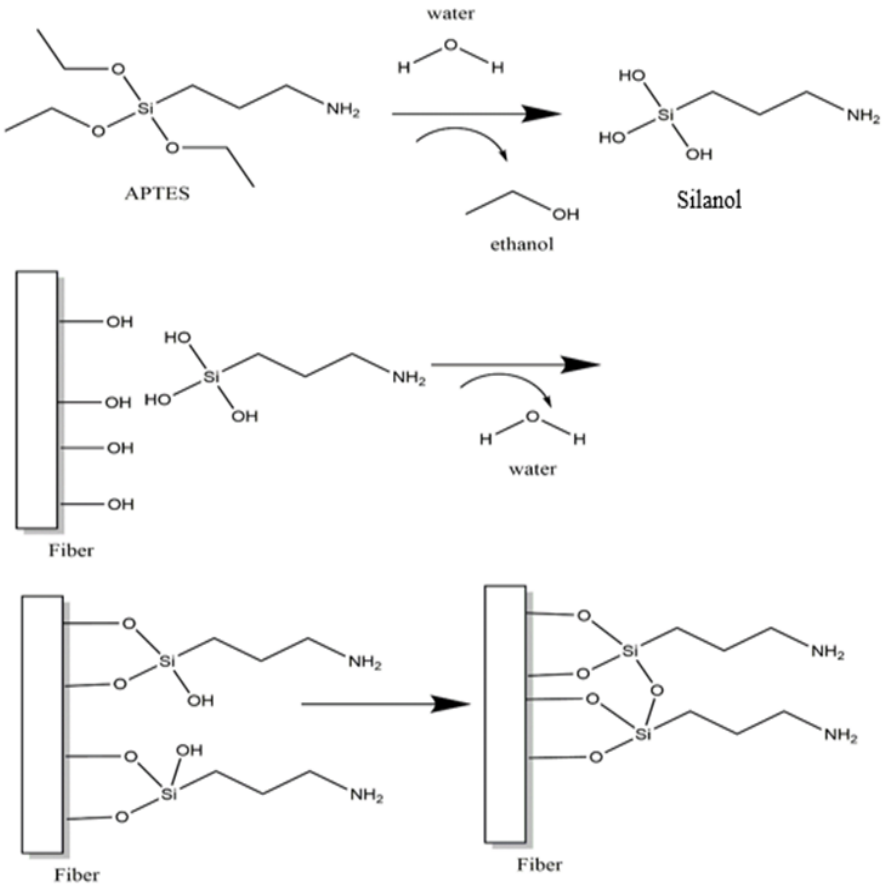


Figure 3. 56 Mechanism of APTES functionalization.

APTES hydrolyses gradually and forms the corresponding silanol R-Si(OH)$_3$, which reacts with surface OH groups to form substrate-O-Si-O-R bonds. Subsequently, during solvent evaporation, the unreacted silanol groups may undergo further condensation with residual hydroxyl groups forming a polysiloxane network.[259] Moreover, in the aqueous medium, the hydrolyzed silanes form dimeric and oligomeric structures because of the condensation of the silanol groups both with each other and with alkoxy groups.[260]

### 3.3.5.1 Solid state $^{13}$C and $^{29}$Si NMR

The solid-state $^{13}$C and 29Si NMR spectra of cellulose and paper with or without APTES treatment are implemented and displayed in **Figures 3.57** and **Figure 3.58**.

The $^{13}C$ NMR spectrum of both commercial cellulose and paper display typical cellulosic signals from 60 to 120 ppm:[258] the main assignments are anomeric C1 (δ≈105ppm); C4 (86−92 ppm crystalline and 79−86 ppm amorphous); C2, C3, and C5 (72−79 ppm); and in the end the C6 carbon (δ ≈ 64 ppm). Compared to the initial (untreated) $^{13}C$ NMR spectra of cellulose and paper, the corresponding APTES treated materials display three new resonances (C7, C8, C9) at around 11, 27, and 45 ppm assigned to the $\alpha CH_2$, $\beta CH_2$, and $\gamma CH_2$ moieties, thus proving successful silylation. Meanwhile, it is obvious to see that after grafting, the C2, C3 peaks of cellulose and paper split into two small peaks, indicating that the reaction between APTES and samples mainly happened at C2, C3 carbons. There is no sign of OEt peaks which can often be seen due to residual Si-OEt group, implying that the silanes are well bound.

Similarly, the solid-state $^{29}Si$ NMR on the APTES treated materials shows two possible presences of $^{29}Si$ structures around -50 ppm to -80 ppm: the linear and three-dimensional structures of silicon. The condensation of silanol groups between the cellulose/papers and APTES did not affect the shifts of the cellulosic C atoms, and silanes are favored over simple hydrolysis to yield a 3D network of polysiloxanes.

The Si atom of the APTES is designated as T, which corresponds to the three (=T) siloxane Si-O bonds attached to the central Si atom and a single Si-C bond present in the molecule.[258] The alkoxy substituents (Si-O-R) in APTES were replaced progressively by silyloxy groups (Si-O-Si) during hydrolysis and condensation. Due to the number of silyloxy (Si-O-Si) groups bound to characterize the Si atom, the structures are called T1 structure which is in about -50 ppm in $^{29}Si$ NMR spetra, T2

structure (linear sequences) which appears approximately -60 ppm and T3 structure (3D oligomer structures) can be observed around -70 ppm in $^{29}$Si NMR. From the $^{29}$Si spectra in **Figure 3.57**, a single T3 structured peak was detected when grafted in acetone. Whilst, T2 and T3 structured peaks were both observed when grafted in ethanol, indicating that the samples grafted in acetone prefer to form more T3 structures. The similar trend was seen from $^{29}$Si spectra in **Figure 3.58** when treated with the paper samples.

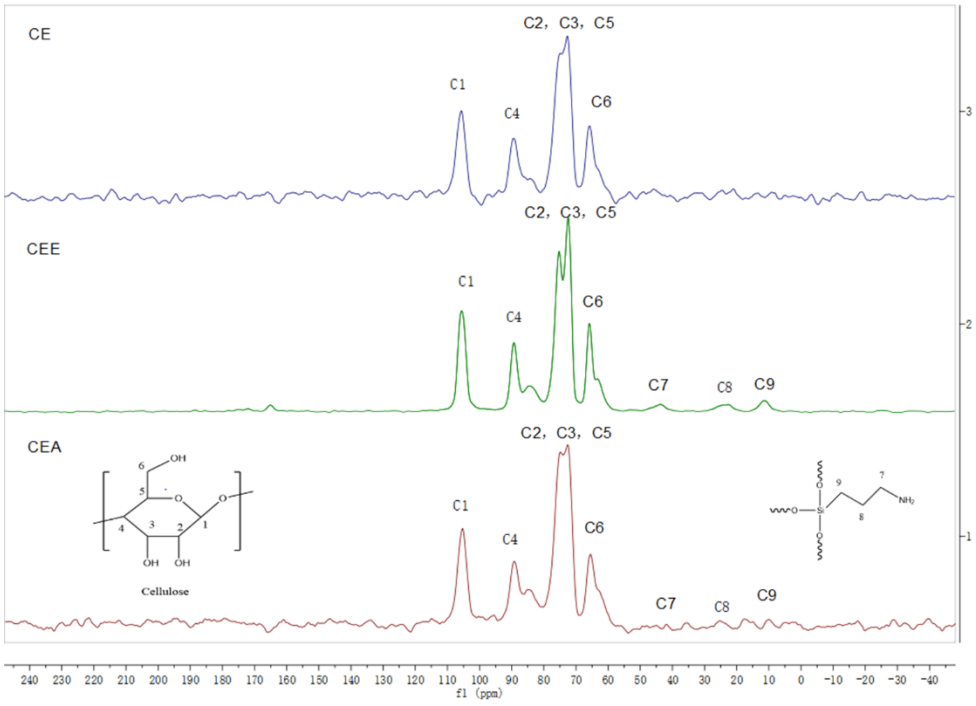

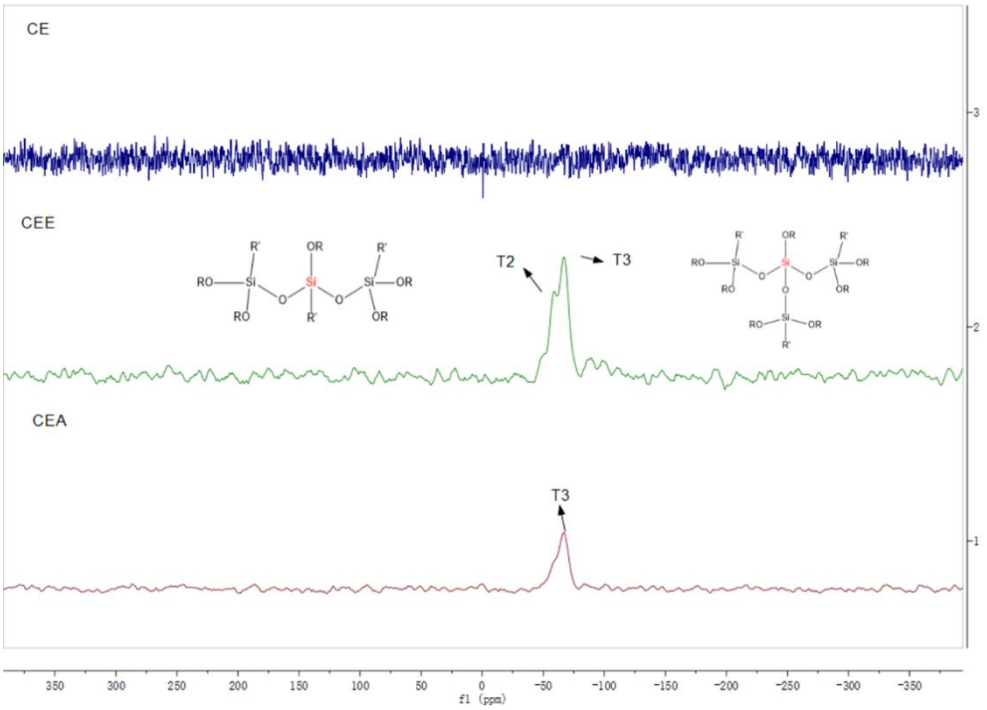


Figure 3. 57 Solid-state $^{13}C$ and $^{29}Si$ NMR spectra of commercial cellulose (CE) treated with ethanol (CEE) and acetone (CEA).

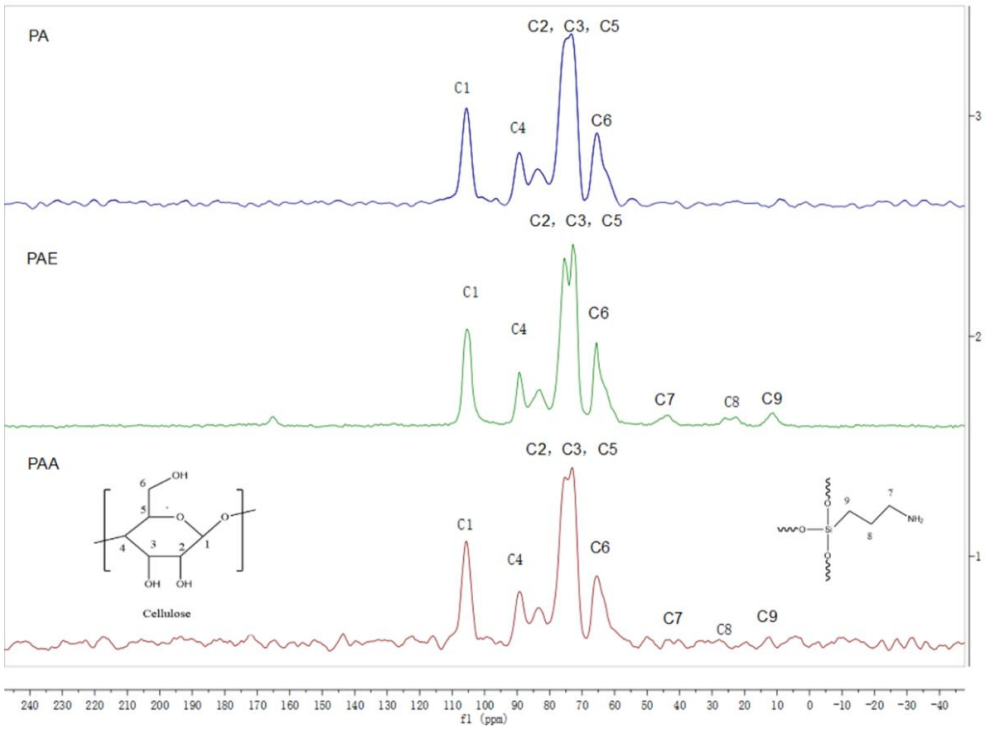

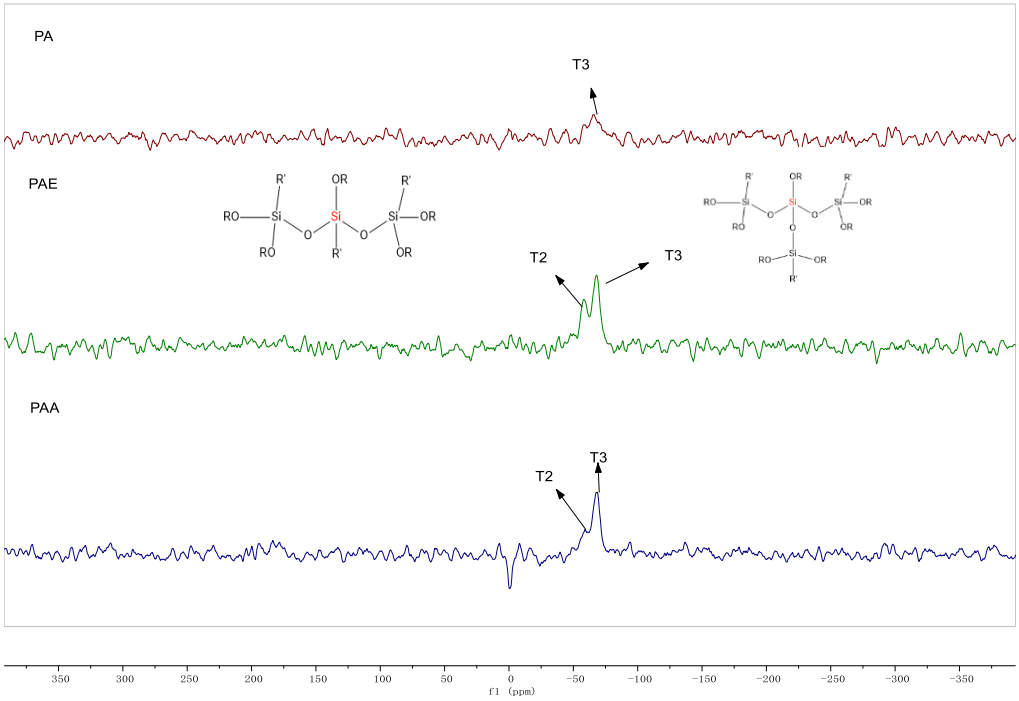


Figure 3. 58 Solid-state $^{13}C$ and $^{29}Si$ NMR spectra of paper (PA) treated with ethanol (PAE) and acetone(PAA).

### 3.3.5.2 SEM

SEM analysis (**Figure 3.59**) is carried out to show the changes of surface morphology features of the materials during the process. From the typical 3D network structures of samples, the change of commercial cellulose during treatment is not significant both in CEE and CEA. Even we have found the $\alpha CH_2$, $\beta CH_2$, $\gamma CH_2$ moieties and T2, T3 structured silicon from these samples via $^{13}C$ and $^{29}Si$ NMR respectively, the samples present a small thin feature and no distinct coatings are detected. This might be due to the low silicate content and achieving not enough surface coverage. On the contrary, a thin white polysiloxane coating is observed on the surface of papers in PAE and PAA, implying that the APTES is successfully grafted on the paper surface via the hydrogen bonds. This also explained the reason that the paper samples after silylation were hydrophobic while the commercial samples have a bad water proof property.

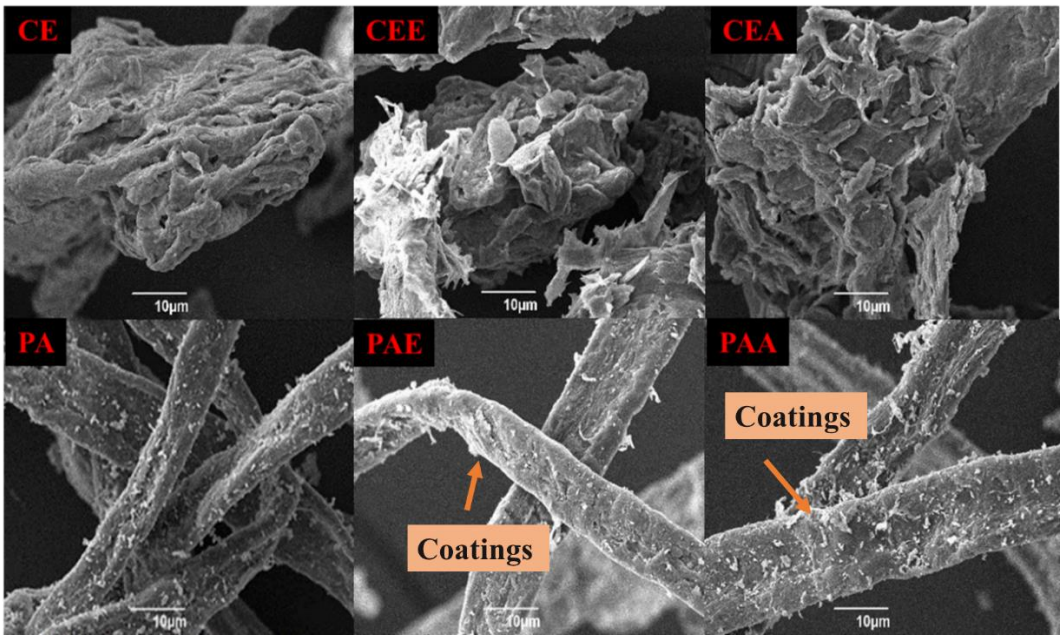


Figure 3. 59 Micromorphology of cellulose and paper during the modification. The images are: original cellulose, (CE) cellulose treated with ethanol, (CEE) cellulose treated with acetone, (CEA) and original paper, (PA) paper treated with ethanol (PAE) and paper treated with acetone (PAA).

### 3.3.5.3 ICP and CHN

The elemental contents of samples are determined by ICP and the results are shown in **Table 3.12**. It is obvious to see that both cellulose and papers have a higher amount of silicon content (19.47 to 551or 7318 ppm and 570.11 to 1616.66 or 5214.59 ppm respectively) after the treatment, implying the successful graft with APTES. For both cellulose and papers, the treatment with acetone leads to a higher silicon content than ethanol (551.49 to 7318.78 ppm and 1616.66 to 5214.59 ppm), this may may be due to the difference H-bonding behavior of acetone and ethanol. Interestingly, the papers have more silicon than cellulose, this is because initial papers have added kaolin which is a silicon aluminium oxide during the processing.

Table 3. 12 Silicon content of cellulose/paper during treatment

| Sample | Silicon content(ppm) | Sample | Silicon content(ppm) |
|---|---|---|---|
| CE | 19.47 | PA | 570.11 |
| CEE | 551.49 | PAE | 1616.66 |
| CEA | 7318.78 | PAA | 5214.59 |

The CHN analysis is displayed in **Table 3.13**. Due to the agent addition during paper manufacture, the contents except CHN of paper is a bit higher (approximately 8%) than cellulose. After the silylation, a significant difference is detected: for all samples, the carbon content decrease (by 1% to 2%), the nitrogen element is increasing from 0 % to about 0.5 % during grafting with APTES which came from the $NH_2$ parts, implying that the APTES have been grafted on the surface of samples. Theoretically the Si content and the N content should correlate 1:1 but CEE / CEA have very different Si contents but smaller N contents, this may be due to the sensitivity of CHN analysis. PAE display a relative different elemental ratio, this may be due to the experimental error.

Table 3. 13 CHN analysis of cellulose/paper during treatment

| Sample type | | | | | | | | | |
|---|---|---|---|---|---|---|---|---|---|
| Before treatment | | | | | After treatment | | | | |
| | %C | %H | %N | Others | | %C | %H | %N | Others |
| CE | 44±0.2 | 6.±0.2 | 0 | 51±0.5 | CEE | 42±0.5 | 6.0±0.1 | 0.5±0.1 | 51±0.2 |
| | | | | | CEA | 42±0.1 | 6.0±0.1 | 1.±0.1 | 50±0.7 |
| PA | 43±0.3 | 5.±0.1 | 0 | 58±0.3 | PAE | 42±0.1 | 6.0±0.2 | 0.4±0.1 | 51±0.3 |
| | | | | | PAE | 35±3.0 | 5.0±0.5 | 0.4±0.1 | 60±4 |

### 3.3.5.4 Thermogravimetric analysis (TGA)

The thermograms and DTG of thermograms of cellulose are displayed in **Figure 3.60**. The initial cellulose shows typical thermal degradation profile of cellulosic substrates, with a maximum decomposition rate around 348 ℃ and approximately 10% residual.

After the modification with APTES in ethanol or acetone, the decomposition temperature slightly increases to approximately 365 ℃, and the residue part retains more mass than pure cellulose (mass loss from 85% to 80% or 70% due to siloxy moieties which have higher decomposition temperatures). For papers, the decomposition temperatures change less than 3 ℃ during the modified, but the residue mortise decrease approximately from 80% to 70% due to the exist of the APTES. Meanwhile, compared to the pure commercial cellulose, the DTG curves of paper based sample present a relative broad peaks especially in PAA samples, some bands which refers to additional agents can be detected at around 320 ºC.

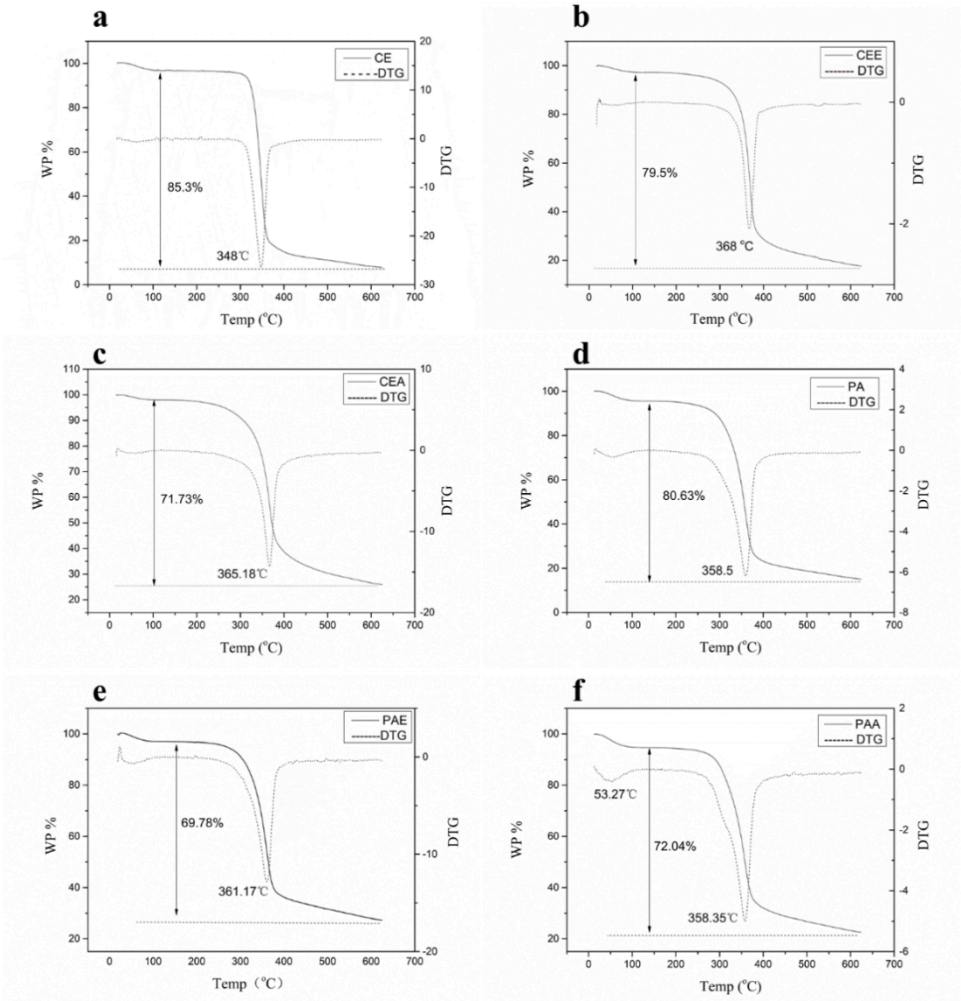


Figure 3. 60 The thermal stability and degradation profile of original and treated cellulose/papers: a. CE; b. CEE; c. CEA; d. PA; e. PAE and f. PAA.

### 3.3.5.5 Test for hydrophobicity

To investigate the hydrophobic properties of final products, a brief water drops experiments of cellulose/papers were implemented. **Figure 3.61** shows the performances of cellulose/papers (from top to bottom is CE, CEE, PA and PAE separately) after 1,5 and 10 drops (from left to right) of deionized water. It can be observed that the initial materials especially cellulose present a hydrophilic property due to the rich hydrogen groups on the surface. Even the modified cellulose shows a bad water proof property, the grafted cellulose still absorbs less water than original one. For paper samples, PAE displays a good hydrophobic function and is still not wet after adding 10 drops of deionized water. The experiment indicated that modification with APTES is successful and effective. However, it should be noticed that the reaction of foam materials during procedure is inherently water-based, thus care should be taken not to over silylate.

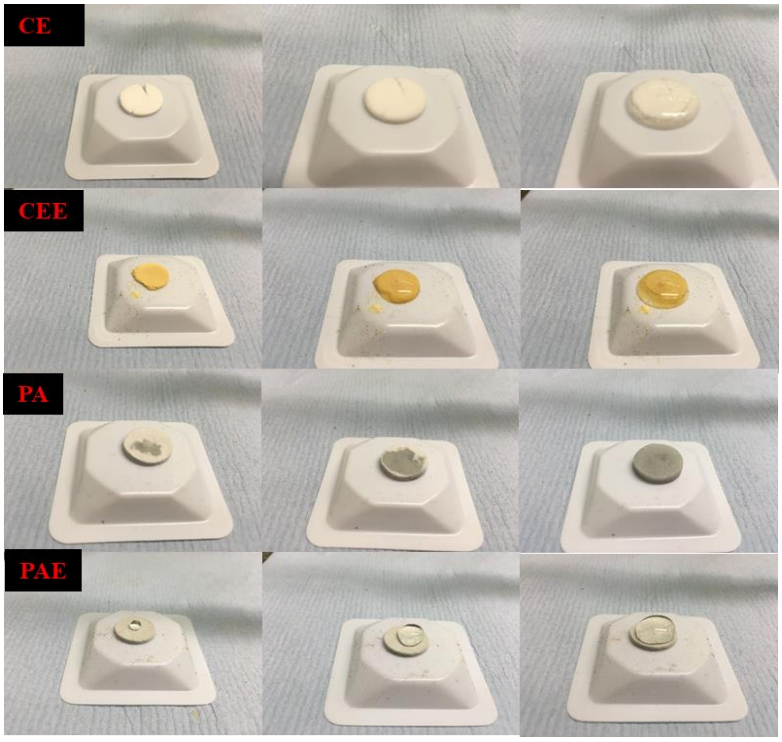


Figure 3. 61 Hydrophobicity test on cellulose/paper post treatment

Chapter 4

# 4 CONCLUSIONS and FUTURE WORK

## 4.1 Conclusions

In conclusion, this thesis shows that biorefineries that deliver chemicals, materials and (bio)energy can be envisaged from valorization of pea, ginger and agri-straw UFSCWs as shown in **Figure 4.1**. As global population continues to increase, unfortunately, there will be no shortage of food waste so its paramount to divert from landfill or incineration in to chemicals, materials and (bio)energy for development of a sustainable 21st century.

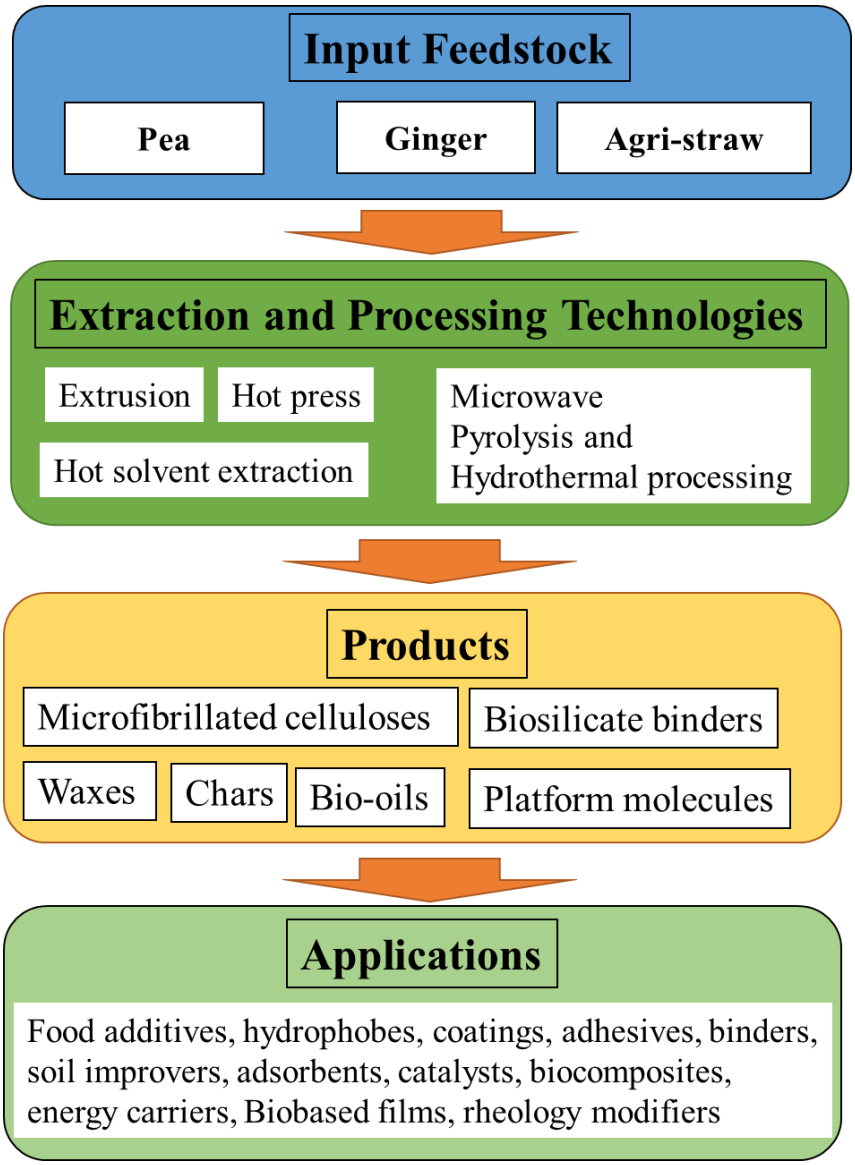


Figure 4. 1 Conceptual UFSCW biorefinery based on pea, ginger and agri-straw input feedstocks

Bioboards, especially wood and toxic-binder (UF, PF and isocyanate), made from under-utilised agri-straws will avoid deforestation and at the same stop the illegal burning of straws post-harvest, which causes significant air-borne pollution as well soil erosion. The manufacture of a SIP entirely from renewable resources is still its infancy but represents an interesting valorization opportunity that promotes resource efficiency, provides shelter and warmth. A concept SIP from bioboards and renewable paper foam material is shown in **Figure 4.2**.

Figure 4. 2 Preliminary prototype of SIP.

The re-utilization UFSCW not only releases the environmental burden, but also promote income for farmers and local community through new jobs, especially in developing countries with large agricultural arising. All the efforts in this thesis complement the UN Sustainable Development Goals, such as, reducing food losses along production and supply chains, reducing poverty & inequality, extending job opportunities, halting deforestation and promoting circular bioeconomy.

In terms of technology, acid-free hydrothermal microwave processing is a promising technology in valorization of UFSCW due to its rapid heating and extraction capability

as well using water alone as a solvent. Microwave pyrolysis has shown to provide bio-oils and energy densify materials so they become potential sources of bioenergy.

The microfibrillated celluloses both from pea and ginger waste could be used as hydrogels which can be used back in food or pharmaceutical products or cosmetics as rheology modifiers (thickeners). Meanwhile, the byproduct including oils, sugars and starch could also be used in a variety of fields: the oils especially ginger oils obtained from the biomass with Soxhlet extraction have nutritional and pharmacological benefits and are very popular in food and medical application. The sugars which come from hydrolysates have economic value as bioresource, they can further convert to bio-based polymers, biofuels or biomaterials via biotechnology.[69] The starch, which is interestingly only extracted from the ginger, can be used as adhesive or food directly or convert to other high value added products.[261] It should be noted isolation of starch was a surprise as the intention was to isolate pectin on addition cold ethanol to MHT hydrolysate.

Bio-oils were rich in both aliphatic and aromatic platform molecules. Furanics are interesting as a source of biobased platform molecules for conversion into further molecules of industrial interest such as furan-2-, 5-dicarboxylic acid.[262] The hydrochars have useful properties including porous structure, high specific surface area, and abundant functional groups, for potential application as soil amendment agents, water/air adsorbents , catalysts, and an energy source.[263, 264]

## 4.2 Limitations and Future work

Although the work was carried out thoroughly, there were still a few limitations in this

thesis, to improve the quality of product and motivate future work.

### 4.2.1 Pretreatment

Pretreatment of biomass is important as it dictates the final quality and characteristics of materials obtained. In this study, only extrusion was investigated which demonstrated it was a feasible way to produce MFCs with better performance. In the future other pretreatment approaches should be considered such as ultrasound,[265] ball-milling,[266] ionic liquids[267]or or green solvents.[268]

### 4.2.2 Improvements in the quality and characterization of MFCs

Hornification of cellulose is a major problem in the defibrillation of cellulose. Hornification is a direct manifestation of the drying process. In this thesis, all samples were oven dried, which leads to hornification. Thus, future work should explore other drying methods such as freeze-drying which is known to limit hornification[208] or explore more diluted and well-dispersed suspensions for homogenization/ultrasonic treatment.[69]

Due to time limitations, further characterisation of MFC hydrogels was not possible. Importantly, the rheological characterization including temperature sweep, structure recovery (the rate and extent of viscosity recovery of the sample after shear) and flow curves (viscosity of the samples at different shear rates) should be explored as they will dictate possible applications.[269, 270]

The formation of biobased films should be explored further either as membranes for gas and liquid separation or as biobased packing materials. The latter is very topical given the global waste plastic issues, whereby, synthetic, non-biodegradable plastics

are polluting our planet.

### 4.2.3 Hydrolysate valorization

The highly valuable products (sugars, small molecules) which were extracted from hydrolysate were only identified and these products can be explored for further potential applications, the sugars are important for the production of either platform molecules or input feedstock for industrial biotechnology processes.[271]

### 4.2.4 Green extractions

In this study, the Soxhlet extraction was implemented to remove the organic compounds (essential oils or wax). However, the use of the organic solvents (ethanol) during washing procedure has a great impact on the greenness of the total process, and environmentally friendly approaches including supercritical $CO_2$ might be better. This green technology can extract non to moderately polar compounds from biomass. Alternatively, superhot water could be explored which becomes less polar at higher temperatures and pressure.

### 4.2.5 Biocomposites

The particle boards made of wheat straw and silicate solution are renewable, fire resistant and low cost. However, a full characterization based in industry standards need to be conducted to explore their full utility.[272] Generally, fibre foam materials have excellent properties of sound absorption, thermal insulation and fire resistance, but the problem is that it is not waterproof which restricts the application. Also, their mechanical strength is not enough for actual utilization as they are often very soft and/or brittle materials. Both improving hydrophobicity through exploring silyating

agents and improving mechanical strength either through addition of fillers or chemical cross-linking needs to be explored.

# References


(1) Worldometer. https://www.worldometers.info/world-population/ (accessed 7 April 2020).

(2) OCDE. Global material resources outlook to 2060: Economic drivers and environmental consequences. **2019**.

(3) Mehariya, S.; Iovine, A.; Casella, P.; Musmarra, D.; Chianese, S.; Marino, T.; Figoli, A.; Sharma, N.; Molino, A., Bio-based and agriculture resources for production of bioproducts. In *Current Trends and Future Developments on (Bio-) Membranes*

(4) IPCC. Special Report on Global Warming of 1.5 ºC,. http://www.ipcc.ch/report/sr15/ (accessed 3 June 2020).

(5) Amsaveni, D.; Ghayathri, D. K.; Venkatesan, S. Optimizing the usage of plastic waste in cement industry using discrete dynamic programming. *Materials Today: Proceedings*, **2020,** *21*, 257-262.

(6) Lacy, P.; Long, J.; Spindler, W., *Toward a Circular Future*. Springer: **2020**.

(7) Pew Research Center. https://www.pewresearch.org/fact-tank/2019/06/17/worlds-population-is-projected-to-nearly-stop-growing-by-the-end-of-the-century/ (accessed 7 April 2020).

(8) United Nations. Transforming our world: the 2030 Agenda for Sustainable Development. https://sustainabledevelopment.un.org/post2015/transformingourworld (accessed 4 June 2020).

(9) United Nations. Transforming our world: the 2030 Agenda for Sustainable Development. https://sustainabledevelopment.un.org/post2015/transformingourworld (accessed 30 October 2019).

(10) Allen, C.; Metternicht, G.; Wiedmann, T. National pathways to the Sustainable Development Goals (SDGs): A comparative review of scenario modelling tools. *Environmental Science & Policy*, **2016,** *66*, 199-207.

(11) United Nations. What is the Paris Agreement? https://unfccc.int/process-and-meetings/the-paris-agreement/what-is-the-paris-agreement (accessed 7 April 2020).

(12) United Nations. About the UN Climate Change Conference - December 2019. https://unfccc.int/about-the-un-climate-change-conference-december-2019 (accessed 7 April 2020).

(13) Anastas, P. T.; Warner, J. C. Principles of green chemistry. *Green chemistry: Theory and practice*, **1998**, 29-56.

(14) US EPA Green Chemistry Program. https://www.epa.gov/greenchemistry (accessed 4 June 2020).

(15) *Catalyzing Growth and Addressing Our World's Sustainability Challenges*; Ooford Economics: 2019.

(16) Chemistry Council. The Chemistry Council Sector Deal. http://ukchemistrygrowth.com/wp-content/uploads/2019/11/Chemistry-Council-Sector-Deal-041119-1.pdf (accessed 7 April 2020).

(17) BioEnergy Consult. The Concept of Biorefinery. https://www.bioenergyconsult.com/biorefinery/ (accessed 4 June 2020).
(18) Alonso, D. M.; Bond, J. Q.; Dumesic, J. A. Catalytic conversion of biomass to biofuels. *Green Chemistry*, **2010,** *12*, 1493–1513.
(19) Cherubini, F. The biorefinery concept: using biomass instead of oil for producing energy and chemicals. *Energy conversion and management*, **2010,** *51*, 1412-1421.
(20) A Linares-Pasten, J.; Andersson, M.; N Karlsson, E. Thermostable glycoside hydrolases in biorefinery technologies. *Current Biotechnology*, **2014,** *3*, 26-44.
(21) Fernando, S.; Adhikari, S.; Chandrapal, C.; Murali, N. Biorefineries: current status, challenges, and future direction. *Energy & Fuels*, **2006,** *20*, 1727-1737.
(22) Dale, B. E. Biomass refining global impact-the biobased economy of the 21st century. *Biorefineries-Industrial Processes and Product*, **2006,** *1*, 41-66.
(23) Lange, J. P. Lignocellulose conversion: an introduction to chemistry, process and economics. *Biofuels, Bioproducts and Biorefining: Innovation for a sustainable economy*, **2007,** *1*, 39-48.
(24) Vernès, L.; Li, Y.; Chemat, F.; Abert-Vian, M., *Biorefinery concept as a key for sustainable future to green chemistry—the case of microalgae*. Springer: **2019**.
(25) Yang, H.; Gözaydın, G. k.; Nasaruddin, R. R.; Har, J. R. G.; Chen, X.; Wang, X.; Yan, N. Toward the shell biorefinery: processing crustacean shell waste using hot water and carbonic acid. *ACS Sustainable Chemistry & Engineering*, **2019,** *7*, 5532-5542.
(26) Khan, M. U.; Ahring, B. K. Anaerobic digestion of biorefinery lignin: Effect of different wet explosion pretreatment conditions. *Bioresource Technology*, **2020,** *298*, 1-9.
(27) Chandel, A.; Da Silva, S. S., *Sustainable Degradation of Lignocellulosic Biomass: Techniques, Applications and Commercialization*. BoD–Books on Demand: **2013**.
(28) Chundawat, S. P.; Donohoe, B. S.; da Costa Sousa, L.; Elder, T.; Agarwal, U. P.; Lu, F.; Ralph, J.; Himmel, M. E.; Balan, V.; Dale, B. E. Multi-scale visualization and characterization of lignocellulosic plant cell wall deconstruction during thermochemical pretreatment. *Energy & Environmental Science*, **2011,** *4*, 973-984.
(29) Bozell, J. J.; O'Lenick, C.; Warwick, S. Biomass fractionation for the biorefinery: heteronuclear multiple quantum coherence–nuclear magnetic resonance investigation of lignin isolated from solvent fractionation of switchgrass. *Journal of agricultural and food chemistry*, **2011,** *59*, 9232-9242.
(30) Song, Q.; Winter, W. T.; Bujanovic, B. M.; Amidon, T. E. Nanofibrillated cellulose (NFC): A high-value co-product that improves the economics of cellulosic ethanol production. *Energies*, **2014,** *7*, 607-618.
(31) Wilkinson, S.; Greetham, D.; Tucker, G. A. Evaluation of different lignocellulosic biomass pretreatments by phenotypic microarray-based metabolic analysis of fermenting yeast. *Biofuel Research Journal*, **2016,** *3*, 357-365.
(32) Kudakasseril Kurian, J.; Raveendran Nair, G.; Hussain, A.; Vijaya Raghavan, G. S. Feedstocks, logistics and pre-treatment processes for sustainable lignocellulosic biorefineries: A comprehensive review. *Renewable and Sustainable Energy Reviews*, **2013,** *25*, 205-219.

(33) Chen, H.; Liu, J.; Chang, X.; Chen, D.; Xue, Y.; Liu, P.; Lin, H.; Han, S. A review on the pretreatment of lignocellulose for high-value chemicals. *Fuel Processing Technology,* **2017,** *160*, 196-206.
(34) Rajinipriya, M.; Nagalakshmaiah, M.; Robert, M.; Elkoun, S. Importance of Agricultural and Industrial Waste in the Field of Nanocellulose and Recent Industrial Developments of Wood Based Nanocellulose: A Review. *ACS Sustainable Chemistry & Engineering,* **2018,** *6*, 2807-2828.
(35) George, A.; Brandt, A.; Tran, K.; Zahari, S. M. S. N. S.; Klein-Marcuschamer, D.; Sun, N.; Sathitsuksanoh, N.; Shi, J.; Stavila, V.; Parthasarathi, R.; Singh, S.; Holmes, B. M.; Welton, T.; Simmons, B. A.; Hallett, J. P. Design of low-cost ionic liquids for lignocellulosic biomass pretreatment. *Green Chemistry*, **2015,** *17*, 1728-1734.
(36) Xu, F.; Sun, J.; Konda, N. V. S. N. M.; Shi, J.; Dutta, T.; Scown, C. D.; Simmons, B. A.; Singh, S. Transforming biomass conversion with ionic liquids: process intensification and the development of a high-gravity, one-pot process for the production of cellulosic ethanol. *Energy & Environmental Science,* **2016,** *9*, 1042-1049.
(37) Yan, Z.; Li, J.; Chang, S.; Cui, T.; Jiang, Y.; Yu, M.; Zhang, L.; Zhao, G.; Qi, P.; Li, S. Lignin relocation contributed to the alkaline pretreatment efficiency of sweet sorghum bagasse. *Fuel,* **2015,** *158*, 152-158.
(38) Laurens, L. M. L.; Nagle, N.; Davis, R.; Sweeney, N.; Van Wychen, S.; Lowell, A.; Pienkos, P. T. Acid-catalyzed algal biomass pretreatment for integrated lipid and carbohydrate-based biofuels production. *Green Chemistry*, **2015,** *17*, 1145-1158.
(39) Murciano Martínez, P.; Bakker, R.; Harmsen, P.; Gruppen, H.; Kabel, M. Importance of acid or alkali concentration on the removal of xylan and lignin for enzymatic cellulose hydrolysis. *Industrial Crops and Products,* **2015,** *64*, 88-96.
(40) Zubrowska-Sudol, M.; Walczak, J. Effects of mechanical disintegration of activated sludge on the activity of nitrifying and denitrifying bacteria and phosphorus accumulating organisms. *Water Res,* **2014,** *61*, 200-209.
(41) Hu, H.; Zhang, Y.; Liu, X.; Huang, Z.; Chen, Y.; Yang, M.; Qin, X.; Feng, Z. Structural changes and enhanced accessibility of natural cellulose pretreated by mechanical activation. *Polymer Bulletin,* **2013,** *71*, 453-464.
(42) Anis, S.; Zainal, Z. A. Study on kinetic model of microwave thermocatalytic treatment of biomass tar model compound. *Bioresour Technol,* **2014,** *151*, 183-90.
(43) Rouches, E.; Herpoël-Gimbert, I.; Steyer, J. P.; Carrere, H. Improvement of anaerobic degradation by white-rot fungi pretreatment of lignocellulosic biomass: A review. *Renewable and Sustainable Energy Reviews,* **2016,** *59*, 179-198.
(44) Alvira, P.; Negro, M. J.; Ballesteros, I.; González, A.; Ballesteros, M. Steam explosion for wheat straw pretreatment for sugars production. *Bioethanol,* **2016,** *2*, 66-75.
(45) Lopez-Linares, J. C.; Ballesteros, I.; Touran, J.; Cara, C.; Castro, E.; Ballesteros, M.; Romero, I. Optimization of uncatalyzed steam explosion pretreatment of rapeseed straw for biofuel production. *Bioresour Technol,* **2015,** *190*, 97-105.
(46) Ravindran, R.; Jaiswal, A. K. A comprehensive review on pre-treatment strategy

for lignocellulosic food industry waste: challenges and opportunities. *Bioresource technology*, **2016,** *199*, 92-102.
(47) Lee, H.; Hamid, S. B. A.; Zain, S. Conversion of lignocellulosic biomass to nanocellulose: structure and chemical process. *The Scientific World Journal,* **2014,** *2014*, 1-20.
(48) Lavanya, D.; Kulkarni, P.; Dixit, M.; Raavi, P. K.; Krishna, L. N. V. Sources of cellulose and their applications—a review. *Int J Drug Formul Res,* **2011,** *2*, 19-38.
(49) Matthews, J. F.; Himmel, M. E.; Crowley, M. F. Conversion of cellulose Iα to Iβ via a high temperature intermediate (I-HT) and other cellulose phase transformations. *Cellulose,* **2012,** *19*, 297-306.
(50) Kontturi, E. Cellulose: Structure, Morphology and Crystalline Forms. *Chem-E2140. Aaito University*, **2015**.
(51) Wada, M.; Chanzy, H.; Nishiyama, Y.; Langan, P. Cellulose IIII crystal structure and hydrogen bonding by synchrotron X-ray and neutron fiber diffraction. *Macromolecules*, **2004,** *37*, 8548-8555.
(52) Buleon, A.; Chanzy, H. Single crystals of cellulose IVII: preparation and properties. *Journal of Polymer Science: Polymer Physics Edition,* **1980,** *18*, 1209-1217.
(53) Dos Santos, N. M. Influence of chemical and enzymatic treatments on a variety of wood pulps on their dissolution in NaOH-water. PhD Thesis, **2013**.
(54) Ramos, L. P. The chemistry involved in the steam treatment of lignocellulosic materials. *Qu ímica Nova,* **2003,** *26*, 863-871.
(55) P érez, J.; Munoz-Dorado, J.; De la Rubia, T.; Martinez, J. Biodegradation and biological treatments of cellulose, hemicellulose and lignin: an overview. *International microbiology,* **2002,** *5*, 53-63.
(56) Tekin, K.; Karag öz, S. Non-catalytic and catalytic hydrothermal liquefaction of biomass. *Research on Chemical Intermediates,* **2013,** *39*, 485-498.
(57) Lavarack, B.; Griffin, G.; Rodman, D. The acid hydrolysis of sugarcane bagasse hemicellulose to produce xylose, arabinose, glucose and other products. *Biomass and bioenergy*, **2002,** *23*, 367-380.
(58) Ge, Y.; Li, Z. Application of lignin and its derivatives in adsorption of heavy metal ions in water: a review. *ACS Sustainable Chemistry & Engineering*, **2018,** *6*, 7181-7192.
(59) Chabannes, M.; Ruel, K.; Yoshinaga, A.; Chabbert, B.; Jauneau, A.; Joseleau, J. P.; Boudet, A. M. In situ analysis of lignins in transgenic tobacco reveals a differential impact of individual transformations on the spatial patterns of lignin deposition at the cellular and subcellular levels. *The Plant Journal,* **2001,** *28*, 271-282.
(60) Heitner, C.; Dimmel, D.; Schmidt, J., *Lignin and lignans: advances in chemistry*. CRC press: **2016**.
(61) Baig, K. S.; Wu, J.; Turcotte, G. Future prospects of delignification pretreatments for the lignocellulosic materials to produce second generation bioethanol. *International Journal of Energy Research,* **2019,** *43*, 1411-1427.
(62) Meng, Y.; Lu, J.; Cheng, Y.; Li, Q.; Wang, H. Lignin-based hydrogels: A review of preparation, properties, and application. *International journal of biological*

*macromolecules*, **2019**, 1006-1019.
(63) Rangan, A.; Manjula, M.; Satyanarayana, K.; Menon, R. Lignin/nanolignin and their biodegradable composites. *Biodegradable Green Composites*, **2016**, 167-198.
(64) Collins, M. N.; Nechifor, M.; Tanasă, F.; Zănoagă, M.; McLoughlin, A.; Stróżyk, M. A.; Culebras, M.; Teacă, C.-A. Valorization of lignin in polymer and composite systems for advanced engineering applications–a review. *International journal of biological macromolecules*, **2019**, 828-849.
(65) The World Bank Global Waste on Pace to Triple by 2100. https://www.worldbank.org/en/news/feature/2013/10/30/global-waste-on-pace-to-triple (accessed 4 June 2020).
(66) Otterdijk, J. G. R. V. Global food losses and food waste - Food and Agriculture Organization of the United Nations. **2011**.
(67) FAO,. Global initiative on food loss and food waste reduction. http://www.fao.org/save-food/en/ (accessed 4 June 2020).
(68) FAO. Global food losses and food waste. http://www.fao.org/save-food/en/ (accessed 4 June 2020).
(69) Macedo de Melo, E. Microfibrillated Cellulose and High-value Chemicals from Orange Peel Residues. PhD Thesis, University of York: **2018**.
(70) FAO. Food wastage footprint: Impacts on natural resources. http://www.fao.org/3/i3347e/i3347e.pdf (accessed 4 June 2020).
(71) Papargyropoulou, E.; Lozano, R.; Steinberger, J. K.; Wright, N.; bin Ujang, Z. The food waste hierarchy as a framework for the management of food surplus and food waste. *Journal of Cleaner Production*, **2014,** *76*, 106-115.
(72) Matharu, A. S.; de Melo, E. M.; Houghton, J. A. Opportunity for high value-added chemicals from food supply chain wastes. *Bioresource technology*, **2016,** *215*, 123-130.
(73) Bilska, B.; Wrzosek, M.; Kołożyn-Krajewska, D.; Krajewski, K. Risk of food losses and potential of food recovery for social purposes. *Waste Management*, **2016,** *52*, 269-277.
(74) Hargreaves, J. S.; Pulford, I. D.; Balakrishnan, M.; Batra, V. S., *Conversion of large scale wastes into value-added products*. CRC Press: **2013**.
(75) Liu, S. Woody biomass: Niche position as a source of sustainable renewable chemicals and energy and kinetics of hot-water extraction/hydrolysis. *Biotechnology advances*, **2010,** *28*, 563-582.
(76) Verma, N.; Bansal, M. C.; Kumar, V. Pea peel Waste: A lignocellulosic waste and its utility in cellulase production by Trichoderma reesei under solid state cultivation. *BioResources*, **2011,** *6*, 1505-1519.
(77) Choi, W. S.; HAN, J. H. Physical and Mechanical Properties ofPea-Protein-based Edible Films. *Food science*, **2001,** *66*, 319-322.
(78) Rao, I. U., *Origin and Introduction of Crop Plants, Cereals and Pulses*. **2007**.
(79) FAO. FAOSTAT. http://www.fao.org/faostat/en/#data/QC (accessed 4 June 2020).
(80) Phillips, J. Processing to valorise green biomass side streams to create new food ingredients. PhD Thesis, University of Nottingham: **2019**.

(81) Venkidasamy, B.; Selvaraj, D.; Nile, A. S.; Ramalingam, S.; Kai, G.; Nile, S. H. Indian pulses: A review on nutritional, functional and biochemical properties with future perspectives. *Trends in Food Science & Technology*, **2019**.
(82) Agriculture in the United Kingdom. https://www.gov.uk/government/collections/agriculture-in-the-united-kingdom (accessed 3 June 2020).
(83) Wadhwa, M.; Bakshi, M. Utilization of fruit and vegetable wastes as livestock feed and as substrates for generation of other value-added products. *Rap Publication*, **2013,** *4*, 1-58.
(84) Nimbalkar, P. R.; Khedkar, M. A.; Chavan, P. V.; Bankar, S. B. Biobutanol production using pea pod waste as substrate: Impact of drying on saccharification and fermentation. *Renewable Energy*, **2018,** *117*, 520-529.
(85) Xia, H.; Houghton, J. A.; Clark, J. H.; Matharu, A. S. Potential Utilization of Unavoidable Food Supply Chain Wastes–Valorization of Pea Vine Wastes. *ACS Sustainable Chemistry & Engineering*, **2016,** *4*, 6002-6009.
(86) Sharma, R.; Rawat, R.; Bhogal, R. S.; Oberoi, H. S. Multi-component thermostable cellulolytic enzyme production by Aspergillus niger HN-1 using pea pod waste: Appraisal of hydrolytic potential with lignocellulosic biomass. *Process Biochemistry*, **2015,** *50*, 696-704.
(87) Müsellim, E.; Tahir, M. H.; Ahmad, M. S.; Ceylan, S. Thermokinetic and TG/DSC-FTIR study of pea waste biomass pyrolysis. *Applied Thermal Engineering*, **2018,** *137*, 54-61.
(88) Gómez, L. D.; Vanholme, R.; Bird, S.; Goeminne, G.; Trindade, L. M.; Polikarpov, I.; Simister, R.; Morreel, K.; Boerjan, W.; McQueen-Mason, S. J. Side by Side Comparison of Chemical Compounds Generated by Aqueous Pretreatments of Maize Stover, Miscanthus and Sugarcane Bagasse. *BioEnergy Research*, **2014,** *7*, 1466-1480.
(89) Mekonnen, T.; Mussone, P.; Khalil, H.; Bressler, D. Progress in bio-based plastics and plasticizing modifications. *Journal of Materials Chemistry A*, **2013,** *1*, 13379-13398.
(90) Shahrajabian, M. H.; Sun, W.; Cheng, Q. Clinical aspects and health benefits of ginger (Zingiber officinale) in both traditional Chinese medicine and modern industry. *Acta Agriculturae Scandinavica, Section B—Soil & Plant Science*, **2019,** *69*, 546-556.
(91) Aly, M. M.; El Sawy, A.; El Gendy, R. A. Comparative study of different shading types on growth and yield of ginger plants. *Middle East J*, **2019,** *8*, 1264-1270.
(92) MarketWatch. https://www.marketwatch.com/press-release/ginger-market-2019-global-share-manufacturing-cost-structure-and-forecast-to-2028-2019-03-21 (accessed 4 June 2020).
(93) Palatty, P. L.; Haniadka, R.; Valder, B.; Arora, R.; Baliga, M. S. Ginger in the prevention of nausea and vomiting: a review. *Crit Rev Food Sci Nutr*, **2013,** *53*, 659-69.
(94) Kou, X.; Ke, Y.; Wang, X.; Rahman, M. R. T.; Xie, Y.; Chen, S.; Wang, H. Simultaneous extraction of hydrophobic and hydrophilic bioactive compounds from ginger (Zingiber officinale Roscoe). *Food chemistry*, **2018,** *257*, 223-229.

(95) Lai, Y.-S.; Lee, W.-C.; Lin, Y.-E.; Ho, C.-T.; Lu, K.-H.; Lin, S.-H.; Panyod, S.; Chu, Y.-L.; Sheen, L.-Y. Ginger essential oil ameliorates hepatic injury and lipid accumulation in high fat diet-induced nonalcoholic fatty liver disease. *Journal of agricultural and food chemistry*, **2016,** *64*, 2062-2071.
(96) Makanjuola, S. A. Influence of particle size and extraction solvent on antioxidant properties of extracts of tea, ginger, and tea–ginger blend. *Food science & nutrition*, **2017,** *5*, 1179-1185.
(97) Omage, J.; Onimisi, P.; Adegbite, E.; Agunbiade, M. The effect of ginger (Zingiber officinale Roscoe) waste meal on growth performance, carcass characteristics, serum lipid and serum cholesterol profiles of rabbit. *Pakistan Journal of Nutrition*, **2007,** *6*, 359-362.
(98) Moreschi, S. R.; Petenate, A. J.; Meireles, M. A. A. Hydrolysis of ginger bagasse starch in subcritical water and carbon dioxide. *Journal of agricultural and food chemistry*, **2004,** *52*, 1753-1758.
(99) Sims, R. E. Biomass, bioenergy and biomaterials: future prospects. *Biomass and Agriculture–Sustainability Markets and Policies. OECD, Paris*, **2004**, 37-61.
(100) Qi, G.; Xiong, L.; Li, H.; Huang, Q.; Luo, M.; Tian, L.; Chen, X.; Huang, C.; Chen, X. Hydrotropic pretreatment on wheat straw for efficient biobutanol production. *Biomass and bioenergy*, **2019,** *122*, 76-83.
(101) Huerta, R. R.; Saldaña, M. D. Sequential treatment with pressurized fluid processing and ultrasonication for biorefinery of canola straw towards lignocellulosic nanofiber production. *Industrial Crops and Products*, **2019,** *139*, 111521.
(102) Kumari, D.; Singh, R. Pretreatment of lignocellulosic wastes for biofuel production: A critical review. *Renewable and Sustainable Energy Reviews*, **2018,** *90*, 877-891.
(103) Luque, R.; Herrero-Davila, L.; Campelo, J. M.; Clark, J. H.; Hidalgo, J. M.; Luna, D.; Marinas, J. M.; Romero, A. A. Biofuels: a technological perspective. *Energy & Environmental Science*, **2008,** *1*, 542-564.
(104) Tabarsa, T.; Jahanshahi, S.; Ashori, A. Mechanical and physical properties of wheat straw boards bonded with a tannin modified phenol–formaldehyde adhesive. *Composites Part B: Engineering*, **2011,** *42*, 176-180.
(105) Medved, S.; Antonović, A.; Jambreković, V.; Čuk, N.; Kunaver, M. In *Wood-based panels as material for sustainable use of natural resources*, Wood is good: transfer of knowledge in practice as a way out of the crisis. Proceedings of the 21st International Scientific Conference, Zagreb, Croatia, 15th October 2010, Faculty of Forestry, University of Zagreb: 2010; pp 73-80.
(106) Grand View Research. Wood Based Panel Market Size, Share, Industry Analysis Report, 2027. https://www.grandviewresearch.com/industry-analysis/wood-based-panel-market (accessed 8 April 2020).
(107) Rahmawati, W.; Haryanto, A.; Tindaon, G. In *Utilization of Purun Tikus (Eleocharis dulcis) as Bioboard Raw Material with Heat Press*, IOP Conference Series: Earth and Environmental Science, IOP Publishing: 2019; pp 1-7.
(108) Elbashiry, E. M.; Chen, J.; Tuo, W.; Ren, Y.; Guo, Z. Review of the pretreatment methods for wheat straw building materials. *Journal of Reinforced Plastics and*

*Composites,* **2018,** *37*, 35-48.
(109) Hýsková, P.; Hýsek, Š.; Schönfelder, O.; Šedivka, P.; Lexa, M.; Jarský, V. Utilization of agricultural rests: Straw-based composite panels made from enzymatic modified wheat and rapeseed straw. *Industrial Crops and Products,* **2020,** *144*, 1-8.
(110) Domínguez-Robles, J.; Tarrés, Q.; Alcalà, M.; El Mansouri, N.-E.; Rodríguez, A.; Mutjé, P.; Delgado-Aguilar, M. Development of high-performance binderless fiberboards from wheat straw residue. *Construction and Building Materials,* **2020,** *232*, 1-11.
(111) Hýsek, Š.; Podlena, M.; Bartsch, H.; Wenderdel, C.; Böhm, M. Effect of wheat husk surface pre-treatment on the properties of husk-based composite materials. *Industrial Crops and Products,* **2018,** *125*, 105-113.
(112) Torkaman, J. Mechanism of Bondability in Uf-bonded Rice Husk Particle Boards by Isocyanate. *Journal of Applied Sciences,* **2019,** *19*, 247-251.
(113) Nicolao, E.; Leiva, P.; Chalapud, M.; Ruseckaite, R.; Ciannamea, E.; Stefani, P. Flexural and tensile properties of biobased rice husk-jute-soybean protein particleboards. *Journal of Building Engineering,* **2020**, 101261.
(114) Chalapud, M. C.; Herdt, M.; Nicolao, E. S.; Ruseckaite, R. A.; Ciannamea, E. M.; Stefani, P. M. Biobased particleboards based on rice husk and soy proteins: Effect of the impregnation with tung oil on the physical and mechanical behavior. *Construction and Building Materials,* **2020,** *230*, 1-6.
(115) Zeleniuc, O.; Brenci, L.-M.; Cosereanu, C.; Fotin, A. Influence of Adhesive Type and Content on the Properties of Particleboard Made from Sunflower Husks. *BioResources,* **2019,** *14*, 7316-7331.
(116) Güler, G. Chemical, physical, and mechanical properties of particleboards manufactured from sodium hydroxide-treated sunflower (Helianthus annuus L.) stalks. *Bartın Orman Fakültesi Dergisi,* **2019,** *21*, 758-770.
(117) Nicolao, E.; Leiva, P.; Chalapud, M.; Ruseckaite, R.; Ciannamea, E.; Stefani, P. Flexural and tensile properties of biobased rice husk-jute-soybean protein particleboards. *Journal of Building Engineering,* **2020,** *30*, 1-5.
(118) Mahieu, A.; Alix, S.; Leblanc, N. Properties of particleboards made of agricultural by-products with a classical binder or self-bound. *Industrial Crops and Products,* **2019,** *130*, 371-379.
(119) Mesquita, R. G. d. A.; Sanadi, A. R.; Marconcini, J. M.; Correa, A. C.; César, A. A. d. S.; Andrade, L. M. F.; Lopes, T. A.; Simão, J. A.; Mendes, L. M. The effect of cellulose nanocrystals in sugarcane bagasse particleboards of pith and fibers. *Cerne,* **2019,** *25*, 203-213.
(120) Gauss, C.; Araujo, V. D.; Gava, M.; Cortez-Barbosa, J.; Savastano Junior, H. Bamboo particleboards: recent developments. *Pesquisa Agropecuária Tropical,* **2019,** *49*, 1-9.
(121) Kariuki, S. W.; Wachira, J.; Kawira, M.; Leonard, G. M. Characterization of Prototype Formulated Particleboards from Agroindustrial Lignocellulose Biomass Bonded with Chemically Modified Cassava Peel Starch. *Advances in Materials Science and Engineering,* **2019,** *2019*, 1-15.
(122) Hernández, D.; Fernández-Puratich, H.; Cataldo, F.; González, J. Particle boards

made with Prunus avium fruit waste. *Case Studies in Construction Materials*, **2020,** *12*, 1-6.
(123) Kim, J.-H.; Shim, B. S.; Kim, H. S.; Lee, Y.-J.; Min, S.-K.; Jang, D.; Abas, Z.; Kim, J. Review of nanocellulose for sustainable future materials. *International Journal of Precision Engineering and Manufacturing-Green Technology*, **2015,** *2*, 197-213.
(124) Hoeng, F.; Denneulin, A.; Bras, J. Use of nanocellulose in printed electronics: a review. *Nanoscale*, **2016,** *8*, 13131-13154.
(125) Kaushik, M.; Moores, A. nanocelluloses as versatile supports for metal nanoparticles and their applications in catalysis. *Green Chemistry*, **2016,** *18*, 622-637.
(126) De France, K. J.; Hoare, T.; Cranston, E. D. Review of Hydrogels and Aerogels Containing Nanocellulose. *Chemistry of Materials*, **2017,** *29*, 4609-4631.
(127) Du, H.; Liu, W.; Zhang, M.; Si, C.; Zhang, X.; Li, B. Cellulose nanocrystals and cellulose nanofibrils based hydrogels for biomedical applications. *Carbohydrate Polymers*, **2019,** *209*, 130-144.
(128) Abdul Khalil, H. P. S.; Davoudpour, Y.; Saurabh, C. K.; Hossain, M. S.; Adnan, A. S.; Dungani, R.; Paridah, M. T.; Islam Sarker, M. Z.; Fazita, M. R. N.; Syakir, M. I.; Haafiz, M. K. M. A review on nanocellulosic fibres as new material for sustainable packaging: Process and applications. *Renewable and Sustainable Energy Reviews*, **2016,** *64*, 823-836.
(129) Moon, R. J.; Martini, A.; Nairn, J.; Simonsen, J.; Youngblood, J. Cellulose nanomaterials review: structure, properties and nanocomposites. *Chem Soc Rev*, **2011,** *40*, 3941-3994.
(130) Garc ́a, A.; Gandini, A.; Labidi, J.; Belgacem, N.; Bras, J. Industrial and crop wastes: A new source for nanocellulose biorefinery. *Industrial Crops and Products*, **2016,** *93*, 26-38.
(131) Market resource report. https://www.marketsandmarkets.com/Market-Reports/nano-cellulose-market-56392090.html?gclid=EAIaIQobChMIq4Xdma-Q4AIVDrHtCh2aGgJQEAAYASAAEgKjtfD_BwE# (accessed 4 June 2020).
(132) Kargarzadeh, H.; Ahmad, I.; Thomas, S.; Dufresne, A., *Handbook of Nanocellulose and Cellulose Nanocomposites*. John Wiley & Sons: **2017**.
(133) Matharu, A. S.; de Melo, E. M.; Remon, J.; Wang, S.; Abdulina, A.; Kontturi, E. Processing of Citrus Nanostructured Cellulose: A Rigorous Design-of-Experiment Study of the Hydrothermal Microwave-Assisted Selective Scissoring Process. *ChemSusChem*, **2018,** *11*, 1344-1353.
(134) Reid, M. S.; Villalobos, M.; Cranston, E. D. Benchmarking Cellulose Nanocrystals: From the Laboratory to Industrial Production. *Langmuir*, **2017,** *33*, 1583-1598.
(135) Rebouillat, S.; Pla, F. State of the Art Manufacturing and Engineering of Nanocellulose: A Review of Available Data and Industrial Applications. *Journal of Biomaterials and Nanobiotechnology*, **2013,** *04*, 165-188.
(136) Salimi, S.; Sotudeh-Gharebagh, R.; Zarghami, R.; Chan, S. Y.; Yuen, K. H. Production of nanocellulose and its applications in drug delivery: A critical review. *ACS Sustainable Chemistry & Engineering*, **2019,** *7*, 15800-15827.

(137) Richel, A.; Jacquet, N. Microwave-assisted thermochemical and primary hydrolytic conversions of lignocellulosic resources: a review. *Biomass Conversion and Biorefinery,* **2015,** *5*, 115-124.
(138) Kostas, E. T.; Beneroso, D.; Robinson, J. P. The application of microwave heating in bioenergy: A review on the microwave pre-treatment and upgrading technologies for biomass. *Renewable and Sustainable Energy Reviews,* **2017,** *77*, 12-27.
(139) Kappe, C. O. Controlled microwave heating in modern organic synthesis. *Angewandte Chemie International Edition,* **2004,** *43*, 6250-6284.
(140) Takahashi, M.; Takenaka, H. DC electrical conductivity of cellulose. *Polymer journal,* **1983,** *15*, 625–629.
(141) Aguilar-Reynosa, A.; Romani, A.; Rodriguez-Jasso, R. M.; Aguilar, C. N.; Garrote, G.; Ruiz, H. A. Microwave heating processing as alternative of pretreatment in second-generation biorefinery: an overview. *Energy Conversion and Management,* **2017,** *136*, 50-65.
(142) Smith, R. E., *Prefab architecture: A guide to modular design and construction*. John Wiley & Sons: **2010**.
(143) Green Modular. What are structural insulated panels? . https://www.green-modular.com/blog/structural-insulated-panels/ (accessed 17 January 2020).
(144) Panjehpour, M.; Abang Ali, A. A.; Voo, Y. L. Structural Insulated Panels: Past, Present, and Future. *Journal of Engineering, Project & Production Management,* **2013,** *3*.
(145) Panjehpour, M.; Ali, A.; Abdullah, A.; Voo, Y. L. Structural Insulated Panels: Past, Present, and Future. *Journal of Engineering, Project & Production Management,* **2013,** *3*, 2-8.
(146) Kawasaki, T.; Kawai, S. Thermal insulation properties of wood-based sandwich panel for use as structural insulated walls and floors. *Journal of wood science,* **2006,** *52*, 75-83.
(147) Chen, Z.; Chen, Z.; Yang, Z.; Hu, J.; Yang, Y.; Chang, L.; Lee, L. J.; Xu, T. Preparation and characterization of vacuum insulation panels with super-stratified glass fiber core material. *Energy,* **2015,** *93*, 945-954.
(148) Binici, H.; Eken, M.; Kara, M.; Dolaz, M. In *An environment-friendly thermal insulation material from sunflower stalk, textile waste and stubble fibers*, 2013 International Conference on Renewable Energy Research and Applications (ICRERA), IEEE: 2013; pp 833-846.
(149) ECO-SEE. Healthier, quieter and more energy efficient buildings. https://www.greenovate-europe.eu/sites/default/files/publications/web-ECO-SEE-booklet.pdf (accessed 17 January 2020).
(150) BBC. Grenfell Tower fire: 'Urgent review' of firefighting resources requested. http://www.bbc.co.uk/news/uk-40543496 (accessed 4 June 2020).
(151) Chang, C. P.; Hung, S. C. Manufacture of flame retardant foaming board from waste papers reinforced with phenol–formaldehyde resin. *Bioresource technology,* **2003,** *86*, 201-202.
(152) Aguilar-Palazuelos, E.; Zazueta-Morales, J. d. J.; Jiménez-Arévalo, O. A.;

Martínez-Bustos, F. Mechanical and structural properties of expanded extrudates produced from blends of native starches and natural fibers of henequen and coconut. *Starch-Stärke,* **2007,** *59*, 533-542.

(153) Glenn, G.; Orts, W.; Nobes, G. Starch, fiber and CaCO3 effects on the physical properties of foams made by a baking process. *Industrial Crops and Products,* **2001,** *14*, 201-212.

(154) Feng, L.; Li, S.; Li, Y.; Li, H.; Zhang, L.; Zhai, J.; Song, Y.; Liu, B.; Jiang, L.; Zhu, D. Super-hydrophobic surfaces: from natural to artificial. *Advanced materials,* **2002,** *14*, 1857-1860.

(155) Cunha, A. G.; Gandini, A. Turning polysaccharides into hydrophobic materials: a critical review. Part 1. Cellulose. *Cellulose,* **2010,** *17*, 875-889.

(156) Balu, B.; Breedveld, V.; Hess, D. W. Fabrication of "roll-off" and "sticky" superhydrophobic cellulose surfaces via plasma processing. *Langmuir,* **2008,** *24*, 4785-4790.

(157) Cady, N. C.; Behnke, J. L.; Strickland, A. D. Copper-Based Nanostructured Coatings on Natural Cellulose: Nanocomposites Exhibiting Rapid and Efficient Inhibition of a Multi-Drug Resistant Wound Pathogen, A. baumannii, and Mammalian Cell Biocompatibility In Vitro. *Advanced Functional Materials,* **2011,** *21*, 2506-2514.

(158) Liao, X.; Zhang, Z.; Liang, Q.; Liao, Q.; Zhang, Y. Flexible, cuttable, and self-waterproof bending strain sensors using microcracked gold nanofilms@ paper substrate. *ACS applied materials & interfaces,* **2017,** *9*, 4151-4158.

(159) Tian, X.; Li, Y.; Wan, S.; Wu, Z.; Wang, Z. Functional surface coating on cellulosic flexible substrates with improved water-resistant and antimicrobial properties by use of ZnO nanoparticles. *Journal of Nanomaterials,* **2017,** *2017*, 1-9.

(160) Yazdanshenas, M. E.; Shateri-Khalilabad, M. One-step synthesis of superhydrophobic coating on cotton fabric by ultrasound irradiation. *Industrial & Engineering Chemistry Research,* **2013,** *52*, 12846-12854.

(161) Xue, C.-H.; Jia, S.-T.; Zhang, J.; Tian, L.-Q.; Chen, H.-Z.; Wang, M. Preparation of superhydrophobic surfaces on cotton textiles. *Science and technology of advanced materials,* **2008,** *9*, 1-7.

(162) Ratajczak, I.; Rzepecka, E.; Woźniak, M.; Szentner, K.; Mazela, B. The effect of alkyd resin on the stability of binding (3-aminopropyl) triethoxysilane with cellulose and wood. *Drewno: prace naukowe, doniesienia, komunikaty,* **2015,** *58*, 91--99.

(163) Ling, P. A.; Ismail, H. Tensile properties, water uptake, and thermal properties of polypropylene/waste pulverized tire/kenaf (PP/WPT/KNF) composites. *BioResources,* **2013,** *8*, 806-817.

(164) Salon, M.-C. B.; Abdelmouleh, M.; Boufi, S.; Belgacem, M. N.; Gandini, A.

Silane adsorption onto cellulose fibers: Hydrolysis and condensation reactions. *Journal of colloid and interface science,* **2005,** *289*, 249-261.
(165) Koga, H.; Kitaoka, T.; Isogai, A. Chemically-modified cellulose paper as a microstructured catalytic reactor. *Molecules,* **2015,** *20*, 1495-1508.
(166) Amantes, B. d. P.; Melo, R. P. d.; Neto, R. P. C.; Marques, M. d. F. V. Chemical treatment and modification of jute fiber surface. *Chemistry & Chemical Technology, 3 (11), 2017*, **2017,** *11*, 333-343.
(167) Hochmańska, P.; Mazela, B.; Krystofiak, T. Hydrophobicity and weathering resistance of wood treated with silane-modified protective systems. *Drewno: prace naukowe, doniesienia, komunikaty,* **2014,** *57*, 99-110.
(168) Ratajczak, I.; Wichłacz-Szentner, K.; Mazela, B.; Hochmańska, P.; Rissmann, I. Silicon compounds as additives improving coating performance: fixation of silicon compounds with cellulose. *European Journal of Wood and Wood Products,* **2010,** *68*, 483-486.
(169) Zain, N. F.; Yusop, S. M.; Ahmad, I. Preparation and characterization of cellulose and nanocellulose from pomelo (Citrus grandis) albedo. *J Nutr Food Sci,* **2014,** *5*, 334.
(170) Traynham, T.; Myers, D. J.; Carriquiry, A.; Johnson, L. Evaluation of water-holding capacity for wheat–soy flour blends. *Journal of the American Oil Chemists' Society,* **2007,** *84*, 151–155.
(171) Palme, A.; Theliander, H.; Brelid, H. Acid hydrolysis of cellulosic fibres: comparison of bleached kraft pulp, dissolving pulps and cotton textile cellulose. *Carbohydrate polymers,* **2016,** *136*, 1281-1287.
(172) Park, S.; Baker, J. O.; Himmel, M. E.; Parilla, P. A.; Johnson, D. K. Cellulose crystallinity index: measurement techniques and their impact on interpreting cellulase performance. *Biotechnology for biofuels,* **2010,** *3*, 1-10.
(173) Tian, G. Renewable materials from renewable resource. PhD Thesis, University of York: **2015**.
(174) Remón, J.; Matharu, A. S.; Clark, J. H. Simultaneous production of lignin and polysaccharide rich aqueous solutions by microwave-assisted hydrothermal treatment of rapeseed meal. *Energy Conversion and Management,* **2018,** *165*, 634-648.
(175) de Melo, E. M.; Clark, J. H.; Matharu, A. S. The Hy-MASS concept: hydrothermal microwave assisted selective scissoring of cellulose for in situ production of (meso)porous nanocellulose fibrils and crystals. *Green Chemistry,* **2017,** *19*, 3408-3417.
(176) Bagaria, A. Isolation and characterization of mesoporous cellulose from citrus and mango waste. PhD Thesis, University of York: **2014**.
(177) Gao, Y.; Xia, H.; Sulaeman, A.; de Melo, E. M.; Dugmore, T. I. J.; Matharu, A. S. Defibrillated celluloses via dual twin-screw extrusion and microwave hydrothermal treatment (MHT) of spent pea biomass. *ACS Sustainable Chemistry & Engineering*, **2019**, 11861–11871.

(178) Kim, Y.-M.; Lee, H. W.; Kim, S.; Watanabe, C.; Park, Y.-K. Non-isothermal pyrolysis of citrus unshiu peel. *Bioenergy Research*, **2015,** *8*, 431-439.
(179) Fan, J.; De bruyn, M.; Budarin, V. L.; Gronnow, M. J.; Shuttleworth, P. S.; Breeden, S.; Macquarrie, D. J.; Clark, J. H. Direct Microwave-Assisted Hydrothermal Depolymerization of Cellulose. *Journal of the American Chemical Society*, **2013,** *135*, 11728-11731.
(180) Hajir, M.; Graf, R.; Tremel, W. Stable amorphous calcium oxalate: synthesis and potential intermediate in biomineralization. *Chem Commun (Camb)*, **2014,** *50*.
(181) Kumar, A.; Negi, Y. S.; Choudhary, V.; Bhardwaj, N. K. Characterization of cellulose nanocrystals produced by acid-hydrolysis from sugarcane bagasse as agro-waste. *Journal of Materials Physics and Chemistry*, **2014,** *2*, 1-8.
(182) Azadfar, M.; Gao, A. H.; Bule, M. V.; Chen, S. Structural characterization of lignin: a potential source of antioxidants guaiacol and 4-vinylguaiacol. *Int J Biol Macromol*, **2015,** *75*, 58-66.
(183) Szymanska-Chargot, M.; Zdunek, A. Use of FT-IR spectra and PCA to the bulk characterization of cell wall residues of fruits and vegetables along a fraction process. *Food biophysics*, **2013,** *8*, 29-42.
(184) Horikawa, Y.; Hirano, S.; Mihashi, A.; Kobayashi, Y.; Zhai, S.; Sugiyama, J. Prediction of lignin contents from infrared spectroscopy: chemical digestion and lignin/biomass ratios of Cryptomeria japonica. *Applied biochemistry and biotechnology*, **2019,** *188*, 1066-1076.
(185) Tian, Z.; Zong, L.; Niu, R.; Wang, X.; Li, Y.; Ai, S. Recovery and characterization of lignin from alkaline straw pulping black liquor: As feedstock for bio‐oil research. *Journal of applied polymer science*, **2015,** *132*, 1-9.
(186) Tejado, A.; Pena, C.; Labidi, J.; Echeverria, J.; Mondragon, I. Physico-chemical characterization of lignins from different sources for use in phenol–formaldehyde resin synthesis. *Bioresource technology*, **2007,** *98*, 1655-1663.
(187) Tai, H.-C.; Li, G.-C.; Huang, S.-J.; Jhu, C.-R.; Chung, J.-H.; Wang, B. Y.; Hsu, C.-S.; Brandmair, B.; Chung, D.-T.; Chen, H. M. Chemical distinctions between Stradivari's maple and modern tonewood. *Proceedings of the National Academy of Sciences*, **2017,** *114*, 27-32.
(188) Kono, H.; Yunoki, S.; Shikano, T.; Fujiwara, M.; Erata, T.; Takai, M. CP/MAS 13C NMR study of cellulose and cellulose derivatives. 1. Complete assignment of the CP/MAS 13C NMR spectrum of the native cellulose. *Journal of the American Chemical Society*, **2002,** *124*, 7506-7511.
(189) S öyler, Z.; Meier, M. A. R. Sustainable functionalization of cellulose and starch with diallyl carbonate in ionic liquids. *Green Chemistry*, **2017,** *19*, 3899-3907.
(190) Simmons, T. J.; Mortimer, J. C.; Bernardinelli, O. D.; Poppler, A. C.; Brown, S. P.; deAzevedo, E. R.; Dupree, R.; Dupree, P. Folding of xylan onto cellulose fibrils in plant cell walls revealed by solid-state NMR. *Nat Commun*, **2016,** *7*, 1-9.
(191) Wang, T.; Yang, H.; Kubicki, J. D.; Hong, M. Cellulose Structural Polymorphism in Plant Primary Cell Walls Investigated by High-Field 2D Solid-State NMR Spectroscopy and Density Functional Theory Calculations.

*Biomacromolecules,* **2016,** *17*, 2210–2222.
(192) Vismara, E.; Gastaldi, G.; Valerio, A.; Bertini, S.; Cosentino, C.; Eisle, G. Alpha cellulose from industrial and agricultural renewable sources like short flax fibres, ears of corn and wheat-straw and its transformation into cellulose acetates. *Journal of Materials Chemistry,* **2009,** *19*, 8678-8686.
(193) Tai, H. C.; Li, G. C.; Huang, S. J.; Jhu, C. R.; Chung, J. H.; Wang, B. Y.; Hsu, C. S.; Brandmair, B.; Chung, D. T.; Chen, H. M.; Chan, J. C. Chemical distinctions between Stradivari's maple and modern tonewood. *Proc Natl Acad Sci U S A,* **2017,** *114*, 27-32.
(194) Zhu, W.; Westman, G.; Theliander, H. The molecular properties and carbohydrate content of lignins precipitated from black liquor. *Holzforschung,* **2015,** *69*, 143-152.
(195) Sannigrahi, P.; Kim, D. H.; Jung, S.; Ragauskas, A. Pseudo-lignin and pretreatment chemistry. *Energy Environ. Sci.*, **2011,** *4*, 1306-1310.
(196) Cheng, H. N.; Neiss, T. G. Solution NMR Spectroscopy of Food Polysaccharides. *Polymer Reviews,* **2012,** *52*, 81-114.
(197) Foston, M.; Katahira, R.; Gjersing, E.; Davis, M. F.; Ragauskas, A. J. Solid-state selective (13)C excitation and spin diffusion NMR to resolve spatial dimensions in plant cell walls. *J Agric Food Chem,* **2012,** *60*, 1419-1427.
(198) Balu, A. M.; Budarin, V.; Shuttleworth, P. S.; Pfaltzgraff, L. A.; Waldron, K.; Luque, R.; Clark, J. H. Valorisation of orange peel residues: waste to biochemicals and nanoporous materials. *ChemSusChem,* **2012,** *5*, 1694-1697.
(199) Cheng, G.; Zhang, X.; Simmons, B.; Singh, S. Theory, practice and prospects of X-ray and neutron scattering for lignocellulosic biomass characterization: towards understanding biomass pretreatment. *Energy & Environmental Science,* **2015,** *8*, 436-455.
(200) Xiao, S.; Gao, R.; Lu, Y.; Li, J.; Sun, Q. Fabrication and characterization of nanofibrillated cellulose and its aerogels from natural pine needles. *Carbohydrate polymers,* **2015,** *119*, 202-209.
(201) Tsubaki, S.; Azuma, J.-i., *Application of microwave technology for utilization of recalcitrant biomass*. InTech: **2011**.
(202) Sofla, M. R. K.; Brown, R. J.; Tsuzuki, T.; Rainey, T. J. A comparison of cellulose nanocrystals and cellulose nanofibres extracted from bagasse using acid and ball milling methods. *Advances in Natural Sciences: Nanoscience and Nanotechnology,* **2016,** *7*, 1-9.
(203) Zhu, H.; Fang, Z.; Preston, C.; Li, Y.; Hu, L. Transparent paper: fabrications, properties, and device applications. *Energy & Environmental Science,* **2014,** *7*, 269-287.
(204) Flórez, N.; Conde, E.; Domínguez, H. Microwave assisted water extraction of plant compounds. *Journal of Chemical Technology & Biotechnology,* **2015,** *90*, 590-607.
(205) Hu, F.; Jung, S.; Ragauskas, A. Pseudo-lignin formation and its impact on enzymatic hydrolysis. *Bioresource technology,* **2012,** *117*, 7-12.
(206) Su, T. C.; Fang, Z.; Zhang, F.; Luo, J.; Li, X. K. Hydrolysis of Selected Tropical

Plant Wastes Catalyzed by a Magnetic Carbonaceous Acid with Microwave. *Sci Rep,* **2015,** *5*, 1-14.
(207) Johansson, L.-S.; Tammelin, T.; Campbell, J. M.; Setälä, H.; Österberg, M. Experimental evidence on medium driven cellulose surface adaptation demonstrated using nanofibrillated cellulose. *Soft Matter,* **2011,** *7*, 10917-10924.
(208) Zimmermann, M. V.; Borsoi, C.; Lavoratti, A.; Zanini, M.; Zattera, A. J.; Santana, R. M. Drying techniques applied to cellulose nanofibers. *Journal of Reinforced Plastics and Composites*, **2016,** *35*, 628-643.
(209) Renard, C.; Weightman, R.; Thibault, J.-F. The xylose-rich pectins from pea hulls. *International journal of biological macromolecules,* **1997,** *21*, 155-162.
(210) Mamman, A. S.; Lee, J. M.; Kim, Y. C.; Hwang, I. T.; Park, N. J.; Hwang, Y. K.; Chang, J. S.; Hwang, J. S. Furfural: Hemicellulose/xylosederived biochemical. *Biofuels, Bioproducts and Biorefining: Innovation for a sustainable economy,* **2008,** *2*, 438-454.
(211) Zain, N. F.; Yusop, S. M.; Ahmad, I. Preparation and characterization of cellulose and nanocellulose from pomelo (Citrus grandis) albedo. *J Nutr Food Sci,* **2014,** *5*, 1-4.
(212) Viamajala, S.; Donohoe, B. S.; Decker, S. R.; Vinzant, T. B.; Selig, M. J.; Himmel, M. E.; Tucker, M. P., *Heat and mass transport in processing of lignocellulosic biomass for fuels and chemicals*. Springer: **2010**.
(213) Mahfoudhi, N.; Boufi, S. Nanocellulose as a novel nanostructured adsorbent for environmental remediation: a review. *Cellulose,* **2017,** *24*, 1171-1197.
(214) Santos, S. F. d.; Tonoli, G. H. D.; Mejia, J.; Fiorelli, J.; Savastano Jr, H. Non-conventional cement-based composites reinforced with vegetable fibers: A review of strategies to improve durability. *Materiales de Construcción,* **2015,** *65*, 1-20.
(215) Karimi, K.; Taherzadeh, M. J. A critical review of analytical methods in pretreatment of lignocelluloses: composition, imaging, and crystallinity. *Bioresource technology,* **2016,** *200*, 1008-1018.
(216) Santos, S. F. d.; Tonoli, G. H. D.; Mejia, J.; Fiorelli, J.; Savastano Jr, H. Non-conventional cement-based composites reinforced with vegetable fibers: A review of strategies to improve durability. *Materiales de Construcción,* **2015,** *65*, 041.
(217) Osong, S. H.; Norgren, S.; Engstrand, P. Processing of wood-based microfibrillated cellulose and nanofibrillated cellulose, and applications relating to papermaking: a review. *Cellulose,* **2016,** *23*, 93-123.
(218) Spence, K. L.; Venditti, R. A.; Rojas, O. J.; Habibi, Y.; Pawlak, J. J. A comparative study of energy consumption and physical properties of microfibrillated cellulose produced by different processing methods. *Cellulose,* **2011,** *18*, 1097-1111.
(219) Mitchell, J.; Webber, J. B. W.; Strange, J. H. Nuclear magnetic resonance cryoporometry. *Physics Reports,* **2008,** *461*, 1-36.
(220) Anovitz, L. M.; Cole, D. R. Characterization and analysis of porosity and pore structures. *Reviews in Mineralogy and geochemistry,* **2015,** *80*, 61-164.
(221) Sadaka, S.; Sharara, M. A.; Ashworth, A.; Keyser, P.; Allen, F.; Wright, A. Characterization of biochar from switchgrass carbonization. *Energies,* **2014,** *7*, 548-567.

(222) Kwapinski, W.; Byrne, C. M.; Kryachko, E.; Wolfram, P.; Adley, C.; Leahy, J. J.; Novotny, E. H.; Hayes, M. H. Biochar from biomass and waste. *Waste and Biomass Valorization,* **2010,** *1*, 177-189.
(223) Hu, X.; Gholizadeh, M. Biomass pyrolysis: A review of the process development and challenges from initial researches up to the commercialisation stage. *Journal of Energy Chemistry,* **2019,** *39*, 109-143.
(224) Kumar, R.; Strezov, V.; Weldekidan, H.; He, J.; Singh, S.; Kan, T.; Dastjerdi, B. Lignocellulose biomass pyrolysis for bio-oil production: A review of biomass pre-treatment methods for production of drop-in fuels. *Renewable and Sustainable Energy Reviews,* **2020,** *123*, 109763.
(225) Wu, C.; Budarin, V. L.; Gronnow, M. J.; De Bruyn, M.; Onwudili, J. A.; Clark, J. H.; Williams, P. T. Conventional and microwave-assisted pyrolysis of biomass under different heating rates. *Journal of Analytical and Applied Pyrolysis*, **2014,** *107*, 276-283.
(226) Wiedemeier, D. B.; Abiven, S.; Hockaday, W. C.; Keiluweit, M.; Kleber, M.; Masiello, C. A.; McBeath, A. V.; Nico, P. S.; Pyle, L. A.; Schneider, M. P. Aromaticity and degree of aromatic condensation of char. *Organic Geochemistry,* **2015,** *78*, 135-143.
(227) Zambon, I.; Colosimo, F.; Monarca, D.; Cecchini, M.; Gallucci, F.; Proto, A. R.; Lord, R.; Colantoni, A. An innovative agro-forestry supply chain for residual biomass: Physicochemical characterisation of biochar from olive and hazelnut pellets. *Energies,* **2016,** *9*, 526.
(228) Qambrani, N. A.; Rahman, M. M.; Won, S.; Shim, S.; Ra, C. Biochar properties and eco-friendly applications for climate change mitigation, waste management, and wastewater treatment: A review. *Renewable and Sustainable Energy Reviews,* **2017,** *79*, 255-273.
(229) Budai, A.; Zimmerman, A.; Cowie, A.; Webber, J.; Singh, B.; Glaser, B.; Masiello, C.; Andersson, D.; Shields, F.; Lehmann, J. Biochar Carbon Stability Test Method: An assessment of methods to determine biochar carbon stability. *International Biochar Initiative,* **2013**, 1-10.
(230) Dieguez-Alonso, A.; Funke, A.; Anca-Couce, A.; Rombolà, A. G.; Ojeda, G.; Bachmann, J.; Behrendt, F. Towards biochar and hydrochar engineering—influence of process conditions on surface physical and chemical properties, thermal stability, nutrient availability, toxicity and wettability. *Energies,* **2018,** *11*, 1-26.
(231) Ghani, W. A. W. A. K.; Mohd, A.; da Silva, G.; Bachmann, R. T.; Taufiq-Yap, Y. H.; Rashid, U.; Ala'a, H. Biochar production from waste rubber-wood-sawdust and its potential use in C sequestration: chemical and physical characterization. *Industrial Crops and Products,* **2013,** *44*, 18-24.
(232) Wang, C.; Wang, Y.; Herath, H. Polycyclic aromatic hydrocarbons (PAHs) in biochar–Their formation, occurrence and analysis: A review. *Organic Geochemistry,* **2017,** *114*, 1-11.
(233) Gao, Y.; Xia, H.; Sulaeman, A.; de Melo, E. M.; Dugmore, T. I. J.; Matharu, A. S. Defibrillated celluloses via dual twin-screw extrusion and microwave hydrothermal treatment (MHT) of spent pea biomass. *ACS Sustainable Chemistry &*

*Engineering*, **2019**.
(234) Hajir, M.; Graf, R.; Tremel, W. Stable amorphous calcium oxalate: synthesis and potential intermediate in biomineralization. *Chemical Communications*, **2014,** *50*, 6534-6536.
(235) Azadfar, M.; Gao, A. H.; Bule, M. V.; Chen, S. Structural characterization of lignin: A potential source of antioxidants guaiacol and 4-vinylguaiacol. *International journal of biological macromolecules*, **2015,** *75*, 58-66.
(236) Idström, A.; Schantz, S.; Sundberg, J.; Chmelka, B. F.; Gatenholm, P.; Nordstierna, L. 13C NMR assignments of regenerated cellulose from solid-state 2D NMR spectroscopy. *Carbohydrate polymers*, **2016,** *151*, 480-487.
(237) Zhao, L.; Smolarkiewicz, I.; Limbach, H.-H.; Breitzke, H.; Pogorzelec-Glaser, K.; Pankiewicz, R.; Tritt-Goc, J.; Gutmann, T.; Buntkowsky, G. Imidazole-doped cellulose as membrane for fuel cells: structural and dynamic insights from solid-state NMR. *The Journal of Physical Chemistry C*, **2016,** *120*, 19574-19585.
(238) Foston, M.; Katahira, R.; Gjersing, E.; Davis, M. F.; Ragauskas, A. J. Solid-state selective 13C excitation and spin diffusion NMR to resolve spatial dimensions in plant cell walls. *Journal of agricultural and food chemistry*, **2012,** *60*, 1419-1427.
(239) Gu, F.; Wang, W.; Cai, Z.; Xue, F.; Jin, Y.; Zhu, J. Y. Water retention value for characterizing fibrillation degree of cellulosic fibers at micro and nanometer scales. *Cellulose*, **2018,** *25*, 2861-2871.
(240) Magomya, A.; Kubmarawa, D.; Ndahi, J.; Yebpella, G. Determination of plant proteins via the kjeldahl method and amino acid analysis: a comparative study. *International journal of scientific & technology research*, **2014,** *3*, 68-72.
(241) Pelissari, F. M.; do Amaral Sobral, P. J.; Menegalli, F. C. Isolation and characterization of cellulose nanofibers from banana peels. *Cellulose*, **2014,** *21*, 417-432.
(242) Huang, Y.; Sun, S.; Huang, C.; Yong, Q.; Elder, T.; Tu, M. Stimulation and inhibition of enzymatic hydrolysis by organosolv lignins as determined by zeta potential and hydrophobicity. *Biotechnology for biofuels*, **2017,** *10*, 1-11.
(243) Ghosh, T.; Katiyar, V. Cellulose-based hydrogel films for food packaging. *Cellulose-based superabsorbent hydrogels. Polymers and polymeric composites: a reference series. Springer, Cham*, **2018**, 1-25.
(244) Shanks, R.; Martinez Pardo, I. Cellulose Solubility, Gelation, and Absorbency Compared with Designed Synthetic Polymers. **2018**.
(245) Chan, S. Y.; Choo, W. S.; Young, D. J.; Loh, X. J. Pectin as a rheology modifier: Origin, structure, commercial production and rheology. *Carbohydrate polymers*, **2017,** *161*, 118-139.
(246) Zhu, J.; Zhang, S.; Zhang, B.; Qiao, D.; Pu, H.; Liu, S.; Li, L. Structural features and thermal property of propionylated starches with different amylose/amylopectin ratio. *International journal of biological macromolecules*, **2017,** *97*, 123-130.
(247) Bergna, H. E.; Roberts, W. O., *Colloidal silica: fundamentals and applications*. CRC Press: **2005**.
(248) Tamai, K.; Ma, J. F. Characterization of silicon uptake by rice roots. *New phytologist*, **2003,** *158*, 431-436.

(249) Ismael, M.; Anjos, R. d.; Salomão, R.; Pandolfelli, V. Colloidal silica as a nanostructured binder for refractory castables. *Refract. Appl. News,* **2006,** *11*, 16-20.
(250) Pfaltzgraff, L.; Clark, J., Green chemistry, biorefineries and second generation strategies for re-use of waste: an overview. In *Advances in Biorefineries* |Publisher: | **Year**; |.
(251) Dodson, J. Wheat straw ash and its use as a silica source. PhD Thesis, University of York: **2011**.
(252) Statista. Paper Industry - Statistics & Facts. https://www.statista.com/topics/1701/paper-industry/ (accessed 8 April 2020).
(253) The 2019 Paper & Plastics Recycling Conference Europe. PPRCE 2019: Global shifts in paper and board production. https://www.recyclingtoday.com/article/pprce-2019-paper-production-globally/ (accessed 8 April 2020).
(254) Srivastava, S. K.; Asthana, A. Study of Ecofriendly Light Weight Bricks using waste Paper—A Review. *Carbon,* **2017,** *5*, 573-577.
(255) MarketWatch. Waste Paper Recycling Market 2019 Global Industry Analysis, Development, Revenue, Future Growth, Business Prospects and Forecast to 2024: 360 Research Reports. https://www.bbntimes.com/global-economy/the-global-paper-industry-still-on-the-rise (accessed 4 June 2020).
(256) Zhang, Z. Renewable Biomass Resources: from waste biomass to novel applications via green chemical technologies. PhD Thesis, University of York: **2015**.
(257) Environmental Audit Committee. Chinese Waste Import Ban inquiry launched. https://www.parliament.uk/business/committees/committees-a-z/commons-select/environmental-audit-committee/news-parliament-2017/chinese-waste-import-ban-launch-17-19/ (accessed 15 January 2020).
(258) Fernandes, S. C.; Sadocco, P.; Alonso-Varona, A.; Palomares, T.; Eceiza, A.; Silvestre, A. J.; Mondragon, I. a.; Freire, C. S. Bioinspired antimicrobial and biocompatible bacterial cellulose membranes obtained by surface functionalization with aminoalkyl groups. *ACS applied materials & interfaces,* **2013,** *5*, 3290-3297.
(259) Vrancken, K. C.; Van Der Voort, P.; Gillis-D'Hamers, I.; Vansant, E. F.; Grobet, P. Influence of water in the reaction of γ-aminopropyltriethoxysilane with silica gel. A Fourier-transform infrared and cross-polarisation magic-angle-spinning nuclear magnetic resonance study. *Journal of the Chemical Society, Faraday Transactions,* **1992,** *88*, 3197-3200.
(260) Jonkheijm, P.; Weinrich, D.; Schröder, H.; Niemeyer, C. M.; Waldmann, H. Chemical strategies for generating protein biochips. *Angewandte Chemie International Edition,* **2008,** *47*, 9618-9647.
(261) Roy Goswami, S.; Dumont, M. J.; Raghavan, V. Starch to value added biochemicals. *Starch-Stärke,* **2016,** *68*, 274-286.
(262) Caes, B. R.; Teixeira, R. E.; Knapp, K. G.; Raines, R. T. Biomass to furanics: renewable routes to chemicals and fuels. *ACS Sustainable Chemistry & Engineering,* **2015,** *3*, 2591-2605.
(263) Al Afif, R.; Anayah, S. S.; Pfeifer, C. Batch pyrolysis of cotton stalks for

evaluation of biochar energy potential. *Renewable Energy*, **2020,** *147*, 2250-2258.
(264) Fang, J.; Zhan, L.; Ok, Y. S.; Gao, B. Minireview of potential applications of hydrochar derived from hydrothermal carbonization of biomass. *Journal of Industrial and Engineering Chemistry*, **2018,** *57*, 15-21.
(265) Ching, T. W.; Haritos, V.; Tanksale, A. Ultrasound-assisted conversion of cellulose into hydrogel and functional carbon material. *Cellulose*, **2018,** *25*, 2629-2645.
(266) Phanthong, P.; Guan, G.; Ma, Y.; Hao, X.; Abudula, A. Effect of ball milling on the production of nanocellulose using mild acid hydrolysis method. *Journal of the Taiwan Institute of Chemical Engineers*, **2016,** *60*, 617-622.
(267) Khalil, H. A.; Davoudpour, Y.; Islam, M. N.; Mustapha, A.; Sudesh, K.; Dungani, R.; Jawaid, M. Production and modification of nanofibrillated cellulose using various mechanical processes: a review. *Carbohydrate polymers*, **2014,** *99*, 649-665.
(268) Chen, M.; Ma, Q.; Zhu, J.; Alonso, D. M.; Runge, T. GVL pulping facilitates nanocellulose production from woody biomass. *Green Chemistry*, **2019,** *21*, 5316-5325.
(269) Schenker, M.; Schoelkopf, J.; Gane, P.; Mangin, P. Influence of shear rheometer measurement systems on the rheological properties of microfibrillated cellulose (MFC) suspensions. *Cellulose*, **2018,** *25*, 961-976.
(270) Dimic‐Misic, K.; Rantanen, J.; Maloney, T. C.; Gane, P. A. Gel structure phase behavior in micro nanofibrillated cellulose containing in situ precipitated calcium carbonate. *Journal of Applied Polymer Science*, **2016,** *133*.
(271) Azhar, S. H. M.; Abdulla, R.; Jambo, S. A.; Marbawi, H.; Gansau, J. A.; Faik, A. A. M.; Rodrigues, K. F. Yeasts in sustainable bioethanol production: A review. *Biochemistry and Biophysics Reports*, **2017,** *10*, 52-61.
(272) ISO 16893:2016 Wood-based panels -- Particleboard 2016.

# Appendix

**Figure A1** GC-MS of ginger essential oil extracted by heptane.

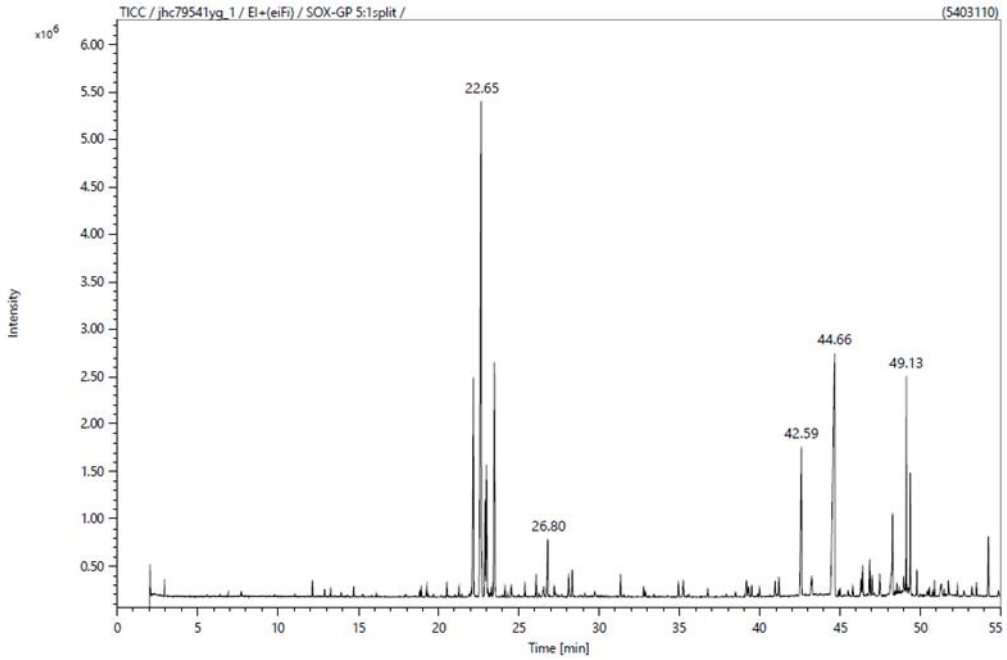

**Figure A2** Flammability test apparatuses; (b) after ignition of one board

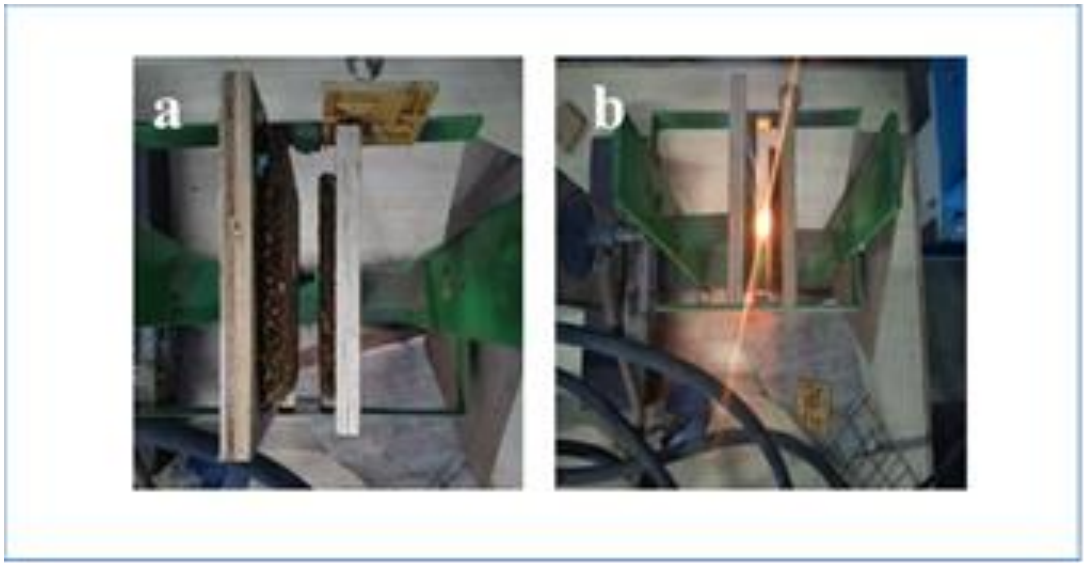

**Figure A3** Fire retardant test apparatuses with single hole burner

**Figure A4 Expanded ATR showing different wax**

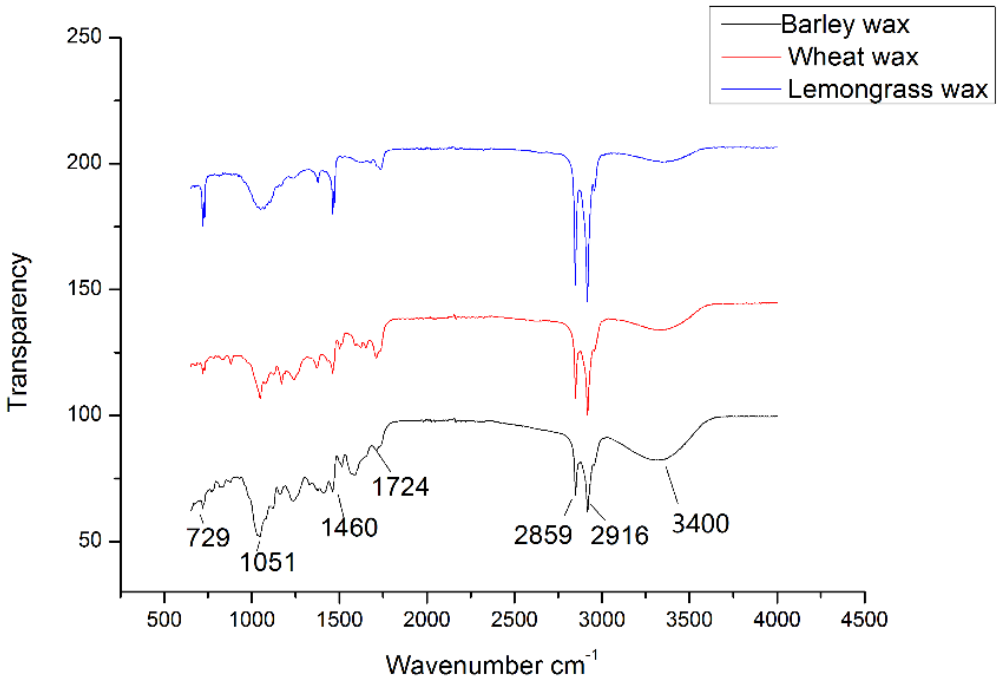

**Figure A5** GC-MS of wax extracted by ethanol

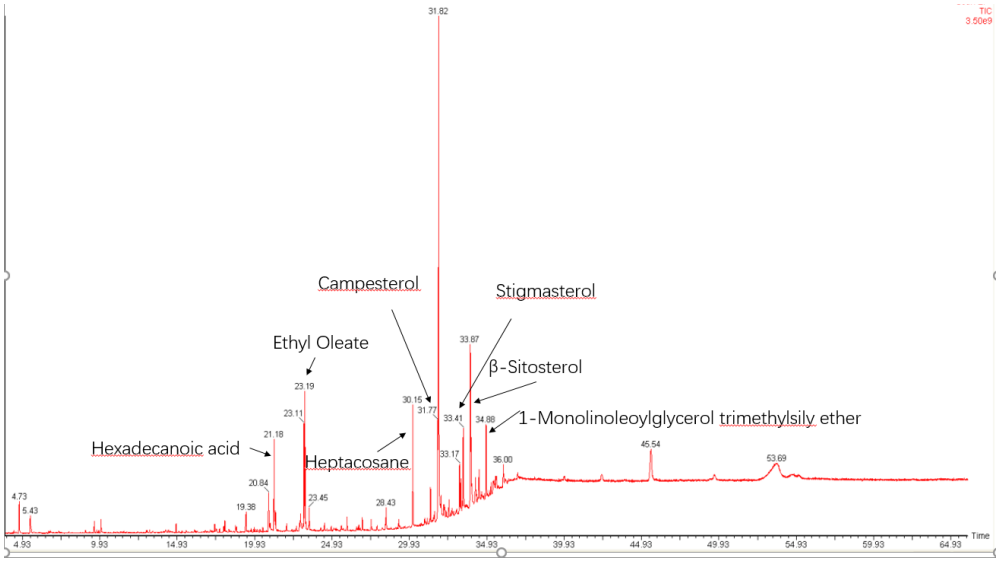

# Abbreviations

| | |
|---|---|
| APTES | 3-Aminopropyl triethoxysilane |
| ATCM | Airborne Toxic Control Measure |
| BET | Brunauer–Emmett–Teller |
| BJH | Barrett–Joyner–Halenda |
| CARB | California Air Resources Board |
| CEA | Cellulose treated in acetone solution |
| CEE | Cellulose treated in ethanol solution |
| CHN | Carbon, hydrogen and nitrogen analysis |
| CrI | Crystallinity Index |
| CMC | Cellulose microcrystalline |
| CNC | Cellulose nanocrystals |
| CNF | Cellulose nanofibrils |
| COP | Conference of the Parties |
| DSC | Differential Scanning Calorimetry |
| DTG | First derivative of thermogravimetric analy |
| EPEA | Extruded pea waste |
| EPS | Expanded Polystyrene |
| EU | European Union |
| FAO | Food and Agriculture Organization |
| FSC | Food Supply Chain |
| GC | Ginger char |

| | |
|---|---|
| GCMS | Gas Chromatography-mass spectrometry |
| GMFC | Ginger microfibrillated cellulose |
| GS | Ginger starch |
| HPLC | High Performance Liquid Chromatography |
| HSC | Honeycomb |
| HWPW | Hardwood Plywood |
| Hy-MASS | Hydrothermal microwave-assisted selective scissoring |
| IBS | Internal Bond Strength |
| ICP | Inductively Coupled Plasma |
| ICP-OES | Inductively Coupled Plasma Atomic Emission Spectroscopy |
| MCC | Microcrystalline cellulose |
| MD | Medium Boards |
| MDF | Medium Density fibre Board |
| MFC | Microfibrillated Cellulose |
| MHT | Microwave hydrothermal treatment |
| Mt | Million tonnes |
| NCC | Cellulose nanocrystal |
| NFC | Nanofibrillar cellulose |
| NMR | Nuclear Magnetic Resonance |
| OSB | Oriented Strand Board |
| PAA | Paper samples treated in acetone solution |
| PAE | Paper samples treated in ethanol solution |

| | |
|---|---|
| PB | Particleboard |
| PEA | Product from pea waste |
| PF | Phenol-formaldehyde |
| PVA | Polyvinyl Alcohol |
| SDG | Sustainable Development Goals |
| SEM | Scanning Electron Microscope |
| SIP | Structural Insulation Panel |
| SSA | Specific Surface Area |
| TGA | Thermogravimetric Analysis |
| Td | Temperature of maximum mass loss rate (TGA) |
| TEM | Transmission electron microscopy |
| TEMPO | 2,2,6,6-Tetramethylpiperidine-1-oxyl radical |
| UF | Urea-Formaldehyde |
| UFSCW | Unavoidable Food Supply Chain Waste |
| UK | United Kingdom |
| UN | United Nations |
| UNFCCC | United Nations Framework to Combat Climate Change |
| USA | United States of America |
| WHC | Water holding capacity |
| WRV | Water retention value |
| XPS | Extruded Polystyrene |
| XRD | X-Ray Diffraction |